DEPARTMENT OF ELECTRONIC & ELECTRICAL ENGINEERING

University of Strathclyde Engineering

# PULSED ELECTRIC FIELD TREATMENT OF *ARTHROSPIRA PLATENSIS* AND *SACCHAROMYCES CEREVISIAE*

A thesis presented in fulfilment of the requirement for

the degree of

**Doctor of Philosophy**

**Si Qin, B.Eng. (Honours), M.Sc.**

**2016**

**Department of Electronic and Electrical Engineering**

**University of Strathclyde**

**Glasgow, UK**

# DECLARATION OF AUTHENTICITY AND AUTHOR'S RIGHTS

‘This thesis is the result of the author’s original research. It has been composed by the author and has not been previously submitted for examination which has led to the award of a degree.’

‘The copyright of this thesis belongs to the author under the terms of the United Kingdom Copyright Acts as qualified by University of Strathclyde Regulation 3.50. Due acknowledgement must always be made of the use of any material contained in, or derived from, this thesis.’

Signed:

Date:

# ACKNOWLEDGEMENTS

I would like to express my sincere thanks and appreciation to a few people who have been invaluable to me throughout the course of this project and in the completion of this thesis.

First and foremost, I would like to acknowledge my supervisors Dr. Igor Timoshkin and Prof. Scott MacGregor for providing me the opportunity to undertake this PhD and their supervision, guidance, encouragement and help throughout the course of this project.

I would also like to thank Dr. Mark Wilson, Dr. Michelle Maclean and Dr. Martin Given for many productive discussions and academic writing suggestions. Thanks also go to Dr. Karen McKenzie, Dr. Tracy White and Mr. David Curry for their assistance in bioscience matters.

Thanks to all the guys in the High-Voltage Mechanical Workshop: David Griffin, Andy Carlin, Sean Doak and Frank May, for all their help with designing and machining many pieces of test cells and equipment.

I would like to thank Faculty of Engineering and Department of EEE of University of Strathclyde for providing the Faculty of Engineering Studentship, without which this PhD could not be possible.

I would also like to express my appreciation for all my colleagues and friends, in particular Yihan Liu and Tong Qiao, for making this PhD an enjoyable journey.

I would also like to thank my family, in particular my father Hanshi Qin and my wife Jingyuan Wei for their tremendous support and understanding.

This thesis is dedicated to my mother.

# ABSTRACT

Pulsed electric field (PEF) can induce irreversible electroporation in the bio-membrane and cause the death of microbial cells without significant thermal effect, which can be used for inactivation of microorganisms and facilitation lysis of microbial cells for lipid extraction. The present study aimed to investigate the efficiency of PEF treatment of *Arthrospira platensis* and *Saccharomyces cerevisiae* using test cells with different types of electrodes and impulses with different waveshapes. An equivalent circuit modelling approach was also proposed and developed to describe the pulsed power system and the microbiological cell in the present study.

The PEF test cells with three types of electrodes were developed in the present study: a traditional stainless steel test cell; a novel low-conductive test cell with 2 μm $TiO_2$-coating on electrode surface; and a novel test cell with non-conductive ceramic electrodes. Effective PEF inactivation of both *A. platensis* and *S. cerevisiae* was achieved using stainless steel and $TiO_2$-coated test cells. Significant improvement in the energy efficacy of the PEF treatment was obtained using the $TiO_2$-coated test cell. However, PEF inactivation of microorganisms in the ceramic test cell required electric fields with magnitude above 80 kV/cm.

Three types of impulses, square impulse, smooth exponential impulse and oscillating exponential impulse were used in the present study. The best energy efficacy was achieved using the smooth exponential impulse for the field levels of 67 kV/cm and 80 kV/cm. A correlation between the pulse waveshape, the electric field magnitude and the inactivation performance was established.

The PEF treatments of *A. platensis* demonstrated that this type of cyanobacteria can be inactivated effectively but rupture of the cell structure was not achieved. The PEF process was capable of induction of the lethal damage to the *A. platensis* cells but not sufficient to cause significant mechanical damage to the cell structure.

# TABLE OF CONTENTS

# Chapter I

## INTRODUCTION

Effective inactivation of undesirable microorganisms has long been a challenge in medical and food industries. Varieties of decontamination and disinfection technologies have been developed to meet this challenge. However, many of the established technologies present limitations in terms of their environmental suitability, their side effects and their economic viability. Therefore, there is a strong continuous demand for the optimisation of established decontamination and disinfection technologies and for the development of novel inactivation methods and approaches.

On the other hand, the products from the microorganism metabolism have attracted significant research and practical interest. For example, microalgae, cyanobacteria and their bio-products have drawn great global attention in the past decades. In the hunt for the alternatives to fossil fuel, these microorganisms turn out to be one of the most promising candidates due to their high lipid content as compared to other food crops and oil seeds, [1]. However, current methods of lipid extraction from microalgae and cyanobacteria are still ineffective and costly. Therefore, novel technologies are urgently required to facilitate lysis of the microbial cells effectively and economically.

First systematically investigated and described in 1967, the process of pulsed electric field (PEF) treatment is based on the application of the high electric field to suspension with microorganisms which can induce lethal effects on these microorganisms, [2-4]. When subjected to an external electric field, pores can be formed in the microbial membrane under certain conditions and this process is called electroporation, [5]. Once the electric field exceeds a critical value, the electroporation process becomes irreversible and causes the death of the microbial

cell. The electroporation process gives the PEF technology the ability to inactivate microorganisms and potentially to facilitate lysis of the microbial cells. Although PEF inactivation of variety of bacteria and yeast has been well documented, limited amount of work has been done to facilitate lysis of microalgae and cyanobacteria using the PEF process. Investigation of PEF induced lysis of one of these lipid-rich microorganisms was one of the research aims of the present study.

As a non-thermal inactivation technology, the PEF method has attracted significant research attention. This method has been employed in various applications over the last two decades and a large number of studies have been conducted to develop the PEF technology. However, there are some fundamental drawbacks which are associated with the traditional PEF treatment. To apply the electric field to microorganisms, the liquid suspension which contains these microorganisms is usually placed between two metallic electrodes. Once high voltage is applied to the electrodes, electro-chemical reactions can occur at the interface between the liquid and the electrodes, which can generate toxic metallic ions and gaseous bubbles. In addition, direct contact between the electrodes and highly conductive suspension results in a high ionic conduction current, which increases the suspension temperature through excessive energy dissipation.

These undesirable effects are unavoidable in the conventional PEF chambers with metallic electrodes. To overcome such negative effects, a novel PEF test cell design was proposed in [6]. This conceptual PEF test cell has two layers of high permittivity ceramic separating the metallic electrodes and the liquid suspension. As a result, there will be no electro-chemical reactions between the metallic electrodes and the suspension, which minimises the possibility of the production of undesirable by-products. Besides, the steady state ionic conduction current through the suspension will be eliminated, which will minimise the thermal effect and can significantly improve the energy efficacy of the PEF process. Implementation of this design in practice and investigation of the PEF performance of this conceptual test cell were the main tasks of the present study.

Over the last few decades, significant amount of studies have also been focused into the investigation of the effects of different operational and biological factors on the PEF process. These factors include the electric field magnitude, pulse waveshape, electrode material, size of the microbial cell, and the temperature and conductivity of the microbial suspension. Very limited amount of work has been conducted in order to investigate the effect of pulse waveshape on the PEF process, a few examples can be found in [7-8]. However, further understanding of the effects of the pulse waveshape on the PEF process will be beneficial and important for optimising the PEF systems and energisation parameters of the PEF process. To address this problem and to improve understanding of the influence of pulse waveshape on the PEF process efficacy, a study of the effect of different pulse waveshapes on inactivation of yeast was conducted in the framework of this project.

Apart from practical PEF studies, significant efforts in the present work were made to establish the mathematic description and to model the PEF process. Accurate modelling of the PEF process can provide valuable information for understanding of the PEF inactivation mechanisms, development of the transient electric field across bio-membrane, and for optimisation of the PEF systems. Since the proposal of the Schwan's equation in 1957, [9], in which the mathematic relationship between the external electric field and the induced trans-membrane potential was established, significant amount of studies have been conducted to model the PEF process using either equivalent circuit models or analytical models. However, the majority of these studies were focused on either the modelling of microbial cell on a micro-scale or the modelling of the PEF system on a macro-scale. The link between these two approaches, micro-scale cell model and macro-scale pulse driving circuit model, is important for further optimisation of the PEF process. To provide this connection, a comprehensive approach which described the pulsed power system and the microbiological cell was proposed and developed in the present study. This approach was used for analysis of the transient electric fields in the test cells (suspension) and across bio-membrane.

An overview of the content of each chapter in the present thesis is given below:

***Chapter II*** *(Background and Literature Review)* provides background information relevant to the field of study which was obtained and analysed during the course of the present project. Background information on microorganisms and current inactivation methods is given. Technical fundamentals of the pulsed power technology are discussed. A comprehensive literature review of the PEF technology including the inactivation mechanisms, design of the PEF chambers, results of PEF inactivation of yeast and algae, and the analysis of the recent PEF studies with a focus into different aspects of the PEF technology is presented in this chapter.

***Chapter III*** *(Modelling of the PEF Process)* presents two models which describe the development of the transient trans-membrane potential. These models include a 2-dimentional equivalent circuit model and an analytical model which describes the PEF treatment in the non-conductive test cell. The obtained results and significant findings from these modelling works are discussed.

***Chapter IV*** *(Development of the PEF Test Cells and PEF System)* presents the details of the design process of two PEF test cells: a conductive stainless steel test cell and a non-conductive ceramic test cell. An impulse generator which produces HV impulses with square waveshape is also introduced in this chapter.

***Chapter V*** *(PEF Treatment of Microorganisms Using the Initial Test Cells)* discusses the experimental procedures and results of the PEF treatment of microorganisms using the PEF system developed in Chapter IV. The results obtained in these tests are presented and the PEF performance of the two test cells is compared.

***Chapter VI*** *(Development of Improved PEF Test Cells and PEF System)* analyses the drawbacks of the developed PEF system and PEF treatment approaches described in Chapter V. An improved stainless steel test cell and a low-conductive $TiO_2$-coated test cell are designed and manufactured based on this analysis. Development of the smooth exponential impulse and oscillating exponential impulse generators is also discussed in this chapter.

***Chapter VII*** *(PEF Treatment on Microorganisms: Improved Test Cells)* investigates the PEF inactivation performance of the re-designed stainless steel test cell and the novel $TiO_2$-coated test cell. The effect of the pulse waveshape on the PEF performance is studied. The energy efficacy of the PEF treatment in different test cells stressed with PEF impulses with different waveshapes is obtained and discussed.

***Chapter VIII*** *(Conclusions and Future Works)* summarises the significant findings from the whole project, highlighting the contribution of the present study to the knowledge in the field of PEF inactivation. Recommendations for future work are also given.

# Chapter II

# BACKGROUND AND LITERITURE REVIEW

## 2.0 General

This chapter presents a literature review of the relevant background information, current researches and the latest developments in the field of PEF inactivation of microorganisms.

This literature review begins with an introduction of the basic background information on microorganisms, which includes the key structural elements of microorganisms, the benefits and hazards of the presence of microorganisms, and the current inactivation and disinfection technologies. The review also discusses the principle of pulsed power technology which underpins the PEF process. Essential elements of pulsed power systems, such as pulse forming methods and high voltage switches, will be described and current applications of the pulsed power technology will be introduced. The PEF inactivation technology, which is the focus of the present study, will be reviewed in details in the final part of this literature review. The principles of the PEF technology and the inactivation mechanisms will be discussed. Introduction to the recent PEF studies into the different factors that can affect the inactivation performance of the PEF process will be presented. These factors include the magnitude of field strength, pulse waveshape, electrodes material and microbial and suspension factors.

Through this critical literature review, the gaps in the acquired knowledge in the field of PEF research will be identified and discussed. The main objectives and aims of the present study which will help to fill the identified gaps in the knowledge and in further development of the PEF technology will be outlined.

## 2.1 Background Information of Microorganism

Since their discovery in the 17th century, the reliable estimate number of different microorganisms is 159,000 species, [10]. The name “microorganism” is given due to the very small sizes of these microscopic organisms with a cell diameter ranging from ~ 0.2 µm to 700 µm, [11]. As the first form of life developed on earth, single-cell microorganisms existed since 3-4 billion years ago, [12-14], and remained the only form of life on earth for the following 3 billion years, [15]. Microorganisms can be classified into two types: prokaryote and eukaryote microorganisms. Figure II.1 shows the typical structures of the prokaryote and eukaryote microorganisms, [16]. Prokaryote microorganisms have structurally simple cells, which lack a cell nucleus and the other membrane bound organelles. Bacteria and archaea are included within the prokaryotic group by their cell structural simplicity. Majority of bacteria can be sub-divided into two types, Gram-positive and Gram-negative, according to their response to Gram staining which highlights the composition of the cell wall, [11]. The eukaryote microorganisms contain relatively complicate organelles and are normally larger than the prokaryote microorganisms. Eukaryote microorganisms include most protists, some fungi, as well as some animals and plants. The following section of the review will introduce critical structures and elements of the microorganisms, the effect of their presence on people’s life and the current inactivation technologies.

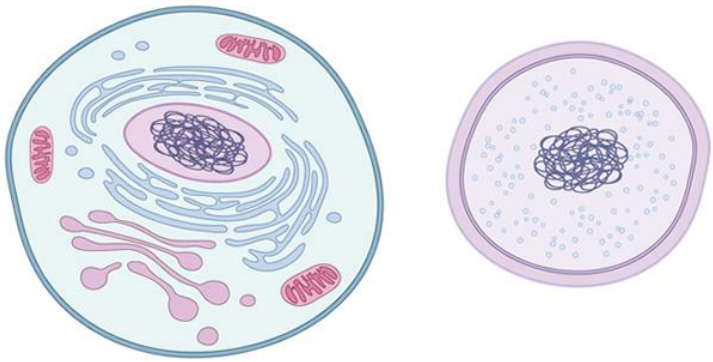

**Figure II.1** Demonstration of typical prokaryote and eukaryote microorganism cells. Eukaryote microorganism (left): contains complicate organelles and is larger in size. Prokaryote microorganism (right): relatively simple structure and is smaller in size. Figures taken from [16].

### 2.1.1 Structures of Microorganism Cell

This section introduces some important components commonly seen in most of the microorganism cells and their key roles in cell's functioning.

#### 2.1.1.1 Cell Wall

The cell wall is the outermost layer of most of the microorganism cell. The basic function of the cell wall is to provide structural strength and protection to a cell, [17]. The cell wall is much stronger than the cytoplasmic membrane in order to withstand the significant osmotic pressure inside the cell, which can be as high as 2 atm in a typical prokaryotic cell, [11], and to prevent cell bursting. The cell wall of microorganism is a relatively permeable structure, which allows the exchange of small molecules between the cell and the surrounding environment.

The composition of the cell wall varies for different microorganisms. In general, all bacterial cell walls contain peptidoglycan and other polysaccharide, [18]. Gram-positive bacteria have a thick cell wall made of peptidoglycan, whereas Gram-negative bacteria have a thinner peptidoglycan layer which is surrounded by an outer membrane. All archaea cell walls contain no peptidoglycan but only polysaccharide and other proteins, [19]. In eukaryotic microorganisms, cell wall of fungi consists mainly of chitin, glucans and proteins, [20], while cell wall of algae consists mainly of cellulose, [21].

#### 2.1.1.2 Cytoplasmic Membrane

The cell membrane, also known as the cytoplasmic membrane, is one of the most critical structures of a cell. The cytoplasmic membrane is a thin layer inside the cell wall and separates the cytoplasm from the surrounding environment, [22]. Unlike the cell wall, the cell membrane is structurally weak and provides minimal protection from osmotic lysis, [11]. However, the most important function of the cytoplasmic membrane is to be selective permeable to ions, proteins and organic molecules. Table II.1 demonstrates the different permeability of the membrane to various molecules, [11]. This critical function allows the membrane to control the

movements of substance entering and exiting the cell and to maintain a relatively constant environment inside the cytoplasm, [23].

The basic structure of the cytoplasmic membrane is a phospholipid bilayer with different types of membrane proteins embedded, as shown in Figure II.2, [24]. The phospholipid bilayer consists of fatty acids, which point inward toward each other, and the hydrophilic portions, which point outward toward cytoplasm or external environment, [25], as demonstrated in Figure II.3, [26].

**Table II.1** Comparative permeability of membranes to various molecules. Data taken from [11].

| **Substance** | **Rate of permeability (relative scale: permeability of water is given as 100)** |
|---|---|
| Water | 100 |
| Glycerol | 0.1 |
| Tryptophan | 0.001 |
| Glucose | 0.001 |
| Chloride ion ($Cl^-$) | 0.000001 |
| Potassium ion ($K^+$) | 0.0000001 |
| Sodium ion ($Ca^+$) | 0.00000001 |

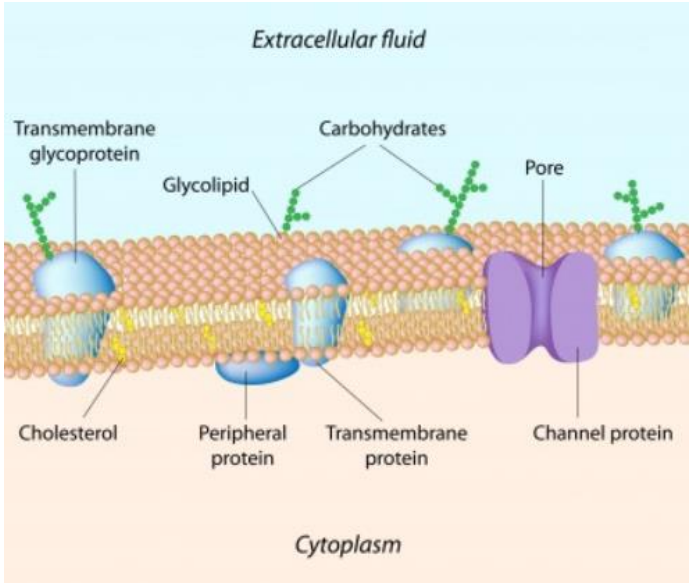


**Figure II.2** Demonstration of a typical structure of the cytoplasmic membrane. Figure taken from [24].

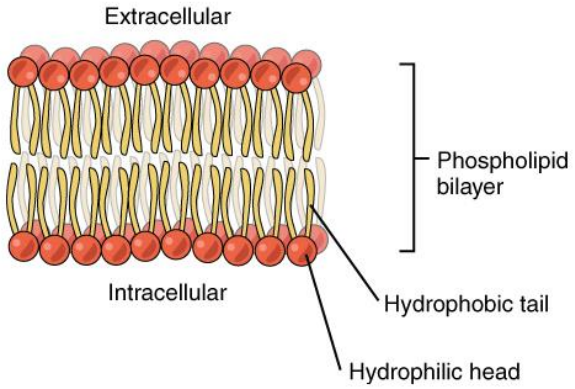


**Figure II.3** Demonstration of a phospholipid bilayer structure. Figure taken from [26].

#### 2.1.1.3 Cytoplasm

The cytoplasm is a liquid or gel-like mixture inside the cytoplasmic membrane. Most of the cell activities occur within the cytoplasm, for example many metabolic pathways and cell division, [27]. Some of the products from the metabolic processes are also stored in the cytoplasm, [11].

The contents of cytoplasm can be divided into three major elements, the cytosol, the organelles and the cytoplasmic inclusions. The cytosol consists mainly of water, inorganic ions and soluble macromolecules. The organelles are sub-structures enclosed by their own lipid bilayers, each having their own specific functions within the cell. The organelles are responsible for most of the cell activities. However, only eukaryote microorganisms have the organelles and the cell activities take place in the cytosol in the prokaryote microorganisms, [28]. The cytoplasmic inclusions are the insoluble substances in the cytoplasm, including glycogen, lipids, pigments and crystals. Many of the metabolic products are cytoplasmic inclusions.

### 2.1.2 Benefits and Hazards of the Microorganisms

Microorganisms exist in every parts of the biosphere on earth and can live in almost every extreme environment conditions. Due to this wide distribution, human beings are in constant contact with microorganisms in everyday life. Microorganisms play a very important role in people's life and influence many aspects of human

civilizations. Some of the benefits of microorganisms, as well as their hazards, will be discussed briefly in this section.

Perhaps the most important value of microorganisms is their crucial role in nutrition recycling in the ecosystem. Many bacteria and fungi act as decomposers in the ecosystem, [29-32]. Almost all types of organic matters can be broke down by these bacteria and fungi, [33]. Apart from this, a lot of soil microorganisms can participate in the nitrogen fixation process and therefore play a vital part in the nitrogen cycles, [34-37].

In addition to their natural functions, microorganisms have been widely used in the biotechnology applications since ancient time. Microorganisms have long been used in the fermentation process in winemaking, brewing, baking, yogurt making and cheese making, [38-43]. Apart from the various applications in food industry, different types of microorganisms have been used in the medical industry to produce variety of antibiotics, [11, 44 and 45]. In modern technology, microorganisms are also exploited in genetic engineering, [46-48].

Recently, the products from the microorganism metabolism, which can be accumulated and stored inside the individual cells, have raised great research interest. Among these microorganisms, microalgae, cyanobacteria and their bio-products have drawn great attention in recent decades, [49-60]. Due to their high protein content and nutritive value, several types of these microorganisms can be used as human and animal nutrition, [50-54]. Microalgae are also reported to be used for cosmetic products, [55-56]. Apart from being used as nutrition directly, extraction of high value molecule from the microalgae and cyanobacteria has also received a great research interest, [56-60]. These high value molecules include fatty acids, pigments and stable isotope bio-chemicals.

Into the late 2000's, microalgae and cyanobacteria drew increasing global attention as the potential sustainable sources for bio-fuel production [1, 61-64]. In the efforts of finding clean and sustainable alternatives for fossil fuel, which is considered to be unsustainable and have environmental impact on the planet, microalgae and

cyanobacteria are now considered to be one of the most promising candidates due to their high lipid content as compared to other food crops and oil seeds [1]. Several methods for cell disruption and lipid extraction have been investigated in order to extract the valuable content from these microalgae and cyanobacteria, [59, 62, 65 and 66]. These methods include high-pressure homogenizer, autoclaving, mechanical homogenizer, addition of chemical solvent and, most recently, pulsed electric field (PEF) technology, [67-71].

Apart from the many benefits the microorganisms can bring, the presence of microorganisms can also be problematic. One of the most significant negative impacts of microorganisms is that they are the sources of many infectious diseases. Many infamous epidemic diseases, such as plague, tuberculosis and anthrax, are caused by pathogenic bacteria. Some of the protozoa are also the cause of diseases such as malaria, dysentery and toxoplasmosis, while some types of fungi are the sources for diseases like ringworm, candidiasis and histoplasmosis.

Apart from the hazards on human's health, microorganisms have significant impact on modern food industry. The presence of microorganisms is one of the most common causes of food spoilage, [72-74]. As a result, consuming food product contaminated by microorganisms can lead to serious food poisoning. Therefore, the presence of microorganisms is strictly controlled in the food industry, [75-76].

## 2.2 Current Methods of Inactivation

Effective inactivation of microorganisms has long been widely needed in many areas, [77]. In the medical industry and healthcare environment, any pathogenic microorganisms need to be eliminated in order to provide safe medical equipment and environment. In the food industry, any undesirable or hazardous microorganisms should be inactivated in food products. In addition, as introduced in Section 2.1.2, inactivation and cell disruption could be a useful tool for biotechnology industry. In this section, some of the traditional inactivation methods will be briefly introduced, as well as some of the emerging new techniques.

### 2.2.1 Thermal Inactivation

Thermal inactivation of microorganisms has a long history, which is one of the most studied inactivation methods and is still widely used in modern industry nowadays. Heat processing of food has been used by people even without any knowledge of microbiology, [78], and doctors in the 18$^{th}$ century knew to burn the surgical equipment or put them into boiling water for sterilization, [79]. Mathematical models of thermal inactivation were first discussed in early 1920's, [80], and have been further developed, [81-83]. The basic principle of the thermal inactivation is that most microorganisms are sensitive to heat, and when subjected to stressful heat conditions cell activity will be hampered or even stopped. Therefore, inactivation of microorganisms can be achieved by exposing the microorganisms to environments above certain temperature for a certain period of time according to their individual heat resistance. For example, one of the established methods for sterilisation in the laboratory environment is to expose the equipment being sterilised at 121 °C for 15 minutes.

However, thermal inactivation has its own limitations. Some microorganisms, such as *Bacillus sporothermodurans* and *Desulfotomaculum nigrificans*, are very resistant to heat, [78]. It requires much higher temperature and much longer heating time to achieve effective inactivation of these microorganisms. Therefore, the thermal method becomes energy consuming and economically unwise in these applications. On the other hand, many applications in the food industry require non-thermal inactivation of microorganisms since the food products themselves have low heat resistance.

### 2.2.2 Chemical Disinfection

Chemical disinfection is another method for microorganism inactivation with long history. Several types of chemical substances have been used for disinfection in medical applications since 19$^{th}$ century and the use of alcohol for sterilisation can be dated back to the 13$^{th}$ century, [79]. The specific characteristics of these chemical substances, such as strong oxidation from chlorine [84], iodine [85] and ozone [86];

and protein precipitate from alcohols [87], can trigger the dysfunction and lysis of the microorganism cells. Traditional chemical substances used for microorganism inactivation includes chlorine and chloride, iodine and iodide, ozone, alcohols and glutaraldehyde. Into the 20$^{th}$ century, new chemical antimicrobials have also been developed for enhanced and safer performance, [88]. The chemical disinfection is widely used in medical application and hospital environments, and it is also employed in other applications, such as water purification and food sterilization.

Although chemical inactivation of microorganisms is very effective, this inactivation method has its own disadvantage. As most of the chemicals used for disinfection require special storage, handle and depose, extra costs are required for these additional operations. Besides, detection for remaining chemical substances after the inactivation process is needed in many applications in order to ensure the safety of the products or environments. In addition, some of the chemical substances and their decomposition products could be hazardous for human beings and environment, [89]. For example, chlorine and chloride need to be carefully dealt with, [90].

### 2.2.3 Ultraviolet Irradiation Inactivation

The capability of inducing damage in microorganism cell of the ultraviolet (UV) irradiation was first recognized in the late 19$^{th}$ century, [91]. Since then, UV inactivation technology has been developed for variety of antimicrobial applications, such as water sterilisation, surfaces disinfection, food processing and air disinfection. The inactivation mechanism of the UV irradiation is the induced damage to the nucleic acids, DNA and RNA of the microorganism's cell, [92]. With the nucleic acids and DNA disrupted, the cells are not able to conduct vital functions and subsequently die, [93]. The inactivation of microorganisms can be achieved by relatively low doses of UV irradiation; therefore this inactivation method is considered inexpensive, [92].

However, it was discovered that exposure to the UV irradiation can cause severe skin burn and leads to skin cancer in human body, [94-96]. Therefore, people are required to avoid exposure to the UV inactivation systems when in operation. Besides, it was

also found that the UV irradiation is able to break chemical bonds [97], as a result, UV disinfection of plastic surface can cause rapid aging of the material.

### 2.2.4 High Pressure Inactivation

The effect of high pressure on microorganisms was first studied in the late 19$^{th}$ century. However, it was not until 1980's this method of inactivation attracted researchers and industries interest again and became an emerging inactivation technology since then, [98-100]. Applying high pressure, normally a few hundreds of MPa, to the microorganism cells can lead to changes to several cell components, [99]. For example, the fluidity of the cell membrane could be changed by the applied high pressure and the membrane-bound Na/K ATPase can no longer function properly, which results a drop in the internal pH and subsequently the death of the cell, [101]. Studies also suggested rapid release of the applied high pressure improves the inactivation performance, [102]

As a non-thermal inactivation method, high pressure inactivation of microorganisms has a number of potential applications in food industry. However, this method still needs to overcome several challenges, [103]. Technically, filling and sealing of the treatment package brings some difficulties under such high pressure. On the other hand, in terms of economic feasibility, the cost of the high pressure inactivation process is still relatively high.

### 2.2.5 High-Intensity Narrow-Spectrum Light Inactivation

High-Intensity Narrow-Spectrum (HINS) light inactivation is a newly developed decontamination technology in the past decade, [104-106]. Inactivation of some bacteria using visible light, specifically blue-light, was reported in the early 2000's, [107-108]. These studies indicated that visible light with wavelength ranging from 400 nm to 420 nm has the capability to inactivate several bacteria, with maximum inactivation at 405 nm, [109]. The inactivation mechanism was reported to be oxygen dependent, [105, 110], photoexcitation of the endogenous porphyrins inside

the bacteria cell leads to the production of highly cytotoxic, oxygen-derived species, such as singlet oxygen.

Unlike the UV irradiation, which has a damaging effect on skin and eyes, the 405 nm HINS light at required minimal inactivating does has no such detrimental effect to humans. Therefore, the HINS light technology allows people to be present while the disinfection process is underway. A study has been conducted where HINS light was used to decontaminate a hospital room while the room was occupied with a MRSA-infected burns patient in [104]. It was shown from this study that the performance of the HINS light disinfection was greater than normal infection control and cleaning activity alone. This result suggested this new decontamination technology has promising potential in various clinical and non-clinical applications.

### 2.2.6 Pulsed Electric Field Treatment

Another emerging inactivation technology in recent decades is the PEF treatment. The phenomenon of disruption of microbial membrane by external electric field was firstly described in the early 20$^{th}$ century, [5]. But it wasn't until the 1960's that the lethal effect of pulsed electric field on microorganisms was found and systematically investigated, [2-4]. When microbial cell is subjected to external electric field, pores are formed in the membrane due to the large induced trans-membrane potential, which is called electroporation process, [5]. If this trans-membrane potential is greater than a critical value (~ 1V), the electroporation process becomes irreversible and results in cell death. As a non-thermal microorganism processing technology, PEF treatment has attracted great research interest and is being developed rapidly since then.

During the past few decades, the PEF treatment technology has been employed in various applications. The most intensively studied PEF application is food preservation, [111-116]. PEF process is capable for inactivating bacteria and other microorganisms without significant thermal effects, which allows the food to be processed without losing its flavors, nutrients and vitamins. The other type of widely studied PEF application is electro-manipulation of cells, [5, 117-122]. Sub-lethal

membrane disruption can be induced to the microorganism cells by the PEF process, which allows several electro-manipulation applications to be possible. These applications include electropermeabilization (electroinjection), [117-120], which allows soluble materials to be injected into the cells; and electrofusion, [120-122], which allows the hybrids or formation of giant cell from the melting of individual cells. Most recently, researches have also been conducted to investigate the feasibility of extracting valuable lipids from microorganism cells, such as microalgae, using PEF treatment [67-71].

As the technology being studied in the present research project, the technical fundamentals of the PEF technology, the inactivation mechanisms, and recent investigations of the effects of different aspects of this technology will be discussed in details in Section 2.4 and Section 2.5.

## 2.3 Microorganisms Used in the Study

One of the microorganisms used in the present PEF study was cyanobacteria *Arthrospira platensis*. *A. platensis* are in the family of *Microcoleaceae*, phylum of *Cyanobacteria* and kingdom of *Eubacteria* [123]. *A. platensis* are also called *Spirulina platensis* due to the spiral shape of the individual cells, as can be seen in Figure II.4. Like other cyanobacteria, *A. platensis* are photosynthetic and aquatic. As a result, *A. platensis* are often called 'filamentous blue-green algae', [124-126]. However, *A. platensis* are not really microalgae as they are prokaryotic microorganisms and the microalgae are eukaryotic microorganisms. *A. platensis* naturally occur in rivers and lakes with high salt content in the subtropical and tropical regions, [124]. *A. platensis* are rich in proteins and fatty acids [127-130] and can be used in medical and food applications. It was also reported that, similar to microalgae, lipid content in *A. platensis* cells is high and could potentially be used as a source of bio-fuel production [1, 130]. Being prokaryotes, the cell structure of the *A. platensis* is simpler as compared to microalgae cells, which suggests *A. platensis* are potentially more likely to be lysed by the PEF treatment. As a comparison, studies of several types of microalgae treated by the PEF process indicated that direct

lysis of the microalgae cells was difficult to achieve, [67, 68, 70, and 71]. Therefore, *A. platensis* has been chosen for treatment by the PEF impulses in the present study.

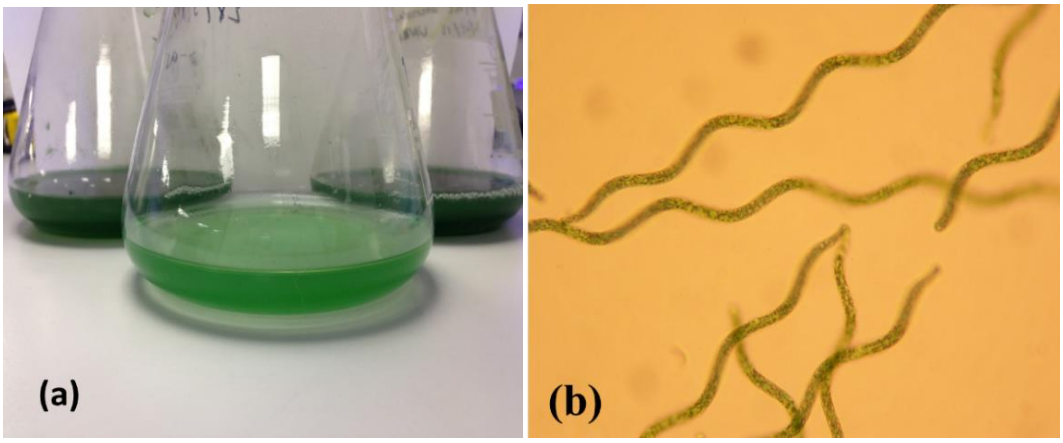


**Figure II.4** (a) *A. platensis* in the growth medium. (b) *A. platensis* cells under microscope (×400 magnification).

The other microorganism used in the present study was yeast *Saccharomyces cerevisiae* (MUCL 28749), which were obtained from The Belgian Co-ordinated Collections of Microorganisms. The species *S. cerevisiae* are in the family of *Saccharomycetaceae*, phylum of *Ascomycota* and kingdom of *Fungi* [131]. *S. cerevisiae* are the most commonly used microorganism in the fermentation process since ancient time [38, 39] and are widely used in winemaking, brewing and baking industry [40]. The shape of *S. cerevisiae* cell is usually spherical or ovoid; *S. cerevisiae* cells have a diameter of 5-10 µm [132]. The reason for choosing *S. cerevisiae* as one of the microorganisms for PEF treatment in the present study is that *S. cerevisiae* are one of the model organisms used in molecular biology studies. As one of the most representative organisms, the culturing and statistical analysis procedures for *S. cerevisiae* are well established, which can be used to determine the PEF treatment performance accurately. In addition, the *S. cerevisiae* cells have rich lipid content similar to the microalgae, [133], which could also be a potential source of bio-fuel production [134-135]. Therefore it is worthwhile to investigate how PEF acts on these species.

## 2.4 Pulsed Power Technology

The technology which underpins the PEF treatment is the pulsed power technology. The purpose of the pulsed power system is to deliver a certain amount of power into a load during a short period of time (impulse). Fundamentally, this is achieved by two steps. The first step is to accumulate the energy into a storage device, which is normally a capacitor, an inductor, or a transmission line, over a relatively long period of time. The second step is to release the energy stored in the storage device into the load by a trigger device, which is normally a high voltage switch, over a relatively short period of time. In this section, the key aspects of the pulsed power technology, such as the pulse generating circuit, the transmission line based pulse forming network and spark-gap high voltage switch, will be discussed. Apart from PEF treatment, other applications based on pulsed power technology will also be introduced briefly in this section.

### 2.4.1 Capacitive Pulse Generating Circuit

Electronic circuits, which are consisted of mainly *RLC* components, are widely used to generate high voltage pulse. These circuits can be broadly categorised into two types, either capacitive or inductive, according to their energy storage device, [136]. In general, capacitive pulse generating circuit is more frequently employed in pulsed power system.

In a capacitive pulse generating circuit, charging capacitor is served as the energy storage device. Figure II.5 shows the schematic diagram of a basic capacitive pulse generating circuit and the typical load (ideal resistive load) voltage curve produced by this circuit.

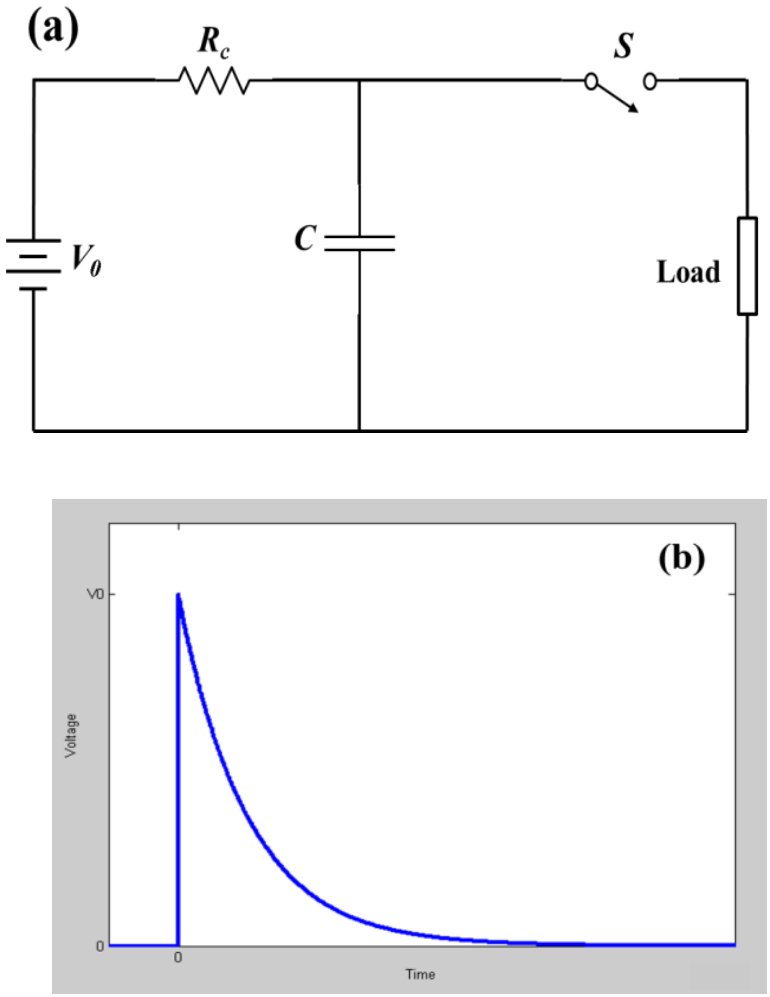


**Figure II.5** (a) Schematic diagram of a simple capacitive pulse generating circuit; (b) Typical load voltage curve produced by this circuit assuming ideal resistive load.

During the charging process, the high voltage switch *S* remains open and the charging capacitor *C* is charged to the supply voltage $V_0$ through the charging resistor $R_c$. The charging resistor limits the charging current during this process. The energy is stored in the charging capacitor in the form of electrical energy and this energy in Joules can be expressed as:

$$E = \frac{C \cdot V_0^2}{2} \tag{II.1}$$

where *C* is the capacitance of the charging capacitor and $V_0$ is the charging voltage. The closing of the high voltage switch triggers the second step, in which the energy

stored in the charging capacitor is delivered to the load. In an ideal condition, the magnitude of the voltage across the load rises to the charging voltage instantaneously, as demonstrated in Figure II.5(b). However, in any practical pulse generating circuit, the rise time of the impulse is increased due to the presence of parasitic inductances of the capacitor, switch, load, and the connecting cables/wires. After reaching the charging voltage, the voltage across the load decays exponentially assuming an ideal resistive load, as demonstrated in Figure II.5(b). The decay process is governed by the resistance of the load and the capacitance of the charging capacitor and can be expressed as Equation II.2.

$$v(t) = V_0 \cdot e^{-\frac{t}{RC}} \tag{II.2}$$

where *v(t)* is the transient voltage across the load, $V_0$ is the charging voltage, *t* is the time, *R* is the resistance of the ideal resistive load and *C* is the capacitance of the charging capacitor.

It can be seen from Equation II.2 that, in such capacitive pulse generating circuit, the maximum voltage across the load is limited by the charging voltage, i.e. the magnitude of the high voltage supply. Normally, the majority of commercially available DC high voltage sources can provide voltage up to 100 kV. For pulsed power applications which require voltage of many tens or hundreds of kV, multi-stages Marx generator is commonly used, [137-138]. Invented by Marx in 1923, [139], Marx generator is a multi-stages capacitive voltage multiplier. Figure II.6 demonstrates the operation of an inverting Marx generator with four stages.

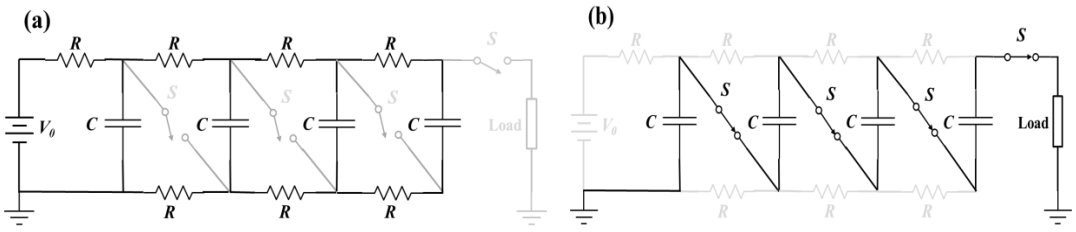


**Figure II.6** Operation of a four stages Marx generator: (a) Charging state; (b) Discharging state.

As can be seen in Figure II.6(a), the switches are open in the charging state and the charging capacitors are connected in parallel. The voltage across each capacitor equals to the charging voltage from the supply, $V_0$. In the discharging state, the switches are closed and the charging capacitors are connected in series, as shown in Figure II.6(b). As a result, voltage with an opposite polarity and with magnitude of $N \cdot V_0$ is developed across the load, where $N$ is the number of charging capacitors (number of stages). Therefore, much higher voltage can be achieved from a pulse generating circuit using a relatively low voltage supply.

In the present study, a pulse power system was designed using the capacitive pulse generating circuit to generate high voltage impulses with smooth and oscillating exponential waveshapes. The design of this pulse power system will be presented in Section 6.4.

### 2.4.2 Inductive Pulse Generating Circuit

Apart from the capacitive pulse generating circuit, the other type of circuit used in pulsed power system is the inductive pulse generating circuit. In an inductive pulse generating circuit, the inductor is served as the energy storage device. Figure II.7 shows the schematic diagram of a basic inductive pulse generating circuit and the typical load (ideal resistive load) voltage curve produced by this circuit.

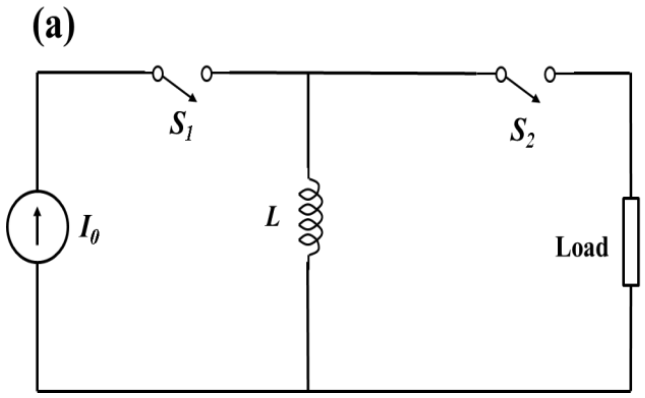

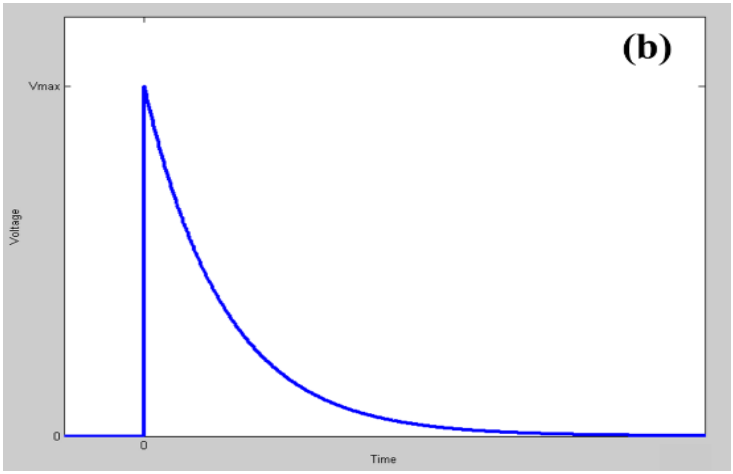


**Figure II.7** (a) Schematic diagram of a simple inductive pulse generating circuit; (b) Typical load voltage curve produced by this circuit assuming ideal resistive load.

Initially, the high voltage switch $S_1$ is closed, $S_2$ is open and a DC current $I_0$ flows through the inductor $L$, which stores the energy in the inductor. Unlike the capacitive pulse generating circuit, the energy stored in the inductor is in two forms: electrical energy and magnetic energy. It was demonstrated in [140] that the stored magnetic energy could be two orders of magnitude larger than the stored electrical energy in a simple inductive pulse generating circuit. The total energy stored in the inductor Joules can be expressed as:

$$E = \frac{L \cdot I_0^2}{2} \tag{II.3}$$

where $L$ is the inductance of the inductor and $I_0$ is the DC current flow through the inductor. The opening of the high voltage switch $S_1$ and closing of $S_2$ trigger the second step, in which the energy stored in the inductor is delivered to the load. In an ideal condition, the magnitude of the voltage across the load rises to the maximum voltage instantaneously, as demonstrated in Figure II.7(b). However, in any practical pulse generating circuit, the rise time of the resulting pulse is increased due to the presence of parasitic inductances of the switch, load, and the connecting cables/wires. The maximum voltage developed across the load is defined by Equation II.4.

$$V_{max} = L\frac{di}{dt} \tag{II.4}$$

where $L$ is the inductance of the inductor, $di/dt$ is the rate of change of the current through the inductor. Therefore, high voltage switch with fast closing time and high $di/dt$ can produce higher peak voltage across the load. After reaching the charging voltage, the voltage across the load decays exponentially assuming an ideal resistive load, as demonstrated in Figure II.7(b). The decay process is governed by the resistance of the load and the inductance of the inductor and can be expressed as Equation II.5.

$$v(t) = V_{max} \cdot e^{-\frac{tR}{L}} \tag{II.5}$$

where $v(t)$ is the transient voltage across the load, $V_{max}$ is the initial peak voltage, $t$ is the time, $R$ is the resistance of the ideal resistive load and $L$ is the inductance of the inductor.

Another example of the inductive pulse generating circuit is the pulse generator using semiconductor opening switch (SOS), as described in [140-141]. The SOS is able to switch high-density current in nanoseconds, which allows high voltage to be generated from inductive storage device. The SOS pulse generator constructed in [141] can produce impulse with pulse voltages 250 kV and has the potential to generate pulse with voltage up to 5 MV. Figure II.8 shows a schematic representation of the SOS pulse generator. In this pulse generator, both switches ($S_1$ and $S_2$) are saturable core inductors. $S_1$ is open initially until the core saturates, which closes the switch and allows $C_1$ discharging into $C_2$ through the forward biased SOS. When $S_2$ closes, the current through the SOS reverses rapidly and eventually opens the SOS. The power stored in $L$ from $C_2$ discharge is then diverted to the load.

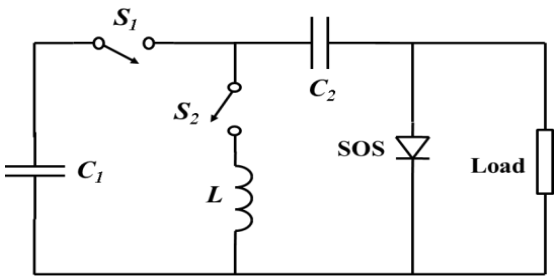


**Figure II.8** Schematic representation of a SOS pulse generator.

### 2.4.3 Combined *RLC* Pulse Generating Circuit

As demonstrated in Section 2.4.1 and Section 2.4.2, typical high voltage impulses generated by both capacitive and inductive pulse generating circuits have an exponential decaying waveshape. However, the waveforms of the impulse could have an impact on the efficiency and energy consumption of the PEF process, as demonstrated in [7]. Different combinations of *R*, *L* and *C* components in the pulse generating circuit allow some flexibility in the forming of the resulting pulse profile. It was shown in [7] that high voltage impulses with square and oscillatory decaying waveshapes could be generated by different combinations of *RLC* components in the pulse generating circuit. Figure II.9 shows the schematic circuit diagram of the square impulse generating circuit developed in [7] and the practical voltage waveform of this square impulse. Figure II.10 shows the schematic circuit diagram of the oscillatory decaying impulse generating circuit developed in [7] and the practical voltage waveform of this oscillatory decaying impulse.

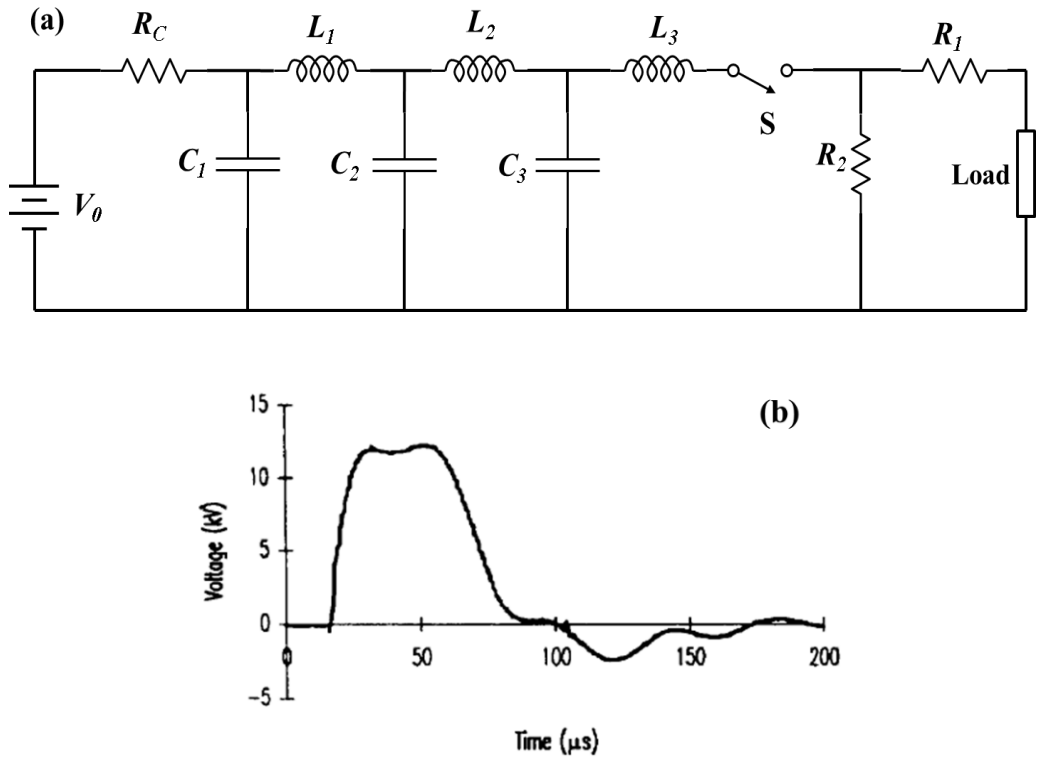


**Figure II.9** (a) Schematic circuit diagram of the square impulse generating circuit, adopted from [7]; (b) Practical voltage waveform of this square impulse, figure taken from [7].

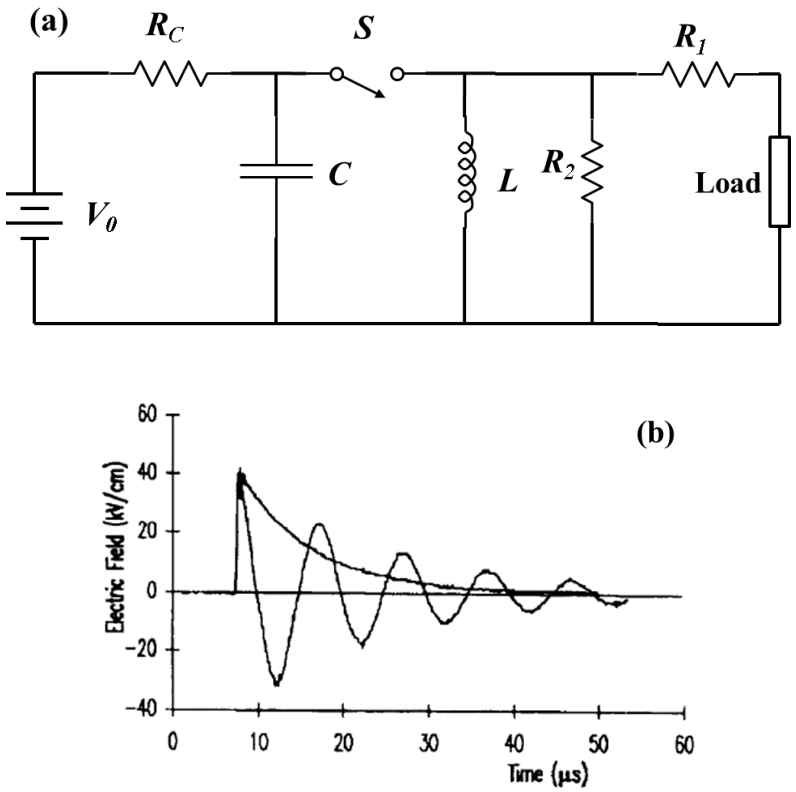


**Figure II.10** (a) Schematic circuit diagram of the oscillatory decaying impulse generating circuit, adopted from [7]; (b) Practical voltage waveform of this oscillatory decaying impulse together with an exponential decaying waveform, figure taken from [7].

### 2.4.4 Transmission Line Based Pulse Forming Network

Instead of using the capacitor or inductor as the energy storage device, a length of transmission line or a transmission line network can be served as the energy storage device in a pulsed power system. The pulse forming line (PFL) or pulse forming network (PFN) based on transmission line is by far the most common technology used in the pulsed power system for the generation of short square impulse. Generation of square impulse can be achieved using a *RLC* pulse generating circuit, as demonstrated in Section 2.4.3, which is relatively simple in terms of circuit construction and inexpensive in cost. However, square impulse generated by simple *RLC* circuit does not have a stable peak, as can be seen in Figure II.9(b), and significant number of *LC* units need to be added in order to achieve a 'flat' peak. On the other hand, transmission line based PFL or PFN can produce square impulse with

stable peak and precise pulse duration. Therefore, despite the relatively high cost and complicate construction procedure, transmission line based PFNs are widely selected for the pulsed power application requiring square impulse.

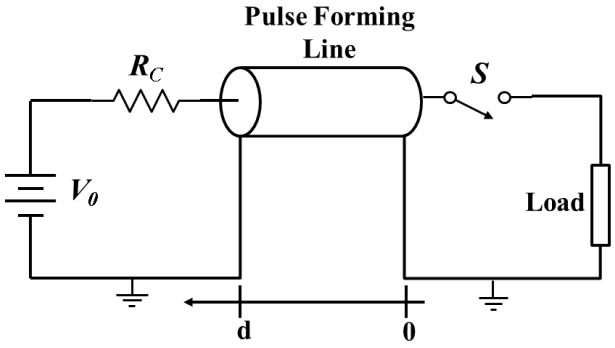


**Figure II.11** Schematic circuit diagram of a simple pulse forming line (PFL).

Figure II.11 shows a schematic circuit diagram of a simple PFL with the length of the transmission line equals to *d*. For a matched load, which the impedance of the load equals to the impedance of the PFL, a voltage of $0.5\ V_0$ will appear across the load when the high voltage switch *S* is closed. At the same time, a pulse with amplitude of $-0.5\ V_0$ propagates down the transmission line toward *d*. When this pulse reaches the high impedance (charging resistor and the HV supply) at *d*, it will be fully reflected and propagates back towards the load. When the reflected $-0.5\ V_0$ pulse reaches the load, the transmission line is discharged completely.

The result of this process is a constant voltage with amplitude of $0.5\ V_0$ appears across the load over a period of time which equals to the total propagation time of the $-0.5\ V_0$ pulse. The total propagation time, which is effectively the pulse duration of the resulting square impulse, can be determined by Equation II.6.

$$T = \frac{2 \cdot d\sqrt{\mu_r \varepsilon_r}}{c} \tag{II.6}$$

where $\varepsilon_r$ is the relative permittivity of the transmission line, $\mu_r$ is the relative permeability of the transmission line, *d* is the length of the transmission line, and *c* is

the speed of light. In an ideal situation, the square impulse generated by this PFL will rise and fall instantaneously. However, in any practical pulse forming line or pulse forming network, the rise time and the fall time of the generated square impulse will be increased and determined by the parasitic inductances in the switch, transmission lines, connecting cables/wires and the load.

It can be seen from the above analysis that, the magnitude of the square impulse generated by a single pulse forming transmission line is only half of the charging voltage from the HV power supply. Improvement in the voltage magnitude of the square impulse generated by transmission line based generator had been made available by Blumlein in 1941, [142]. Figure II.12 shows the schematic circuit diagram of a Blumlein pulse generator.

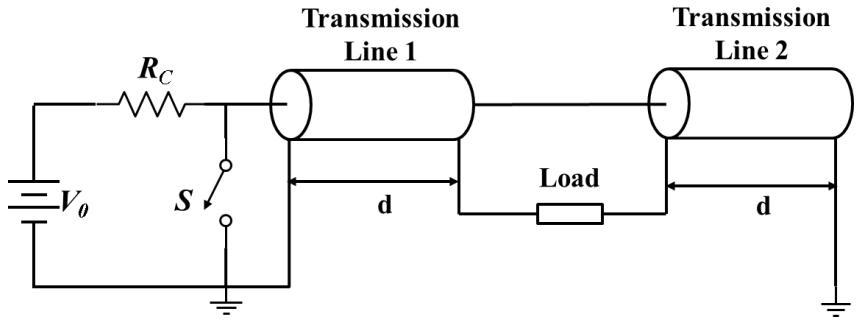


**Figure II.12** Schematic circuit diagram of a Blumlein pulse generator.

As can be seen from Figure II.12, in a Blumlein pulse generator, the load is connected in series between two transmission lines with identical length *d*. Consider a matched load in this configuration, the impedance of the load is twice of the impedance of each transmission line. When the HV switch *S* is closed, a pulse with voltage magnitude of $V_0$ is triggered and travels through Line 1 toward the load. Once this pulse reaches the load, it is half reflected back to Line 1 and half transmitted into Line 2, resulting in two symmetrical voltage pulses with 0.5 $V_0$ magnitudes but opposite polarity, which propagate away from the load. As a result, a voltage with magnitude of $0.5V_0 - (-0.5V_0) = V_0$ appears across the load. These two voltage pulses then reach the end of each transmission line simultaneously and

will be reflected towards the load. Once both voltage pulses reach the load, the transmission lines are discharged completely.

The result of this process is a constant voltage with magnitude of $V_0$ appears across the load over a period of time which equals to the total propagation time of the two ± 0.5 $V_0$ pulses. The total propagation time, which is effectively the pulse duration of the resulting square impulse, can also be determined by Equation II.5. The significance of this Blumlein design is that the voltage magnitude of the resulting square impulse is doubled as compared to the single PFL when using HV supply with the same charging voltage. In addition, the other advantage of the Blumlein design is that the HV switch can now be grounded. As a comparison, the HV switch in a single PFL configuration is located on the high voltage charging line, as can be seen in Figure II.11, which complicates the technical requirement for the triggering electronics.

Since the invention of Blumlein generator, efforts have been made to improve the performance and practical aspects of the Blumlein transmission line generator, [143-145]. For example, a nominal voltage gain of 4 has been achieved using a stacked-Blumlein generator developed in [143] and a pulse repetition rate of 1.1 MHz has been achieved using the Blumlein configuration designed in [145].

Apart from Blumlein configuration, other configurations of the transmission line based PFN have also been developed and used in variety of pulsed power applications, [146-152]. Marx generators based on transmission line networks rather than *RC* components were used in the pulsed power studies reported in [146-148]. In the pulsed power studies reported in [149-150], the *RC* based Marx generators were used to drive the PFL and PFN. Another type of transmission line based generator, the self-matched generator, was also described and developed in [151-152], where signal reflection can be eliminated regardless of the load impedance.

### 2.4.5 Spark-Gap Switches

As demonstrated in Section 2.4.1-2.4.4, one of the key components in the pulsed power system is the high voltage switch. In most of the pulsed power system, the forming and delivery of the high voltage impulse is triggered by the actions of the high voltage switches. Therefore, the performance of the HV switch can significantly influence the overall performance of the pulse generator.

In general, there are few critical requirements for the selection of switch in pulsed power system. First and foremost, the switch must be able to withstand the high voltage and the high power during the fast closure process. Besides, the switch should be able to recover from the closed state in a relatively fast time in order to allow the re-application of the charging voltage. This is one of the common requirements in pulsed power applications where fast pulse repetition rate is needed. In addition, the 'jitter', which is the statistical variation in the delay times between impulses, should be low in order to achieve a stable repetition rate.

Varity of the high voltage switch have been designed and developed for different pulsed power applications for decades. All these HV switches can be broadly divided into three categories: spark-gap discharge switch, surface discharge switch and semiconductor switch, [153]. Among the three types of switch, the spark-gap discharge switch is the most intensively used switch in variety of pulsed power applications. The spark-gap switches are capable of operating with: high voltage (100's V-100's kV), high current (kA), high *dV/dt*, high *dI/dt*, and can provide fast closing time (10's of ns) with low jitter (few ns), [154]. In the present study, the two high voltage switches used in the pulsed power system are both spark-gap switch. Therefore, a review of this particular type of switch will be presented in this section.

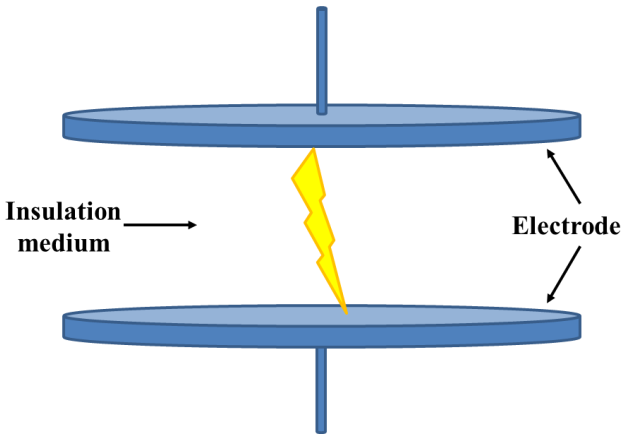


**Figure II.13** Basic structure of a spark-gap discharge high voltage switch.

As can be seen in Figure II.13, the basic structure of a spark-gap switch is two electrodes separated by an insulation medium, which is normally gas or liquid. When a discharge (spark) is triggered and develops between the two electrodes through the insulator, the switch closes. Spark-gap switches can be sub-divided by the triggering mechanisms, which include self-breakdown, trigatron triggering, field distortion triggering, corona stabilised triggering, ultraviolet triggering, laser triggering and electron beam triggering, [136]. A self-breakdown spark-gap switch and a corona stabilised spark-gap switch are used in the pulsed power systems in the present study. The triggering mechanisms of these two types of spark-gap switches will be discussed in the following sections.

### 2.4.5.1 Self-Breakdown Spark-Gap Switch

Self-breakdown or self-closing switches, which is robust, reliable and cost-effective, is the most basic and popular spark-gap discharge switch in pulsed power industry, [140]. The closure of the self-breakdown switch is triggered when the voltage across the electrodes exceeds the threshold voltage for dielectric breakdown between the switch electrodes. In order to operate the self-breakdown switch with different closing criteria, as required in many of the pulsed power applications, this threshold voltage should be adjustable.

In the case of gas insulation, the threshold breakdown voltage is governed by Paschen's law, which the breakdown voltage of gas is a function of the product of gas pressure and gap length ($p \times d$). Therefore, change of the threshold voltage of a self-breakdown switch can be achieved by either changing the inter-electrode distance or changing the gas pressure in between the two electrodes. To change the inter-electrode distance, adjustable or moving electrode topology is required. However, as reported in [155], the moving electrode topology makes the switch more complex and less reliable. Therefore, in pulsed power industry, majority of the self-breakdown switches are designed to be fixed electrode and pneumatically operated switch, which the threshold voltage is controlled by changing the gas pressure in the switch.

Self-breakdown switches are extensively used in the high voltage generators such as the Marx generators. In the present study, an adjustable self-breakdown spark-gap switch was used in one of the pulsed power system for high voltage impulse generation. This switch and the other components of the pulsed power system will be presented in Section 6.4.

#### 2.4.5.2 Corona Stabilised Spark-Gap Switch

One of the limitations of the spark-gap switch is its relatively poor repetition capability. Fast repetition of a spark-gap switch is limited by the slow recovery rate of the insulating gas medium. This is caused by the presence of high current density discharge channel during the switch closure process, which results in strongly heated gas, strongly heated metal and slowly deionizing plasma at the electrodes. Several technologies have been developed to improve the repetition capability of the spark-gap switch, [136]. One method is to force the gas to flow at an optimal velocity in the switch, which removes the hot plasma. Generator using this switch design can operate at a pulse repetition rate of $10^2$-$10^3$ Hz. The other approach is to use spark-gaps with multi-avalanche volume discharge, which reduces the current density significantly. Generator using this switch design can achieve $10^4$ Hz pulse repetition rate.

Into the 2000s, another approach to improve the repetition capability of spark-gap switch was proposed in [156-157]. This is achieved by introducing highly non-uniform field inside the switch, which allows the corona stabilisation to occur. Introduction of the highly non-uniform field can be achieved by different electrode topologies [156-159] or by intentional sharp edged electrodes [160]. Figure II.14 shows a schematic diagram of a corona stabilised switch with intentional sharp edged disc electrodes.

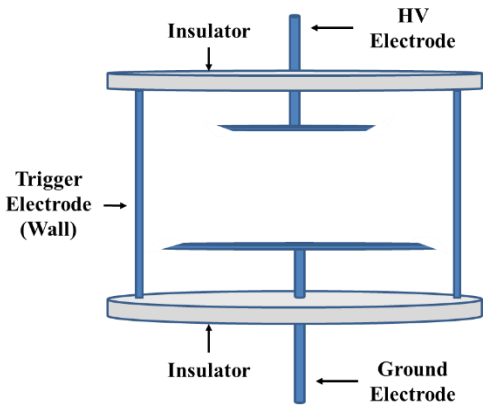


**Figure II.14** Schematic diagram of a corona stabilised switch with intentional sharp edged disc electrodes.

As can be seen in Figure II.14, the edges of both HV and ground electrodes are sharpen in order to create non-uniform field distribution when the electrodes are energised. Due to this non-uniform field, electron produced in the high-field region is attached by the electronegative gas (such as $SF_6$) inside the switch and space charge is accumulated in the low-field region. Above a critical voltage, which is considerably lower than the main gap breakdown voltage, corona discharge occurs at the edge of the ground electrode. However, the space charge accumulated in the low-field region shields the HV electrode and prevents the breakdown. By adjusting the pressure of the gas, this pre-trigger state can be reached at the required voltage. Application of the trigger pulse to the trigger electrode (the chamber wall) creates overvoltage in the low field region resulting in a complete discharge and the switch is closed. After closure, the switch returns back to the pre-trigger state and therefore allows fast repetitive triggering.

In the present study, a corona stabilised spark-gap switch was used in one of the pulsed power system. This switch and the other components of this pulsed power system will be introduced in Section 4.3.

### 2.4.6 Environmental and Biological Applications of Pulsed Power Technology

The rapid development and advancement of the pulsed power technology in the past decades has enabled the optimisation of established and creation of variety applications in different industry areas: such as high power microwave source; lighting and EMP simulation; material processing; military application; and, as the focus of the present study, biological applications, [161].

Apart from the pulsed electric field treatment, other pulsed power technologies are also widely used for biological applications: such as gas discharge; water discharge; and pulsed light treatment. Pulsed power system can be used to generate discharge in air. Pulsed discharges in air are used for sterilisation of bacteria such as *Escherichia coli* and *S. typhimurium* in order to achieve air or surface decontamination, [162-163].

Water discharge can be sub-divided into two categories: corona discharge and arc discharge. Corona discharge can be produced in a non-uniform electric field, as described in Section 2.4.5.2. Application of pulsed corona discharge in liquid can generate several antimicrobial sources: free radicals, electrons, and oxidative species, [164]. On the other hand, arc discharges are produced by introducing completely dielectric breakdown in the treated fluid. In addition to the antimicrobial effects produced by corona discharge, the arc discharges generate shockwave and produce toxic metallic ions in the fluid, [165-166]. However, both types of water discharge treatments are not suitable for food processing, as toxic compounds are generated during the discharge process.

The development of the pulsed power technology also allows the evolution of some traditional microorganism inactivation technology, such as the UV inactivation

described in Section 2.2.3. Traditional UV inactivation is a continuous treatment which requires relatively long treatment duration and is limited in the effectiveness of the inactivation performance, [167]. On the other hand, the pulsed UV system can utilise high peak power for faster inactivation and spectral range optimisation, [147, 168].

## 2.5 Pulsed Electric Field Inactivation

As briefly introduced in Section 2.2.6, PEF treatment has attracted significant research interest and has been developing rapidly since it was first described in the 1960s. As the technology being investigated in the present study, a critical and detailed review of all aspects of the PEF technology is necessary and important. In this section, the main mechanisms of microbial inactivation in the PEF process will be discussed. Important PEF studies over the past few decades of PEF treatment of yeast and microalgae will be reviewed. Some of the famous PEF chamber designs will be introduced as well. Recent investigations into the effects of different aspects of the PEF technology will also be discussed in details in this section.

### 2.5.1 Mechanisms of PEF Inactivation

Lethal effect of pulsed electric field on microorganisms was first systematically investigated and described by Sale and Hamilton in 1967, [2-4]. Subsequent studies have been conducted continuously to investigate the exact inactivation mechanism of the PEF process. It is generally believed that the main inactivation mechanism is the irreversible electroporation in the cell membrane.

When microbial cell is exposed to an external electric field, a larger membrane potential is developed at the two poles of the membrane, [169]. When this induced membrane potential reaches a critical value, a dielectric breakdown occurs on the membrane and results membrane pores to be formed in the membrane. The formation of the membrane pores was firstly described in [170] and was firstly visualised using transmission electron microscope in [171]. This phenomenon is now widely accepted and is called electroporation.

The critical membrane breakdown voltage has been found to be ~ 1V, [5]. It was showed in [172] that, at this critical voltage, if the external electric field is applied as a short pulse (<1 μs), the resulting membrane pores are resealable and no permanent damage is induced to the cell. In certain conditions, which the time of exposure to the external electric field is large (> 1 μs) or the induced membrane voltage is high (>1 V), the electroporation process becomes irreversible, which introduces permanent damage to the cell and results in cell death.

Numerous efforts have been made to establish the mathematic relationship between the external field strength and the induced membrane voltage. The most famous expression is the Schwan equation, which was developed by Schwan in 1957, [9]. A spherical model of the cell was considered in [9], as demonstrated in Figure II.15, the membrane of the cell was assumed to be non-conductive. The Schwan equation is expressed as:

$$\Delta\varphi = \frac{3}{2} ER \cos\alpha \tag{II.7}$$

where $\Delta\varphi$ is the induced membrane potential, $E$ is the external electric field, $R$ is the radius of the cell and $\alpha$ is the angle between the membrane site and the field direction. It can be seen from the Schwan equation that the induced membrane potential is linearly correlated to the magnitude of external field strength and the diameter of the microbial cell. The voltage developed on the membrane increases as the applied electric field increases and higher membrane potential will be developed on a larger cell. It can also be learned from Equation II.7 that the membrane potential varies along the surface of the cell and depends on the angle between the particular position of the membrane and the field direction. Therefore, it is easy to see that maximum membrane potential is developed at the 'poles' of the cell (closest to the electrode), where $\cos\alpha = 1$.

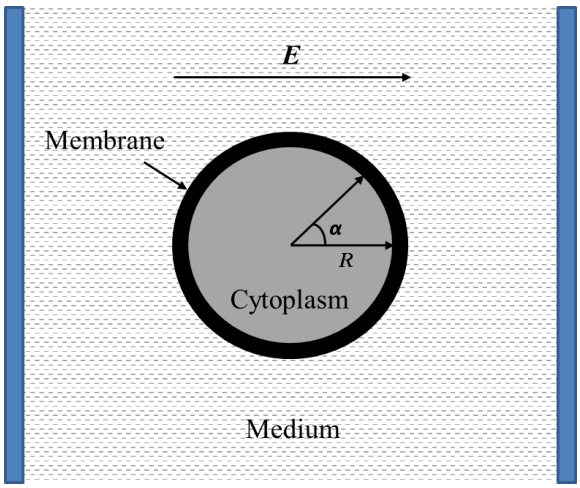


**Figure II.15** Demonstration of the cell model used in [9].

After Schwan, others continued to develop the mathematic model based on the principle and approach developed by him in order to consider the cell's physical and electrical properties more precisely. In [5, 173], the conductivity of the membrane and the membrane thickness were taken into account and the resting membrane potential difference was also considered in [5]. Effects of surface conductance and deformational forces on the membrane permeabilisation were taken into account in [174]. While in [175-176], development of the membrane potential in an ellipsoidal cell was evaluated. Recently, Timoshkin *et al* presented the development of the transient response of the membrane potential to an external electric field between a different electrodes topology, in which the metal electrodes are covered by a layer of high permittivity ceramic, [6].

Development of these mathematic descriptions of the membrane potential provides a good reference in the designing of PEF treatment system for specific applications. In the present study, the transient model described in [6] acts as an inspiration for the design of a novel non-conductive PEF test cell, and will be introduced and analysed in Section 3.2.

Apart from the electroporation process, other electrical and electro-chemical activities take place during the PEF process. For example, metallic ions are released from the electrode into the liquid suspension due to the electro-chemical reaction

when voltage is applied to the metallic electrodes. Studies have shown that the presence of the metallic ions has an impact on the inactivation of microorganisms, which will be discussed in Section 2.5.4.3. The other major electrical activity during the PEF process is the ionic conduction. When liquid suspension with relatively high conductivity (few S/m) is placed between the metallic electrodes, ionic conduction current, which can be as high as few hundreds of Amperes, will flow through the liquid suspension, [7, 177]. However, the effect of ionic conduction in the inactivation of microorganism during PEF process has never been separately investigated by the time when the present study started. Therefore, the inactivation mechanism of the PEF process cannot be regarded solely as the irreversible electroporation process.

### 2.5.2 Design of PEF Chambers

PEF chamber is one of the vital components in the PEF treatment system. The general purpose of the PEF chamber is to house the liquid suspension to be treated and to deliver high voltage impulses to the suspension. In some cases, the design of the PEF chamber also implements the cooling requirement in order to maintain a relatively low temperature for the PEF system. Basically, a PEF chamber is composed of two electrodes held in position by insulating material, which forms a treatment region containing the liquid suspension.

The PEF treatment process can be divided into the batch or continuous mode. In the batch processing, a static PEF chamber is used. In this case, a specific amount of the fluid are treated as a unit governed by the volume of the treatment region of the PEF chamber. In the PEF process with the continuous mode, the fluid to be treated is flowing into and emitted from the continuous PEF chamber at a certain steady flow rate. Due to their small treatment volume, static PEF chambers are mainly suitable for laboratory use for investigating the effects of relevant factors on the PEF treatment process. On the other hand, continuous PEF chambers are more efficient for the large scale PEF operation.

Over the years, various PEF chambers have been developed, constructed, manufactured and used by a number of universities, research groups and private industries for their respective PEF studies. In this section, some of the typical PEF chamber designs will be reviewed.

### 2.5.2.1 Static Chamber

A U-shaped static PEF chamber was developed and used in the first systematic PEF study conducted by Sale and Hamilton in 1967, [2-4]. As shown in Figure II.16, this PEF chamber contains two carbon electrodes supported by brass blocks, and a U-shaped polythene spacer placed between the electrodes to form the treatment region. A coolant path is hollowed out in the brass block for coolant circulation in order to control the temperature of the fluid sample. The maximum magnitude of the electric field which this PEF chamber can withstand was limited to 30 kV/cm. This limitation was due to the electrical breakdown of the air above the fluid sample.

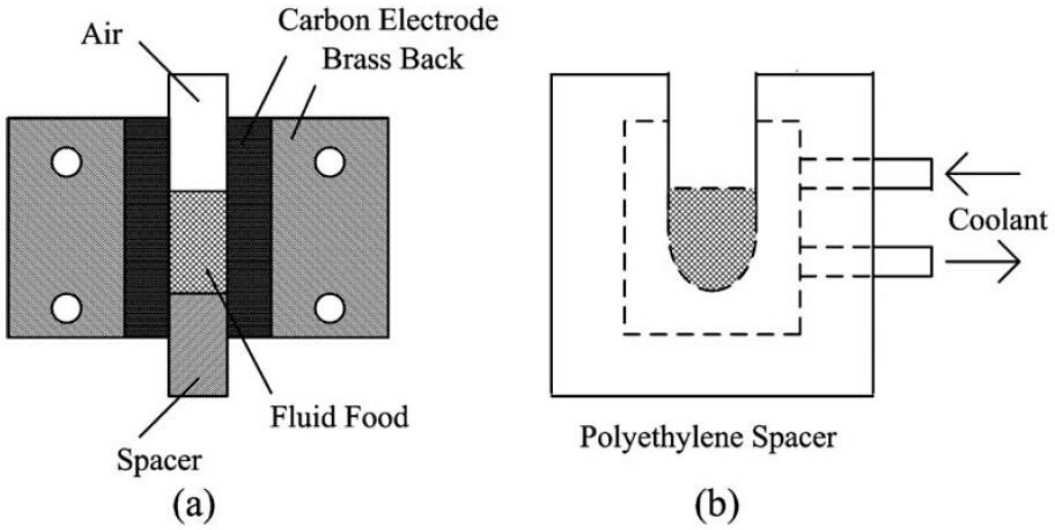


**Figure II.16** The static PEF chamber designed by Sale and Hamilton: (a) cross section view of the chamber. (b) U-shaped treatment region and coolant path. Figure taken from [178].

A similar static PEF chamber was designed by Grahl and Markl, [179], as shown in Figure II.17. This PEF chamber was consisted of two rectangular carbon-brass

electrodes which were separated by a rectangular Plexiglas frame with a thickness of 0.5 cm. The volume of the treatment region of this PEF chamber was 25 $cm^3$ (5 cm×10 cm×0.5 cm). The fluid to be treated was filled into this PEF chamber by a syringe through the filler hole at the top of the chamber. Unlike the PEF chamber designed by Sale and Hamilton, no cooling measure was taken in this chamber design. The maximum electric field strength of 30 kV/cm was used in [179] without any electrical breakdown of the air above the filler-hole.

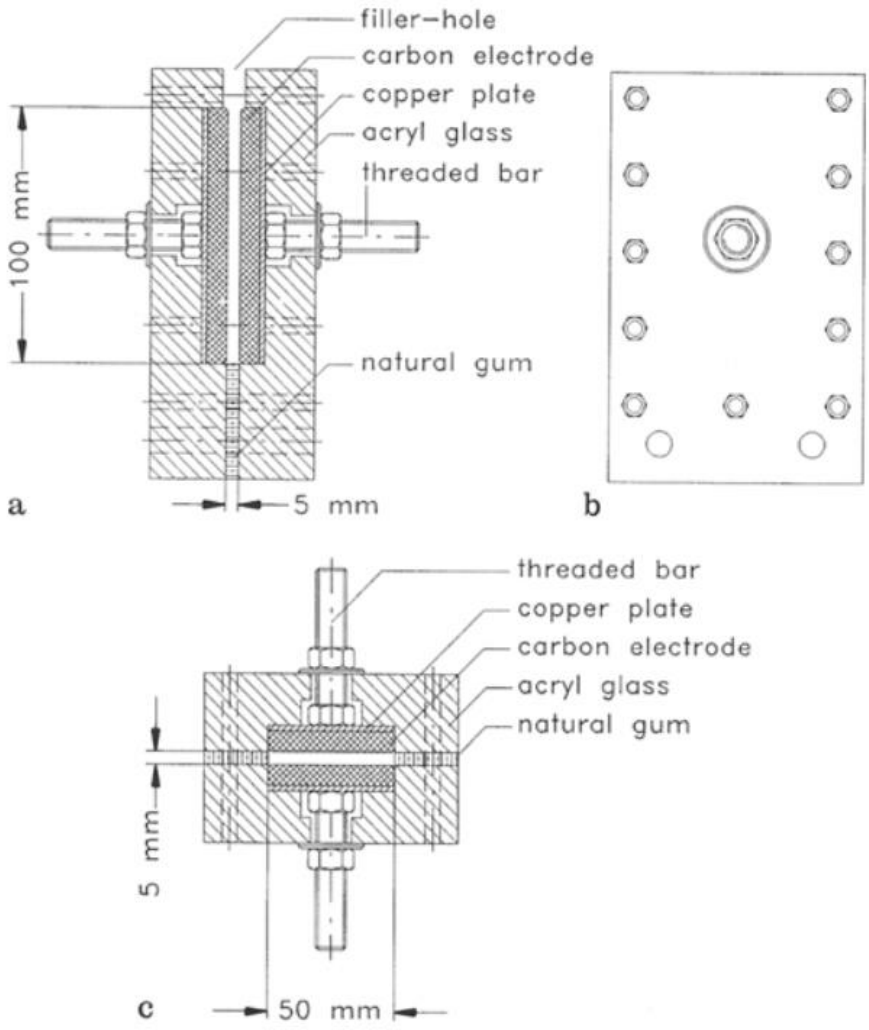


**Figure II.17** The static PEF chamber designed by Grahl and Markl: (a) longitudinal section; (b) frontal view; (c) cross-section. Figure taken from [179].

Another laboratory scale static PEF chamber was designed and patented by Dunn and Pearlman, [180], as shown in Figure II.18. This PEF chamber was consisted of two parallel-plane stainless steel electrodes and a cylindrical nylon spacer. The two electrodes were separated by the spacer and the gap between the electrodes was maintained at 5 mm. The chamber had an effective treatment volume of 39 $cm^3$ as the inner diameter of the electrodes was 10 cm. The fluid to be treated in this chamber is introduced through the small filling port on one of the electrodes. This filling port can also be used for measuring the fluid temperature during the PEF treatment process.

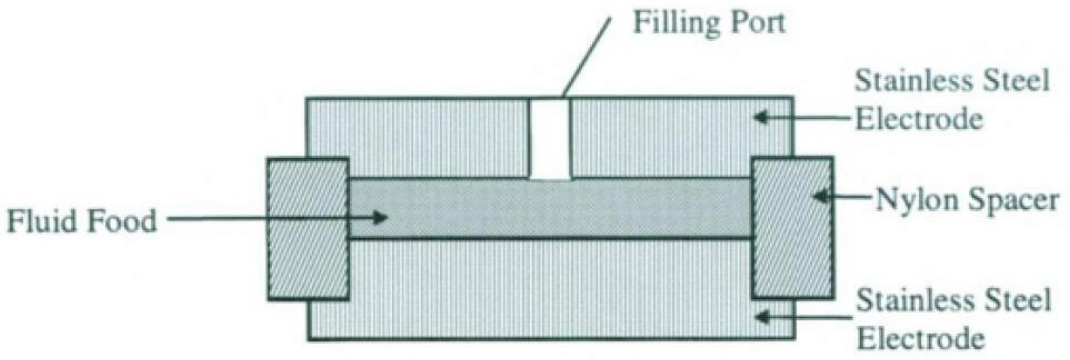


**Figure II.18** The static PEF chamber designed by Dunn and Pearlman, figure taken from [116].

The research group in Washington State University (WSU) designed and constructed a disk-shaped static PEF chamber in [7], as shown in Figure II.19. In this chamber design, two round-edged, disk-shaped, mirror surfaced stainless steel electrodes were held and separated by a polysulfone spacer. The effective area of the electrode was 27 $cm^2$ and the inter-electrode distance could be adjusted to either 0.95 cm or 0.5 cm, which gave the chamber a treatment volume of 25.7 $cm^3$ and 13.5 $cm^3$ respectively. Cooling of the PEF chamber during PEF treatment was achieved by circulating the coolant through jacket built into the electrodes. The maximum electric field strength up to 70 kV/cm could be applied to this PEF chamber.

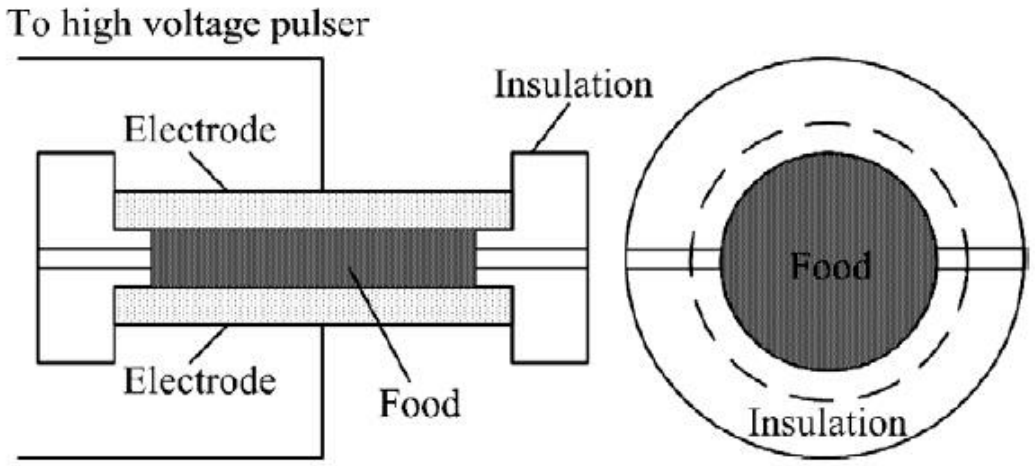


**Figure II.19** The static PEF chamber designed by the WSU research group, figure taken from [178].

Majority of the static PEF chamber designs employ the parallel-plane electrodes topology as this electrode configuration provides a uniform electric field distribution in the treatment region, which enable the vast majority of the fluid being subjected to a sufficient electrical stress. Nevertheless, static PEF chamber with other topology has also been designed. As shown in Figure II.20, a PEF chamber with wire-cylinder electrode topology was designed by Matsumoto *et al*. [181]. This static PEF chamber was consists of a cylinder aluminum electrode with inner diameter of the 20 mm and wire platinum electrode with diameter of 1 mm. The length of the chamber was 110 mm which formed a treatment region with volume of 38 $cm^3$. The maximum magnitude of the electric field used in this PEF chamber was 20 kV/cm. However, this electrode configuration resulted in an uneven field distribution: the field strength near the cylinder wall was much lower than that in the central axis of the chamber. To compensate this effect, a rotor was employed at the bottom of the chamber which introduced agitation of the fluid during the PEF process. When yeast *S. cerevisiae* was treated in this PEF chamber, 2 more $\log_{10}$ reduction in the surviving yeast population was achieved when the induced agitation was applied, [181].

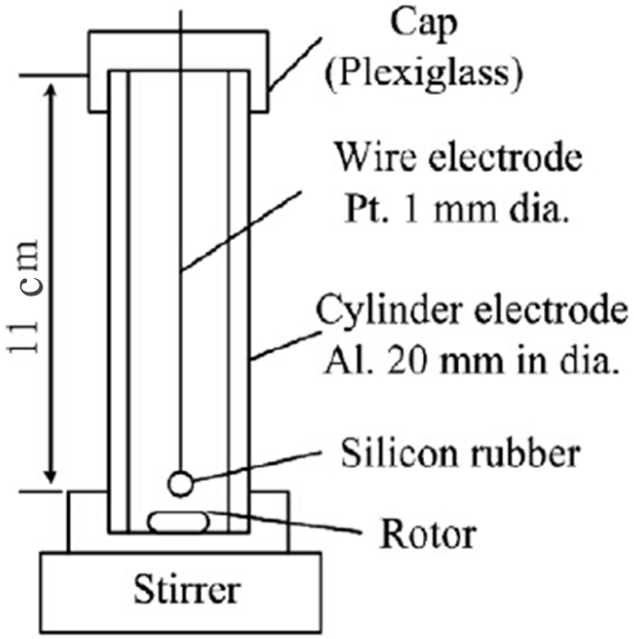


**Figure II.20** The static PEF chamber with wire-cylinder electrodes designed by Matsumoto *et al.*, figure taken from [178].

#### 2.5.2.2 Continuous Chamber

In order to scale up the PEF system and to improve PEF performance, researchers commonly modified their initial static chambers to design the continuous PEF chambers and the chambers normally share similar configuration. As shown in Figure II.21, a continuous PEF chamber designed by the research group in WSU had a similar design as their static PEF chamber (Figure II.19). This continuous-flow PEF chamber consisted of two disk-shaped stainless steel electrodes which were separated by a polysulfone spacer. The baffled flow channel was created inside the chamber to increase the total time the fluid exposed to pulsed electric field. Similar to the static PEF chamber, the cooling of the chamber was achieved by circulating coolant through the jacket built into the electrode. The operating parameters for the PEF system using this continuous chamber were: inter-electrode gap of 0.95 or 0.51 cm; chamber volume of 20 or 8 $cm^3$; electric field strength of 35 or 70 kV/cm; liquid sample flow rate of 1200 or 6 ml/min, [182-183].

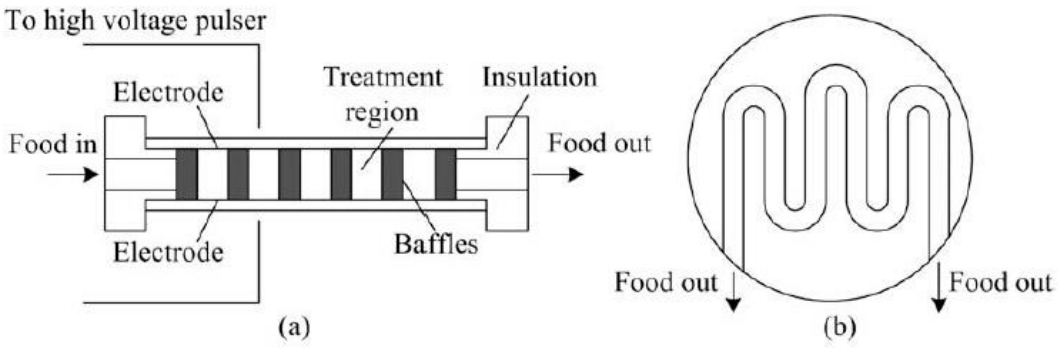


**Figure II.21** The continuous PEF chamber designed by the WSU research group: (a) cross section view; (b) top view. Figure taken from [178].

Dunn and Pearlman also adapted their static PEF chamber (Figure II.18) to design a continuous chamber, [180], as shown in Figure II.22. This design employed two parallel-plane electrodes separated by a spacer made from dielectric insulator. In this continuous PEF chamber, the fluid being treated was separated from the electrodes by ion conductive membranes. The regions between the membranes and the electrodes were filled with electrolyte solutions in order to facilitate electrical conductions. These electrolyte solutions were circulated in order to remove the products from the electrolysis process and reduce the concentration of ionic components. Another continuous PEF chamber with different topology was also designed by Dunn and Pearlman, [180], as shown in Figure II.23. In this design, the treatment region in the chamber was divided into several reservoir zones by the conical insulators and these reservoir zones were connected through the orifices created by the conical insulators. The fluid being treated in this chamber passed through each of these zones and the total treatment time was therefore increased.

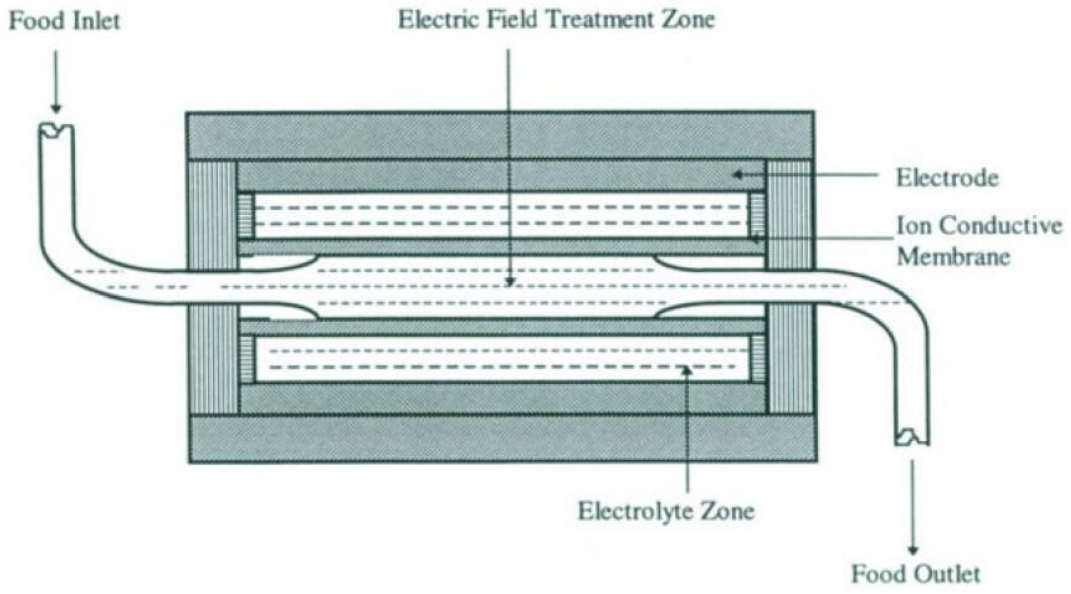


**Figure II.22** A continuous PEF chamber designed by Dunn and Pearlman, figure taken from [116].

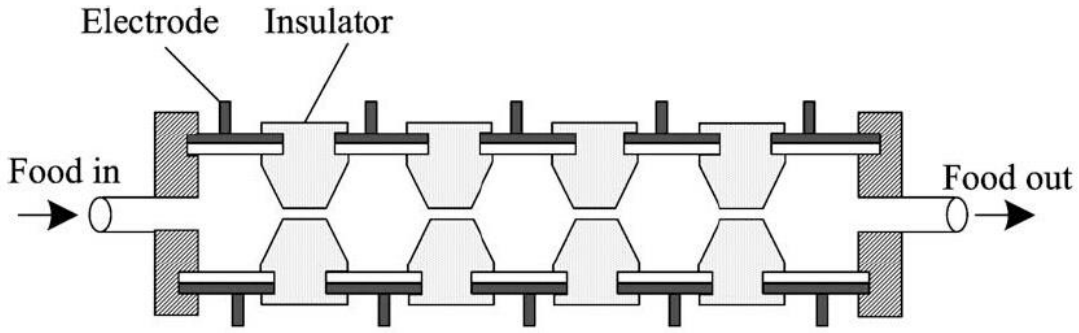


**Figure II.23** Another continuous PEF chamber designed by Dunn and Pearlman, figure taken from [178].

Unlike the static PEF chambers, the continuous chambers allow different electrode configurations to be employed as the flowing of the fluid results greater treatment uniformity. As a result, continuous PEF chambers with variety of electrode configurations have been designed in order to achieve field enhancement. Sensoy *et al.* designed a continuous PEF chamber which features enhanced electric field in the treatment region in [184], as shown in Figure II.24. The electrodes and the insulators

in this design had a conical shape so that the electric field strength in the treatment region was enhanced.

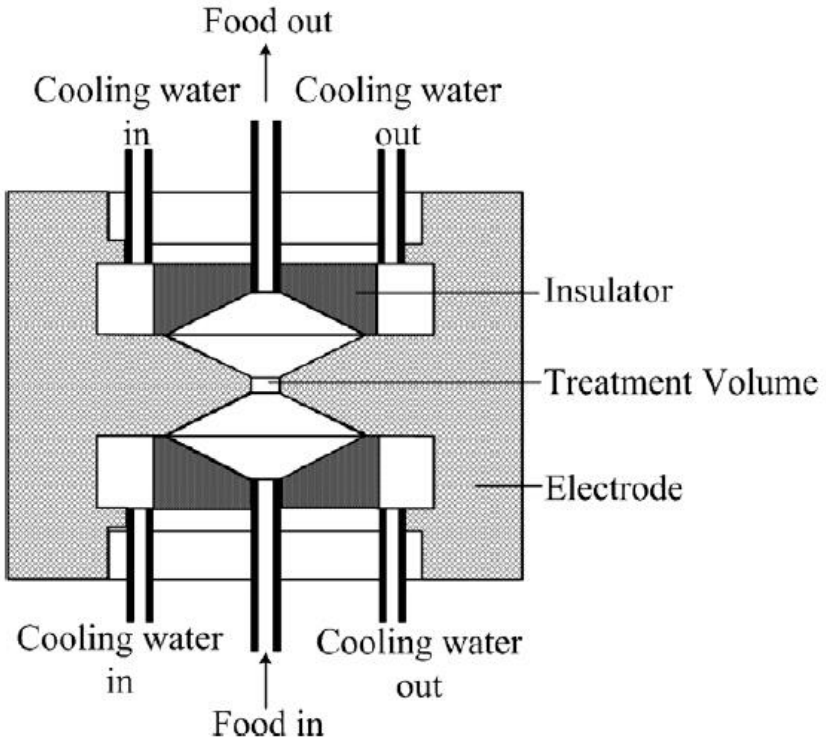


**Figure II.24** The continuous PEF chamber designed by Sensoy *et al*., figure taken from [116].

Another continuous PEF chamber with coaxial configuration was developed by the WSU research group in [185]. As shown in Figure II.25, the outer electrodes were designed to have a protruded section in order to enhance the electric field in the treatment region and reduce the field strength in the remaining parts of the chamber. Coolant paths were built into both electrodes so that the temperature of the chamber could be maintained during the PEF treatment. The whole chamber had an approximate outer diameter of 13 cm and the total height of this chamber was ~ 20 cm. Flow rates from 30 to 120 liter/hr were achieved in the PEF system using this continuous PEF chamber in [186].

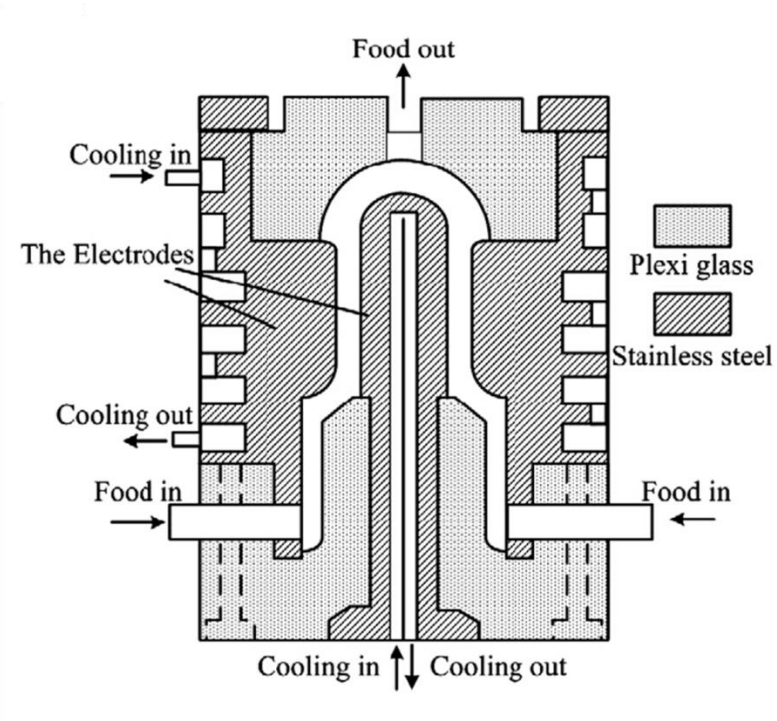


**Figure II.25** The continuous PEF chamber with coaxial configuration designed by the WSU research group, figure taken from [178].

A similar coaxial continuous PEF chamber was designed by Pizzichemi and Occhialini in [187], as shown in Figure II.26. The inner electrode of this PEF chamber was movable so that the equivalent resistance of the chamber can be adjusted in order to match the pulse generator and achieve optimal performance.

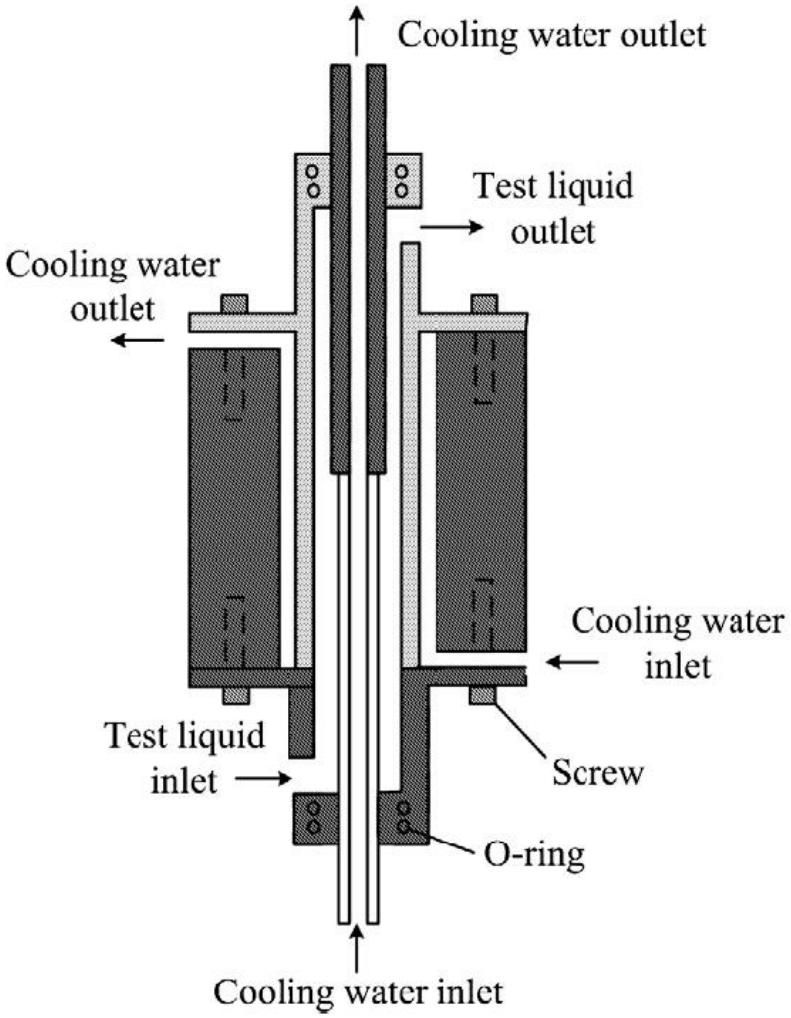


**Figure II.26** The continuous PEF chamber with coaxial configuration designed by Pizzichemi and Occhialini, figure taken from [178].

### 2.5.2.3 Non-direct Contact Chamber

As can be seen from Figure II.16-II.26, the fluid being treated in a PEF chamber has a direct contact with the metal electrodes in majority of the PEF chamber designs, with the exception of the chambers designed by Dunn and Pearlman (Figure II.22-II.23) in which the fluid was separated with the electrodes by an ion conductive membrane. However, direct contact between the liquid and electrode can generate different types of by-products during PEF process, which will be discussed in detail in Section 2.5.4.3. The presence of these by-products can contaminate the fluid being processed and is regarded as undesirable, especially in PEF systems designed for

food processing. Therefore, apart from the Dunn and Pearlman's designs, several attempts have been made to design a PEF chamber which separates the fluid with the metallic electrodes.

As shown in Figure II.27, a static coaxial PEF chamber which separated the liquid sample and the electrodes was designed by Lubicki and Jayaram in [188]. In this design, the fluid being treated was filled in the glass tube which surrounded the inner electrode. The region between the electrodes outside the glass tube was filled with conductive liquid which had similar permittivity as the fluid sample. The PEF study using this chamber indicated that bacteria *Yersinia enterocolitica* were effectively inactivated by the PEF process without direct contact with the metallic electrodes, [188]. However, it was also revealed in [188] that no inactivation was observed if the conductive filling liquid outside the tube was replaced by non-conductive transformer silicon oil.

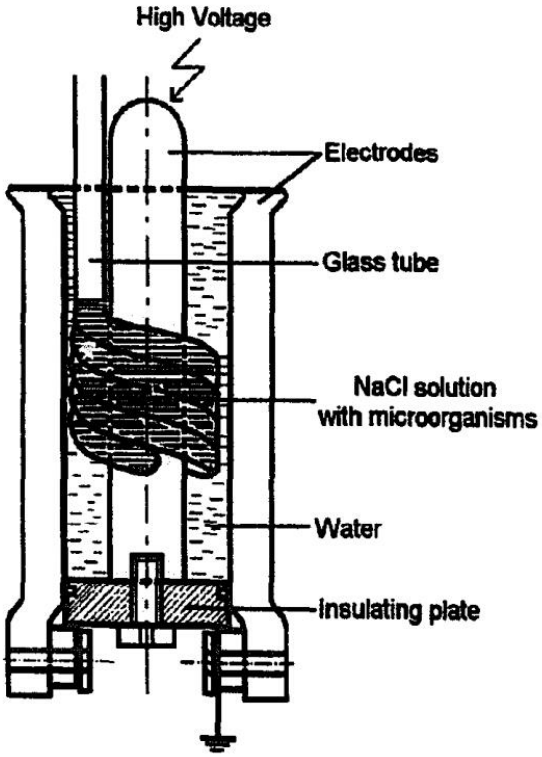


**Figure II.27** The static PEF chamber designed by Lubicki and Jayaram, figure taken from [188].

Timoshkin *et al*. proposed a conceptual PEF chamber in [6] which the metallic electrodes and the liquid being treated were separated by a layer of high permittivity ceramic material, as demonstrated in Figure II.28. Such design can eliminate the electro-chemical reaction between the metallic electrodes and the liquid sample and its undesirable by-products.

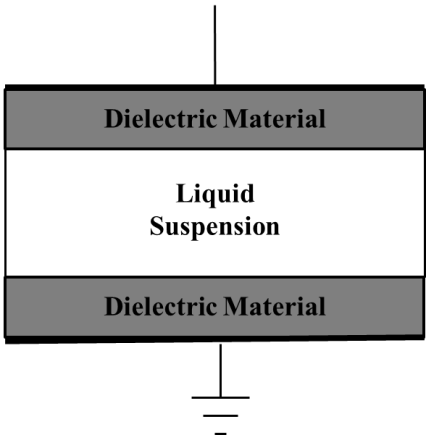


**Figure II.28** Schematic diagram of the PEF chamber with dielectric layers proposed by Timoshkin *et al.*

Novac *et al*. constructed a PEF chamber with similar design in [189], as shown in Figure II.29. The ceramic material used in this design had a relative permittivity of 3200 and formed a treatment region with a volume of 4.5 $cm^3$. In the PEF study reported in [189], *E. coli* were subjected to 100 PEF impulses in this PEF chamber with electric field strength from 130 kV/cm to 200 kV/cm. The results obtained from this PEF study demonstrated that *E. coli* were effectively inactivated by the PEF process in this chamber: 4-$\log_{10}$ reduction in surviving population at 130 kV/cm and 6-$\log_{10}$ reduction at 200 kV/cm. This PEF study also revealed that the temperature of the liquid sample did not increased during the PEF process.

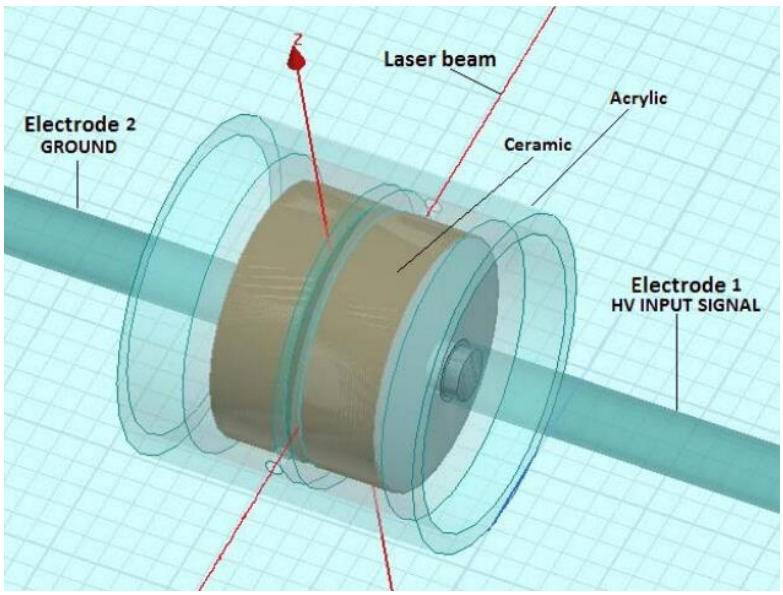


**Figure II.29** PEF chamber with ceramic material designed by Novac *et al*., figure taken from [189].

### 2.5.3 PEF Inactivation of Microorganisms

Several types of microorganisms have been widely used in PEF studies, including *E. coli*, *S. cerevisiae*, *Bacillus subtilis*, *Staphylococcus aureus*, *Lactobacillus* and *Pseudomonas*. Among these microorganisms, *S. cerevisiae* [7, 179, 181, 185, 190-196] and *E. coli* [7, 179, 191, 197-201] are the most intensive studied microorganisms, as the presence of *S. cerevisiae* is one of the major causes of food spoilage while the *E. coli* is an important indicator of fecal contamination of food. In the 2010's, as the microalgae and cyanobacteria draw increasing research attention as the promising bio-fuel source, several studies have been conducted to investigate the potential of PEF assisted inactivation and lipid extraction of these microorganisms [67-71]. Some of the important PEF studies of yeast and microalgae will be reviewed in this section.

#### 2.5.3.1 PEF Treatment of Yeast

In general, *S. cerevisiae* cells are more susceptible to the PEF treatment than other microbial cells, which is most likely due to their large cell size. Qin *et al.* studied the inactivation of *S. cerevisiae*, *E. coli* and *S. aureus* using a continuous PEF system in

[185]. The three types of microorganisms, which were suspended in simulated milk ultrafiltrate (SMUF) liquid, were subjected to exponential decay impulse with peak field strength of ~ 60 kV/cm and pulse duration of ~ 40 μs. It was reported that 5-$\log_{10}$ reduction in *S. cerevisiae* population was observed after the application of 8 pulses. As a comparison, application of 30 and 40 pulses were required to achieve the same log reduction for *E. coli* and *S. aureus* respectively. Qin *et al*. concluded that *S. cerevisiae* cells were less resistant to the PEF treatment due to their larger size (linear dimensions of ∼6 μm) as compared to *E. coli* (2.2 μm×0.9 μm) and *S. aureus* (linear dimensions of ∼1 μm).

The high susceptibility of the *S. cerevisiae* cells to the PEF process is also confirmed by the low critical electric field ($E_c$) and critical treatment time ($t_c$) required for inactivation. Grahl and Markel reported a study of PEF treatment of *S. cerevisiae* in different suspension mediums in [179]. The following values were reported for *S. cerevisiae* suspended in sodium alginate: $E_c$ = 5.4 kV/cm and $t_c$ = 0.4 μs at 24.8 kV/cm; in UHT milk: $E_c$ = 4.7 kV/cm and $t_c$ = 19.8 μs at 24.8 kV/cm. As a comparison, for *E. coli* cells suspended in sodium alginate: $E_c$ = 14 kV/cm and $t_c$ = 4.5 μs at 24.8 kV/cm; in UHT milk: $E_c$ = 12.7 kV/cm and $t_c$ = 130.2 μs at 24.8 kV/cm. It was also suggested in [179] that 5-$\log_{10}$ reduction in *S. cerevisiae* population was possible at electric field magnitude as low as 7 kV/cm and energy input as low as 10 kJ/liter could be achieved for optimal treatment condition.

Jacob *et al*. studied the PEF treatment on *S. cerevisiae* cells in different growing phases in [192]. It was reported that yeast cells in the logarithmic phase were more sensitive to PEF process than the cells in the stationary phase: 75% of the yeast cells in stationary phase survived after 4 pulses with electric field strength of 30 kV/cm, while only 5% of the cells in logarithmic phase survived after 4 pulses at 11 kV/cm. The similar results were reported by Gaskova *et al*. in [190], where *S. cerevisiae* were subjected to rectangular impulses with duration of ~ 200 μs. It was found that the killing rate of the yeast cell in the logarithmic phase was nearly 100% at 16 kV/cm, whereas the killing rate of the stationary cells was less than 30% with electric field strength up to 28 kV/cm.

In [7], Qin *et al*. compared the performance of PEF treatment on *S. cerevisiae* using impulses with different waveshapes. *S. cerevisiae* cells, which were suspended in apple juice in a static PEF chamber, were subjected to square (~ 50 µs) and exponential decaying (~ 150 µs) impulse with field strength at 12 kV/cm. It was reported that ~ 4-$\log_{10}$ reduction in the *S. cerevisiae* population was observed after the application of 10 pulses for both types of the impulses. However, the study revealed that the energy efficiency for the square impulse was 91% and the energy efficiency for the exponential decaying impulse was only 64 %. Therefore, based on the results obtained in [7], Qin *et al*. concluded that impulse with square waveshape has the better energy efficiency in PEF process.

Aronsson and Ronner investigated the effect of pH, water activity and temperature on PEF treatment of *S. cerevisiae* in [191]. In this study, *S. cerevisiae* cells were suspended in 0.9 % NaCl solution and the suspension was subjected to 20 square impulses with 25 kV/cm field magnitude and 4 µs duration in a continuous PEF system. The range of pH of the suspension being investigated was from 4.0 to 7.0, the range of water activity of the suspension being investigated was from 1.0 to 0.94 and two temperature levels (10 °C and 30 °C) was investigated. It was found that the effect of pH and water activity on PEF treatment of *S. cerevisiae* was statistic insignificant. However, it was reported that increase in the suspension temperature significantly enhanced the killing effect of PEF for *S. cerevisiae*, as averaging 2 more $\log_{10}$ reductions in the population was observed at higher temperature.

Harrison *et al*. used the transmission electron microscopy (TEM) to assess the PEF inactivation of *S. cerevisiae* in [193]. In this PEF study, *S. cerevisiae* cells were suspended in apple juice and were subjected to 64 exponential decaying impulse with 40 kV/cm field magnitude and 4 µs duration in a static PEF system. The results obtained from the TEM observation gave little evidence to support the electroporation process as the major inactivation mechanism for *S. cerevisiae*. It was found that disruption of the *S. cerevisiae* cellular organelles was observed more frequently than the disruption of the cell membrane. Harrison *et al*. suggested the cytological disruption as an alternative inactivation mechanism to the widely accepted electroporation process.

The energy consumption for PEF inactivation of *S. cerevisiae* varies among the reported PEF studies, which was in the range from few tens to a few hundreds of kJ/liter. Mizuno and Hayamizu reported the energy input in the PEF treatment on *S. cerevisiae* was 126 kJ/liter for 3-$\log_{10}$ reduction in the surviving *S. cerevisiae* population in [194]. Matsumoto *et al.* reported a 84 kJ/liter energy consumption for 5-$\log_{10}$ inactivation of *S. cerevisiae* in [181]. In the PEF study conducted by Zhang *et al.*, the energy consumption was 77 kJ/liter when the surviving population of *S. cerevisiae* was reduced by 6-$\log_{10}$ in [195]. However, for the same 6-$\log_{10}$ reduction, energy consumption of 300 kJ/liter was reported in the PEF study conducted by Ohshima *et al.* in [196].

#### 2.5.3.2 PEF Treatment of Microalgae

Unlike the PEF studies on *S. cerevisiae* and other yeast and bacteria, which have been conducted for years and cover almost all aspects of the PEF process, PEF research on microalgae is at a very early stage and focuses mainly on the feasibility of PEF induced or assisted lipid extraction from microalgae.

Zbinden *et al*. investigated PEF treatment on green microalgae *Ankistrodesmus falcatus* in [67]. In this study, *A. falcatus* cells were subjected to exponentially decaying impulses with a characteristic decay time of 360 ns and a peak field magnitude of 45 kV/cm. The PEF chamber used in [67] had a parallel-plane topology and consisted of two stainless steel electrodes. The PEF process was used as the pre-extraction treatment to disrupt the cell structure and followed by the solvent extraction. The solvents used in the study were ethyl acetate, methanol and water. The efficiency of the PEF treatment was assessed by comparison of lipid extraction and by microscopic inspection of an algae cell stained with propidium iodide. It was found in the study that, PEF treatment with a specific energy of 26 MJ/kg (dry weight) resulted in lysis ~90% of the *A. falcatus* cells and the lipid yield of PEF-treated *A. falcatus* was increased by 130% as compared with untreated *A. falcatus*.

Eing *et al*. conducted PEF study of another type of microalgae, *Auxenochlorella protothecoides* in [68]. The *A. protothecoides* cells were subjected to square impulses

with electric field magnitude of 35 kV/cm and pulse duration of 1 µs. The efficiency of the PEF process was assessed by measuring of intracellular stored biomass, total organic carbon content (TOC), and carbohydrates released by the PEF process. The lipid extraction using ethanol from the treated and untreated *A. protothecoides* was also compared. It was found that PEF treatment with 2 MJ/kg specific energy resulted in ~ 433 % increase in release of intracellular stored biomass, ~ 400% increase in the release of TOC, ~ 1000% increase in the release of carbohydrates and ~ 500% increase in lipid yield as compared with untreated *A. protothecoides*.

Grimi *et al*. studied the PEF treatment of microalgae *Nannochloropsis sp*. for selective extraction of ionic components, pigments, and proteins and compared its performance with other cell disruption methods in [70]. The *Nannochloropsis sp*. cells were subjected to HV impulses with 20 kV/cm of field magnitude and 10 µs of pulse duration. The results obtained in this study showed that PEF process allowed selective extraction of water soluble ionic components, microelements, small organic compounds and water soluble proteins from *Nannochloropsis sp*. However, PEF treatments were ineffective for extraction of pigments as compared to other cell disruption methods such as ultrasonication and high pressure homogenization.

The feasibility of direct PEF induced lipid extraction from *A. protothecoides* was investigated by Goettel *et al*. in [71]. In this study, *A. protothecoides* cells were treated by square impulses with field magnitudes of 23-43 kV/cm and pulse duration of 1 µs. In order to visualise the lipids inside the *A. protothecoides* cells and potential release by the PEF process, the cells were dyed with Nile Red. The Nile Red stained *A. protothecoides* cells were analyzed by light and fluorescence microscopy after the PEF treatment to detect any leakage of the lipid content. The results obtained in [71] showed that no lipid content was detected outside the *A. protothecoides* cells after the PEF process, which suggested that PEF treatment did not cause spontaneous release of lipids from *A. protothecoides.*

### 2.5.4 Factors Influencing PEF Inactivation Performance

In recent decades, numerous studies have been focused into investigation of the factors that can affect the inactivation performance of the PEF process. These factors include the magnitude of electric field strength, the pulse waveshape, selection of the electrode material, as well as the microbial and suspension factors. Understanding of the effect of these factors can allow the optimisation of the design of PEF system and the selection of treatment parameters. Recent studies into the effects of these factors are reviewed in the following sections.

#### 2.5.4.1 Magnitude of Electric Field

As discussed in Section 2.5.1, the main inactivation mechanism in the PEF process is the electroporation process, which is triggered when the membrane potential reaches the critical value of 1 V. It was also demonstrated that this membrane potential has a strong correlation with the magnitude of the external electric field. Therefore, the field strength of the applied electric field during the PEF treatment has a significant impact on the PEF inactivation performance and critical field strength needs to be reached in order to trigger PEF inactivation.

Although mathematical relation between the external electric field strength and the membrane potential has been established in many studies, the value of this critical field strength, $E_C$, varies significantly among different practical studies. Firstly, the value of $E_C$ varies among different microorganisms. It was reported in [179] that inactivation of *S. cerevisiae* can be observed at a critical field value of 4.7 kV/cm. In [202], $E_C$ was obtained for several microorganisms: 4 kV/cm for *E. coli*; 6 kV/cm for *Klebsiella pneumonia*; 8 kV/cm for *Candida albicans* and *Pseudomonas aeruginosa*. The variation in $E_C$ between different microorganisms is mainly the result of different microbial characteristics among microorganisms: such as the type of Gram staining, cell size, and growth stage of the microbial cell. The effects of these microbial factors on PEF treatment performance will be detailed in Section 2.5.4.4.

Secondly, the value of $E_C$ varies even for the same types of microorganism, as was demonstrated in [179, 202-203] where *E. coli* were subjected PEF treatment in these studies. However, a correlation between the pulse duration and this variation of $E_C$ for *E. coli* can be established. The reported $E_C$ values and their corresponding pulse duration were: 13.7 kV/cm (not specified) [179], 4 kV/cm (36 μs) [202], 4.9 kV/cm (50 μs) [203] and 40 kV/cm (2 μs) [203]. It can be concluded that higher field strength is required for PEF inactivation if shorter pulse is used. This conclusion shows a good agreement with the finding presented in [172], which stated that irreversible electroporation could be achieved by inducing higher membrane potential or maintaining the critical membrane potential for a longer time.

However, using the critical field strength can only lead to minimum PEF inactivation, as demonstrated in [179, 202], in which only 0.2-$\log_{10}$, i.e. 37 %, reduction of the microbial population was observed using the critical field strength. When the field was increased to 7 kV/cm, the population reduction of *S. cerevisiae* was increased to 5-$\log_{10}$ (99.999%) [179]. While in [202], when the field was increased to 10 kV/cm, the population reduction of *E. coli* increased to 3-$\log_{10}$ (99.9%) and the population reduction of *C. albicans* increased to 2-$\log_{10}$ (99%) when the field was increased to 12 kV/cm.

The results from these studies indicate that the field strength should be ~ 10 kV/cm in order to achieve useful levels of inactivation. In recent developed PEF treatment systems [67, 68, 197, and 204], the field strength is commonly selected to be above 30 kV/cm in order to achieved reliable and effective PEF inactivation. It has also been shown that further increase in the magnitude of field strength could result in a more prominent inactivation effect. For example, PEF treatment with field strength up to 110 kV/cm was used to inactivate *E. coli* in [177]. The results obtained in [177] demonstrate that for field exceeds 60 kV/cm, the surviving population of *E. coli* decreases significantly as compared with lower field strength. However, such high field strength normally requires reasonably short duration (typically sub-μs) of PEF impulses in order avoid formation of spark breakdown between the electrodes.

### 2.5.4.2 Pulse Waveshape

As demonstrated in Section 2.4, two most frequently used pulse waveshapes in the pulsed power system are the square and exponential waveshapes. Generation of an exponential impulse is normally relatively simple and inexpensive, which can be achieved by simple lumped elements pulse generating circuit. On the other hand, generation of a square impulse normally requires a transmission line based pulse forming network, which is relatively complex in construction and costly. Therefore, understanding of the effect of these two waveshapes on the performance of PEF process can be beneficial for the optimisation of pulsed power system design.

Qin *et al* conducted a PEF study [7] to investigate the effect of these two waveshapes on the PEF inactivation performance. Three types of microorganisms, *E. coli*, *S. cerevisiae* and *B. subtilis*, were treated by PEF impulses with square and exponential decaying waveshapes in [7]. The waveforms of the square and exponential decaying impulses used in [7] are shown in Figure II.30. PEF impulse with these two waveshapes had the same peak magnitude of field strength and identical energy was delivered to the liquid suspension by each impulse. It was reported in [7] that impulses with square waveshape was more energy efficient than the impulses with exponential decaying waveshape. Qin *et al* stated that the long decaying tail of the exponential decaying impulse could be ineffectual for inducing lethal electroporation. Therefore, the exponential decaying impulse was less energy efficient than in the case of the square impulse.

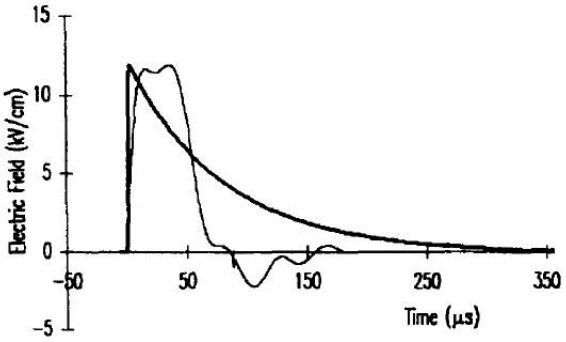


**Figure II.30** Waveforms of the square and exponential decaying impulses used in [7], figure taken from [7].

However, PEF study [7] was the only reported work which was focused on the comparison of PEF inactivation efficiency between square and exponential impulse. After Qin *et al*, a mathematic correlation between the frequency components of the pulse waveshape and the survival fraction was established by Love in [205], which demonstrated in a quantitative way that the square impulse has stronger inactivation effect over the impulse with other waveshapes. However, the establishment of some of the coefficients in this mathematic correlation was based on the experimental results from [7]. Therefore, the study reported in [205] should be regarded as a mathematic description of the results from [7], rather than an independent evaluation.

In addition, the magnitude of the field strength used in [7] was 12 kV/cm, which was only above the 10 kV/cm critical field strength that allows effective PEF inactivation, as demonstrated in Section 2.5.4.1. Therefore, it suggests that within most of the exponential decaying impulse duration, the field magnitude was below the critical value as the impulse started to the decay gradually after reaching the peak. Therefore, it would be beneficial to conduct another PEF study to investigate the PEF inactivation efficiency of the two pulse waveshapes using a different field magnitude in order to obtain a better understanding of the actual effect of the pulse waveshape on the PEF process.

Apart from square and exponential waveshapes, HV impulses with other waveshapes are also used in PEF studies, such as oscillatory impulse and bipolar impulse. A comparison of the PEF inactivation efficiency between oscillatory decaying and exponentially decaying impulses was made in [7]. The waveforms of the oscillatory and exponentially decaying impulses used in [7] are shown in Figure II.10(b). It was reported that the oscillatory decaying impulse was the least efficiency impulse as compared to the exponentially decaying impulse. The result was explained in [7] that the oscillations of the external electric field did not allow the charge accumulation at the membrane and reduced the inactivation efficiency. The results were in line with some analytical studies of the transient process of the development of the trans-membrane potential, [206-207].

Studies of the effects of bipolar impulses on PEF inactivation efficiency were also reported in [7, 8, and 208]. Comparison between the bipolar and monopolar impulses was made in [7]. It was reported that bipolar impulses were more lethal than the monopolar impulses. The reason was explained by that, the change in orientation of the electric field causes a corresponding change in the direction of the movement of charge molecules on the microbial membrane, which enhanced the electrical stress on the membrane. A similar result and the same explanation was reported by Ho *et al*. in [208], in which microorganism *P. fluorescens* was treated by PEF process using both bipolar and monopolar triangular impulses. However, contradicting results were reported by Beveridge *et al*. in [8], where *E. coli*, *L. monocytogenes*, and *B. cereus*, were subjected to PEF treatment using both bipolar and monopolar square impulses. The results from this study show that superior PEF inactivation efficiency was obtained consistently in the PEF process using monopolar impulses. An explanation was given in [8] that the pulse duration used in the study (1μs) was relatively short as compared with the PEF study in [7], in which the pulse duration was over 50 μs, so that the bipolar impulse used in [8] was effectively an oscillating impulse. Figure II.31 and Figure II.32 show the bipolar impulses used in [7] and [8] respectively.

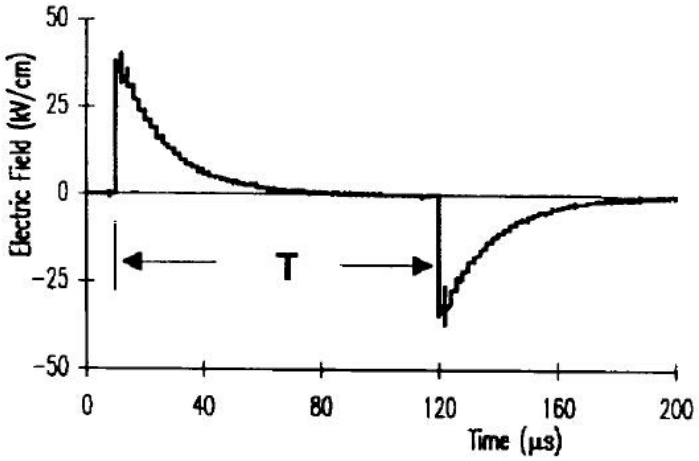


**Figure II.31** Waveforms of the bipolar impulse used in [7], figure taken from [7].

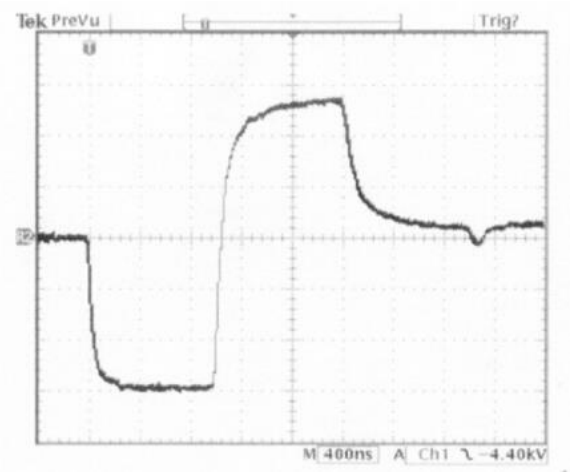


**Figure II.32** Waveforms of the bipolar impulse used in [8], figure taken from [8].

### 2.5.4.3 Electrode Material

As introduced in Section 2.5.1, during PEF process when metallic electrodes are used, metal ions can be generated and introduced into the liquid suspension due to electro-chemical reaction. Many studies demonstrate that the presence of these metallic ions has an antimicrobial effect. Therefore, selection of the electrode material is critical for the design of the pulsed electric field system. For example, for a PEF system design for food processing, presence of these undesirable metallic ions should be minimised, while for a PEF system focus on bacteria inactivation, the presence of these metallic ions can improve the overall inactivation performance.

The electro-chemical reaction, which is called electrolysis, occurs when metallic electrodes are in contact with electrolyte and subjected to the applied voltage. This electrolysis process produces not only the metallic ions, but also the gaseous products: oxygen is generated at the anode and hydrogen at the cathode when the electrolyte is water. The type of ions generated in the electrolysis process depends on the material of the electrodes. In most of the PEF applications, stainless steel and aluminium are selected as the PEF electrodes, and only a few studies investigate the effect of copper electrodes, [165]. In the case of copper, aluminium and stainless steel electrodes, the resulting ions in the liquid suspension are $Cu^{2+}$, $Al^{3+}$ and $Fe^{2+}/Fe^{3+}$ respectively.

It was demonstrated in [165] that the presence of $Cu^{2+}$ showed the most significant antimicrobial effect. In [165], discharges were generated between two electrodes in order to introduce metallic ions into the liquid suspension between the electrodes which contains *E. coli*. The results showed that after 10 discharges, 90% of the *E. coli* population was inactivated when iron core electrodes were used, and the reduction in *E. coli* population became 99 % and 99.9% when aluminium core and copper core electrodes were used respectively. Therefore, copper electrodes are rarely used in PEF system.

However, in the study reported in [209], the antimicrobial effect of ferric ions is more pronounced then the aluminium ions when the ion concentrations were kept the same. It was shown that when ions concentration was 2.5 mM, ~ 17% of the DC-3F cells were inactivated with the presence of ferric ions while only ~ 5% of the cells population was reduced with the presence of aluminium ions. On the other hand, however, aluminium is much more reactive than the stainless steel, which suggests more $Al^{3+}$ can be released into the liquid suspension during PEF process. This was confirm in the same study [209], after the application of the same number of impulses, the concentration of the $Al^{3+}$ was ~ 0.5 mM higher as compared with the concentration of the ferric ions ($Fe^{2+}$/$Fe^{3+}$). The highly reactive aluminium produces more gaseous products in the electrolysis process. During the PEF process, the accumulation of these gaseous molecules can form bubbles between the electrodes, which leads to undesirable dielectric breakdown in the PEF test cell [153]. In addition, it was reported in [210] that the presence of $Al^{3+}$ can affect the membrane electroporation process. As a comparison, the stainless steel has a relatively high corrosion resistance and relatively low electro-chemical reactivity [211]. Therefore, stainless steel is a typical choice for the electrode of PEF systems used in experiments and industrial installations, especially for food processing.

Apart from the metallic ions and gaseous molecules, other undesirable toxic by-products can be generated by the electro-chemical reaction between the metallic electrode and liquid suspension during PEF process: such as chlorine [198], hypochloric/hypochlorous acid [212] and hydrogen peroxide [212].

Recently, a conceptual PEF test cell was proposed by Timoshkin *et al*. in [6] which the metallic electrodes and the liquid suspension are separated by a slab of high permittivity ceramic material, as demonstrated in Figure II.28. This novel concept of PEF test cell design can potentially eliminate any electro-chemical reaction and the toxic by-products, as there is no direct contact between the metallic electrode and the liquid suspension. The probability of undesirable dielectric breakdown can also be reduced as no bubble can be generated by the electrolysis process. The other advantage of this concept is that the ionic conduction current through the liquid suspension will be eliminated with the presence of the dielectric ceramic. As the ionic conduction current is associated with the energy dissipation during the PEF procedure, elimination of the ionic conduction current suggests significant improvement in energy consumption could potentially be achieved using this non-conductive PEF test cell design. However, practical PEF experiments using such conceptual PEF test cell have not been reported in anywhere at the time when the present project started.

#### 2.5.4.4 Microbial Factors

As mentioned in Section 2.5.4.1, the characteristics of the microorganisms have a notable impact on the PEF inactivation performance, particularly on the critical magnitude of applied electric field. These microbial factors include the cell size, the type of gram staining, and the growth stage of the microbial cell.

Among these factors, the size of the microbial cell has the most significant impact on the PEF inactivation performance. As can be seen from the Schwan equation (Equation II.7), the induced membrane potential has a linear correlation with the size of the microbial cell. With the application of external electric field with the same magnitude, greater voltage will be developed across the membrane in a cell with larger diameter, which suggests microorganisms with larger cell size are more sensitive to PEF process. This is confirmed in the practical PEF studies reported in [185, 213]. It has been shown in [185], that *S. cerevisiae* cells (with linear dimensions of ~6 μm) were more susceptible to the PEF treatment than *S. aureus* cells (with linear dimensions of ~1 μm). It was also reported in [213], that an

increased susceptibility of *B. subtilis* to the PEF treatment was observed as compared with smaller *S. aureus*.

Comparison of the susceptibility to PEF treatment between the types of Gram strain of the bacteria has also been made in a few PEF studies [8, 116, and 202]. It was reported in [116] and [202] that Gram-negative bacteria were generally more susceptible to the PEF process than the Gram-positive bacteria. The potential reason for these obtained results was given in [116], which is due to the thick peptidoglycan layer in the Gram-positive bacteria. However, it was shown in [8] that there was no significant difference in the susceptibilities of the three bacteria being investigated: *E. coli* (Gram-negative), *L. monocytogenes* (Gram-positive), and *B. cereus* (Gram-positive).

Several studies also investigated the effect of the growth stage of the microorganism on the performance of pulsed electric field treatment. The critical electric field for *E. coli* of different growth stages was determined in [202]. The results obtained in [202] demonstrated that electric field of 8 kV/cm was necessary to start PEF inactivation of *E. coli* in the stationary phase while $E_C$ was only 2 kV/cm for the *E. coli* in log phase. In other PEF studies [190, 199, and 203], microorganisms in the stationary or lag phases all demonstrated less susceptibility to the PEF process as compared to the same microorganism in the log growth phase.

On the other hand, many food-borne pathogenic bacteria are able to adapt to sub-lethal inimical stresses and become more resistant to the lethal levels of the same source of stress, as reported in [214]. However, very little is known about whether this phenomenon is applicable to of stresses induced by PEF process.

#### 2.5.4.5 Characteristics of Suspension

Characteristics of the liquid suspension, which include the temperature, the electrical conductivity and the pH of the suspension, also produce a notable effect on the PEF process, as demonstrated in many PEF studies, [173, 191, 199, 200-201, 215-219].

As discussed in Section 2.2.1, microorganisms can be inactivated by the thermal process alone. Therefore, the suspension temperature is clearly an influential factor in the PEF process. Although pulsed electric field treatment is widely regarded as a non-thermal processing technology, the thermal effect of the PEF process can be governed by the rate of energy dissipation in the liquid suspension. If large amount energy is delivered to the suspension over a short period of time, the temperature of the suspension can be increased significantly. As a result, increase in suspension temperature is commonly observed during PEF process. The effect of the suspension temperature on PEF inactivation performance has been investigated in several PEF studies, [199-200], where temperature of the suspension was maintained at different level during PEF process. It was demonstrated in [199] that 2-$\log_{10}$ reduction in the *E. coli* population can be achieved by 20 exponential decaying impulses at 40 °C, while the same reduction in population required 50 impulses when the temperature was reduced to 30 °C. Similar tendency was reported in [200], in which *E. coli* was subjected to PEF impulse at two temperature levels. The obtained results showed that 6.5-$\log_{10}$ reduction in population was achieved at 55 °C and less than 1-$\log_{10}$ reduction was recorded when suspension temperature was maintained at 32 °C. The results obtained in these studies show a good agreement with the investigation of electroporation process described in [5], which illustrated that the critical membrane potential reduces significantly as the temperature increases: 2 V at 4 °C and 0.5 V at 37 °C. Although high temperature can improve the inactivation performance of the PEF process, increase of the suspension temperature during PEF process is regarded as undesirable in many pulsed electric field applications and cooling system is employed to maintain the suspension temperature at a relatively low level.

The other factor which can affect the PEF process is the electrical conductivity of the liquid suspension. The suspension conductivity can affect the PEF process in multiple ways. First of all, study into mathematic description of the induced membrane potential indicates that higher suspension conductivity would result a higher trans-membrane voltage, [173]. However, from the electrical point of view, suspension with high conductivity creates several engineering difficulties. PEF chamber containing liquid suspension can be equivalent to a resistive load in a pulsed

power system. Increase in the suspension conductivity reduces the equivalent resistance of the load. When connecting to a *RC* pulse generating circuit, this low resistance load will results a shorter pulse duration. When connecting to a transmission line based PFN, load with low resistance will result in a low load voltage and reflection due to the mismatched between the load resistance and the PEF impedance. On the other hand, when subject to the same electric field, higher ionic conduction current will flow through suspension with higher conductivity. This ionic conduction current is associated with the energy dissipation in the suspension and the resulting Joule heating. As a result, greater increase in the suspension temperature will be seen in the suspension with higher conductivity, which is undesirable in many PEF applications. More importantly, the energy efficacy of the PEF system will be reduced as more energy is dissipated into the suspension. However, in most of the PEF application, especially for the food processing, the conductivity of the suspension fluid is relatively high, in the range of $10^{-1}$-$10^{0}$ S/m [112]. The conceptual non-conductive PEF test cell design, proposed in [6], can potentially overcome this engineering difficulty. With the presence of the dielectric layer, ionic conduction current through the liquid suspension can be eliminated regardless the suspension conductivity.

Another suspension factor which can affect the PEF inactivation performance is the pH of the suspension. The influence of the pH on the PEF efficiency depends on the type of microorganism as it was shown in different PEF studies [191, 201, 215-219]. Greater inactivation has been reported for lower pH solution which contains for *E. coli* [191, 201] and *L. monocytogenes* [215]. However, greater inactivation has been achieved at higher pH values of solution with *S. enteriditis* [216], and *S. senftenberg* [215]. Other studies reported that the inactivation performance was unaffected by the change of pH [3, 217]. However, it should be noted that the strong inactivation performance observed in low pH environment can be a synergistic killing effect of the combination of PEF and acids, as reported in [218]. It was also reported in [219] that Gram positive bacteria are more resistant to PEF treatment at neutral pH environment than Gram negative bacteria. However in acid conditions, Gram negative bacteria show more resistance to PEF process than Gram positive bacteria.

## 2.6 Discussion

This chapter reviewed the relevant information gathered over the duration of the present project. Basic background information about microorganism and the current inactivation methods were introduced at the beginning of this review. In the second part of this review, fundamentals of the pulsed power technology, such as the pulse forming systems and the high voltage switch were discussed. Finally, a comprehensive review of the pulsed electric field (PEF) technology was conducted in this chapter. The main inactivation mechanism and other potential mechanism of the PEF process were introduced. Discussion about the recent PEF studies into the effects of different operational and biological factors on the PEF process were presented. Although numerous studies have been conducted over the past few decades and significant results have been achieved for almost all aspects of the PEF technology, there are still gaps in understanding of this process. Also, there is a need to improve inactivation and energy efficiency of the PEF process which will help to develop commercially viable applications of this technology.

Firstly, a novel concept of the PEF chamber design was proposed by Timoshkin *et al* in [6]. This conceptual chamber design, in which the liquid suspension and the metallic electrodes are separated by layers of high permittivity ceramic, could potentially improve the performance of PEF process in several aspects. The separation of the metallic electrodes and the liquid suspension eliminate the electrolysis process during the PEF treatment. As a result, production of metallic ions and other toxic by-products and generation of the gas bubbles can be prevented. In addition, no ionic conduction current will flow through the suspension regardless of the suspension conductivity, which can significantly reduce the thermal effect of the PEF process. More importantly, the absence of the ionic conduction current can improve the energy efficacy of the PEF process significantly. However, construction of such PEF test cell and practical PEF study using this conceptual test cell has never been conducted at the beginning of the present study.

Secondly, there is a lack of the study into the effect of the pulse waveshape on the inactivation performance of PEF process. Although a valuable and creditable work

has been conducted by Qin *et al* [7] and Beveridge [8] to investigate the effects of square, exponential decaying, oscillating decaying impulses and bipolar impulses, they are seemingly the only studies which focus on this aspect. However, the field strength used in [7] was just marginally higher than the critical field strength which can effectively induce lethal electroporation process. As a result, the PEF inactivation tendency and efficiency for different impulses obtained in [7] could potentially be the synergistic effect of the pulse waveshape and the magnitude of field strength. No study has ever been conducted to compare the effect of pulse waveshape using an elevated level of electric field strength.

Microalgae and cyanobacteria draw increasing global attention in the past decade as the potential sustainable source for bio-fuel production due to its high lipid content as compared to other food crops and oil seeds. Several methods, such as high-pressure homogenizer, autoclaving, mechanical homogenizer, and chemical solvent, have been investigated for cell disruption and lipid extraction. As the main inactivation mechanism of the PEF process is the induced irreversible electroporation on the microbial membrane, the PEF technology can potentially be used to facilitate the lysis of microalgae and cyanobacteria cells and extraction of lipid content. At the time when the present project started, only handful of work has been conducted and little was known about the performance of PEF treatment on microalgae. The results from these studies indicated that direct lysis of the microalgae cells by PEF treatment were difficult to achieve. On the other hand, cyanobacteria, which have relatively simpler cell structure, could potentially be more susceptible to the PEF process.

Therefore, the main objectives of the present project can be summarised as follows:

- To design and construct a non-conductive PEF test cell and to conduct practical PEF treatment using the designed non-conductive PEF test cell to investigate the PEF performance of such design.

- To investigate the effect of pulse waveshapes on the inactivation performance of the PEF process using elevated electric field strength to acquire a further understanding of the effect of pulse waveshape.

- To conduct PEF treatment on cyanobacteria to investigate the effect of PEF process on cyanobacteria cells and to establish if cell lysis could be achieved by the PEF treatment.

# Chapter III

# MODELLING OF THE PEF PROCESS

## 3.0 General

This chapter presents the simulation models of the transient electric field across the bio-membrane during the PEF process. Two types of models have been developed: a model based on the equivalent circuit approach and a physical analytical model. A 2-dimensional equivalent circuit model of the microbial cell includes layers of bio-membrane and the cell wall. The response of this model to an external electric field was simulated using the *OrCAD® PSpice* software in order to investigate the effect of this layer of cell wall on the development of trans-membrane potential.

The analytical model used in this chapter is based on paper [6]. This analytical approach was adopted in the present study to investigate the transient response of the trans-membrane potential to external electric field. This model includes two layers of dielectric material separating the metallic electrodes of the PEF test cell and the liquid suspension in order to implement the proposed non-conductive PEF cell topology as discussed in Section 2.5.2.3. The simulations based on this model were conducted using the *MathWork® Matlab* software.

The obtained results, significant findings and their critical analysis are presented in this chapter. These results provide valuable suggestions and guidelines for the practical design of PEF systems and for optimisation of the PEF treatment regimes, which will be discussed in the following chapters.

## 3.1 Equivalent Circuit Model of Microbiological Cell

In physics and electronics, equivalent circuit model which consists of several lumped circuit elements (resistors, capacitors and inductors) is commonly used to describe

passive electrical properties of materials. Such approach can also be used for modelling of microbial cells exposed to the electric fields, [174, 206, 220-221]. To implement an equivalent circuit model of a microbial cell, different elements of the cell structure are represented as a lumped-element circuit in which the electrical connections between all cell elements and their own electrical properties are described by series-parallel, resistors-capacitors combinations. For example, a planar bilayer membrane was represented by a simple equivalent circuit in [220], where the membrane was modelled by parallel combined capacitance *C* and resistance *R* while $R_0$ represented the external charging pathway, as shown in Figure III.1. The trans-membrane potential $\Delta U(t)$, which is induced by the application of external voltage $V_0$, can therefore be evaluated as a voltage developed across *R* and *C* connected in parallel. In [174], a biological cell was modelled as a lumped equivalent circuit, where the cell membrane was represented by $R_M$ and $C_M$, the cytoplasm was represented by $R_C$, the cell suspension was represented by $R_S$ and $C_S$, and $R_L$ represented the external circuit resistance, as shown in Figure III.2. Such equivalent circuit model implemented in *OrCAD® PSpice* software will allow the investigation the response of microbial cell and its sub-elements to the external voltage source *V(t)*.

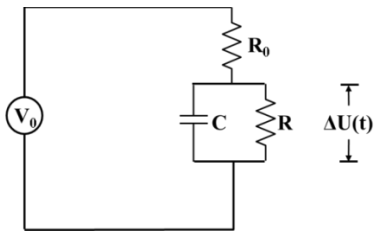


**Figure III.1** Equivalent circuit model of a planar bilayer membrane, [220].

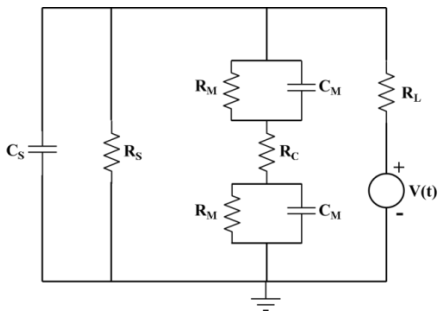


**Figure III.2** Equivalent circuit model of a biological cell, [174].

### 3.1.1 2-Dimentional Equivalent Circuit Model

The shape of the microbial cell varies between different microorganisms, from the most common spherical shaped to rod shaped or even spiral shaped microorganisms [11]. Precise representation of the geometry of microbial cell can be extremely difficult. Even for an ideal spherical shaped cell, the equivalent circuit model of such cell can be very complex, as demonstrated in [206]. In [206], the spherical shaped cell and its surrounding suspension were modelled as a 5×5×5 matric of resistor-capacitor lumped circuit elements. The cell was located in the center cube and the surrounding 124 cubes represented the surrounding suspension so that electric field distortion in the surrounding suspension caused by the spherical shaped cell was simulated. The resulting equivalent circuit model contained over two hundreds of *RC* components. For the purpose of the equivalent circuit model in present study, such complexity was not necessary.

For a simple approximation, a microbial cell subjected to external electric field can be modelled as a cube inside plane-plane electrodes, as shown in Figure III.3. The external electric field can be generated by applying voltage to the electrodes. It was reported in [221] that maximum trans-membrane potential which triggered electroporation process would appear at the 'polar caps', which are the regions nearest to the electrodes in a spherical cell. The equivalent of these 'polar caps' in a cubical model is the planes which facing the electrodes (side A and D in Figure III.3). It was also demonstrated in [206] that trans-membrane potentials were ~ 0 V on the planes that are perpendicular to the electrodes (side B, C, E and F in Figure III.3).

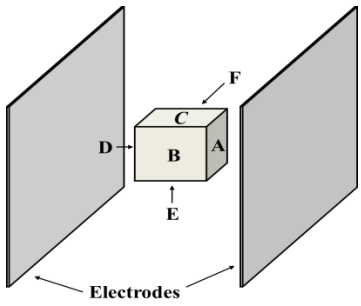


**Figure III.3** Cubical model of a microbial cell between two electrodes.

Therefore, the 3D cubical model can be reduced to a 2-dimential model if the effect of those planes perpendicular to the electrode (side B, C, E and F) is neglected. As shown in Figure III.4, the microbial cell is represented as a series of parallel layers along the axis perpendicular to the electrode. From left to right in between the two electrodes, these layers represent the external suspension, the membrane, the cytoplasm, the membrane and the external suspension. Each of these layers can then be represented by a parallel resistor-capacitor combination according to the passive electrical properties of each layer. Therefore, an equivalent circuit representation of this model can be formed by connecting these *RC* equivalents of all the layers together, as shown in Figure III.5. The resulting equivalent circuit model will allow the evaluation of the transient response to an external electric field to be made. For example, the transient trans-membrane potential will be equivalent to the voltage across the parallel combined $R_M$ and $C_M$.

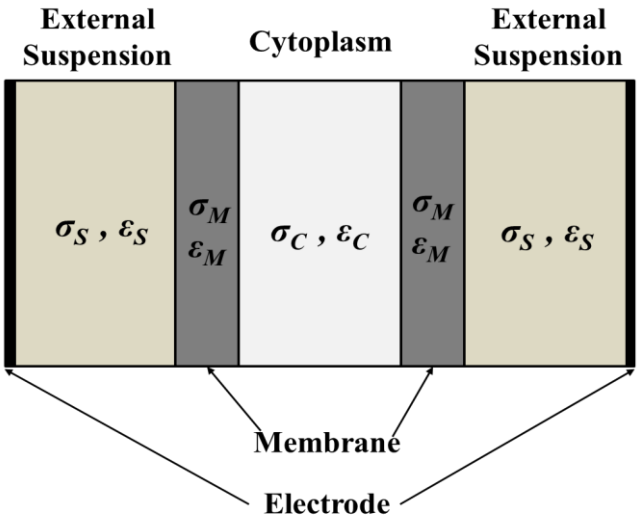


**Figure III.4** 2-dimentional representation of the microbial cell between two electrodes. The figure is for demonstration only, the scale in the figure does not reflect the true ratio between different cell structures.

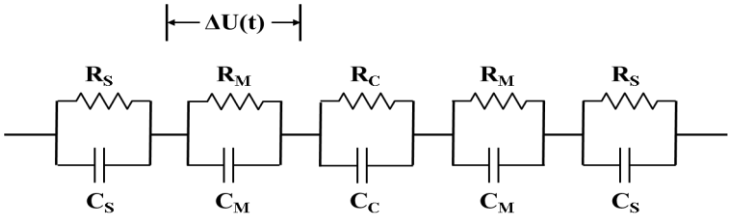


**Figure III.5** Equivalent circuit representation of the 2-dimentional model of microbial.

As mentioned in Section 2.1.1, a microbial cell is normally enclosed by a layer of cell wall outside the cytoplasmic membrane. However, it was widely believed that the main inactivation mechanism of the pulsed electric field treatment is the electroporation process of the cytoplasmic membrane. Therefore, the cell wall was rarely represented in equivalent circuit models of the electroporation process. However, it would be interesting to investigate potential effect of cell wall on the development of trans-membrane potential when the microbial cell is exposed to the external electric field. Therefore, two layers of the cell wall were added to the 2-dimentional cell model. The modified model and its equivalent circuit representation are shown in Figure III.6 and Figure III.7 respectively.

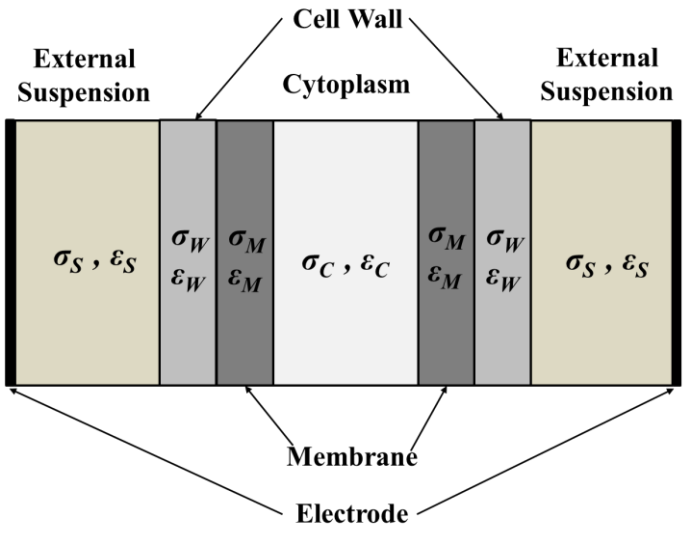


**Figure III.6** 2-dimentional representation of the microbial cell between two electrodes with cell wall included. The figure is for demonstration only, the scale in the figure does not reflect the true ratio between different cell structures.

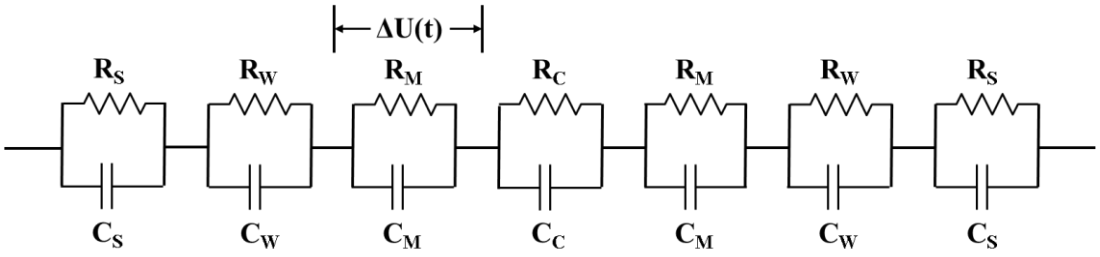


**Figure III.7** Equivalent circuit representation of the 2-dimentional model of microbial including the cell wall.

### 3.1.2 Electrical Properties of Microbial Cell

In order to simulate the transient response to the external electric field using the equivalent circuit model developed in the previous section, the value of the *RC* components needs to be evaluated first. The *RC* equivalents can be determined by the electrical characters of the cell structures. For a 2-dimemtional model, the following equations can be used to estimate the value of *RC* components.

$$R = \frac{d}{\sigma \cdot A} \tag{III.1}$$

$$C = \frac{\varepsilon_0 \cdot \varepsilon_r \cdot A}{d} \tag{III.2}$$

where $d$ is the thickness of each layer of the cell structures, $\sigma$ is the conductivity of each cell structure, $A$ is the surface area of plane parallel to the electrode, $\varepsilon_0$ is the permittivity of free space and $\varepsilon_r$ is the relative permittivity of each cell structure. The electrical properties of each layer of the cell structure will be discussed in the following sections.

#### 3.1.2.1 Cytoplasm

As introduced in Section 2.1.1.3, the cytoplasm is a complex fluid and contains ions, nutrients, proteins, membrane bound organelles and other essential components. All these components can affect the dielectric properties of the cytoplasm. In several

studies, the values of relative permittivity of cytoplasm are provided and they are in the range from 50 to 200, [222-224]. Since the major content of the cytoplasm is water, it was decided to use 80 as the value of relative permittivity of the cytoplasm for the equivalent circuit model used in the present study. The same value was also selected in the modelling works in [6, 206-207].

In terms of conductivity, the cytoplasm can effectively be considered as a highly conductive water solution due to the presence of large amount of ions, [224]. Publications show that the conductivity of cytoplasm can be in the range of 0.2-10 S/m, [222-223 and 225]. In the present model, it was decided to use 0.5 S/m as the conductivity of the cytoplasm, the same value was used in [6].

The thickness of the cytoplasm is effectively the diameter of the microbial cell, as the thickness of membrane and cell wall is 3 orders of magnitude smaller than the diameter of a typical microbial cell. Although the diameter of a microbial cell can vary from ~ 0.2 µm to ~ 700 µm, [11], most of the microorganisms have a cell diameter of a few µm. Therefore, 5 µm was selected as the diameter of the cell, i.e. the thickness of the cytoplasm layer, in the present modelling work. The same value was also used in [6, 206-207].

#### 3.1.2.2 Cytoplasmic Membrane

The cytoplasmic membrane is a thin layer between the cell wall and the cytoplasm, as introduced in Section 2.1.1.2. The basic structure of the cytoplasmic membrane is a phospholipid bilayer with different types of membrane proteins embedded. As a result, the relative permittivity of the membrane was reported to be in the range of 2-10, [222, 224, and 226]. It was decided to use 2 as the relative permittivity of the membrane for the present study, the same as in [6, 174, 206-207, 220-221].

One of the most important functions of the membrane is a selective transport of ions. However, transportation of the ions is regulated by channel proteins, therefore under normal circumstances, the cytoplasmic membrane is regarded as highly non-conducting, [224]. It was reported in [227], where impedance characteristics of the

membrane were investigated in frequency domain, that the membrane showed capacitive characteristic and the capacitance was estimated to be 1.05 μF/cm$^2$ at low frequency. Based on this consideration, the membrane was modelled as an ideal capacitor in several modelling works, [6, 206-207]. However, an estimated conductivity of bio-membrane was found to be reported in the range of $10^{-8}$-$10^{-4}$ S/m, [226-227]. Therefore, $10^{-6}$ S/m was selected as the conductivity of the membrane for the present modelling study.

The thickness of the cytoplasmic membrane was estimated to be ~ 4-10 nm, [11, 224]. As in [6], the thickness of 5 nm was selected to represent the membrane layer in the present 2-dimentional model.

#### 3.1.2.3 Cell Wall

The cell wall is the outermost layer of a microbial cell. Most cell walls have a porous structure in order to exchange small molecules and ions with surrounding environment. As a result of being an ion exchanger, the electrical properties of the cell wall varies with the concentration of the ions in surrounding suspension, [226, 228]. Different studies showed that the conductivity of the cell wall is in the range of 0.01-1 S/m, [227, 229]. The relative permittivity of the cell wall was found to be at 60 in [227]. The thickness of the cell wall varies from 10-80 nm, [11]. It was decided to use 40 nm, 0.1 S/m and 60 as the thickness, conductivity and relative permittivity of the cell wall respectively in the present modelling work.

#### 3.1.2.4 Liquid Suspension

The electrical properties of the liquid suspension which surrounds the microbial cell are different in different PEF experiments. In general, the conductivity of the surrounding suspension is relative high, which can reach ~ 15 S/cm as in [68]. In the modelling studies reported in [206-207], the conductivity of the surrounding suspension was selected to be $10^{-4}$ S/m. However, this value of suspension conductivity is unrealistic in practical PEF treatment. Therefore, it was decided to use 0.1 S/m, which is more commonly used in PEF studies, as the conductivity of the

surrounding suspension in the present model. As for relative permittivity, 80 was widely used in modelling work, [6, 174, 206-207, 220-221]. This is a reasonable estimation as the suspension is a water-based solution in majority of the PEF studies. Therefore, the relative permittivity of surrounding suspension used in the present modelling study was 80. The thickness of the suspension layers in the present 2-dimentional model was 5 μm, which is identical to the diameter of a typical microbial cell.

Based on these considerations, the value of the *RC* representation of each layer in the 2-dimentional model can be calculated according to Equation III.1-III.2. The surface area of each layer was 25 $\mu m^2$ considering a 5 μm cell diameter. The results are listed in Table III.1 and will be used in *PSpice* simulation in Section 3.1.3.

**Table III.1** Electrical parameters used for equivalent circuit model.

| Layer | Thickness | Conductivity | Relative Permittivity | Equivalent Resistance | Equivalent Capacitance |
|---|---|---|---|---|---|
| **Suspension** | 5 μm | 0.1 S/m | 80 | 2 MΩ | 0.00354 pF |
| **Cell Wall** | 40 nm | 0.1 S/m | 60 | 16 kΩ | 0.332 pF |
| **Membrane** | 5 nm | $10^{-6}$ S/m | 2 | 200 MΩ | 0.0885 pF |
| **Cytoplasm** | 5 μm | 0.5 S/m | 80 | 400 kΩ | 0.00354 pF |

### 3.1.3 *PSpice* Simulations

With the value of the *RC* components defined, the equivalent circuit model can now be used to simulate the transient response of the cell to an external electric field in *PSpice*. The equivalent circuit shown in Figure III.7, with *RC* values given in Table III.1, was implemented in *PSpice*. The circuit was connected to a pulse voltage source, which was set up to simulate a square impulse. The square impulse had a rise time and fall time of 10 ps, duration of the ON-time was 5 μs and the magnitude of the impulse was 45 V. As the total thickness of the 2-dimentional model is ~ 15 μm, therefore field strength of 30 kV/cm was simulated. The results of the *PSpice* simulations are shown in Figure III.8.

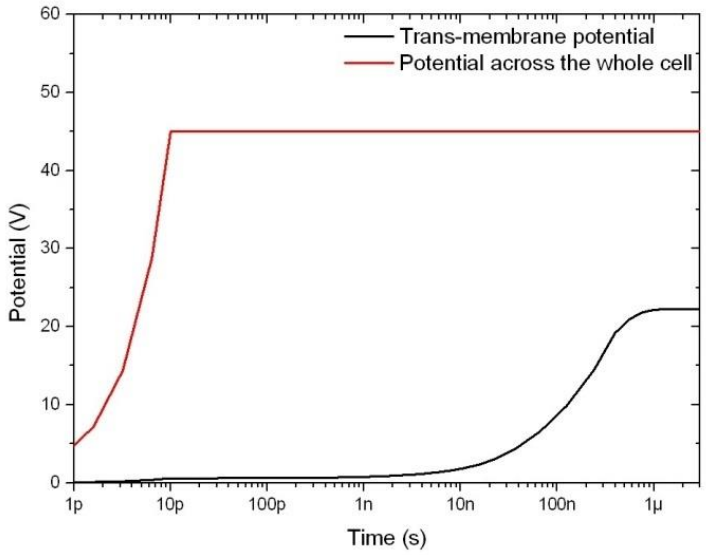


**Figure III.8** *PSpice* simulations using 2-dimentional equivalent circuit model. The black line indicates the dynamic of the trans-membrane potential. The red line shows the transient potential across the whole cell.

As can be seen from Figure III.8, the potential across the whole cell reaches its peak value after ~ 10 ps, which is the rise time of the pulse voltage source. However, the development of the trans-membrane potential is a relatively slow process. The trans-membrane potential starts to develop at ~ 10 ns and reaches its peak value at ~ 1 µs. The delay and slow rate of the process of the development of trans-membrane potential is associated with membrane polarisation and charge accumulation processes as discussed in [6]. In general, the result from the current modelling work shows a good agreement with the simulation results obtained in [206-207]. However, modelling of the cell wall was not conducted in these works while the cell wall was considered in the present study. This suggests the effect of the cell wall on the dynamic of the trans-membrane potential is minimal. To investigate the exact effect of the cell wall on the transient charging process, an equivalent circuit model excluding the cell wall layers (Figure III.5) was also subjected the same pulse voltage source using the same *RC* parameters listed in Table III.1. The dynamic of the trans-membrane potential of the two simulations are compared and showed in Figure III.9.

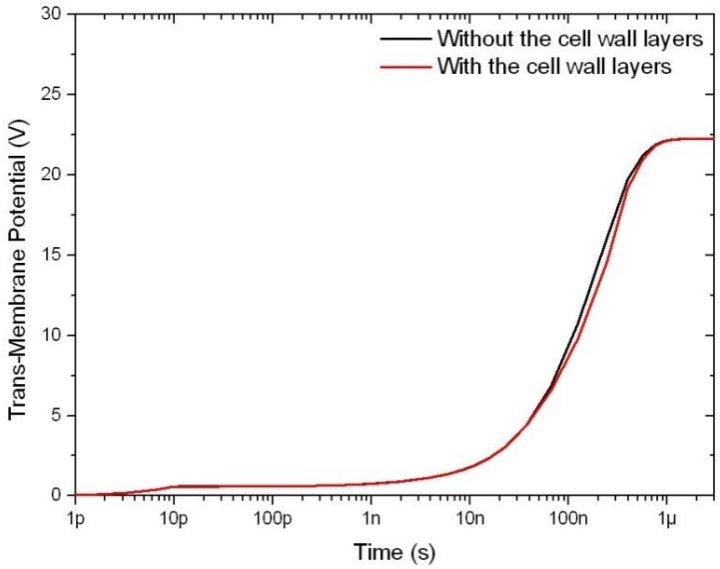


**Figure III.9** Comparison between the transient trans-membrane potentials using the 2-dimentional equivalent circuit models with/without the cell wall layers. Black line: model without the cell wall layers. Red line: model with the cell wall layers included.

The result from this comparison confirmed that the presence of cell wall has a minimum effect of the development of the trans-membrane potential. As can be seen from Figure III.9, the presence of cell wall slightly delays the development of the trans-membrane potential. Apart from this, the dynamic of transient trans-membrane potential is very similar using the two models and the peak magnitude of this potential are the same in both cases. This result can be explained by the unique electrical characteristics of the cell wall. As discussed in Section 3.1.2.3, the cell wall of the microbial cell can be regarded as an ions exchanger and therefore its electrical properties vary with the surrounding suspension. As a result, the conductivity and the relative permittivity of the cell wall are similar to that of the surrounding suspension, as listed in Table III.1. Therefore, the cell wall layer is effectively an extended layer of suspension and has a little impact on the dynamic of trans-membrane potential.

It can be concluded from this equivalent circuit modelling work that the presence of the cell wall has minimum influence on the dynamic of transient membrane potential when the microbial cell is subjected to an external electric field. Neither the

membrane charging time nor the peak trans-membrane potential is significantly affected by the cell wall.

## 3.2 Analytical Model of the Field across Membrane

As introduced in Section 2.5.2, Timoshkin *et al* proposed a novel design of dielectric test cell for PEF treatment in [6]. The transient electric field strength across the microbial membrane during the PEF treatment in such test cell was analysed using an analytical model. Inspired by this paper, a dielectric PEF test cell was designed and developed in the present study. Therefore, the analytical work presented in [6] is considered as important for the present study and it is necessary to introduce and to discuss this model here. This analytical model will be presented in the following sections, the simulation results and the significant findings from this analytical model will be discussed as well.

### 3.2.1 Transient Electric Field across Bio-membrane

The dielectric PEF test cell proposed in [6] consisted of two identical parallel slabs of high permittivity ceramic, as demonstrated in Figure III.10. The space between the dielectric slabs is the treatment region of the PEF test cell which contains microorganism suspension. The other surface of the dielectric slabs is connected to a metal layer, forming the HV and ground electrodes.

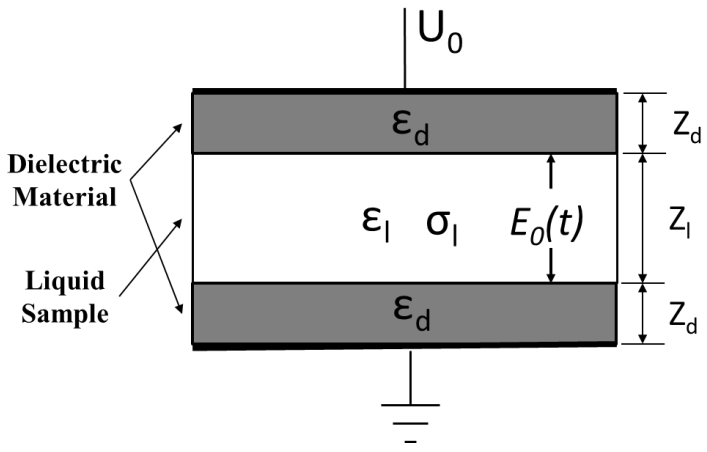


**Figure III.10** Schematic diagram of the PEF chamber with dielectric slabs proposed in [6].

To analyse the dynamic of the electric field inside the treatment region, the Ohmic conduction approach, described in [207], was applied in [6]. Using this Ohmic conduction approach, the time dependent effective field in the treatment region, $E_0(t)$, can be expressed as Equations III.3-III.15. The detailed derivation of these expressions is provided in Appendix A.1.

$$E_0(t) = E_L e^{-t/\tau_f} \tag{III.3}$$

$$E_L = U_0 \left( z_l + 2\frac{\varepsilon_l}{\varepsilon_d} z_d \right)^{-1} \tag{III.4}$$

$$\tau_f = \left( \frac{\varepsilon_l}{\varepsilon_d} + 2\frac{Z_l}{Z_d} \right) \frac{\varepsilon_0 \varepsilon_d}{\sigma_l} \tag{III.5}$$

where $U_0$ is magnitude of the unit step external voltage source, in which potential equals to $U_0$ at $t = 0^+$; $z_d$ and $z_l$ represent the width of the dielectric barrier and treatment region respectively; $\varepsilon_d$ and $\varepsilon_l$ represent the relative permittivity of the dielectric barrier and the liquid suspension in the treatment region respectively; $\varepsilon_d$ is the permittivity of the free space; $\sigma_l$ is the conductivity of the liquid suspension; $E_L$ is the Laplacian electric field in the treatment region and $\tau_f$ is the characteristic field relaxation time, also calls Maxwell-Wagner relaxation time. This time determines the time of existence of the field in the liquid due to the Maxwell-Wagner surface polarisation mechanism.

To investigate the transient potential across the membrane when microbial cell is subjected to the external electric field in the dielectric PEF test cell, a spherical model of a microorganism cell was employed in [6]. As demonstrated in Figure III.11, the membrane of the microbial cell was modelled as a non-conducting spherical shell, which enclosed the cytoplasm and suspended in the surrounding liquid.

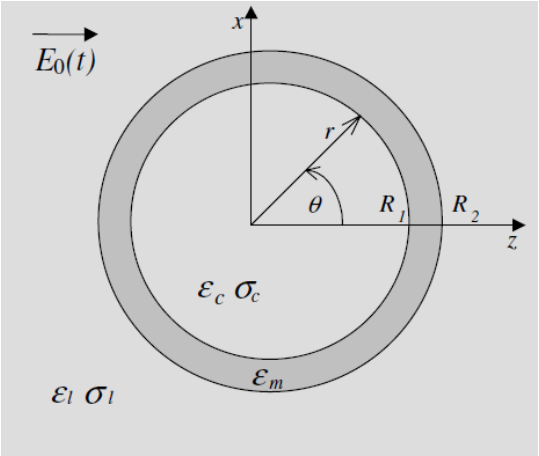


**Figure III.11** Spherical shell model of a microbial cell, figure taken from [6].

A spherical coordinate system has been used to obtain the transient response of the membrane to the time-varying electric field $E_0(t)$. By applying the same Ohmic conduction approach, the time dependent maximum electric field on the membrane, which occurs at the 'poles' of the membrane, can be written as Equation III.6. The detailed derivation of this expression and its coefficients is provided in Appendix A.2.

$$E_{max}(t) = -A_m(t) + 2B_m(t) \cdot R_1^3 \qquad \text{(III.6)}.$$

where $R_1$ is the radius of the cytoplasm region; $A_m(t)$ and $B_m(t)$ are coefficients relating to: radius of the cytoplasm ($R_1$) and the microbial cell ($R_2$); relative permittivity of the cytoplasm($\varepsilon_c$), the membrane ($\varepsilon_m$) and the surrounding liquid ($\varepsilon_l$); conductivity of the cytoplasm ($\sigma_c$) and the surrounding liquid ($\sigma_l$); the Laplacian electric field in the treatment region ($E_L$); and the Maxwell-Wagner relaxation time ($\tau_f$).

The analytical model developed above can now be used to model the transient response of the trans-membrane potential to an external electric field in a dielectric PEF test cell. The modelling of this transient process was conducted using *Matlab* software and the parameters used in the model are shown in Table III.2. The result of this analytical model is showed in Figure III.12.

**Table III.2** Parameters used for the analytical model

| Parameter | Value |
|---|---|
| External voltage | 30 kV |
| Thickness of the dielectric slab, $z_d$ | 5 mm |
| Width of the treatment region, $z_l$ | 1 cm |
| Radius of the cytoplasm, $R_1$ | 5 µm |
| Radius of the cell, $R_2$ | 5.005 µm |
| Relative permittivity of the dielectric slab, $\varepsilon_d$ | 3000 |
| Relative permittivity of the cytoplasm, $\varepsilon_c$ | 80 |
| Relative permittivity of the membrane, $\varepsilon_m$ | 2 |
| Relative permittivity of the surrounding liquid, $\varepsilon_l$ | 80 |
| Conductivity of the cytoplasm, $\sigma_c$ | 0.5 S/m |
| Conductivity of the membrane, $\sigma_m$ | 0 S/m |
| Conductivity of the surrounding liquid, $\sigma_l$ | 0.01 S/m |

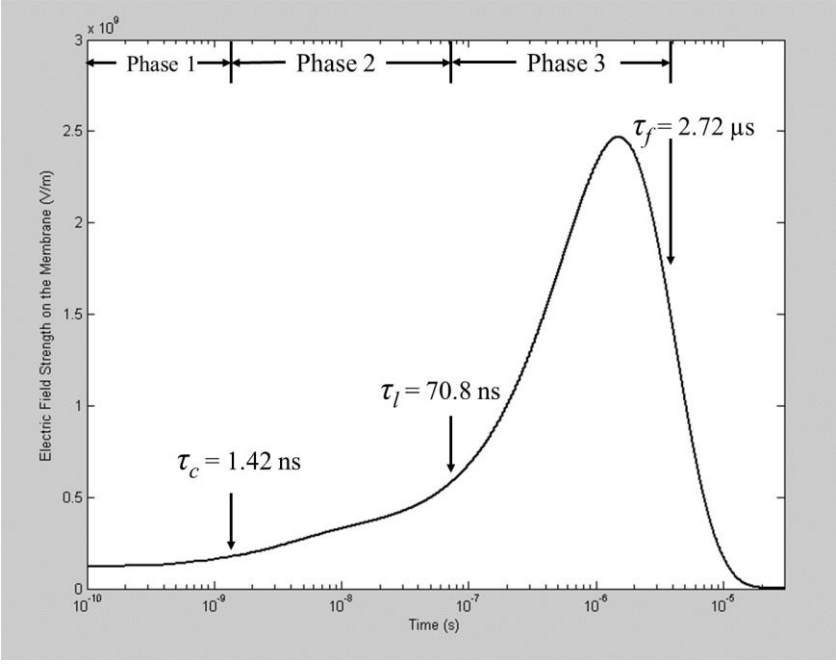


**Figure III.12** The transient response of the electrical field at the poles of a spherical membrane.

As can be seen from the figure, the evolution of the membrane potential after the application of external voltage is a relatively slow process, which is in reasonable agreement with the result of equivalent circuit model. The development of the electric field in the membrane was separately described in 3 distinct physical phases in [6].

In phase 1, shortly after the application of the voltage, the polarization processes in the membrane, the cytoplasm and the surrounding liquid have purely dielectric characters. The electric field is determined solely by the dielectric permittivity of these layers of the cell during this phase. The duration of this phase is defined by the characteristic time of the highly conductive cytoplasm $\tau_c = \varepsilon_0 \varepsilon_c / \sigma_c$, which is 1.42 ns in the present analytical model.

In the second phase, free charges start to accumulate on both internal and external surfaces of the membrane due to the ionic motion in the electric field. The characteristic time of cytoplasm ($\tau_c$) and surrounding liquid ($\tau_l$) determine the duration of this charge accumulation process on internal and external surfaces of the membrane respectively. As the conductivity of the surrounding liquid is much lower than the conductivity of the cytoplasm, the characteristic time of the surrounding liquid is much longer than that of the cytoplasm. Therefore the duration of this phase is determined by the longer characteristic time $\tau_l$, which is 70.8 ns in the present analytical model.

In phase 3, free charges continue to accumulate on the external surface and the electric field on the membrane tends to reach its maximum steady state value. However, with the presence of the dielectric barrier, the effective electric field inside the treatment region starts to decrease due to the Maxwell-Wagner field relaxation process, as discussed in Section 3.2.1. This field relaxation process results a drop in the electric field on the membrane. The duration of this phase is determined by the Maxwell-Wagner field relaxation time $\tau_f$, which is 2.72 μs in the present analytical model.

It can be learned from the above analysis that the Maxwell-Wagner field relaxation process has a significant impact on the dynamic of trans-membrane potential in a dielectric PEF test cell. Unlike the conductive PEF cell, maximum steady state electric field on the membrane could not be reached or maintained due to this field relaxation process in a dielectric PEF cell.

### 3.2.2 Effects of Cell Properties on Transient Field across Membrane

As discussed in Section 3.2.1, the transient trans-membrane potential is determined by different electrical and physical parameters of the microbial cells in a dielectric PEF test cell. However, only the typical values were selected for these parameters in the modelling described in Section 3.2.2. Although the selected parameters and the resulting field is a good representation of parameters used for the PEF treatment of microorganisms, it is important to investigate the effect of variation of these parameters on the transient process in the dielectric PEF test cell. As discussed in Section 3.1.2, the electrical and physical properties of microbial cells vary. Therefore, it was decided to conduct additional modelling using the varying parameters listed in Table III.3. When one of the parameters was being investigated, the rest of the parameters were set to the typical value. The results of this investigation are showed in Figure III.13-III.20.

**Table III.2** Varying Parameters used for the analytical model

| Parameter | Typical Value | Range |
|---|---|---|
| Radius of the cytoplasm, $R_1$ | 5 µm | 0.1 - 350 µm |
| Thickness of membrane, $d = R_2 - R_1$ | 5 nm | 4 – 10 nm |
| Conductivity of the cytoplasm, $\sigma_c$ | 0.5 S/m | 0.2 - 10 S/m |
| Relative permittivity of the membrane, $\varepsilon_m$ | 2 | 2 – 10 |

#### 3.2.2.1 Size of the Microbial Cell

Figure III.13 and Figure III.14 show the effects of varying cell diameter on the maximum field across bio-membrane. Figure III.13 compares the transient response

for the electrical field in the membrane using the upper value, typical and lower values of cell radius. Figure III.14 shows the change in maximum electric field in the membrane as a function of the radius of the cell. It can be seen from these two figures that the size of the microbial cell produces a significant impact on the development of the electric field strength across the membrane in the dielectric PEF test cell. The maximum field strength across the membrane increases significantly as the diameter of the microbial cell increase, which suggests that microorganisms with a larger cell radius will be subjected to a higher trans-membrane potential during PEF treatment using the dielectric PEF test cell. As a result, lethal electroporation process is more likely to occur in microorganisms with a larger cell size when the subjected to the same treatment conditions as compared with smaller microorganisms. This finding shows a good agreement with the PEF study reported in [185, 213]. This conclusion is confirmed experimentally in [185] and [213] that microorganisms with larger cell size are more susceptible to the PEF treatment than the microorganisms with smaller cell size. It should be noted that PEF studies in [185, 213] were conducted using a traditional metallic PEF test cell. Therefore, this finding from the present modelling study indicates that similar result should be observed using the dielectric PEF test cell.

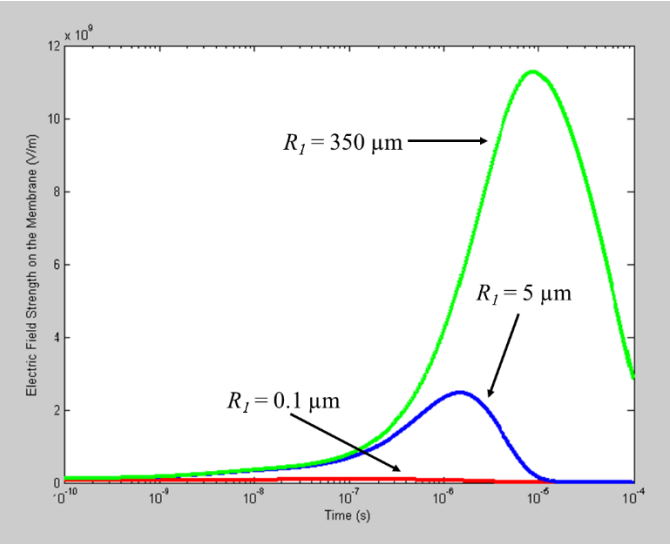


**Figure III.13** The transient response of the electrical field at the poles of a spherical membrane with different cytoplasm radiuses: $R_1$ = 350 µm (green line); $R_1$ = 5 µm (blue line); $R_1$ = 0.1 µm (red line).

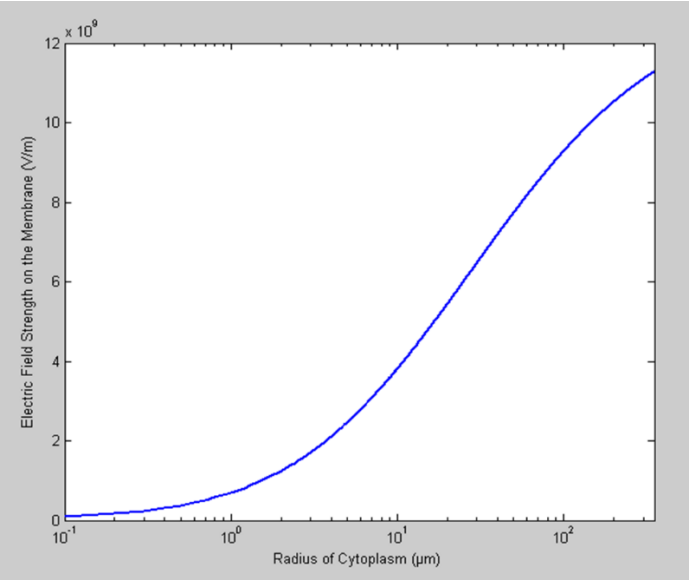


**Figure III.14** Maximum electric field across the membrane as a function of the radius of the cytoplasm.

### 3.2.2.2 Thickness of Membrane

Figure III.15 and Figure III.16 show the effects of varying membrane thickness on the development of the field across the membrane. Figure III.15 compares the transient response of the electrical field in the membrane using the upper, typical and lower values of membrane thickness. Figure III.16 shows the change in maximum electric field across the membrane as a function of the membrane thickness. It can be seen from the figures that the thickness of the membrane has a notable impact in the development of the electric field strength on the membrane in the dielectric PEF test cell. The maximum field strength on the membrane decreases gradually as the thickness of the membrane increases. However, in the range of parameters being investigated, the resulting maximum electric fields across the membrane had the same order of magnitude for all tested parameters. As value of the membrane thickness does not vary significantly for different microorganisms and remains in the range of 4-10 nm as reported in literature. The results obtained in the present study suggested that membrane thickness does not affect the transient value of electric field across the membrane as significant as the size of the microbial cell.

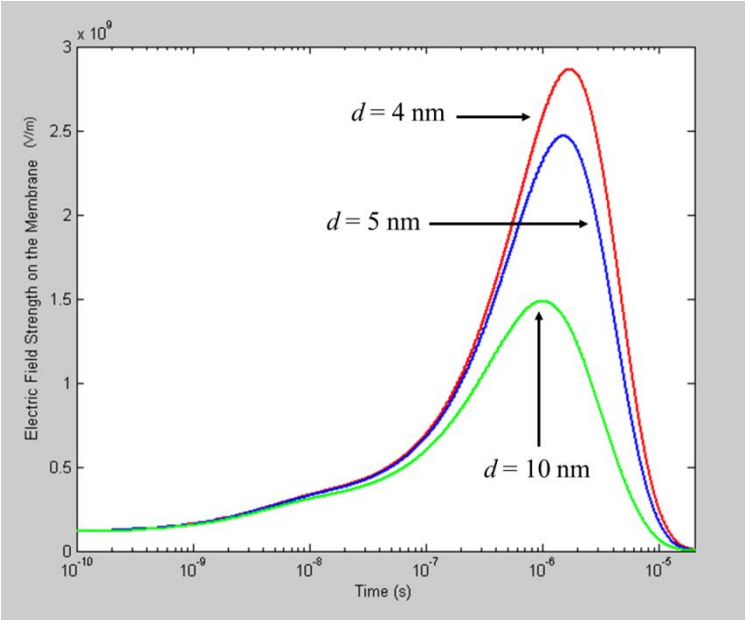


**Figure III.15** The transient response of the electrical field at the poles of a spherical membrane with different membrane thickness: $d$ = 10 nm (green line); $d$ = 5 nm (blue line); $d$ = 4 nm (red line).

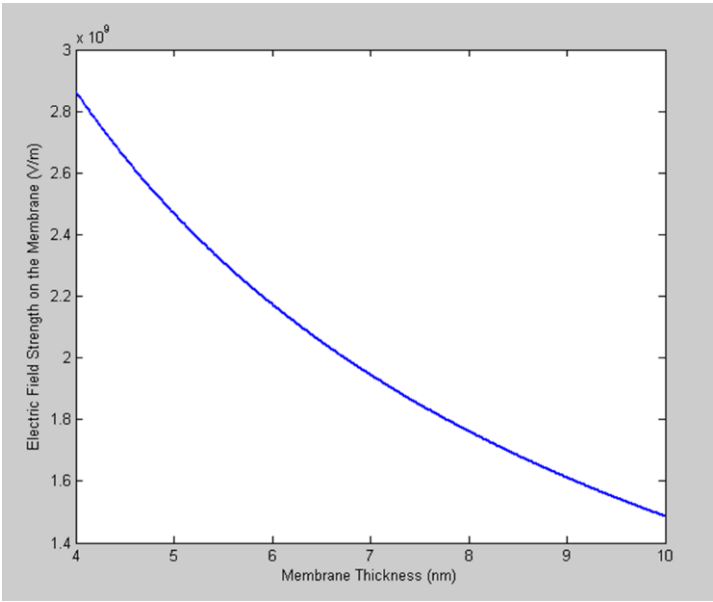


**Figure III.16** Maximum electric field across the membrane as a function of the thickness of the membrane.

### 3.2.2.3 Electrical Conductivity of Cytoplasm

Figure III.17 and Figure III.18 show the effects of varying conductivity of cytoplasm. Figure III.17 compares the transient response of the electrical field in the membrane

using the higher, typical and lower values of the electrical conductivity of cytoplasm. Figure III.18 shows the change in the maximum electric field across the membrane as a function of the electrical conductivity of cytoplasm. It can be seen from the figures that the electrical conductivity of cytoplasm has a minimal impact in the development of the electric field strength across the membrane in the dielectric PEF test cell. As indicated in Figure III.17, the difference in cytoplasm conductivities only affects the first phase in the transient process. As discussed in Section 3.2.1, the initial phase of the transient process is the polarisation process in the cell. This phase which lasts up to $10^{-8}$ s is purely governed by the dielectric characters of different cell structure, especially by the highly conducting cytoplasm. Therefore, the cytoplasm conductivity affects the polarisation process significantly. However, as demonstrated in Figure III.18, the maximum field strength across the membrane barely changes as the cytoplasm conductivity changes. This is because the second and third phases of the transient process are mainly governed by the electrical properties of the membrane and the surrounding liquid. Therefore, as the present study suggested, the cytoplasm conductivity produces insignificant effect on the transient process of the trans-membrane potential for the range of parameters which were being used in the present study.

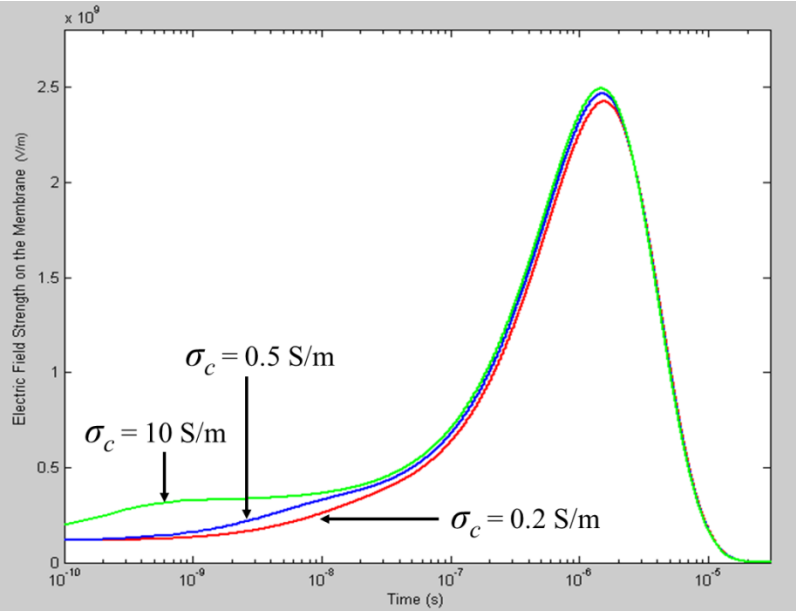


**Figure III.17** The transient response of the electrical field at the poles of a spherical membrane with different cytoplasm conductivity: $\sigma_c$ = 10 S/m (green line); $\sigma_c$ = 0.5 S/m (blue line); $\sigma_c$ = 0.2 S/m (red line).

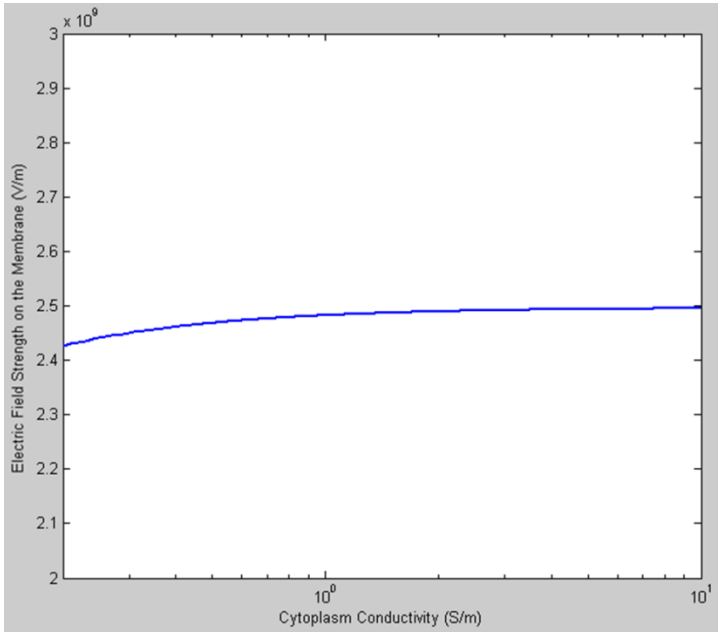


**Figure III.18** Maximum electric field across the membrane as a function of the conductivity of the cytoplasm.

#### 3.2.2.4 Relative Permittivity of Membrane

Figure III.19 and Figure III.20 show the effects of variation in the relative permittivity of the membrane on the transient electric field. Figure III.19 compares the transient response of the electrical field across the membrane using the upper, middle and lower (typical) values of the relative permittivity of membrane. Figure III.20 shows the change in the maximum electric field across the membrane as a function of the relative permittivity of the membrane. It can be seen from these figures that the relative permittivity of membrane has a notable impact on the development of the electric field strength across the membrane in the dielectric PEF test cell. The maximum field strength across the membrane reduces as the relative permittivity of the membrane increases. However, for the range of permittivity used in the present study, the maximum field across the membrane has the same order of magnitude. On the other hand, lower $\varepsilon_m$ results in a slightly faster Maxwell-Wagner field relaxation process, as demonstrated in Figure III.19. In general, it can be concluded that relative permittivity of membrane influences the transient development of the trans-membrane potential in the dielectric PEF test cell. Accurate estimation of this value could provide a better understanding of the transient electro-

mechanical mechanisms which could result into lethal electroporation effects during PEF treatment.

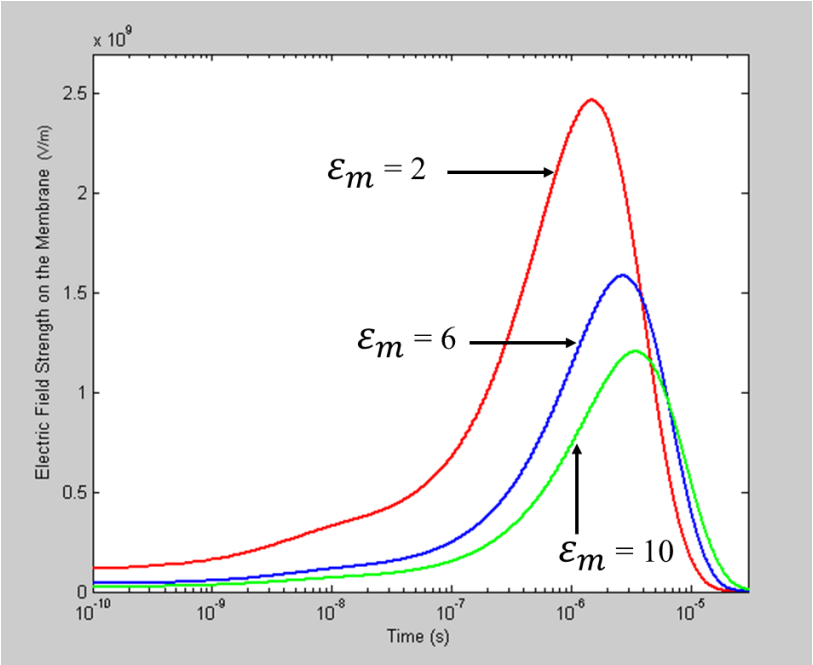


**Figure III.19** The transient response of the electrical field at the poles of a spherical membrane with different relative permittivity of membrane: $\varepsilon_m$ = 10 (green line); $\varepsilon_m$ = 6 (blue line); $\varepsilon_m$ = 2 (red line).

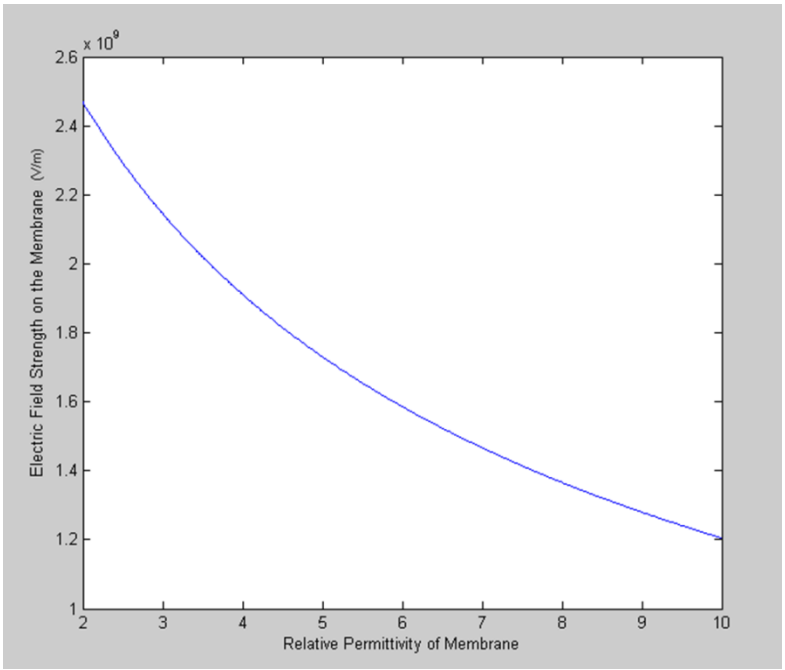


**Figure III.20** Maximum electric field across the membrane as a function of the relative permittivity of the membrane

### 3.2.3 Effects of Electrical Conductivity of Suspension on Transient Field across Membrane

The analysis conducted in the previous section reveals the significance of different electrical and physical properties of the microbial cell in the transient process of the trans-membrane potential and electric field in a dielectric PEF test cell. However, these parameters are determined by the microorganism's natural properties and they are beyond control in a practical PEF process. Therefore, investigation into the effect of controllable parameters on transient fields across membrane can provide valuable information for optimisation of the practical PEF process.

As was shown in Section 3.2.2, the Maxwell-Wagner field relaxation process has a significant impact on the dynamic of trans-membrane potential and field in the dielectric PEF test cell. Unlike in the case of the conductive PEF test cell, the maximum steady state electric field across the membrane could not be reached or maintained due to this field relaxation process in the dielectric PEF test cell. As can be seen from Equation III.5, $\tau_f$ is determined by several parameters, such as the ratio between the thickness of the dielectric barrier and the width of the treatment region, the permittivity of the dielectric barrier, and the conductivity of the surrounding liquid. Among all these factors, the conductivity of the surrounding liquid is the only controllable parameter in a practical PEF process. Therefore, it is necessary to find out an optimal conductivity range for preparation of the practical PEF study. It was decided to investigate the effect of the liquid conductivity on the dynamic of the transient trans-membrane potential and field using the analytical model with conductivity value which varies in the range $10^{-6}$-$10^{1}$ S/m. The results of this investigation are shown in Figure III.21-III.23.

As can be seen from these figures, the suspension conductivity has significant influence on the development of the transient trans-membrane potential. Figure III.21 compares the transient response of the electrical field across the membrane for the upper, typical and lower values of the suspension conductivity. Figure III.22 shows the maximum electric field across the membrane in the dielectric test cell as a function of the electrical conductivity of the suspension. The figure shows that, for

conductivity less than $10^{-1}$ S/m, the maximum electric field will not be affected significantly by the choice of liquid suspension. However, once the conductivity exceeds 0.1 S/m, the maximum field observed across the membrane drops significantly, as demonstrated in Figure III.21 (green line). On the other hand, as shown in Figure III.21 (red line) and Figure III.23, low conductivity can significantly increase the time required for the electric field across the membrane to reach its maximum value. Therefore, taking both findings into consideration, it can be suggested that a suspension with the electrical conductivity in the range of $10^{-3}$-$10^{-2}$ S/m should be used for the optimal development of trans-membrane potential, as a relatively short time is required for the membrane electric field to reach its relatively high maximum value.

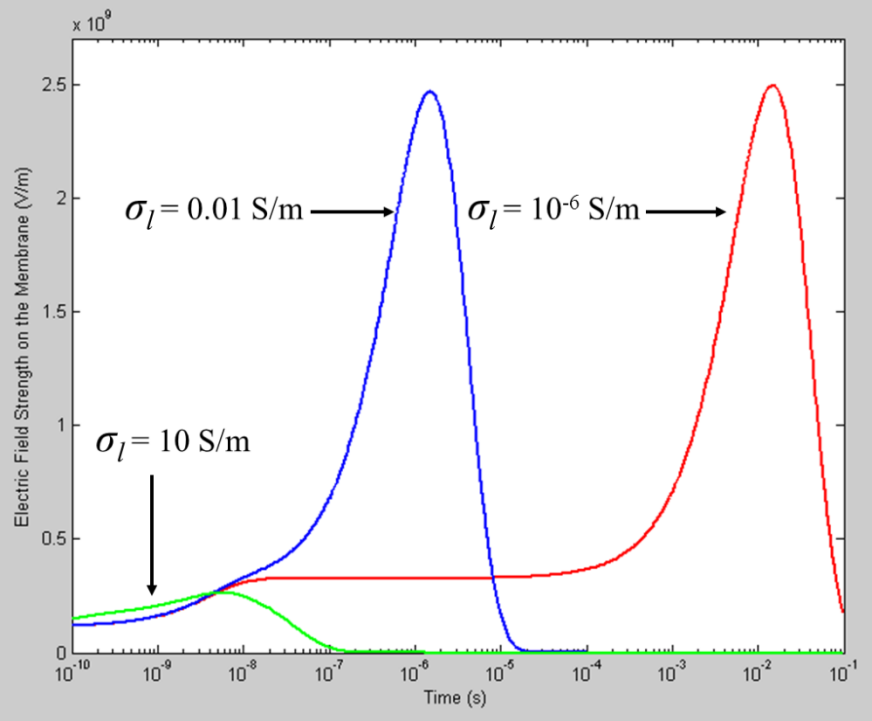


**Figure III.21** The transient response of the electrical field at the poles of a spherical membrane with different suspension conductivity: $\sigma_c$ = 10 S/m (green line); $\sigma_c$ = 0.01 S/m (blue line); $\sigma_c$ = $10^{-6}$ S/m (red line).

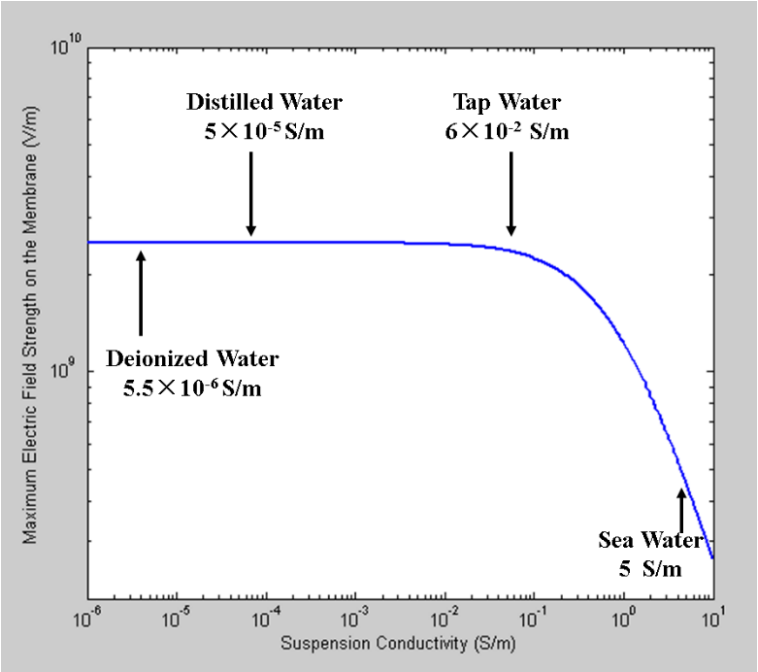


**Figure III.22** Maximum electric field across the membrane as a function of the conductivity of the surrounding liquid. Conductivity of typical liquids are also highlighted in the figure.

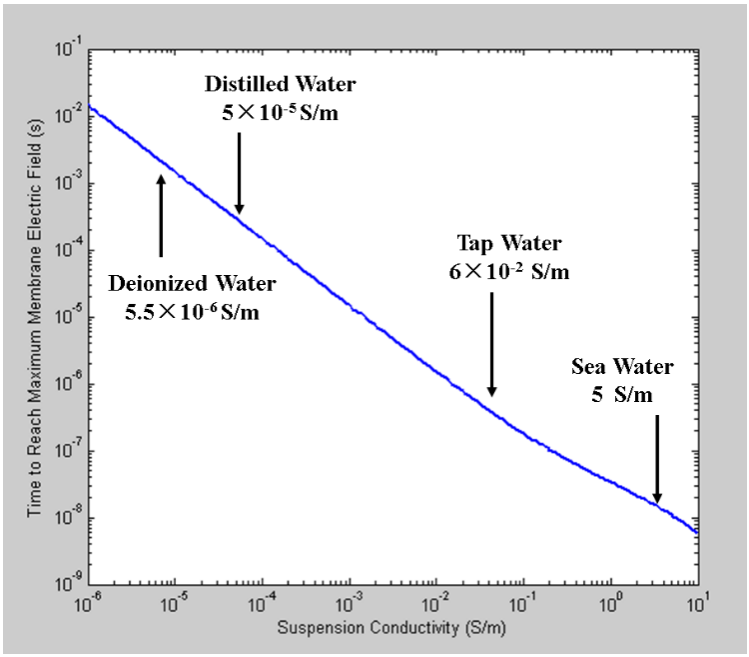


**Figure III.23** Time required reaching maximum electric field across the membrane as a function of conductivity of surrounding liquid. Conductivity of typical liquids are also highlighted in the figure.

## 3.3 Discussion

This chapter was focussed on the analysis of the transient behaviour of the field across the membrane of the microorganism in suspension in a non-conductive dielectric PEF cell. The developed models include an equivalent circuit model and an analytical model. The obtained results provide a better understanding of the transient process during the PEF treatment and lead to useful suggestions for practical design of PEF systems and optimisation of experimental PEF studies.

A 2-dimensional equivalent lumped element circuit model of the microbial cell, which includes a cell wall, was developed and the transient process in the cell was modelled using *OrCAD® PSpice* software. The transient response to the application of an external electric field was simulated using this model. The results obtained in this study indicated that the development of the trans-membrane potential is a relatively slow process (~1μs), which is in a good agreement with other models presented in the literature, [206-207]. The results of this study also revealed that the cell wall has a minimum impact on the dynamic of trans-membrane potential and field as the cell wall, from the electrical point of view, is effectively an extended layer of the surrounding suspension.

The analytical model based on the work in [6] was introduced and analysed in this chapter. This analytical modelling was conducted using the *MathWork® Matlab* software in order to investigate the transient response of the trans-membrane potential to an external field in a dielectric PEF test cell. The proposed PEF test cell consisted of two identical parallel slabs of high permittivity ceramic which form a treatment region between them filled with a liquid suspension. The results obtained using this analytical model indicate that the Maxwell-Wagner field relaxation process has a significant impact on the dynamic of trans-membrane potential and field in the dielectric PEF test cell. Unlike the conductive PEF test cell, the maximum value of the electric field across the membrane could not be reached or maintained due to fast field relaxation process.

Additional analysis has also been conducted to investigate the effect of different electrical and physical properties of the microbial cell on the dynamic of transient membrane electric field. The results obtained in this chapter suggest that the size of the microbial cell has a significant impact on the development of the field strength across the membrane. Microorganisms with a larger cell size will be subjected to a significantly higher trans-membrane potential during PEF treatment using the dielectric PEF test cell. Other parameters such as membrane thickness, cytoplasm electrical conductivity and relative permittivity of the membrane, have less significant influence on the transient process of the field strength across the membrane in the dielectric PEF test cell. Similar analysis has also been conducted to investigate the effect of the electrical conductivity of the suspension on the dynamic of transient membrane electric field. The result from this analysis suggests that the suspension with conductivity in the range of $10^{-3}$-$10^{-2}$ S/m should be used in the practical PEF studies for the optimal development of trans-membrane potential.

Based on the conducted analysis and obtained and discussed results, the parameters for practical PEF study has been developed and this study will be conducted in the next phase of the present project. The design of the PEF system including PEF test cell, the design of the PEF study based on this system and the obtained results will be discussed in the following chapters.

# Chapter IV

# DEVELOPMENT OF THE PEF TEST CELL AND PEF SYSTEM

## 4.0 General

This chapter presents the initial development of the PEF test cells and the PEF system. Two PEF test cells, a traditional test cell with stainless steel electrodes and a novel PEF test cell with ceramic electrodes, have been designed and manufactured at this stage of the research. Stainless steel was selected as the electrode material due to its corrosion resistance and relatively low electro-chemical reactivity, as discussed in Section 2.5.4.3. This material is a typical choice for the electrode of the tests systems used in pulsed electric field inactivation experiments and industrial installations, [7, 113, 230-232]. The ceramic capacitor with one electrode removed, due to its high permittivity and non-conductive characteristic, was selected as electrodes in the non-conductive PEF test cell, which was proposed in [6]. Based on the previously published papers, [7, 8, 113, 230, and 233], it has been decided to design both PEF test cells using parallel-plane topology. The PEF treatment system, which consists of the designed test cells, an HV pulse generator and some accessories, will also be described in this chapter.

## 4.1 Design of Metallic PEF Test cell

A PEF test cell equipped with parallel plane stainless steel electrodes was designed and developed. This treatment PEF cell was used in a number of pulsed electric field inactivation tests which produced encouraging results. The inactivation results obtained with this test cell will be presented and discussed in Chapter V. However, during the PEF tests, some drawbacks in the design of this PEF test cell were exposed. These drawbacks include trapping air bubbles, potential dead zones and

field strength limitation, and will be discussed in Chapter VI. All these factors limited successful application of this PEF test cell for the pulsed electric field inactivation.

### 4.1.1 PEF Test cell Topology

One of the most popular PEF test cell electrode topology is a parallel-plane electrode topology, [7, 8, 113, 230, and 233]. In order to eliminate potential field enhancement at the electrode edges, disk-shaped electrodes were used in the PEF test cell. Figure IV.1 shows the exploded view of the PEF test cell used in the PEF tests presented in this Chapter. The test cell body is made of nylon. Two stainless steel electrodes are separated by a 3-mm thick dielectric spacer. When fully assembled, the electrode sits between the spacer and a dielectric cover. There are 4 outstanding screws evenly distributed over the exterior of the test cell, these nylon screws pass through the holes in the test cell body and are fixed by screw caps in order to keep the test cell tightly assembled. Figures IV.2 - IV.4 show the cross-sectional view of the three test cell components, the cover, the electrode and the spacer, respectively. In order to transfer the liquid suspension in and out of the test cell, a small inlet hole was drilled in the spacer. A simplified cross-sectional view of the assemble PEF test cell is shown in Figure IV.5.

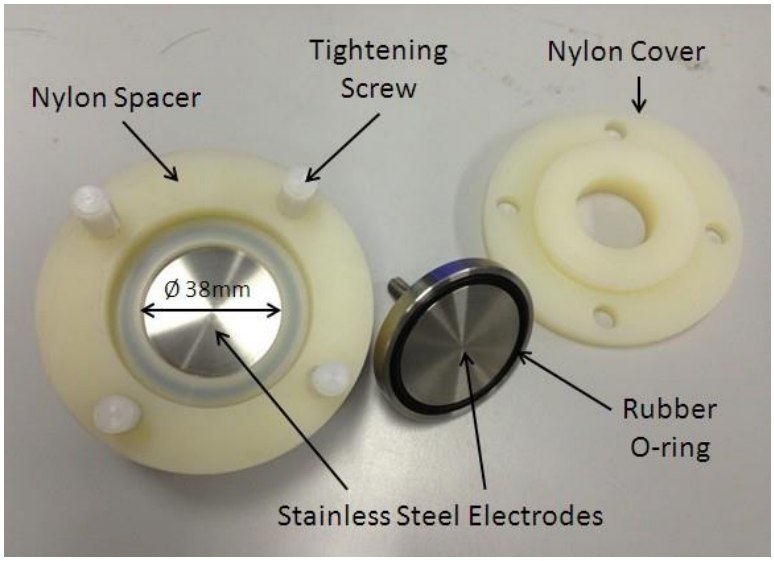


**Figure IV.1** Exploded view of the stainless steel PEF test cell.

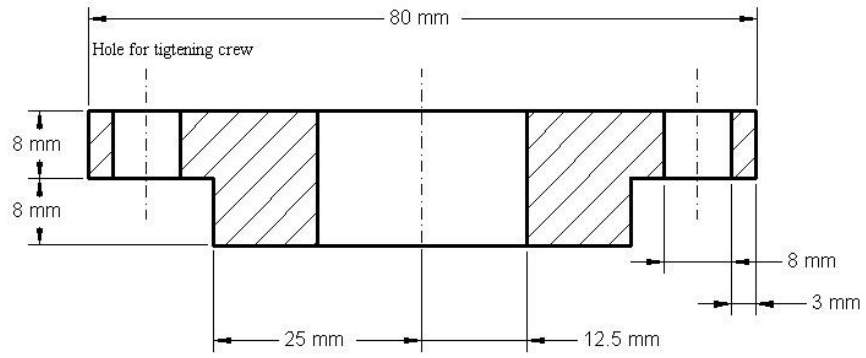


**Figure IV.2** Cross-sectional view of the cover of the metallic cell design.

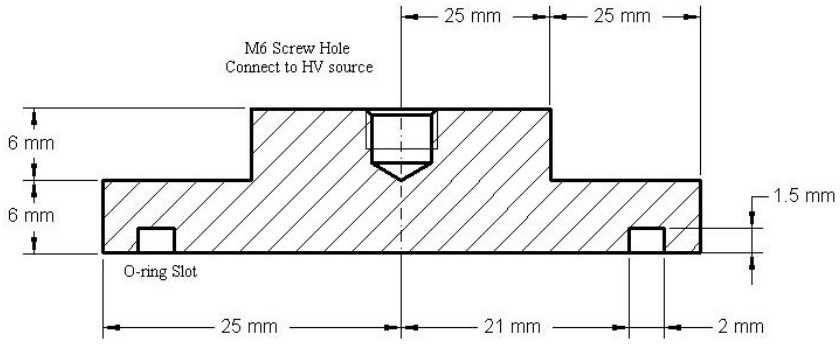


**Figure IV.3** Cross-sectional view of the electrode of the metallic cell design.

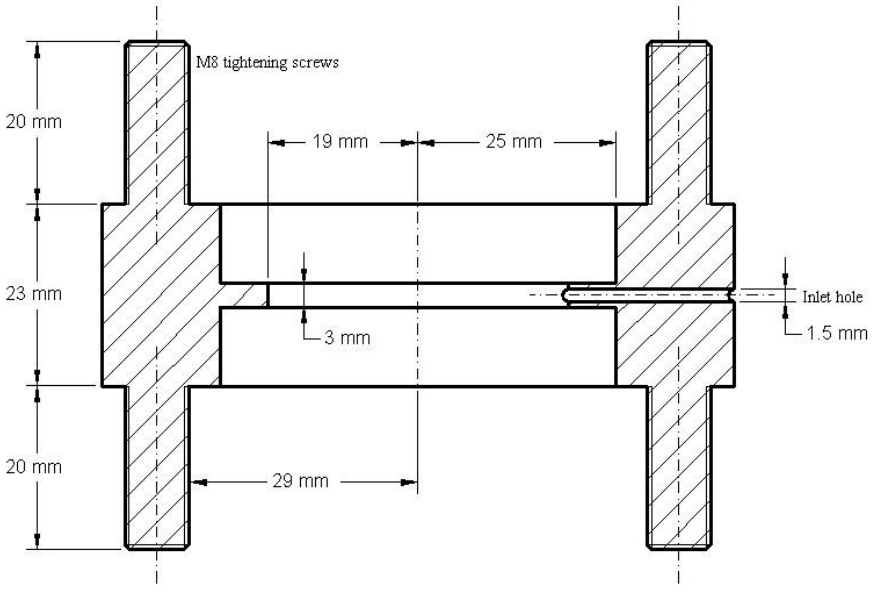


**Figure IV.4** Cross-sectional view of the spacer of the metallic cell design.

As discussed in Section 2.5.4.1, in the PEF treatment systems developed in [67, 68, 197, and 204], the field strength was usually selected to be above 30 kV/cm in order to achieve reliable and effective PEF inactivation of microorganisms. The electric field across the sample in the PEF test cell can be calculated by the following equation:

$$E = \frac{V}{d} \tag{IV.1}$$

where $V$ is the voltage applied to the PEF cell electrodes and $d$ is the distance between the electrodes. As the pulse generator used in the project had a maximum output of 30 kV, an inter-electrode distance of 1 cm will provide the field strength required for effective PEF treatment. However, as mentioned in Section 2.6, one of the project aims was to investigate the efficiency of the PEF treatment using a higher field strength. Therefore, the inter-electrode distance in this initial PEF test cell design was set to 3 mm, which provided a maximum field strength of 100 kV/cm and covered the range of field strengths required in the present research project.

The radius of the exposed electrode surface, where liquid sample with microorganism is in direct contact with the electrodes, was 19 mm. The resulting volume of the test cell was 3.4 ml, which provided sufficient amount of liquid suspension for assessment of the PEF treatment performance. The diameter of the inlet port was 1.5 mm, which allowed the needle of the syringe to pass through.

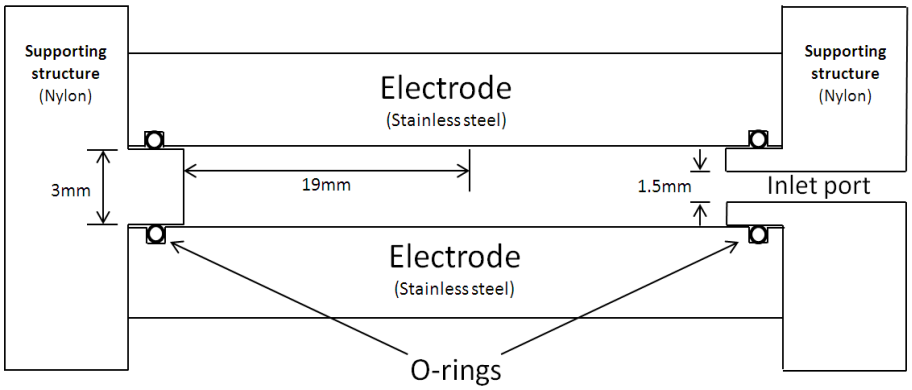


**Figure IV.5** Simplified cross-sectional view of assemble test cell.

A proper sealing of the test cell is essential for conduction of PEF experiments. Leakage of the liquid suspension from the test cell will not only create inaccurate results but also introduce air bubbles inside the test cell, which will certainly result in an electrical breakdown under this level of field strength. The sealing was achieved by introducing rubber O-ring slots on the surface of the electrodes, as can be seen in Figure IV.1 and Figure IV.5. Two rubber O-rings were tightly fit into the slot on each electrode. The test cell was sealed as the electrodes were pressed towards the spacer.

### 4.1.2 Selection of Materials

As discussed in Section 2.5.4.3, variety of different metals has been used to manufacture electrodes for PEF test cells, including copper, aluminium and stainless steel. Among all the material, stainless steel was most widely used in PEF treatment as it is regarded a safe material when in contact with foodstuff. Electro-chemical reactions, which introduce undesirable ions and other toxic chemical by-product into the sample, are likely to occur when copper or aluminium is used as electrodes, [165, 209-210]. Although these by-products may help to achieve higher degree of inactivation of microorganisms being treated, the main focus of this research project was to investigate the effect of electric field in the PEF treatment. Therefore, stainless steel was selected as material for manufacturing the PEF test cell electrodes.

In terms of the spacer and cover, several factors were taken into consideration during selection of appropriate materials. Firstly, the dielectric strength of this material should be sufficient to withstand the applied electric field. Secondly, the machinability of the material needs to allow accurate machining. Thirdly, the rigidness of the material should be relatively high to maintain the required geometric parameters when the test cell is assembled. The cost of the material also should be considered. Taking all those factors into considerations, nylon, with dielectric strength of 236 kV/cm [234], was selected as the material of the spacer and covers.

## 4.2 Design of Dielectric PEF Test cell

The main objective of this research project was to investigate the feasibility of using of a non-conductive test cell in the PEF process. To implement this idea, a dielectric test cell with two non-conducting electrodes, created from ceramic capacitors, was also designed and built.

### 4.2.1 Selection of the Material

As discussed in Section 2.5.4.3, the basic idea of the non-conductive PEF test cell is to cover the metallic electrode with a layer of dielectric barrier, as demonstrated in Figure IV.6. In the figure, $Z_d$ and $Z_l$ represent the width of the dielectric barrier and liquid suspension respectively and $\varepsilon_d$ and $\varepsilon_l$ represent the relative permittivity of the dielectric material and the liquid suspension respectively. In this model, the static state electric field strength across the liquid suspension can be evaluated by the following equation:

$$E_l = \frac{U_0}{Z_l + 2\frac{\varepsilon_l}{\varepsilon_d} Z_d} \tag{IV.2}$$

It can be concluded from the equation that, the ratio between the permittivity of the liquid suspension and the dielectric barrier has a significant impact on the field strength in the sample. The permittivity of the dielectric barrier needs to be higher than the permittivity of the liquid suspension to ensure sufficient field is applied to the sample. If $\varepsilon_d$ is equal to or less than $\varepsilon_l$, the field will be concentrated on the dielectric barrier, resulting in much lower field in the suspension. As the liquid suspension contains mostly water, the value of $\varepsilon_l$ is around 80. Therefore, the relative permittivity of the dielectric material needs to be at least 80 or higher. Some of the dielectric materials, such as nylon and PTFE, are therefore not suitable for this application as the relative permittivity of these materials is only ~ 2.

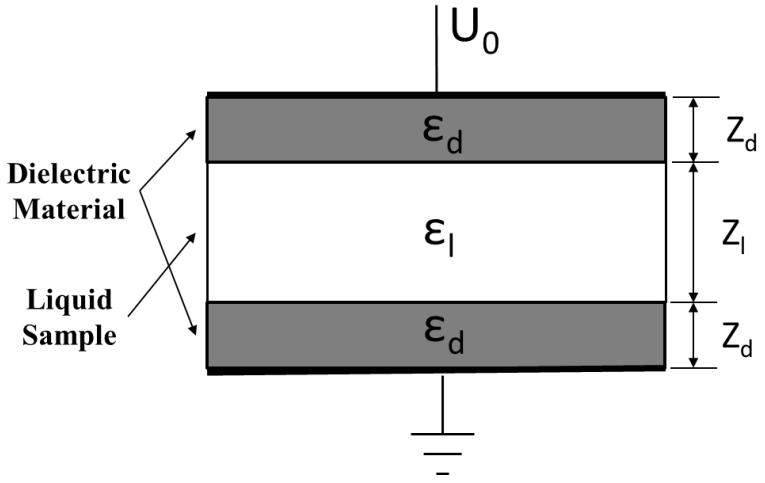


**Figure IV.6** Schematic diagram of the proposed PEF test cell with dielectric barriers.

The initial idea was to use an adhesive to bond the metallic electrode to a layer of high permittivity dielectric material. However, such approach raised technical difficulties in manufacturing. It was advised by the manufacturing staff that solid and uniform bonding between such two materials was difficult to achieve. In addition, the presence of the adhesive between the dielectric and the metallic electrode would introduce additional complexity in field distribution within the test cell. Therefore, alternative approach should be considered.

After reconsideration, it was decided to use a body of the commercially available high voltage ceramic capacitor as a potential alternative electrode. The permittivity of ceramic material used in the HV capacitors is typically in the range from a few 100's to few 1000's. Figure IV.7 shows the cross sectional view of a typical HV ceramic capacitor. As can be seen from the figure, this ceramic capacitor employs an electrode-ceramic-electrode topology and is usually coated with insulation material such as an epoxy resin. The capacitor was cut along the red dashed line, as shown in Figure IV.7, the larger remaining part was used as an dielectric electrode. The ceramic material acts as the dielectric barrier and is firm in contact with the metallic electrode.

Therefore, two identical cylindrical ceramic capacitors, each with a nominal capacitance of 3 nF, were selected to manufacture the dielectric electrodes. These

capacitors have been cut as the figure suggests and the cut surfaces have been polished to make them as smooth as possible. The end products of the dielectric electrodes are shown in Figure IV.8.

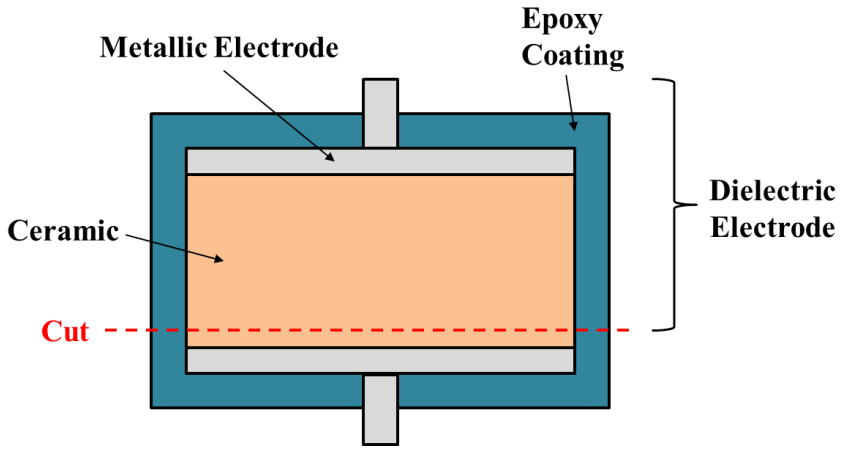


**Figure IV.7** Cross sectional view of a typical ceramic capacitor.

### 4.2.2 Topology of the Test cell

Since the ceramic capacitors were cylindrical, the designed test cell with non-conductive electrodes had the same topology as the metallic test cell shown in Figure IV.5. The two capacitors, which played a role of the dielectric electrode, were separated by a dielectric spacer as shown in Figure IV.8. Similar to the stainless steel test cell, the electrode sat between the spacer and a dielectric cover when fully assembled. There were 4 plastic studs evenly distributed on the spacer, which passed through corresponding threaded holes in the cover, and connected to 4 screw caps in order to keep the test cell tightly closed. A small inlet hole was drilled on the side of the spacer in order to inject liquid suspension in the test cell before the test and to remove the suspension after the application of HV impulses.

To be consistent with the stainless steel cell design and provide direct comparison between the two test cells, the distance between the dielectric electrodes was kept at 3 mm by the spacer. However, the volume of the ceramic test cell was slightly larger than the volume of the test cell with stainless steel electrodes (~ 5.9 ml) due to the

larger radius of the ceramic capacitor. The diameter of the inlet hole was 1.5 mm, the same as the stainless steel test cell.

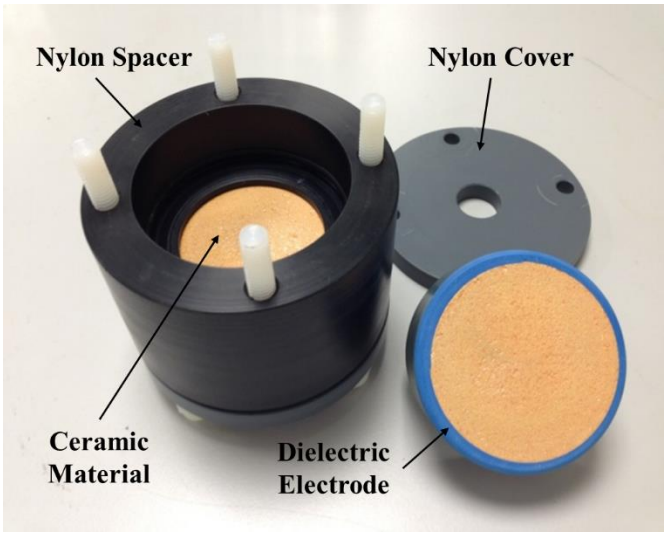


**Figure IV.8** Exploded view of the ceramic PEF test cell.

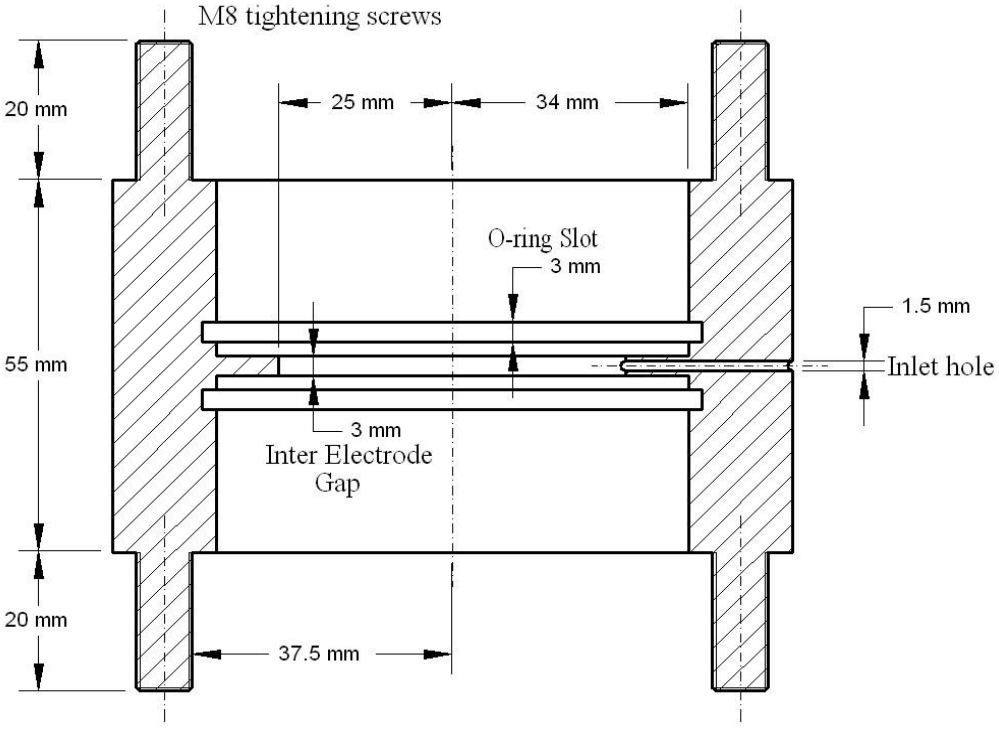


**Figure IV.9** Cross-sectional view of the spacer of the ceramic cell design.

A tight sealing of the dielectric test cell was essential for successful PEF treatment. Any leakage of the liquid suspension will create inaccurate results and introduce air bubbles inside the test cell. The sealing was achieved by placing rubber O-ring between the electrodes and the spacer. However, unlike in the case of the metallic test cell, where an O-ring slot can be easily cut on the surface of the stainless steel electrodes, the O-ring slots cannot be cut onto the ceramic surfaces (electrodes). The ceramic body of the capacitors used to manufacture the dielectric electrodes was hard but fragile, which was impossible to machine accurately. The solution to this problem was to cut the O-ring slots on the nylon spacer, as shown in Figure IV.9. Two rubber O-rings were tightly fit into the slot on each side of the spacer and the test cell was sealed as the electrodes were pressed towards the spacer.

## 4.3 Pulse Generating System

A ready-made pulse generator was used in the project to generate square impulse. This pulse generator, shown in Figure IV.10, was manufactured by SAMTECH Ltd (UK), and consisted of several discrete units: a high voltage power supply, a trigger generator, a corona stabilised switch, a pulse forming network and a voltage gain network. Figures IV.11 and IV.12 show the schematic diagram of electrical configuration of this impulse generator and a practical square impulse waveform generated by this generator during the PEF experiment in the present study. Some of the key components of this square impulse generator will be briefly introduced in the following sub-sections.


**Figure IV.10** The square impulse generator. Manufactured by SAMTECH Ltd. (UK).

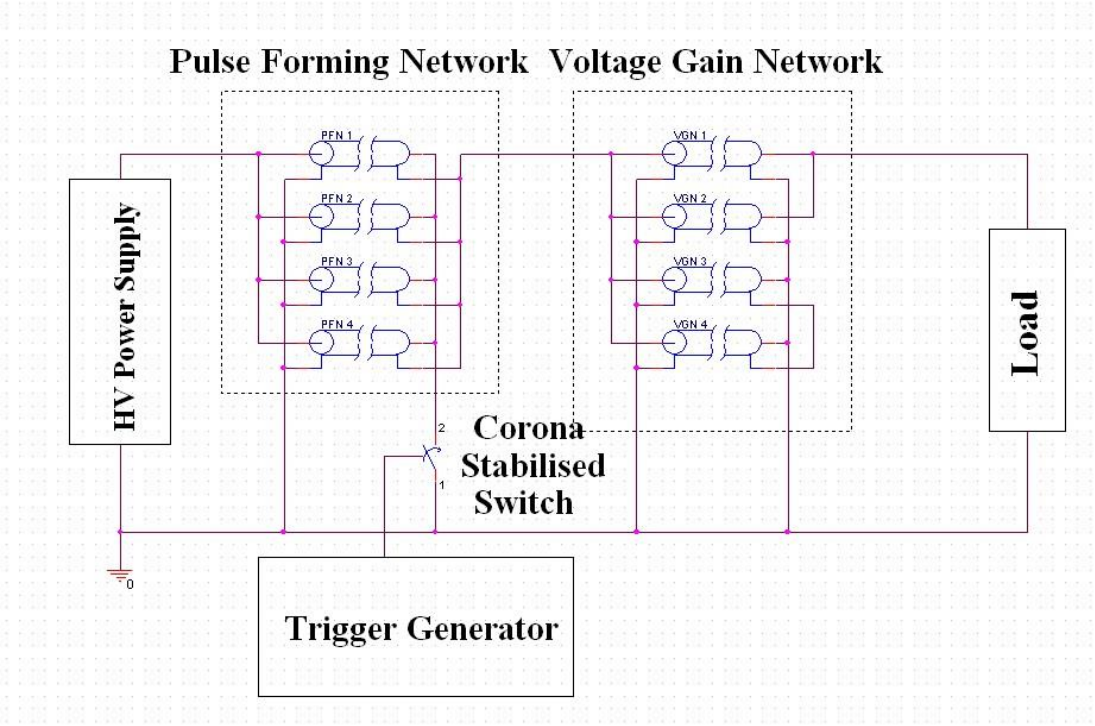


**Figure IV.11** Schematic diagram of electrical configuration of the square impulse generator. PFN stands for pulse forming network; VGN stands for voltage gain network.

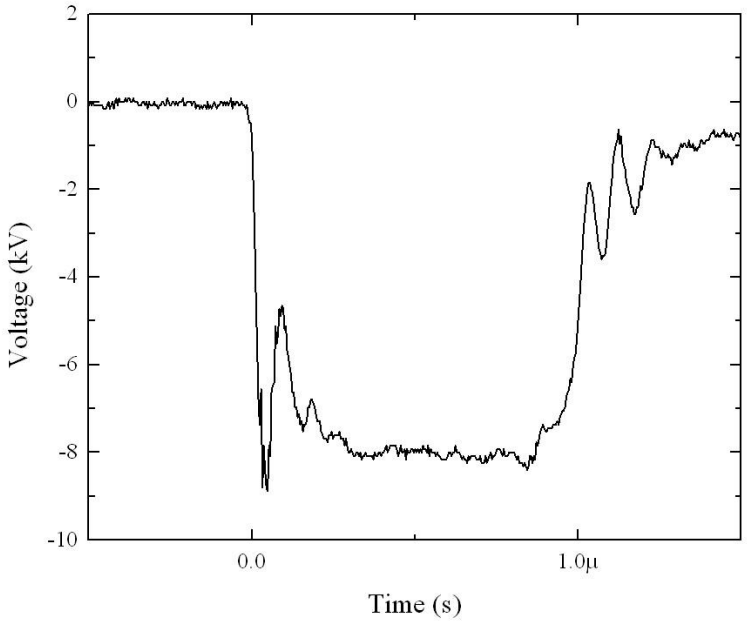


**Figure IV.12** Practical square impulse waveform generated by SAMTECH pulsed power supply.

### 4.3.1 Pulse Forming and Voltage Gain Network

As shown in Figure IV.11, the pulse forming network (PFN) consists of four URM67 transmission lines, with identical length of 100 meters. The transmission lines are connected in parallel. Therefore, as described in Section 2.4.4, this PFN is effectively four single pulse forming lines (PFL) connected in parallel. According to Equation II.6, the resulting square impulse has a pulse duration of ~ 1 μs. As the impedance of the URM67 cable is 50 Ω, the total impedance of this PFN is 12.5 Ω. For the single pulse forming line, the magnitude of the output voltage of the PFL is half of the charging voltage if a matched 12.5 Ω load is connected.

In order to increase the output voltage, a 1:2 voltage gain network is connected to the PFN, as shown in Figure IV.11. This voltage gain network consists of four 100 meter transmission lines as well. For the transmission line network configuration displayed in Figure IV.11, $V_{out} = 2\ V_{in}$ and $Z_{out} = 4\ Z_{in}$. Therefore, the output impedance of the voltage gain network is 50 Ω and the magnitude of the output voltage will equals to the charging voltage if a matched 50 Ω load is connected.

### 4.3.2 Corona Stabilised Spark-Gap Switch

A corona stabilised spark-gap switch is used in this pulse generator to trigger the PFN described in Section 4.3.1. The principle and closing mechanism of this type of switch is described in Section 2.4.5.2. A schematic diagram of the switch is shown in Figure IV.13. As shown in the figure, the switch consists of two plane-plane disc electrodes with sharp edges, which enable the forming of highly non-uniform electric field inside the switch.

As detailed in Section 2.4.5.2, the two main electrodes will be energised to the required voltage, which should be below the self-breakdown voltage of the two main electrode but sufficient enough to develop a complete breakdown when the trigger impulse is applied to the trigger electrode. Therefore, two characteristic breakdown voltages define the working envelop of this switch: the self-breakdown voltage of the main electrodes, $V_b$, and the trigger threshold voltage, $V_{th}$. When the voltage applied

on the HV electrode is higher than $V_b$, an electrical breakdown will occur between the HV electrode and the ground electrode without a trigger impulse. On the other hand, when the applied voltage is lower than $V_{th}$, closure of the switch cannot be triggered by the application of the trigger signal. Both $V_b$ and $V_{th}$ can be changed by adjusting the gas pressure in the switch, as shown in Figure IV.14, to provide desired voltage output. For example, if a 20 kV output voltage is required, the pressure of the switch should be changed to around -0.4 ~ -0.2 bars (gauge).

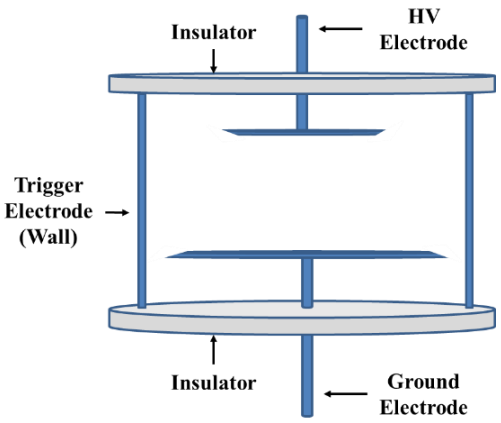


**Figure IV.13** Schematic diagram of the corona stabilized spark-gap switch.

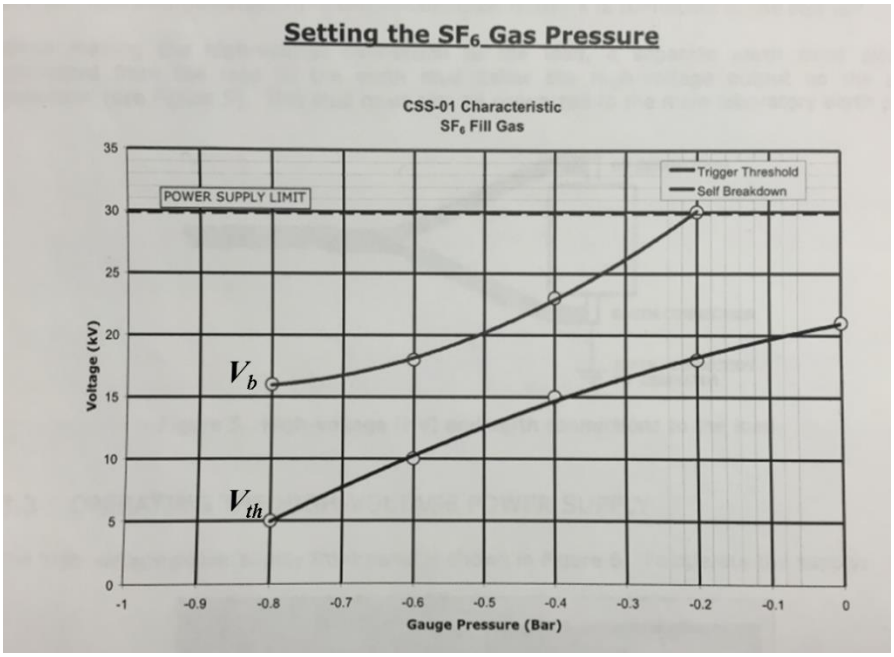


**Figure IV.14** Characteristic curves for the switch (filled with $SF_6$), [235].

The switch was originally designed to use $SF_6$ as the filling gas and can be operated under charging voltage varying from 10 kV to 30 kV. It was decided to use an environment friendly gas (air) as the filling gas instead of $SF_6$. Tests were conducted to examine the capability of the air-filled switch. The new characteristic curve of the air-filled switch is shown in Figure IV.15. It can be seen from the figure, the air-filled switch can also cover the same voltage range from 10 kV to 30 kV. However, it requires much higher pressure to provide the same voltage output. For the same 20 kV output, the air-filled switch now requires an air gauge pressure at least 1.5 bars. The recommended maximum pressure of the switch is 2 bars (gauge). As a result, the maximum charging voltage is limited to around 24 kV according to the new characteristic curves shown in Figure IV.15.

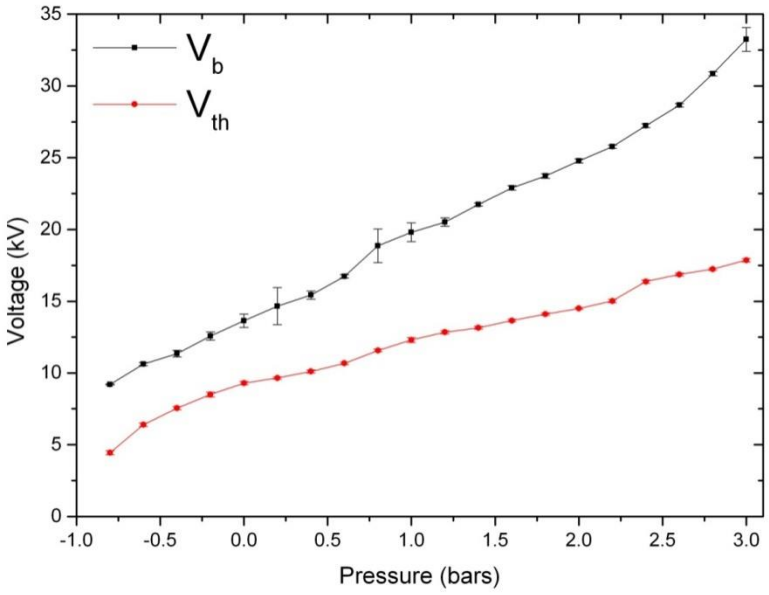


**Figure IV.15** Characteristic curves for the switch (filled with air). Error bars show standard deviation (n=10).

### 4.3.3 Trigger Generator

A trigger generator unit is employed in this pulse generator to deliver fast trigger voltage pulses to the trigger electrode of the corona stabilised spark-gap switch, as shown in Figure IV.11, thereby activate the pulse forming network. The trigger generator can be operated in either single-shot mode or continuous mode. In

continuous mode, the frequency of the triggering impulse can be adjusted from 0.1 Hz to 10 Hz, results a pulse repetition rate range of 0.1 to 10 pulses per second (pps).

## 4.4 Other Components of the PEF System

### 4.4.1 Matching Resistor

As mentioned in Section 4.3.1, the square impulse generator has an impedance of 50 Ω. In order to achieve maximum power transfer to the load and to minimise signal reflection, it is beneficial to provide an impedance matching between the load and the generator. Therefore, the impedance of the load should be 50 Ω. In the PEF experiments, the load is the effectively the PEF test cell with the liquid suspension inside. Therefore, the impedance of the PEF test cells should be evaluated first. The test cells can be represented by the *RC* equivalents of the liquid suspension inside assuming ideal electrodes are used. Figure IV.16 shows the *RC* equivalents of both stainless steel and ceramic PEF test cells.

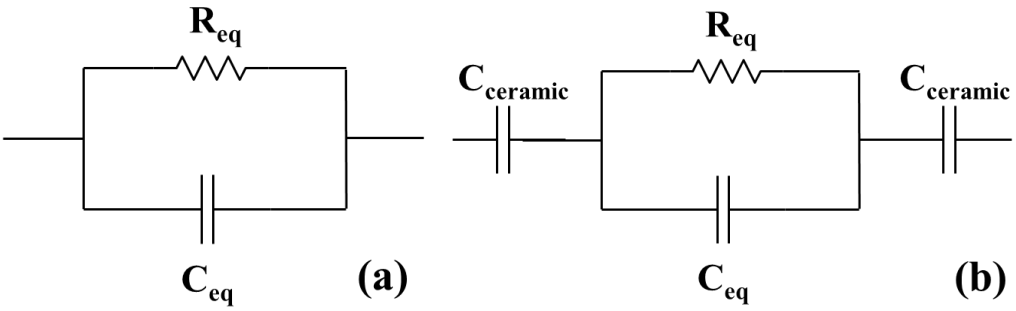


**Figure IV.16** (a) *RC* equivalent of the stainless steel test cell. (b) *RC* equivalent of the ceramic test cell.

As can be seen from the figures, the stainless steel test cell is modelled as parallel connected equivalent resistor $R_{eq}$ and equivalent capacitor $C_{eq}$ of the liquid suspension. The ceramic test cell is modelled as the RC equivalent of the liquid suspension series connected with two capacitors, which represent the ceramic

material. Therefore, the equivalent impedance of the PEF test cells can be estimated using the following equations.

$$R_{eq} = \frac{d}{\sigma \cdot A} \quad \text{(IV.3)}$$

$$C_{eq} = \frac{\varepsilon_0 \cdot \varepsilon_r \cdot A}{d} \quad \text{(IV.4)}$$

$$\frac{1}{Z_{metallic}} = \frac{1}{R_{eq}} + j\omega C_{eq} \quad \text{(IV.5)}$$

$$Z_{dielectric} = \frac{1}{j\omega C_{ceramic}} + \frac{1}{\frac{1}{R_{eq}} + j\omega C_{eq}} + \frac{1}{j\omega C_{ceramic}} \quad \text{(IV.6)}$$

where $d$ is the distance between the electrodes, $\sigma$ is the conductivity of the liquid suspension, $A$ is the surface area of the electrode, $\varepsilon_0$ is the permittivity of free space and $\varepsilon_r$ is the relative permittivity of the liquid suspension.

As suggested in Section 3.2.4, liquid suspension with conductivity in the range between $10^{-3}$-$10^{-2}$ S/m will be optimal for effective PEF treatment. Therefore, the liquid suspension of microorganisms was prepared based on this consideration in actual experiments and had a conductivity of a few tens of μS/cm, which will be introduced in detail in Section 5.1.1-5.1.3. In the stainless steel test cell, the equivalent resistance of the sample was ~ 1 kΩ and the equivalent capacitance was ~ 200 pF according to Equation IV.3 and Equation IV.4. In the ceramic test cell, the equivalent resistance and capacitance of the sample were ~ 800 Ω and ~ 400 pF respectively. As the voltage waveform (Figure IV.12) of the impulse produced by this generator system indicated, the high voltage impulse had a relatively flat top with minimal oscillations. To simplify the calculation, the frequency component can be neglected and the PEF system was seen as a DC system, therefore the impedance of the stainless steel PEF test cell was effectively its equivalent resistance, which was ~ 1 kΩ. On the other hand, the DC impedance of the ceramic test cell was effectively infinity.

As demonstrated, the equivalent impedances of both PEF test cells were much larger than the impedance of the impulse generator. Therefore, a 50 Ω resistor was connected with the PEF test cell in parallel to match the impedance of the pulse generator, as shown in Figure IV.17.

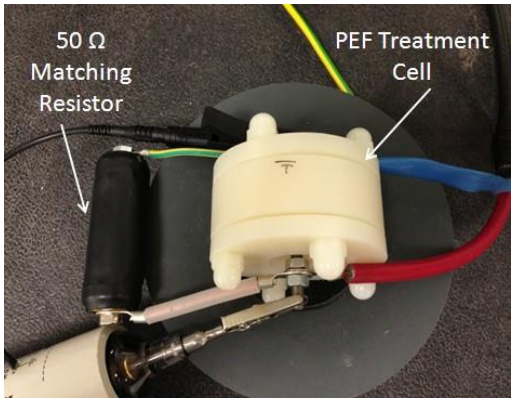


**Figure IV.17** The 50 Ω matching resistor connected with the stainless steel PEF test cell in parallel.

### 4.4.2 Diagnostic Devices

The high voltage diagnostic devices used in this work to monitor the real-time impulse waveform across the PEF test cell included an HV voltage probe and a digitising oscilloscope, Figure IV.18. The HV voltage probe used in this system was a Tektronix P6015A probe with a division ratio of 1000:1. This probe has a bandwidth of 75 MHz and can be used to measure HV impulses with magnitude up to 40 kV, which covers the range of the voltage used in the project. The voltage probe is connected to a Tektronix TDS2024 oscilloscope. The oscilloscope has a bandwidth of 200 MHz and a sampling rate of 2 GS/s.

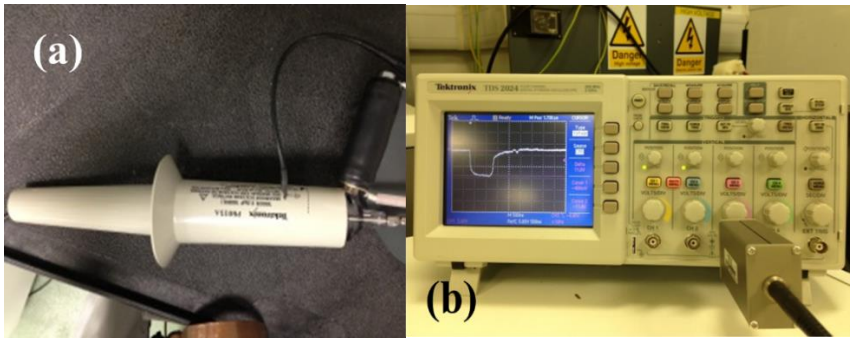


**Figure IV.18** (a) Tektronix P6015A 1000:1 HV Probe. (b) Tektronix TDS2024 oscilloscope.

## 4.5 Discussion

This chapter introduced the design process of the PEF test cells used for preliminary experiments. A traditional metallic test cell and a novel dielectric test cell have been designed.

The metallic test cell and the dielectric test cell employ very similar geometry, which is cylindrical parallel plate to plate electrode with a 3 mm inter-electrode distance. The electrodes of the metallic cell are made of stainless steel while the electrodes of the dielectric cell are made from commercially available ceramic capacitors. The supporting structures of the test cells, i.e. the spacers and the covers, are made of nylon. The equivalent impedances of the test cells are also identified in order to design the PEF treatment system to achieved optimal performance.

The pulse generator used in the preliminary experiment is also described in this chapter. This square impulse generator can produce repeated negative impulse with duration of 1 μs. The original generator with $SF_6$ filled switch can provide stable output voltage up to 30 kV. With the replacement of $SF_6$ with air, the maximum stable output voltage from the generator is reduced to around 24 kV. The impedance of the pulse generator is 50 Ω, which is much less than the estimated impedances of the PEF test cells. Therefore, in order to achieve maximum power transfer and minimised signal reflection, a 50 Ω matching resistor will be connected to the test cells in parallel during PEF treatment to match the impedance of the generator.

The designed PEF test cells and the PEF system, described in this chapter, will be used to conduct a series of preliminary PEF treatments on microorganisms. The results of these preliminary experiments will be introduced in next chapter.

# Chapter V

# PEF TREATMENT OF MICROOGANISMS USING THE INITIAL TEST CELLS

## 5.0 General

As described in Chapter IV, two PEF test cells were designed and constructed. A PEF system which included these two test cells and a square impulse generator were prepared for preliminary PEF experiments. The traditional metallic PEF test cell with stainless steel electrodes was used to carry out initial proof-of-principle PEF tests and to provide reference results for the dielectric PEF cell. The novel dielectric test cell with ceramic electrodes was used to conduct identical experiments in order to investigate whether the idea of non-conducting PEF test cell can achieve satisfactory result in practical experiment.

In this chapter, the preparation process of the microorganisms used in the experiments will be introduced first. The methods to be used to determine the microbiological efficiency of the PEF treatment will also be described in this chapter. The experiment procedures will be presented and the PEF treatment results obtained using both test cells will be discussed.

The results obtained in the PEF experiments demonstrated that successful PEF inactivation of microorganisms can be achieved using the stainless steel PEF test cell. However, the PEF tests in which ceramic PEF test cell was employed indicate that satisfactory practical PEF performance cannot be achieved in the proposed ceramic test cell design and HV impulses produced by the pulsed power system used in the present study. The reasons for this unsatisfactory performance of the ceramic test cell and potential ways of overcoming these drawbacks in the design of non-conductive PEF treatment system will be discussed in Chapter VI.

The analysis of the specific energy consumption of the PEF process in the stainless steel test cell has been conducted and the obtained results are compared with the literature data. The results showed that significant improvement in the specific energy consumption has been achieved in the present study as compared with literature data. The analysis and discussion of the reasons for this improvement in the energy efficiency is presented in this chapter.

## 5.1 Preparation of Test Suspension with Microorganisms

### 5.1.1 Conductivity of Liquid Suspension

As mentioned in Section 3.2.4, the optimum conductivity of the liquid suspension containing microorganism sample should be in the range of $10^{-2}$ ~ $10^{-3}$ S/m in order to allow optimal development of trans-membrane potential in practical PEF tests. Using liquid suspension with conductivity higher than the recommended value can significantly reduce the maximum field strength developed across on the biological membrane due to the Maxwell-Wagner field relaxation process, which could cause ineffective PEF process in the ceramic test cell. On the other hand, using liquid suspension with conductivity lower than the recommended value will increase the time required for the development of trans-membrane potential and to reach its maximum value in both test cells, which may exceed the pulse duration. Therefore, it was decided to prepare liquid suspension with the conductivity satisfying the recommendation from the modelling result obtained in Section 3.2.4, which can provide a relatively short membrane charging time in both test cells and a relatively long Maxwell-Wagner relaxation time in the ceramic test cell. The conductivity of the liquid suspension was measured by a conductivity meter, Jenway 4150, each time prior to the PEF treatment experiment.

### 5.1.2 Preparation of *A. platensis*

The growth medium for *A. platensis* was *Zarrouk* medium, described in [236]. The *Zarrouk* medium was prepared using sterilized distilled water supplemented with the salts list in Table V.1. Fresh *Zarrouk* medium inoculated with *A. platensis* was

placed inside a stationary light incubator to allow the growth of the *A. platensis*. The lights inside the incubator were set to a 12 hours diurnal cycle and the temperature was remained constant at 25 ºC. Therefore natural conditions were simulated within laboratory conditions, which provided the best available condition for the *A. platensis* to grow.

**Table V.1** Components and the formula of *Zarrouk* medium and its characteristic. All chemicals are obtained from Sigma Aldrich UK.

| **Component** | **Concentration (g/1000 ml)** |
|---|---|
| $NaHCO_3$ | 16.8 |
| $NaNO_3$ | 2.5 |
| $K_2SO_4$ | 1 |
| NaCl | 1 |
| $K_2HPO_4$ | 0.5 |
| $MgSO_4 \cdot 7H_2O$ | 0.2 |
| $Na_2EDTA$ | 0.08 |
| $CaCl_2$ | 0.04 |
| $FeSO_4 \cdot 7H_2O$ | 0.01 |
| $H_3BO_3$ | 0.00286 |
| $MnCl_2 \cdot 4H_2O$ | 0.0018 |
| $ZnSO_4 \cdot 7H_2O$ | 0.00022 |
| $CuSO_4 \cdot 5H_2O$ | 0.00008 |
| $(NH_4)_6MoO_{24}$ | 0.00002 |
| **Characteristic of the *Zarrouk* Medium** | |
| Electrical Conductivity | 1.5-3 S/m |
| pH | 8.38 ± 0.06 |

Fully grown (35 ~ 40 days) *A. platensis* was used for the PEF treatment experiment. However, as the growth medium contains mainly electrolytes, the conductivity of this growth medium, ~ (1.5-3) S/m, was 1000 times' higher than the recommended conductivity value (Section 5.1.1). Therefore, *A. platensis* cell were removed from the growth media and re-suspended into a lower conductivity solution before PEF treatment. To do so, the growth medium containing the *A. platensis* cell was centrifuged at 4300 rpm for 10 minutes in the centrifuge, Heraeus Labofuge 400R, as

shown in Figure V.1. After centrifugation, the supernatant, which contained mainly conductive growth medium, was discarded. The precipitated biomass, which contained the *A. platensis* cells, was re-suspended in distilled water. This centrifugation and washing process was conducted three times and the resulting *A. platensis* solution had a conductivity of (2.26 ± 0.45) $\times 10^{-3}$ S/m. This solution satisfied the conductivity requirements as outlined in Section 5.1.1 and therefore can be used in the PEF experiments. However, it should be noted that highly diluted solutions could put additional stress on microbial cells due to changes in the extracellular environment. Therefore, all the control (untreated) samples were put into the same suspension with required conductivity. The same approach was also used in [237], in which a PEF study was conducted to extract protein from microalgae *Nannochloropsis* and *Chlorella*.

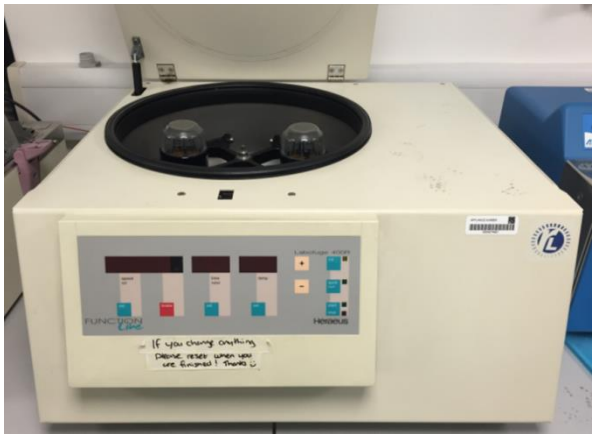

**Figure V.1** Heraeus Labofuge 400R centrifuge.

### 5.1.3 Preparation of *S. cerevisiae*

Unlike the *A. platensis*, the reproducing cycle of the *S. cerevisiae* is much shorter. The growth of *S. cerevisiae* can reach the end of the exponential phase within 20 hours when incubated in fresh medium under optimal conditions, [238].

In the present study, the *S. cerevisiae* sample was cultured in 100 ml solution of Malt Extract Broth (CM0057, Oxoid Ltd, UK) for 20 hours in a shaking incubator, New Brunswick Classic C25KC refrigerated incubator shaker, as shown in Figure V.2.

The incubator was set to rotate at 120 rpm and the temperature was remained constant at 30°C, which is the optimal temperature for culturing *S. cerevisiae*, [239]. Similar to the growth medium of *A. platensis*, this broth medium was also highly conductive. Therefore, the *S. cerevisiae* suspension was centrifuged at 4300 rpm for 10 minutes in the centrifuge after incubation. The *S. cerevisiae* cells were then re-suspended in 100 ml 0.05% Mycological Peptone (LP0040, Oxoid Ltd, UK) solution. The resulting *S. cerevisiae* suspension had a conductivity of $(1.82 \pm 0.13) \times 10^{-2}$ µS/cm, which satisfied the conductivity requirements as outlined in Section 5.1.1. Similar to the *A. platensis* sample, the centrifuge and dilution process was also applied to the control (untreated) *S. cerevisiae* sample.


**Figure V.2** New Brunswick Classic C25KC refrigerated incubator shaker.

## 5.2 Assessment of Efficiency of PEF Treatment

Several methods were used to determine the performance of the PEF treatment experiment in the present study. The assessments of *A. platensis* and *S. cerevisiae* were different and will be introduced in the following sections separately.

### 5.2.1 Assessment of PEF Treatment of *A. platensis*

Two methods were used to assess the performance of PEF treatment on *A. platensis*. Visual inspection of the *A. platensis* cell was conducted to provide direct

examination of the damage caused by the PEF treatment. The growth of the *A. platensis* was also monitored by plotting its growth curve to determine the damage.

#### 5.2.1.1 Visual Inspection

An optical microscope, Nikon Eclipse E400 as shown in Figure V.3(a), was used to inspect the *A. platensis* cell visually. A drop of *A. platensis* suspension was placed onto the surface of a glass slide, as shown in Figure V.3(b). The glass slide containing cells was then placed under the microscope and viewed at ×400 magnification. Both PEF-treated and untreated *A. platensis* suspensions were visually inspected using this method. The images of the PEF-treated and untreated cells are compared to determine any structural damage caused by PEF treatment.

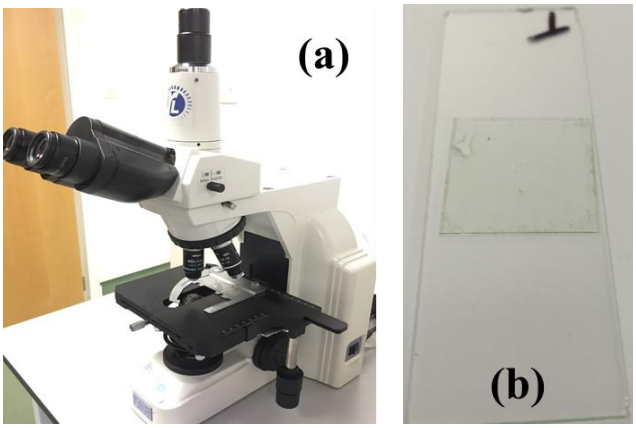


**Figure V.3** (a) Nikon Eclipse E400 microscope. (b) Glass slide with a drop of *A. platensis* suspension on the surface.

#### 5.2.1.2 Growth Curve Measurement

In addition to visual inspection, the growth curve of the *A. platensis* was monitored to assess the damage caused by the PEF treatment. The inspiration behind this idea was that the *A. platensis* suspension became denser and greener as the *A. platensis* cell grew and reproduced, as can be seen in Figure V.4. Therefore, the growth of the *A. platensis* can be quantified by measuring the optical absorption of the suspension. To do so, 0.1 ml of the suspension was transferred into 20 ml fresh growth medium. The optical absorption at 545 nm, which is the wavelength of green light and can be used to detect photosynthesis pigments, of the new 20 ml suspension was measured

by a spectrophotometer every 2 or 3 days. The spectrophotometer, Thermo Spectronic Biomate 5, is shown in Figure V.5. Figure V.4 shows a typical growth curve of the untreated *A. platensis*. The growth curves of both PEF-treated and untreated *A. platensis* samples were measured and compared to assess the performance of PEF treatment.

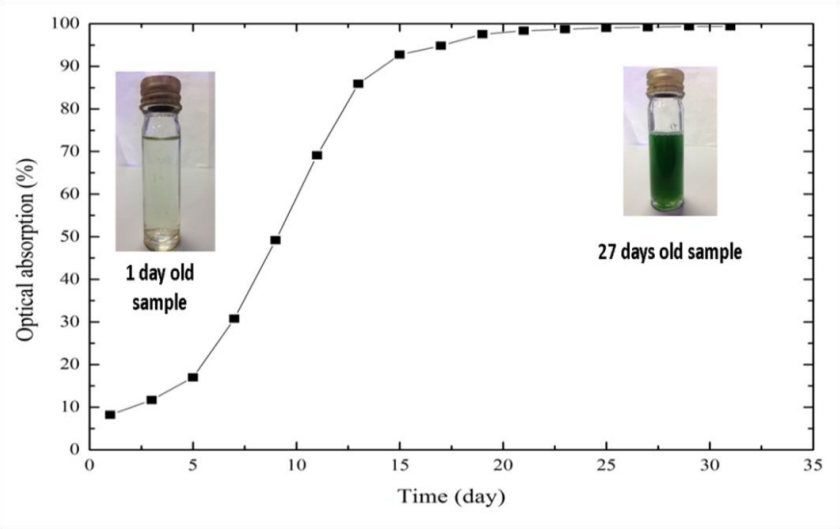


**Figure V.4** Growth curve of untreated *A. platensis* sample.

**Figure V.5** Thermo Spectronic Biomate 5 spectrophotometer.

### 5.2.2 Assessment of PEF Treatment of *S. cerevisiae*

The performance of PEF treatment on *S. cerevisiae* was assessed by calculating the reduction in population after treatment. To do so, the *S. cerevisiae* sample needed to be enumerated accurately before and after the PEF treatment. For enumeration of *S. cerevisiae*, specific amount of *S. cerevisiae* sample was plated onto agar plates and incubated for 24 hours at 30 ºC. Two plating methods, namely spiral plating and spread plating, were used to plate the *S. cerevisiae* sample. The appropriate plating method was selected based on the expected surviving population. The population of

the *S. cerevisiae* sample was determined by counting the number of *S. cerevisiae* colony on the agar plate after incubation.

The agar used for enumeration of *S. cerevisiae* was Malt Extract Agar (CM0059, Oxoid Ltd, UK). 50 grams of the agar powder was added into 1 liter of distilled water to prepare the agar solution. The solution was then sterilized at 121 ºC for 15 minutes in an autoclave. After sterilization, the agar solution was poured onto petri dishes and solidified as it cooled down to make up agar plates. The plates were placed into an incubator at 37 ºC for 24 hours to detect any contamination prior to be used in the experiment.

#### 5.2.2.1 Spiral Plating Method

When the expected surviving population of the *S. cerevisiae* sample was in the range of $10^5$ ~ $10^3$ Colony Forming Units per Millilitre (CFU/ml), spiral plating method was used. This is an automatic plating method using an automated spiral plater, WASP 2 from Don Whitley Scientific Ltd. UK, as shown in Figure V.6. The plater dispensed 50 µl of the liquid *S. cerevisiae* suspension onto the surface of the rotating agar plate. The placement of the liquid suspension was in the shape of Archimedean Spiral and was in logarithmic decrease, as can be seen in Figure V.7(a). After 24 hours' incubation, the *S. cerevisiae* colonies were enumerated manually using a colony counter. A counting grid was centered at the agar plate, each marked grid division corresponded to a known constant volume of the plated liquid suspension. Therefore the population density of the *S. cerevisiae* suspension in CFU/ml was calculated by counting the colony number in a selected division and comparing the number with a supplied reference chart.

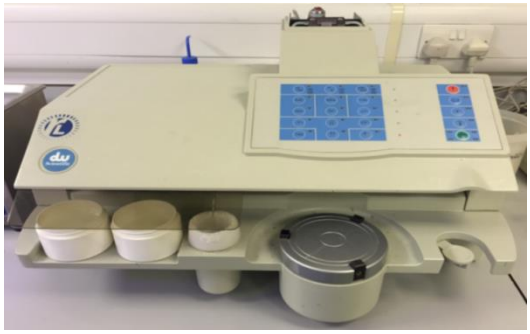

**Figure V.6** Don Whitley Scientific Ltd. WASP 2 automated spiral plater.

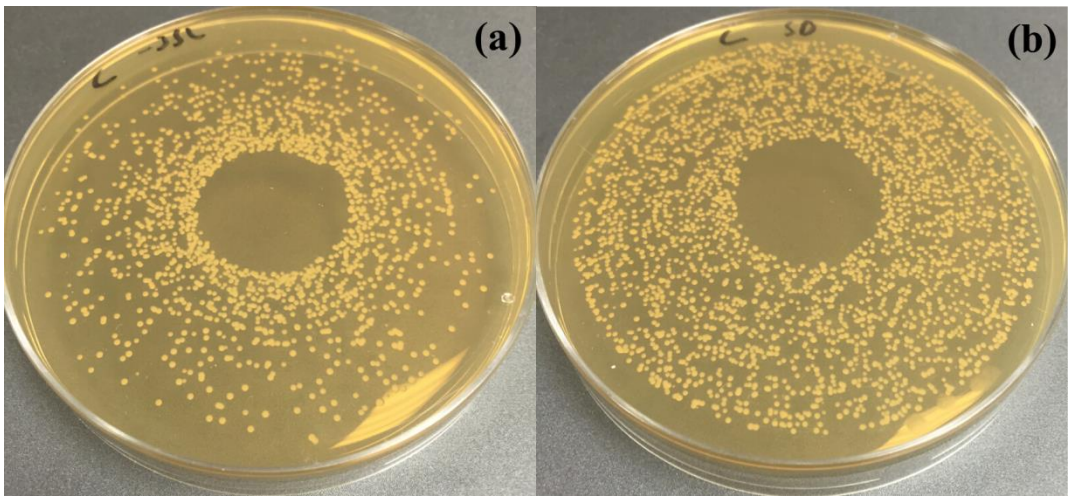


**Figure V.7** (a) Spiral plate: logarithmic distribution. (b) Spread plate: linear distribution.

#### 5.2.2.2 Spread Plating Method

When the expected surviving population of the *S. cerevisiae* sample was in the range of $10^3$ ~ $10^2$ CFU/ml, spread plating method was used. This plating method can be done manually or automatically using the same WASP 2 automated plater described above. The plater can also dispense 100 µl of the liquid suspension linearly on the surface of the rotating in the shape of Archimedean Spiral, as shown in Figure V.7(b). To do it manually, 100 µl of the liquid *S. cerevisiae* suspension was transferred onto the agar plate using a pipette (Gilson, UK). The suspension was evenly distributed on the surface of the agar plate using an L-shape spreader. Both manually and automatically prepared plates were then incubated at 30 ºC for 24 hours. After incubation, the number of the *S. cerevisiae* colonies on the plate was counted and the population density of the *S. cerevisiae* suspension in CFU/ml was calculated by multiplying this number by 10, which is the dilution factor.

If the expected surviving population of the yeast sample was less than ~ $10^2$ CFU/ml, the manual spread plating method was used to obtain an accurate result. In this case, 500 µl or 1 ml of the *S. cerevisiae* suspension was transferred onto the agar plate using a pipette and was evenly distributed on the surface of the agar by an L-shape spreader. The plates were placed into the incubator after the liquid solution on the plates' surface became completely dry. After the incubation, population density of

the *S. cerevisiae* suspension in CFU/ml was calculated by multiplying the number of the colonies on the plate by 2 in the case of 500 µl sample. In the case of 1 ml sample being plated, the number of the colonies equalled to the population density in CFU/ml.

## 5.3 PEF Treatment of *A. platensis*

A series of proof-of-principle PEF treatment experiments were conducted using the stainless steel test cell and the ceramic test cell. At this stage of the present study, the HV impulses with square waveshape were used in the PEF treatment experiments in which PEF test cells described in Chapter IV were used. The obtained results provided valuable information and guideline for the optimisation of the test cells and the subsequent experiments using the modified PEF test cells. This section introduces the experiment procedures and the results obtained from these experiments. The significance of the obtained results is also discussed.

### 5.3.1 Experimental Procedures

The suspension of *A. platensis*, prepared as described in Section 5.1.2, was transferred into the PEF test cell via a syringe. The test cell was then connected to the square impulse generator in parallel with the 50 Ω matching resistor. Two levels of voltage outputs from the generator, 10 kV and 20 kV, were used in the experiment. The corresponding electric field strengths across the PEF test cell were 33 kV/cm and 67 kV/cm respectively. The *A. platensis* sample was then subjected to 50, 100, 500 and 1000 impulses. It was found during the experiments that, in the case of 500 and 1000 impulses tests, the total time required for the experiment was relatively long that the *A. platensis* cells precipitated in the bottom of the test cell. Therefore, in order to minimise the sedimentation effect, the suspension were mixed within the test cell after every 250 impulses.

As introduced in Section 5.1.2, the preparation procedure of the suspension involved 3 times of centrifugation and washing process, which can apply considerable mechanical force on the *A. platensis* cells. Therefore, untreated but centrifuged

*A. platensis* sample was used as control sample to exclude the effect of centrifugation when analysed the performance of PEF treatment. The effect of centrifugation process on the *A. platensis* was analysed by compared centrifuged and un-centrifuged samples.

To check if the PEF treatment caused significant increase in the sample temperature, which could potentially contribute to microbial inactivation, the temperature of the treated samples was monitored using a thermocouple (Kane-May KM340, K-type) before and immediately after each experiment.

All PEF experiments were conducted in triplicate, which allow statistical representation of the obtained results.

### 5.3.2 Results of PEF Treatment in the Stainless Steel Test Cell

This section discusses the obtained experimental results of PEF treatment of *A. platensis* in the stainless steel test cell using high voltage impulses with square waveshape.

#### 5.3.2.1 Visual Inspection

Figure V.8 shows the images of individual *A. platensis* cells for untreated, centrifuged and PEF treated samples. As can be seen from the figure, the visual appearances of the centrifuged and PEF treated *A. platensis* cell were significantly different from that of the untreated sample. While there is a slight difference between the centrifuged and PEF treated samples. Since both centrifuged and PEF treated sample have been centrifuged for a considerable period of time, the visual observation result suggested that the mechanical force induced by the centrifuge process may cause some internal structural changes to the cell. This is supported by a PEF study reported in [240], in which the microalgae *Nannochloropsis oculata* cells were ruptured by mechanical force when treated by a blender, as shown in Figure V.8(d). However, from the results of growth curve measurement, the centrifuged *A. platensis* sample remained viable while the PEF treated sample were non-viable.

Therefore, it suggested that the PEF treatment induced damage to the cell which was invisible at this scale of magnification. Unlike mechanical treatment reported in [240], no rupture or external damage was detected in neither centrifuged nor PEF treated sample in the experiments.

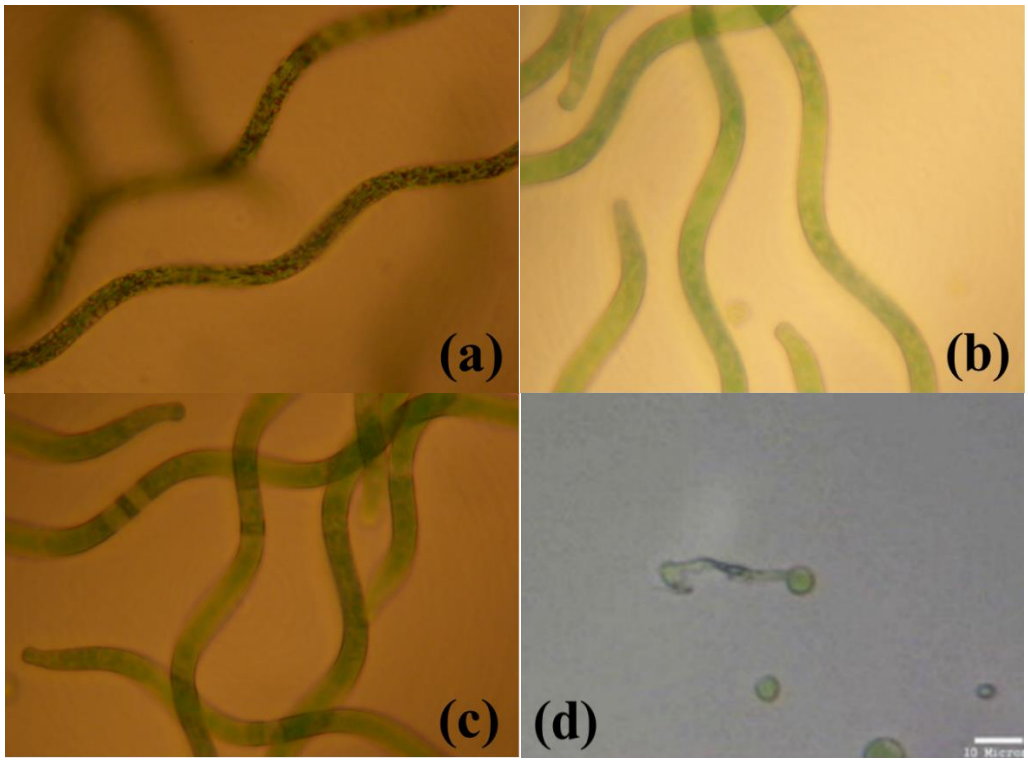


**Figure V.8** Individual *A. platensis* cells under microscope (×400 magnification) (a) Untreated sample. (b) Centrifuged sample. (c) PEF treated sample (33 kV/cm, 500 pulses). (d) *N. oculata* treated by blender, figure taken from [240].

#### 5.3.2.2 Growth Curve Measurement

Figure V.9 and Figure V.10 show the growth curves for the PEF treated *A. platensis* sample. The results shown in these figures demonstrated that the effect of PEF treatment on *A. platensis* cell was significant using the stainless steel test cell in present study.

In the group treated by 33 kV/cm field strength, as shown in Figure V.9, no growth of the *A. platensis* was observed by 15 days with 500 or more pulses. Optical

absorption at day 15 was even slightly decreased as compared to day 1, which was potentially due to the lysis process of the dead cells and the loss of chlorophyll. These no-growth curves indicated that the vast majority of the *A. platensis* cells in the sample have been inactivated by the applied impulses. However, the inactivation efficacy with smaller numbers of impulses (<500) was not as consistent as PEF treatment using higher numbers of impulses (⩾500). When treated with 100 HV impulses, two independent tests demonstrated inactivation tendency represented in Figure V.9 and a third run showed *A. platensis* growth curve similar to that of the centrifuged curve. When treated with 50 impulses, only one independent test out of 3 showed inactivation of *A. platensis* while two other runs showed that *A. platensis* continued to grow as demonstrated in Figure V.9. These results suggested that *A. platensis* can be inactivated by 50 or 100 impulses, but the effect was not consistent for electrical parameters (50, 100 impulses at 33 kV/cm) used in these tests. Larger numberss of impulses (500, 1000) were required to achieve stable inactivation performance.

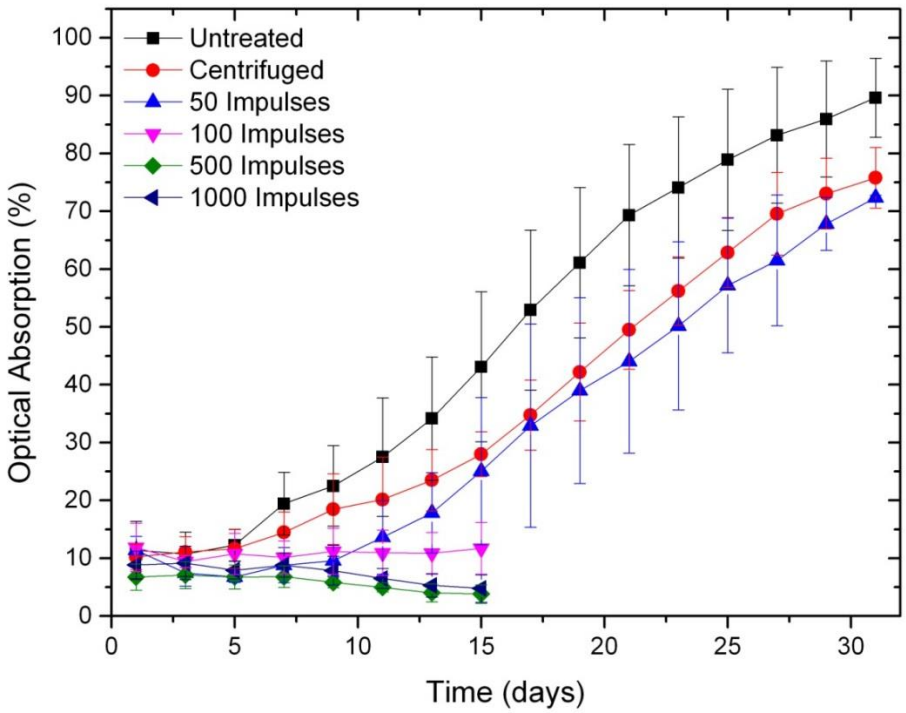


**Figure V.9** Growth curves for untreated, centrifuged and PEF treated (33 kV/cm) *A. platensis* sample. Data points are the average value of triplicate treatments (with the exception of the 50 and 100 impulses groups, in which one outlying treatment is excluded), error bars show standard deviation (n=3).

In the group treated by 67 kV/cm field strength, as shown in Figure V.10, the effect of the HV square impulses was more pronounced. As can been seen in Figure V.10, the growth curves for *A. platensis* treated by all different numbers of impulses demonstrated no sign of growth. These results indicated that virtually all *A. platensis* cells have been inactivated after PEF treatment with 50 or more impulses. Under these field conditions, no treated sample showed an increasing optical density, indicating that reliable inactivation of the *A. platensis* have been achieved.

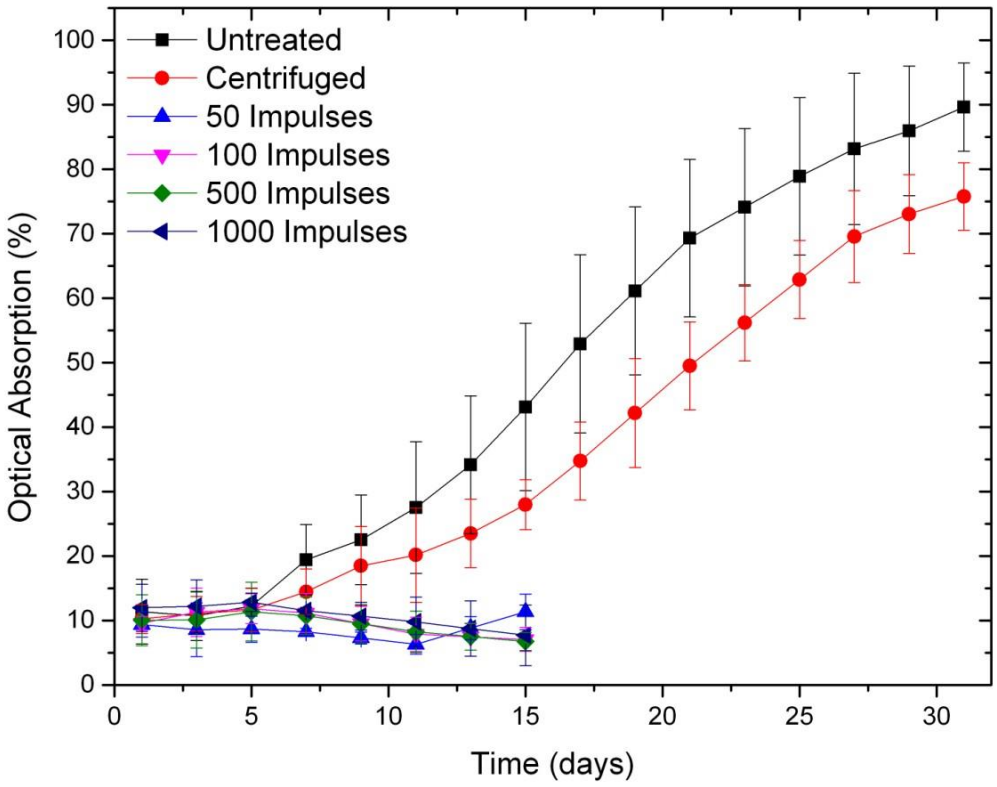


**Figure V.10** Growth curves for untreated, centrifuged and PEF treated (67 kV/cm) *A. platensis* sample. Data points are the average value of triplicate treatments, error bars show standard deviation (n=3).

The obtained growth curves showed that reliable inactivation of the *A. platensis* can be achieved using ~ 500 and more impulses with the field magnitude of 33 kV/cm. When the field strength was doubled to 67 kV/cm, the number of impulses required for reliable inactivation was reduced to ~ 50.

#### 5.3.2.3 Temperature Measurement

As mentioned in Section 5.3.1, the temperature of the treated samples was monitored before and immediately after each treatment test. The result of these measurements showed that the PEF treatment regime used in the current study did not cause significant temperature increase. The maximum registered increase in the sample temperature did not exceed ~ 2°C. This was different from the majority of the PEF treatment studies, [7, 67, and 241]. It was reported in [67] that PEF treatment resulted in a 50 °C increase in the temperature of the sample when both pre-cooling of the microalgae suspension and ice-jacket cooling during treatment were employed.

The reason of the insignificant temperature increase observed in the present study was the use of low conductivity liquid suspension. In order to reduce the conductivity of the liquid suspension, centrifugation and subsequent re-suspension of the *A. platensis* cells in distilled water was carried out three times, resulting in a significant reduction of the conductivity of the solution: the conductivity of all tested samples was in the range of $(2.26 \pm 0.45) \times 10^{-3}$ S/m. In contrast, the sample solutions with significantly higher conductivities in the range of a few S/m were used in [241] and [7] in PEF treatment (0.9% NaCl solution and apple juice, respectively). A much higher conductivity will cause a high conduction current through the sample and significant Joule heating due to this current. As a result, a noticeable increase in temperature after PEF treatment was reported: the temperature of the PEF treated samples increased by a few 10's of ºC. Therefore, the insignificant temperature rise observed in the present experiments was explained by the low conductivity of liquid solutions used in the tests.

#### 5.3.2.4 Specific Energy Consumption

The specific energy consumption during the PEF treatment refers to the amount of energy dissipated in the liquid suspension in the PEF test cell normalised by the mass of the sample (J/kg). This specific energy consumption was estimated analytically by using the equivalent circuit model. The PEF test cell was considered to form a parallel *RC* circuit, as described in Section 4.4.1. The equivalent resistance *R*

represented the conduction through the liquid suspension in the test cell. The capacitance *C* represented the capacitance of the test cell and *C* is connected in series with a resistance, $R_{ESR}$, associated with the losses in the polarisation process.

The energy which dissipated in the test cell can therefore be represented as the sum of the Joule energy due to ionic conduction in the liquid, $E_J$, and the energy associated with displacement current due to polarisation process in the test cell, $E_{pol}$. The Joule energy dissipated in the PEF test cell can be calculated by the following equations:

$$E_J = \frac{N \cdot \int V^2(t) \cdot dt}{R} \quad \text{(V.1)}$$

$$R = \frac{d}{\sigma \cdot A} \quad \text{(V.2)}$$

where *N* is the number of impulses applied, *V(t)* is the voltage across the test cell, *R* is the equivalent resistance of the test cell, *d* is the distance between the electrodes, $\sigma$ is the conductivity of the liquid suspension and *A* is the surface area of the electrode.

It should be noted that the temperature of the liquid suspension has an impact on the conductivity of the suspension. However, it has been confirmed that the sample temperature changes slightly during the PEF treatment. Therefore, this change in temperature and the resulting change in the conductivity of liquid sample should be taken into account in order to ascertain potential changes in the equivalent resistance during the PEF treatment. To do so, the conductivity of the liquid suspension was measured after the PEF treatment and compared with the pre-treatment conductivity value. The result showed that the maximum increase in conductivity due to the PEF treatment did not exceed ~ 3.6 %. Therefore, the constant value of the equivalent resistance, *R*, obtained by Equation V.2 was used for the Joule energy calculations. Using the actual voltage waveform in calculation, it was found that the resulting Joule energy, $E_J$, was 77 mJ per pulse and 308 mJ per pulse in the case of 33 kV/cm and 67 kV/cm pulses respectively.

The energy which was dissipated in the test cell due to displacement current can be calculated by the following equations:

$$E_{pol} = N \cdot R_{ESR} \cdot \int \left( C \frac{dV(t)}{dt} \right)^2 \cdot dt \quad \text{(V.3)}$$

$$R_{ESR} = \frac{tan\delta}{2\pi \cdot f \cdot C} \quad \text{(V.4)}$$

$$C = \frac{\varepsilon_0 \cdot \varepsilon_r \cdot A}{d} \quad \text{(V.5)}$$

where $R_{ESR}$ is the equivalent series resistance of the capacitor in the lumped circuit model, $f$ is the frequency which corresponds to the rise and fall times of the impulse, $C$ is the equivalent capacitance of the test cell, $\varepsilon_0$ is the permittivity of free space, $\varepsilon_r$ is the relative permittivity of the liquid suspension and $tan\delta$ is the ratio of the imaginary and real parts of permittivity of the suspension.

The displacement current, $C \cdot dV(t)/dt$, was calculated using the actual voltage waveforms obtained during the PEF treatment. $tan\delta$ was modelled with the dissipation factor of water, which is $1.94 \times 10^{-4}$, at 25°C for $f$ = 4 MHz, according to [242]. This frequency corresponded to the rise and fall times of the HV impulses used in the PEF treatments. The values obtained using Equations V.3-V.5 for the capacitive energy component, $E_{pol}$, were 0.036 mJ per pulse for 33 kV/cm and 0.150 mJ per pulse for 67 kV/cm.

As can be seen, the capacitive energy components were significantly (3 orders of magnitude) lower than the corresponding Joule energy components. Therefore, the total specific energy during the PEF treatment can be approximated by the Joule energy losses only.

The results from the growth curve measurements indicated that the reliable inactivation of the *A. platensis* was achieved by 500 pulses with the field magnitude

of 33 kV/cm. The volume of the test cell was 3.4 ml, and the concentration of *A. platensis* cells was ~ 13 g/l, therefore the specific energy required to achieve inactivation of the *A. platensis* was ~ 0.87 MJ/kg. In the case of 67 kV/cm PEF treatment, the number of impulses which were required to achieve reliable inactivation was reduced to ~ 50, and specific energy consumption in this case was ~ 0.35 MJ/kg.

Specific energy consumption of the PEF treatment achieved in this study was significantly lower than the energy consumption reported in the literature. For example, it was reported in [67] and [68] that energies of 26 MJ/kg and 2 MJ/kg were used in the PEF treatment respectively. These values are at least ~ 10 times higher than the specific energy value obtained in this study. Several potential reasons could explain such significant difference in the specific energy consumption. First, the conductivity of the *A. platensis* suspension used in this study (~ 20 µS/cm) was significantly lower than that in other's reports: the *A. protothecoides* suspension used in [68] had a conductivity of 0.15 S/cm. The low conductivity of suspension used in the present study results in a lower conduction current in the test cell, and therefore lowers the energy dissipation.

Although the size of microorganisms may make them more sensitive to the HV impulses, it is believed that this factor does not make significant contribution to the observed reduction in the energy consumption as compared with the literature data. It has been shown experimentally in [185] that the *S. cerevisiae* (with linear dimensions of ~ 6 µm) was more susceptible to the PEF treatment than the *S. aureus*, with linear dimensions of ~ 1 µm. The authors of [213] also attributed an increased susceptibility of the *B. subtilis* to the PEF treatment as compared with *S. aureus* of smaller size. Although the *A. platensis* used in the present work and the microalgae sepsis used in [67] and [68] were different, linear dimensions of the individual microorganism cells have the same order of magnitude (10's of µm [123]). Therefore, it was concluded that the size factor did not play a dominant role in the observed reduction in the specific energy consumption and it was mainly due to the use of low conductivity *A. platensis* suspension. However, further investigation into the exact

mechanisms and factors which may result in lower specific inactivation energy is required.

### 5.3.3 Results of PEF Treatment in the Ceramic Test Cell

This section presents and discusses the experimental results of the PEF treatment of the *A. platensis* using the ceramic test cell.

#### 5.3.3.1 Visual Inspection

Figure V.11 shows the images of the untreated, centrifuged and PEF treated individual *A. platensis* cells. Unlike the PEF treatment using metallic test cell, as can be seen from the figures, the visual appearances of the PEF treated sample cell was very similar to the centrifuged sample. The significant different between the PEF treated and untreated sample was likely to be the result of the centrifuge process. In addition, the results of growth curve measurement indicated the PEF treated sample using the ceramic test cell kept growing after the treatment. This suggested PEF treatment using the ceramic test cell may not induce any damage to the *A. platensis* cells. No rupture or external damage can be detected in PEF treated sample either.

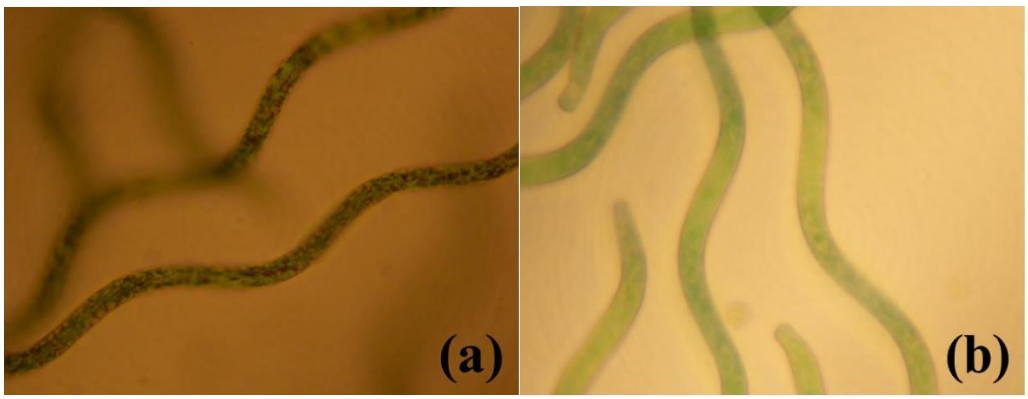

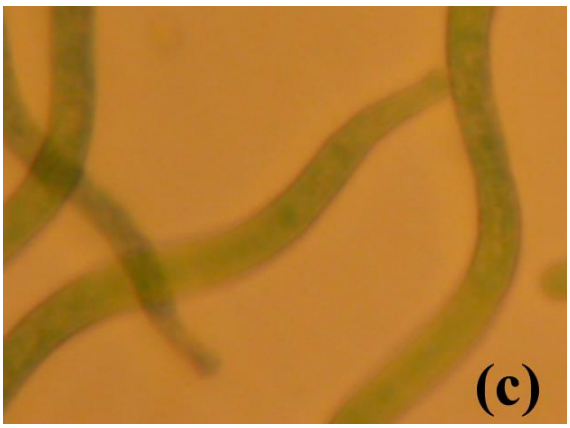


**Figure V.11** Individual *A. platensis* cells under microscope (×400 magnification): (a) untreated sample; (b) centrifuged sample; (c) PEF treated sample (33 kV/cm, 500 pulses).

### 5.3.3.2 Growth Curve Measurement

The Figure V.12 and Figure V.13 show the growth curves for the PEF treated, untreated and centrifuged *A. platensis* samples. The results shown in these figures suggested that PEF treatment in the ceramic test cell did not produce noticeable effect on *A. platensis*. All growth curves for untreated, centrifuged and PEF treated *A. platensis* samples were similar and the differences between them were statistically insignificnat.

As can be seen in Figure V.12 and Figure V.13, optical absorptions of all the PEF treated samples started to increase around day 11 after PEF treatment regardless of field strength and number of impulses. These growth curves indicated that virtually no damage has been done to the *A. platensis* cells during the PEF treatment in the ceramic test cell. The vast majority of the *A. platensis* cells in the sample survived the treatment with the maximum field strength of 67 kV/cm and maximum number of impulses of 1000.

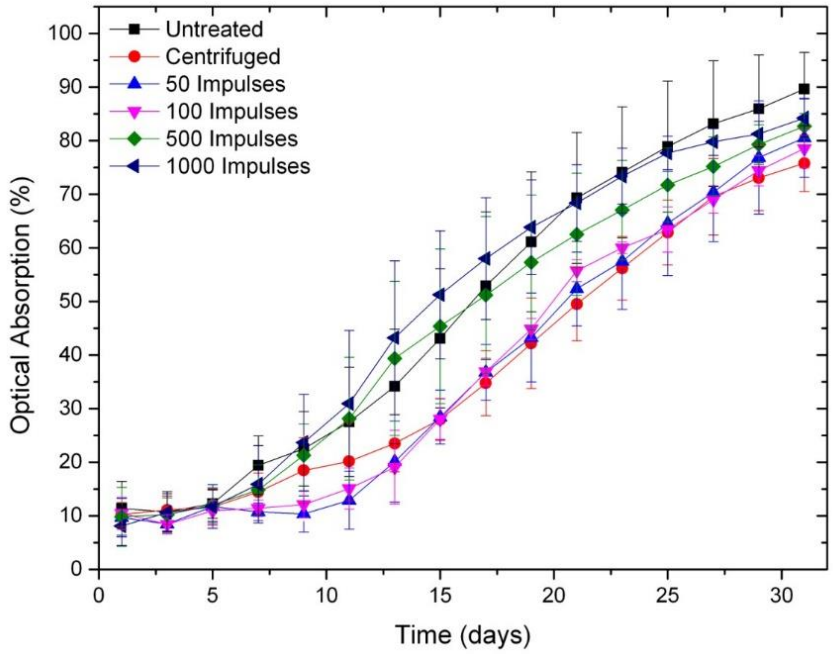


**Figure V.12** Growth curves for untreated, centrifuged and PEF treated (33 kV/cm) *A. platensis* sample. Data points are the average value of triplicate treatments, error bars show standard deviation (n=3).

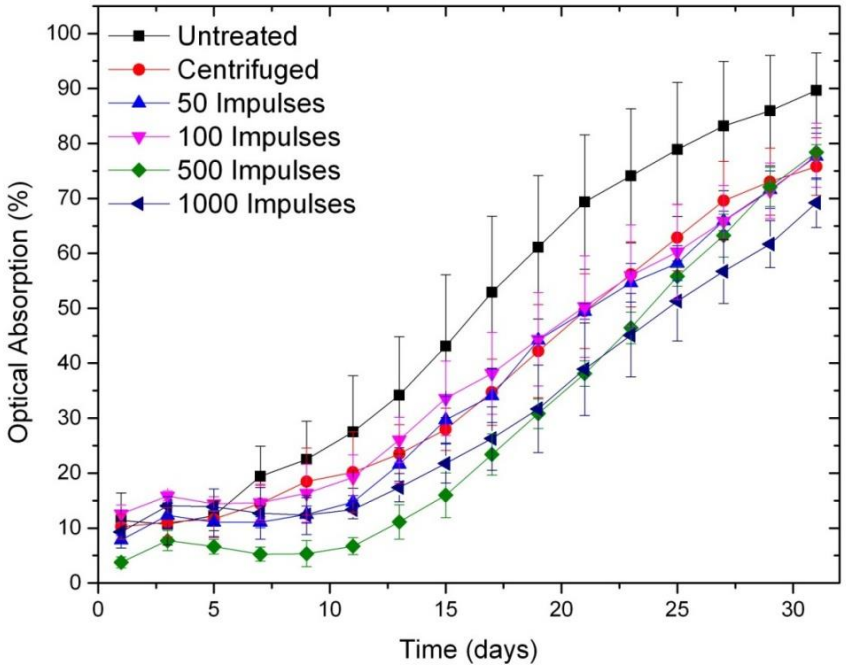


**Figure V.13** Growth curves for untreated, centrifuged and PEF treated (67 kV/cm) *A. platensis* sample. Data points are the average value of triplicate treatments, error bars show standard deviation (n=3).

#### 5.3.3.3 Temperature Measurement

Measurements of the sample temperature have also been conducted in the case of the ceramic test cell experiments. The results of these measurements showed that no change in temperature has been detected in all experiments in which the ceramic test cell was used. It was reported in [243] that the PEF treatment using a similar test cell limited the increase of the temperature significantly as compared with the traditional metallic test cell. However, this absence of the temperature increase observed in the present study could not be simply explained by the use of non-conductive ceramic test cell. Considering the results from visual inspection and growth curve measurements, it was possible to suggest that the electric field in the ceramic test cell relaxed over very short period of time without producing thermal or biological effects.

### 5.3.4 PEF Treatment of *A. platensis*: Summary of Results

The PEF treatment of *A. platensis* in both test cells produced valuable results which provided very useful information for the subsequent research. A brief summary of these results is provided below.

- Reliable PEF inactivation of the *A. platensis* was achieved in the metallic test cell by 500 square HV impulses with field strength of 33 kV/cm. This number was reduced to 50 pulses when the field magnitude was increased to 67 kV/cm.

- No damage to the external structure of the *A. platensis* cells was observed using an optical microscope with ×400 magnification. However, inactivation of the *A. platensis* confirmed that critical internal structural damage and cell dysfunction was induced by PEF treatment in the stainless steel test cell.

- The use of low conductivity solution helped to reduce the specific energy consumption significantly. The specific energy consumption of the PEF

treatment using the stainless steel test cell was at least 10 times lower than those values reported in the literature.

- The use of low conductivity solution also helped to reduce the heating effect during the PEF treatment. The maximum increase in temperature recorded during the experiments was ~ 2°C, which was significantly lower than temperature values reported in the literature for the PEF treatment in traditional metallic test cell.

- The PEF treatment using the ceramic test cell produced no inactivation results, which suggested that *A. platensis* was not subjected to strong enough or long enough electric field during the PEF treatment in the ceramic test cell.

## 5.4 PEF Treatment of *S. cerevisiae*

PEF treatment experiments of *S. cerevisiae* were also conducted using the initial designs of the PEF test cells, described in Chapter IV. Similar to the *A. platensis* experiments, square HV impulses were used for the PEF treatment of *S. cerevisiae*. These experiments also provided valuable information for the subsequent optimisation and improvement of the treatment of *S. cerevisiae* using the new PEF test cells. This section describes the experiment procedures and the obtained results. Significant findings and conclusions are highlighted and discussed in this section.

### 5.4.1 Experimental Procedures

Similar to the *A. platensis* PEF experiment, the suspension of *S. cerevisiae*, prepared as described in Section 5.1.3, was transferred into the PEF test cell via a syringe. The test cell was then connected to the square impulse generator in parallel with the 50 Ω matching resistor. Voltage magnitude of the generator output was set to 10 kV and 20 kV, which resulted in the electric field strength of 33 kV/cm and 67 kV/cm respectively. The liquid suspension containing *S. cerevisiae* were subject to 50, 100, 250, 500 and 1000 HV impulses. The population density of the *S. cerevisiae* sample was measured, as described in Section 5.2.2, prior and after the PEF treatment to

detect any inactivation induced by the PEF treatment. Temperature of the *S. cerevisiae* suspension was also measured before and after the PEF treatment to detect any thermal effects. All experiments were conducted in triplicate and the resulting data points represented an average of 3 independent measurements.

## 5.4.2 Results of PEF Treatment in the Stainless Steel Test Cell

This section presents the obtained experimental results of PEF treatment of *S. cerevisiae* using the stainless steel test cell. Analysis and discussion of the results are also presented in this section.

### 5.4.2.1 Temperature Measurements

Similar to the case of PEF treatment of *A. platensis* in the metallic test cell, the maximum increase in the temperature registered in the *S. cerevisiae* PEF experiments was less than 3 °C. The reason of this insignificant thermal effect could also be the use of low conductivity liquid suspension. In the *S. cerevisiae* PEF tests, the 0.05% Mycological Peptone was used as the suspending media to reduce the conductivity of the liquid suspension, which provided a conductivity of $(1.82 \pm 0.13) \times 10^{-2}$ S/m. This value was significantly lower than those reported in the literature, where significant heating of the liquid sample were reported. Therefore, the use of low conductivity sample solution was the most probable reason for this insignificant thermal effect, as explained in Section 5.3.2.3.

### 5.4.2.2 Inactivation Tendency

Figure V.14 shows the result of population count of the *S. cerevisiae* before and after PEF treatment using the stainless steel test cell. The results of these measurements were presented as the mean of surviving populations ($\log_{10}$ CFU/ml) and its standard deviation obtained from 3 independent PEF treatments. As can be seen from the figure, 2-$\log_{10}$ of reduction in population was achieved by 500 impulses with the field strength of 33 kV/cm. When the field strength was doubled, a 3-$\log_{10}$ of reduction was achieved by 500 impulses. In general, the PEF treatments using 67 kV/cm field strength provided 1-$\log_{10}$ more reduction in surviving population as

compared with the 33 kV/cm field strength with the same number of impulses. However, no further reduction in the surviving population was achieved with an increase in the pulse number. The inactivation curves seem to be saturated after 500 impulses, as can be seen in Figure V.14. This 'tailing' suggested that complete inactivation, as be seen in *A. platensis* experiments, was not achieved in the *S. cerevisiae* PEF experiment using the same metallic test cell.

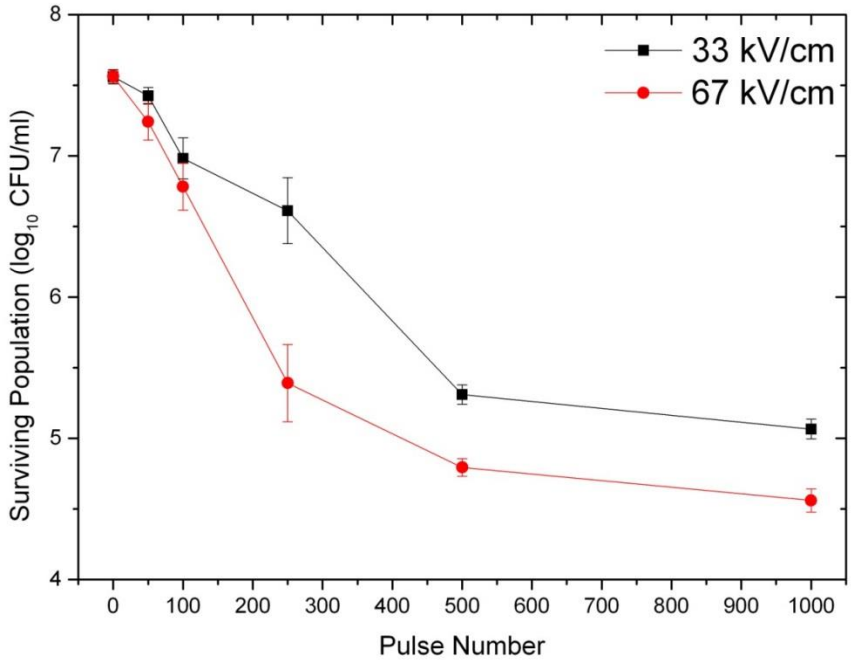


**Figure V.14** Surviving population of *S. cerevisiae* ($log_{10}$ CFU/ml) as a function of number of impulses. Data points are the average value of triplicate treatments, error bars show standard deviation (n=3).

## 5.4.3 Result of PEF Treatment in the Ceramic Test Cell

This section discusses and analyses the obtained experimental results of the PEF treatment of the *S. cerevisiae* in the ceramic test cell.

### 5.4.3.1 Temperature Measurements

Similar to the *A. platensis* PEF experiment using the ceramic test cell, no changes in the temperature have been detected in all *S. cerevisiae* experiments using the same

ceramic test cell. Considering the results from population counting, which will be introduced in the following section, it was likely that the *S. cerevisiae* cells were not exposed to the expected electric field (in terms of magnitude and duration) during the PEF process.

#### 5.4.3.2 Inactivation Tendency

The results of population count of *S. cerevisiae* before and after PEF treatment using the ceramic test cell are shown in Figure V.15. It can be seen from the figure, that no reduction in the *S. cerevisiae* population was achieved during the PEF treatment regardless of the field strength and pulse number in use. Once again, this result indicated that the *S. cerevisiae* cells remained viable after the PEF treatment in this ceramic test cell. Taken the *A. platensis* results into consideration, it suggested that the field strength inside the ceramic test cell was far less than the expected value. As a result, microorganisms treated in this ceramic test cell remained unaffected during the treatment. The potential reasons for the ineffectual PEF inactivation performance of the ceramic test cell will be discussed in Section 6.1.1.

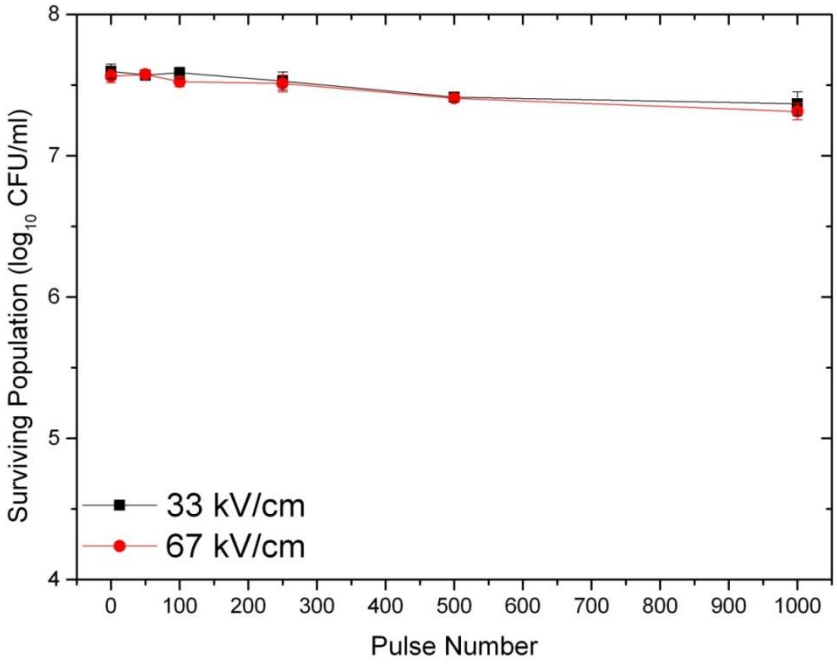


**Figure V.15** Surviving population of *S. cerevisiae* ($\log_{10}$ CFU/ml) as a function of number of impulses. Data points are the average value of triplicate treatments, error bars show standard deviation (n=3).

### 5.4.4 PEF Treatment of *S. cerevisiae*: Summary of Results

A summary of the results of the PEF treatment of *S. cerevisiae* using both test cells is provided in this section.

- The *S. cerevisiae* can be inactivated by the PEF treatment using the stainless steel test cell. 2-$\log_{10}$ of reduction in population was achieved by the application of 500 HV impulses with field strength of 33 kV/cm. Further 1-$\log_{10}$ reduction was achieved when the field strength increased to 67 kV/cm by the same number of impulses.

- Complete inactivation (7-$\log_{10}$ reduction in population) of the *S. cerevisiae* cells was not achieved using the stainless steel test cell. No further inactivation was observed after 500 impulses with both field strengths, leading to a 'tailing' effect in the inactivation curve.

- The use of low conductivity sample solution helped to reduce the heating effect of samples during the PEF treatment in stainless steel test cell. Similar to the *A. platensis* PEF tests, the maximum increase in temperature recorded during the *S. cerevisiae* PEF experiments was less than 3 °C.

- Similar to the *A. platensis* experiments, the PEF treatment of *S. cerevisiae* in the ceramic test cell produced no inactivation. *S. cerevisiae* was not inactivated using this dielectric test cell.

## 5.5 Discussion

The results of the PEF treatment of the *A. platensis* and *S. cerevisiae* using both stainless steel and ceramic test cells were presented in this chapter. The obtained results and main conclusions were also presented and discussed.

In general, the PEF treatment using the stainless steel test cell results in successful inactivation of both *A. platensis* and *S. cerevisiae*. As demonstrated in this chapter,

*A. platensis* was inactivated by 500 square impulses with field magnitude of 33 kV/cm and reliable inactivation was achieved by the application of 50 impulses if the field strength was doubled to 67 kV/cm. Although the *A. platensis* were successfully inactivated by the PEF treatment, the visual inspection of the individual cells revealed that no visible external structural damaged was produced. This finding suggested that the PEF treatment only induced an internal damaged and dysfunction of the microorganism cells. While in the *S. cerevisiae* experiments, 2-$\log_{10}$ reduction in *S. cerevisiae* population was achieved by 500 impulses at 33 kV/cm, further 1-$\log_{10}$ reduction was achieved by the increase in the field strength to 67 kV/cm.

The specific energy of the PEF treatment was also evaluated using the data from the *A. platensis* experiment using the metallic test cell. The results indicated that the specific energy consumption in the present study was much lower than the values reported in literature. It was calculated that the specific energy consumption in current study for reliable inactivation of *A. platensis* was as low as 0.35 MJ/kg. However in other microalgae studies [67, 68], the reported specific energy consumptions were 26 MJ/kg and 2 MJ/kg. The main reason of this improvement in energy efficacy was due to the use of low conductivity sample solution. This lower conductive solution reduced the conduction current significantly during the PEF treatment and therefore less energy was dissipated as Joule heating. The other benefit of using the low conductivity solution was therefore the elimination of heating effect commonly seen in other PEF studies.

Although inactivation of the microorganisms by the PEF treatment was successfully achieved using the stainless steel cell, some drawbacks of the current design were also discovered during the experiments. Electrical breakdowns occasionally occurred between the electrodes during PEF treatments. In addition, complete inactivation of *S. cerevisiae* was not achieved even by the application of 1000 impulses with the maximum field strength of 67 kV/cm, which raised a suspicion of potential low field areas (dead zones) in the stainless steel test cell. On the other hand, in the case of PEF treatment using the ceramic test cell, experiments with both *A. platensis* and *S. cerevisiae* confirmed that inactivation of microorganisms was not achieved by the current non-conductive test cell. The drawbacks of the stainless steel test cell and the

ineffective ceramic test cell both called for an improvement for the test cell design, which will be discussed in next chapter.

# Chapter VI

# DEVELOPMENT OF IMPROVED PEF TEST CELLS AND PEF SYSTEM

## 6.0 General

In Chapter V, it was demonstrated that the use of the non-conductive ceramic test cell in the PEF treatment was ineffective. On the other hand, it was shown that the use of low conductive solutions improves the energy efficacy of the PEF process and reduces the Joule heating. This important result supports the idea of utilising non-conductive or low-conductive PEF test cells and suggests that further improvements in the energy efficacy could be achieved if conduction through the sample can be reduced or totally eliminated. Therefore, it is important to analyse the potential reasons for the ineffective inactivation performance of the ceramic test cell and to find an alternative approach to implement such idea.

On the other hand, some drawbacks of the stainless steel test cell were discovered during the PEF experiments even though positive inactivation results have been achieved with this test cell. The initial design of the metallic cell led to occasional electrical breakdowns between the test cell's electrodes due to the presence of air bubbles. In addition, the results from the *S. cerevisiae* experiments suggested that potential dead zones may exist in the test cell. Therefore, it was also important to improve the design in order to optimize the PEF performance.

As the design of both dielectric and metallic test cells should be modified, it was decided to redesign both test cells for the subsequent PEF experiments. The drawbacks of the metallic test cell and the potential reasons for the ineffective performance of the dielectric cell will be analysed in this chapter. The redesigning process, based on the results obtained, will also be presented in this chapter.

One of the main objectives of this research is to investigate the effect of different pulse waveform on the PEF performance. Therefore, not only square impulses, but also two other types of the pulse waveforms will be used in the PEF treatment together with the modified test cells. The development of two pulse generators, which produce impulses with smooth exponential and oscillating exponential waveforms, will also be discussed in this chapter.

## 6.1 Drawbacks and Limitations of the Initial Test Cell Designs

Although preliminary PEF tests using the initially designed stainless steel test cell produced promising results, some drawbacks and limitations of this design were also found. The obtained results from the experiments using the ceramic test cell also indicate that the PEF process in this test cell was not efficient (no noticeable inactivation effects were recorded). This section will analyse potential reasons for the ineffective performance of the ceramic test cell and specific drawbacks of the stainless steel test cell and will provide an overview of potential solutions to these problems.

### 6.1.1 Potential Reasons for the Ineffectiveness of the Ceramic Cell

#### 6.1.1.1 Maxwell-Wagner Relaxation of Electric Field

During the PEF treatment, the field magnitude applied to the sample is obtained by measuring the voltage across the PEF test cell. This method provides an accurate estimation of the field in the liquid sample in the case of the metallic test cell. The stainless steel electrode can be seen as an ideal conductive electrode and the field strength across the sample can be calculated as voltage across the gap between the electrodes divided by the gap length. However, in the case of ceramic test cell, the Maxwell-Wagner field relaxation process takes place. As described in Section 3.2.1, this Maxwell-Wagner field relaxation process results in a field collapse between the dielectric layers with a characteristic collapse time equals to the Maxwell-Wagner relaxation time, $\tau_{MW}$. This suggests that the field strength in the liquid sample inside

the ceramic test cell collapses shortly after the pulse is applied. Therefore, the Maxwell-Wagner relaxation time of this ceramic test cell should be calculated according to Equation III.5. For the convenience of reading, this equation is showed here as Equation VI.1.

$$\tau_{MW} = \left(\frac{\varepsilon_l}{\varepsilon_d} + 2\frac{Z_l}{Z_d}\right)\frac{\varepsilon_0 \varepsilon_d}{\sigma_l} \qquad \text{(VI.1)}$$

where $\varepsilon_d$ and $\varepsilon_l$ represent the relative permittivity of the ceramic material and the liquid suspension respectively, $Z_d$ and $Z_l$ represent the width of the ceramic barrier and liquid suspension respectively and $\sigma_l$ is the conductivity of the liquid suspension.

Using Equation VI.1 and practical parameters of the test cell and liquid suspension, the Maxwell-Wagner relaxation time of the ceramic cell was found, $\tau_{MW}$ = 0.127 µs, which is only ~ 13% of the duration of the HV square impulse. To verify this calculation, a *PSpice* model of the PEF system with the ceramic cell was developed as direct measurements of the actual voltage drop across liquid suspension in the ceramic cell during PEF treatment are impossible. Figure VI.1 shows the equivalent circuit diagram of the PEF system developed in *PSpice*. The ceramic test cell is modelled as a *RC* equivalent circuit described in Section 4.4.1. The square impulse generator was also modelled using the lumped element circuit approach as described in Section 4.3.

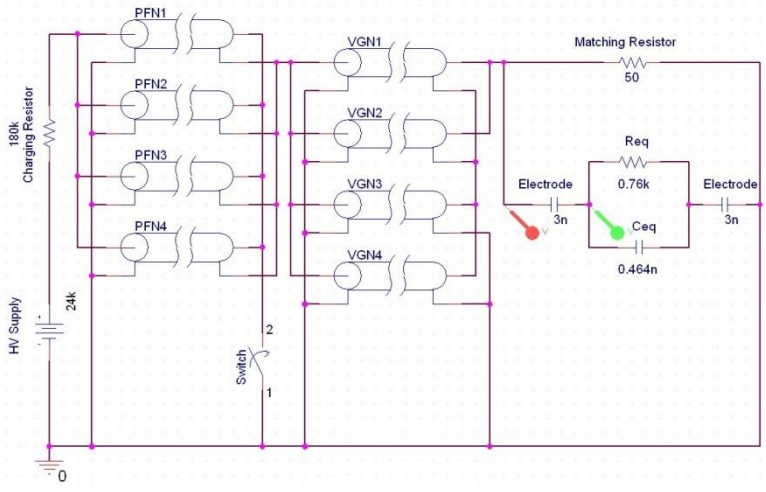


**Figure VI.1** Equivalent circuit diagram of the PEF system with ceramic test cell. PFN stands for pulse forming network; VGN stands for voltage gain network.

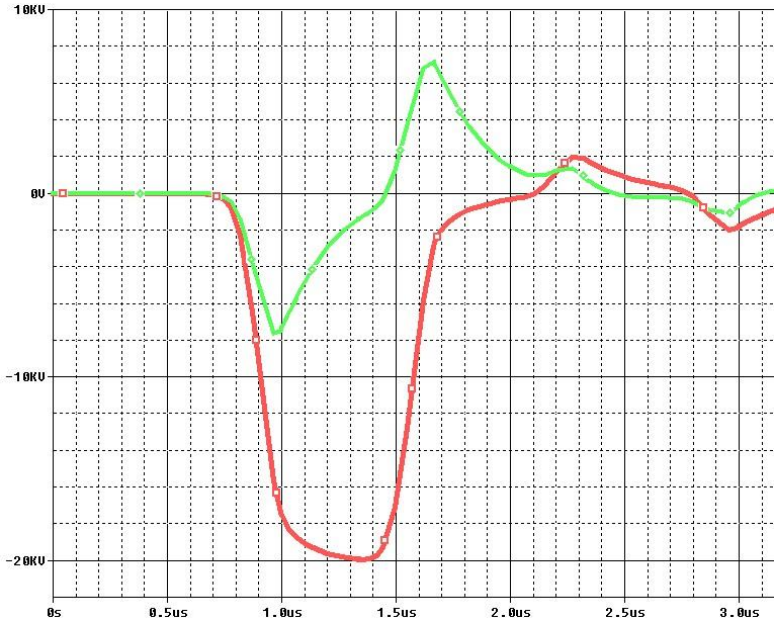


**Figure VI.2** Result of the *PSpice* simulation of PEF treatment using ceramic test cell. The voltage waveform in red indicates the voltage across the whole ceramic test cell; the voltage waveform in green indicates the voltage across the liquid suspension inside the ceramic test cell.

The result of the *PSpice* simulation is shown in Figure VI.2. As can be seen in the figure, the actual voltage across the cell rises to 90% of its maximum value after ~ 0.3 µs and starts to collapse at ~ 0.7 µs after the application of the impulse. However, the voltage drop across the liquid suspension behaves differently: it reaches its maximum value at ~ 0.3 µs after pulse application and then starts to collapse. The peak magnitude of the voltage drop in the liquid sample is significantly lower than the maximum voltage across the test cell. Despite 20 kV peak voltage across the whole ceramic test cell, the actual peak voltage across the liquid suspension can only reach ~ 8 kV. The result obtained from the *PSpice* simulation confirms the Maxwell-Wagner field relaxation process occurs in the ceramic test cell. Due to this Maxwell-Wagner field relaxation process, the voltage across the liquid suspension could not reach its maximum value as shown in Figure VI.2. This result indicates that the field strength applied to the sample could be much smaller than the expected value and its duration is only ~ 30 % of the pulse duration in the actual PEF treatment.

Also, as demonstrated in Section 3.1.3, an additional time is required for the trans-membrane potential to rise due to polarisation and charge accumulation process across the membrane. Therefore, the trans-membrane potential and its transient time could be further reduced and shorten by the combination of these two processes and the Maxwell-Wagner field relaxation process. To evaluate this combined effect on the trans-membrane potential, the analytical model described in Section 3.2.2 was conducted again with the practical parameters which were used in the PEF experiments described in Chapter V. The results of this simulation are shown in Figure VI.3 and Figure VI.4. Figure VI.3 demonstrates how the field strength across the microbial membrane is changing when the sample is treated in the ceramic test cell. As can be seen, the field strength peaking at the $\tau_{MW}$, which is 0.127 µs, before collapse due to the Maxwell-Wagner process. However, when compared with the trans-membrane potential of the bio-membrane in a sample treated in the stainless steel test cell, as shown in Figure VI.4, the peak field magnitude is only ~ 10% of the peak field magnitude achieved in the stainless steel cell.

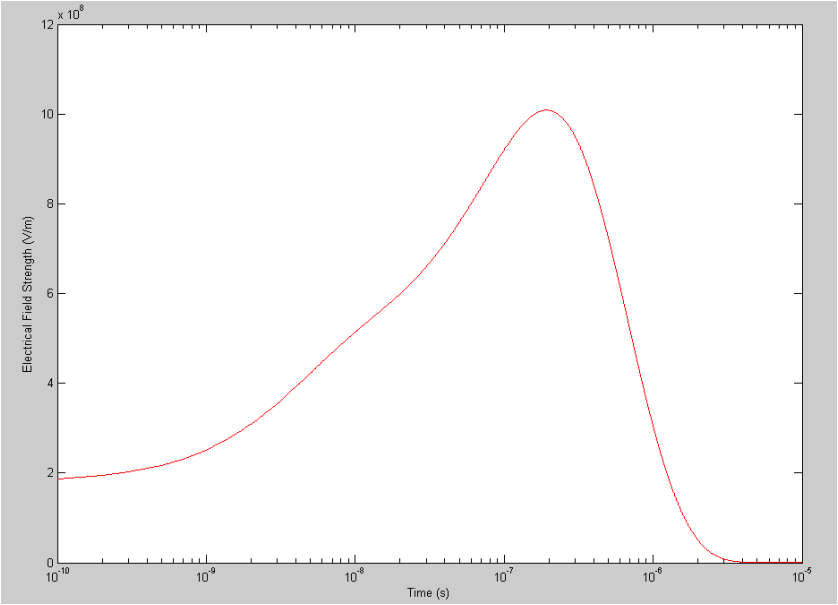


**Figure VI.3** Electric field strength across the microbial membrane when sample is treated in the ceramic test cell.

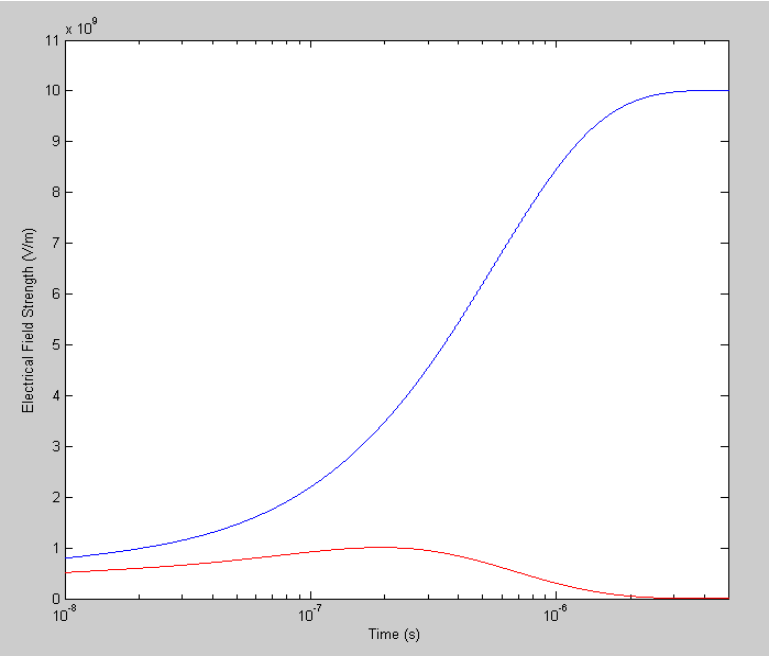


**Figure VI.4** Comparison between the electric field strength across the microbial membranes when samples are treated in the ceramic test cell (red line) and stainless steel test cell (blue line).

It can be concluded from these simulations that the Maxwell-Wagner field relaxation process plays a significant role in the PEF treatment process in the ceramic test cell. Due to this field relaxation, the actual field strength inside the test cell is much lower (40%) as compared to the field strength across the whole test cell. In addition, due to the initial polarisation and charge accumulation processes, the trans-membrane potential could only reach an even smaller value, which is only ~ 10 % as compared to the sample being treated in the stainless steel test cell. These simulation results suggest that the external electric field needs to be significantly higher in order to have sufficient field strength across the liquid suspension and microbial membrane in this ceramic test cell. In the non-conductive PEF study reported in [189], a similar design of the non-conductive PEF test cell was used. This study reported on a successful inactivation of *E. coli* in the ceramic test cell. However, the field strength used in [189] was significantly higher (from 130 kV/cm to 200 kV/cm) than the field strength in the present study. The maximum field strength used in the PEF experiments described in Chapter V was 67 kV/cm, which was only half of the minimum field used in [189]. The results obtained in [189] confirmed the conclusion

from the above simulations that significantly higher field strength is required for successful inactivation of microorganism in a ceramic test cell. The relatively low field strength used in Chapter V could result in lower trans-membrane potentials due to the Maxwell-Wagner relaxation process, so that the lethal electroporation process may not occur under these conditions.

#### 6.1.1.2 Ceramic Electrode Surface

The surfaces of the stainless steel electrodes designed in Section 4.1 were polished to a mirror finish. However, the same degree of smoothness was not achieved in the ceramic electrodes surfaces. Due to mechanical properties of the ceramic material, the surface of this ceramic had visible degree of roughness when the capacitor is cut. Although all possible efforts were made to polish the ceramic surfaces, these surfaces remained uneven due to the small pits, as shown in Figure VI.5. As a result, the field distribution in the vicinity of these electrodes can be distorted by this uneven surface.

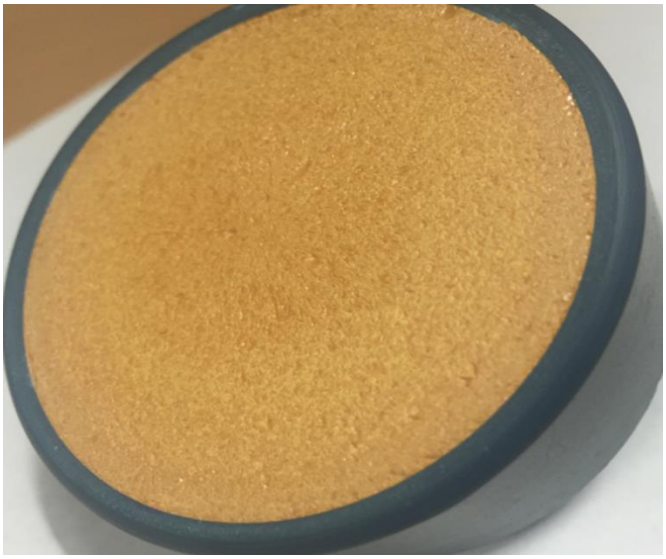

**Figure VI.5** Close look at the surface of the dielectric electrode.

#### 6.1.1.3 PEF Experiment with Higher Field Strength

As discussed in the previous sections, the higher electric field strength might be required in order to achieve successful inactivation of microorganism using the

ceramic test cell. Therefore, PEF treatment of *S. cerevisiae* in the ceramic test cell was conducted using the highest possible field strength obtained using the pulse generator described in Section 4.3. Due to technical restrictions, as demonstrated in Section 4.3, the maximum operating voltage generated by this pulsed power system with a stable pulse repetition rate was 24 kV. Therefore, the maximum field strength could be increased to 80 kV/cm with 3 mm inter-electrode gap.

The *S. cerevisiae* samples were prepared following the procedure described in Section 5.1.3. The *S. cerevisiae* suspension was transferred into the ceramic test cell and subjected to 50, 100, 250, 500 and 1000 square impulses with field magnitude of 80 kV/cm. The surviving population of the *S. cerevisiae* in CFU/ml was then compared with the untreated sample. The results of these PEF tests are shown in Figure VI.6.

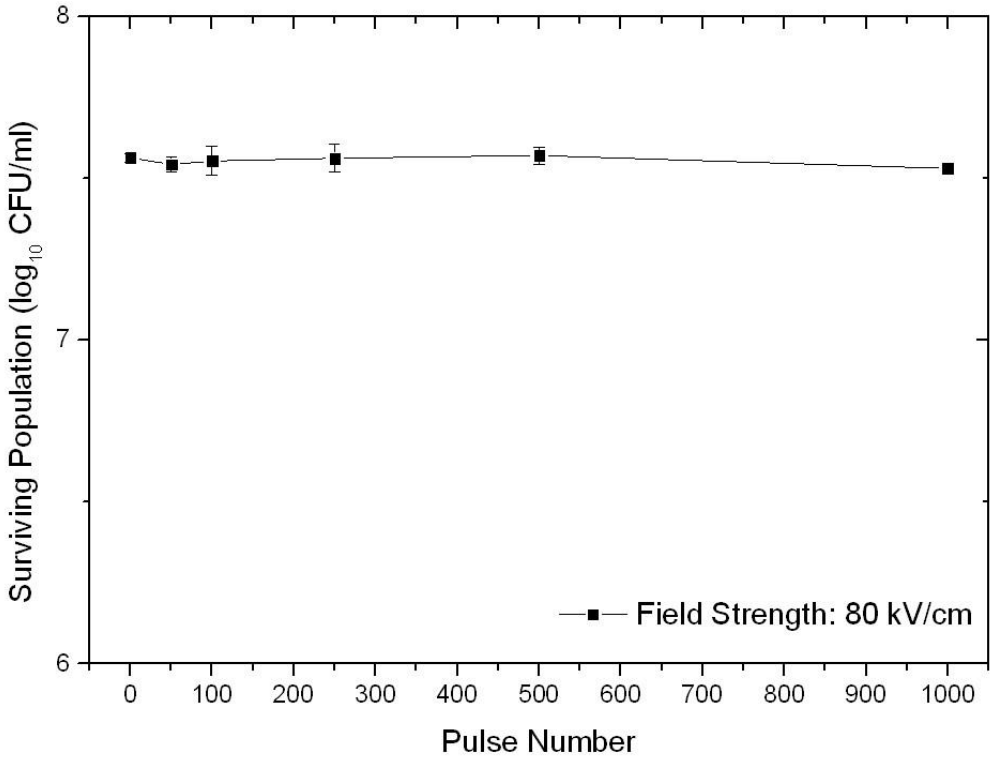


**Figure VI.6** Surviving population of *S. cerevisiae* ($log_{10}$ CFU/ml) as a function of number of impulses. Data points are the average value of triplicate treatments, error bars show standard deviation (n=3).

As Figure VI.6 shows, no inactivation of *S. cerevisiae* was achieved using 80 kV/cm field strength and 1000 or less square impulses in the ceramic test cell. This test suggested that much higher electric field strength was required in order to achieve inactivation of microorganism using this ceramic test cell. As shown in [189], the minimum field strength needed for successful inactivation in a similar ceramic test cell was 130 kV/cm. However, the PEF performance using the field strength lower than 130 kV/cm has not been investigated in that study. Therefore, based on the results obtained in the present study and the results reported in [189], it was possible to state that the critical electric field strength for PEF inactivation could lies between 80 kV/cm and 130 kV/cm for a non-conductive ceramic test cell.

## 6.1.2 Drawbacks of the Stainless Steel Cell

### 6.1.2.1 Electrical Breakdown inside the Test cell

One of the significant drawbacks observed during PEF experiments using the stainless steel test cell was the occasional electrical breakdowns between the electrodes. The cause of these breakdowns is the presence of air bubbles inside the test cell. As discussed in Section 2.5.4.3, gaseous bubbles can be generated by the electrolysis process during the PEF treatment, which normally triggers electrical breakdown after the application of a few impulses. However, during the PEF experiments described in Chapter V, some of the breakdowns occurred immediately after the application of the first HV impulse which suggests air bubbles existed before the PEF treatment.

Due to the position of the inlet hole, which was located in the middle of the inter-electrodes gap, small air bubbles can be introduced into the liquid suspension in the test cell during the filling procedure. In addition, as the inlet hole was relatively small and the test cell was a closed-top cell, it was difficult to inspect visually whether any air bubbles remain in the cell after filling it with the liquid suspension. The presence of such air bubbles caused undesirable electrical breakdowns inside the test cell during the PEF process, which not only interrupt the PEF treatment but also damage the surfaces of the electrodes, leaving breakdown pits on the electrode

surface. These breakdown pits with sharp edges increased the probability of undesirable electrical breakdown further

#### 6.1.2.2 Low Field Zones

The experimental results of the PEF test with *S. cerevisiae* in the stainless steel cell suggest that potential zones with low electric field ("dead" zones) may exist inside the test cell. The obtained results indicate that 3-$\log_{10}$ reduction in the yeast population can be achieved by 500 PEF impulses, which means that 99.9 % of the yeast population in the sample had been inactivated by the HV impulses. However, the rest of the *S. cerevisiae* population in the sample, 0.1 %, still remained viable even if the pulse number was increased to 1000. Therefore, it was suggested that potentially there were dead zones in the stainless steel test cell, which accounted for 0.1 % of the total sample volume.

In order to identify these potential "dead" zones in which the field strength was lower than the critical field required for inactivation, an electrostatic field distribution in the cell was modelled using *QuickField* software. The result of this modelling is shown in Figure VI.7. As this figure shows, the majority of the treatment volume has a uniform field distribution. However, there are some areas where the field strength is much lower than the uniform field strength in the center of the test cell. Figure VI.8 shows the local field distribution in these "dead" zones. As highlighted in the figure, two types of "dead" zones have been identified. "Dead Zone" 1 is the small gap between the electrode and the nylon spacer created by the presence of the O-rings. "Dead Zone" 2 is the inlet hole for the syringe. The electric field strength in these areas is almost zero. Therefore, microorganisms in these areas remain untreated during the PEF process. This modelling result could explain the reason why complete inactivation was not achieved in this stainless steel test cell: a small portion of the liquid suspension remained untreated in these low-field zones.

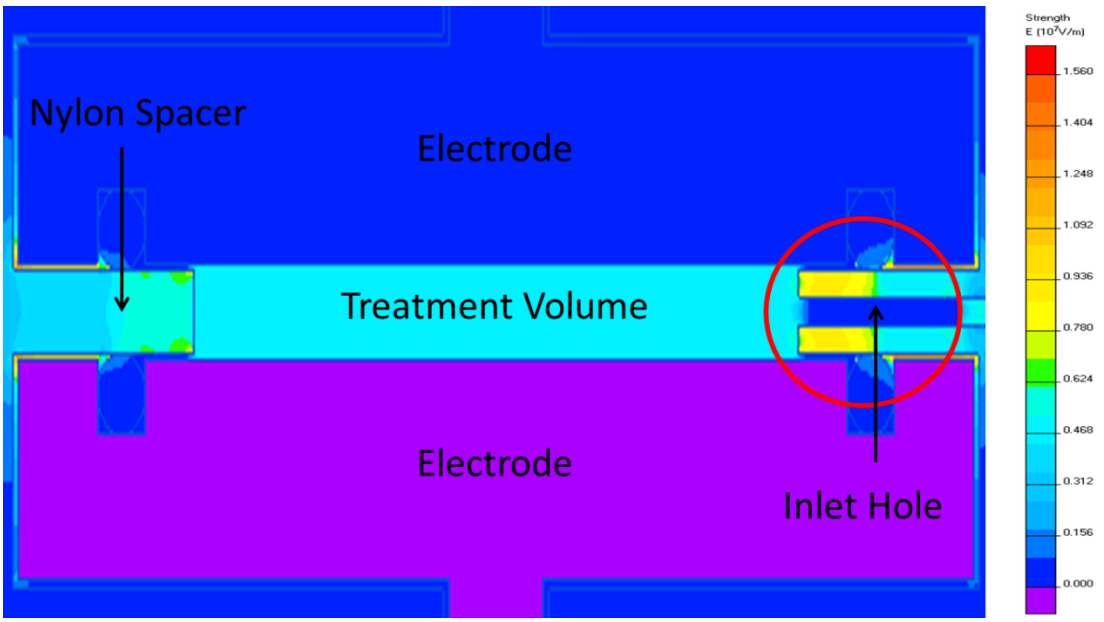


**Figure VI.7** Electrostatic field distribution in the metallic cell.

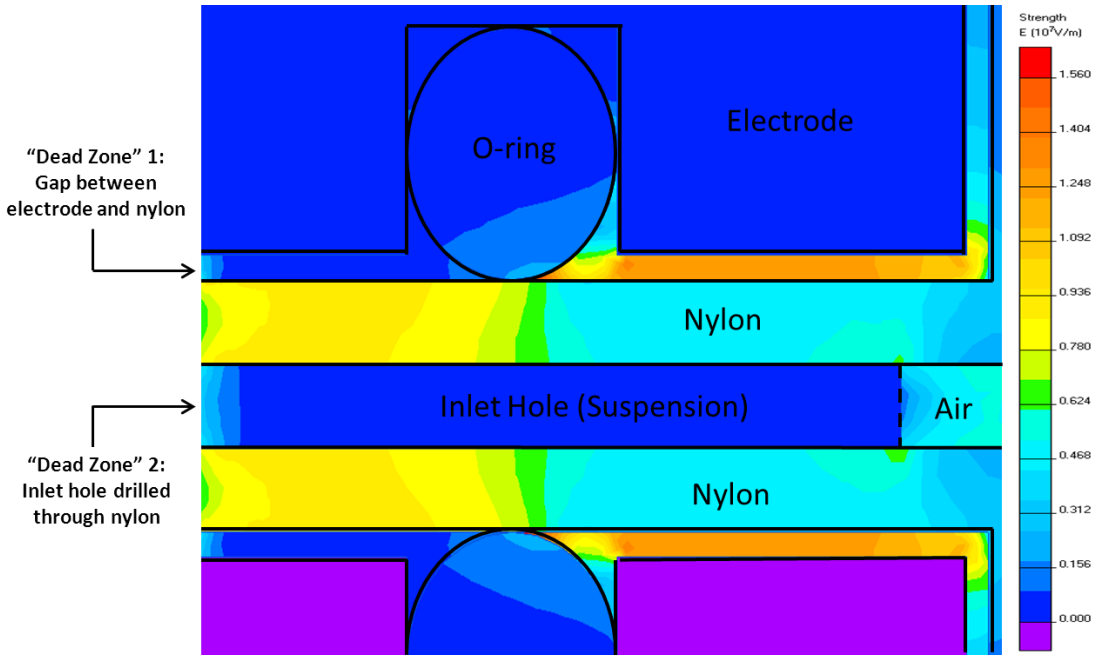


**Figure VI.8** Local electric field distribution in the potential dead zones.

### 6.1.2.3 Field Strength Limitations

As discussed in Section 4.3, it was found that due to some technical restrictions including operational performance of the pulsed power switch filled with air and

mismatch between the load impedance (PEF test cell) and the generator, the maximum operation voltage generated by this pulsed power system was 24 kV. As a result, the maximum field strength across the sample inside the test cell was limited to ~ 80 kV/cm according to Equation IV.1. Therefore, with the limited output voltage from the pulse generator, this stainless steel test cell with 3 mm inter-electrode gap was no longer suitable for PEF treatment with elevated levels of electric field and a modified test cell with smaller inter-electrode gap is required for this purpose.

## 6.2 Modified Design of the Metallic Test cell

Analysis of the drawbacks identified during the preliminary PEF tests was discussed in Section 6.1. This analysis leads to the conclusion that redesigning of the metallic test cell is required. A new design of metallic PEF test cell aims to achieve the following objectives: to avoid the presence of air bubble inside the PEF test cell after filling procedure; to enable the inspection and removal of any trapped air bubble; to eliminate potential low field zones identified in Section 6.1.2.2; and to enable PEF tests with elevated electric field strength.

### 6.2.1 New Metallic Test Cell Topology

In order to eliminate air bubbles in the test cell, an open-top topology for the test cell was proposed. The advantage of such open-top design is in natural upward movement of air bubbles formed in the liquid suspension during the filling process due to the buoyant force. In addition, such open top design allows visual inspection to be conducted. Air bubbles inside the test cell can be discovered prior to the test and any trapped air bubbles can be removed by tipping it out using a needle. Besides, the open-top design does not require an inlet hole as liquid is transferred into the cell using open top. Therefore, one of the potential dead zones, identified in Section 6.1.2.2, can be eliminated.

The open top test cell is equipped with two parallel plane stainless steel electrodes which are separated with an Π-shaped PTFE spacer as shown in Figure VI.9(a). The electrodes and the spacer are tighten by 7 sets of nylon screws, as shown in Figure

VI.9(b). The rectangular shape of the electrodes is needed to fit in the internal structure of a pressurised chamber used in the PEF treatment system, which will be introduced and discussed in Section 6.4.3.

To achieve a higher electric field magnitude using the square-pulse HV generator, the inter-electrode distance should be reduced according to Equation IV.1. In an attempt to achieve the field strength of 200 kV/cm, as used in [189], 1 mm inter-electrode gap was used. The electrode cross-section (their length and width) was selected to provide sufficient volume of liquid suspension for post treatment microbiological analysis.

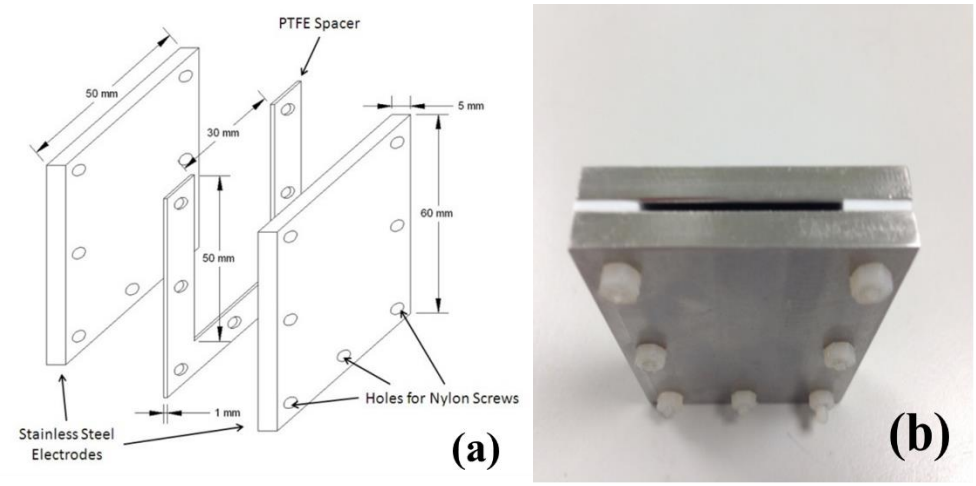


**Figure VI.9** Re-designed metallic PEF test cell. (a) Schematic diagram of exploded metallic test cell. (b) Fully assembled metallic test cell.

## 6.2.2 Electrode and Spacer Materials

The electrodes used in this new test cell were manufactured of stainless steel, as in the case of the original test cell (Section 4.1.2). However, the 1 mm Π-shaped spacer was made of PTFE rather than nylon, which was used as the spacer material in the original test cell design, as the rigidness of nylon makes it very difficult to manufacture the spacer with the required shape. The choice of PTFE was proven to be a right one as this material provides a stable shape and maintains required thickness when compressed with nylon screws. In addition, a relative softness of

PTFE means a good sealing can be achieved by compression of the electrodes and the spacer. Therefore, O-rings were no longer needed and the other potential dead zone due to the presence of O-rings, as identified in Section 6.1.2.2, can be eliminated.

## 6.3 Design of a $TiO_2$-Coated Test Cell

In the case of PEF treatment with non-conductive dielectric electrodes, the Maxwell-Wagner field relaxation process will lead to a field collapse with a characteristic time equals to the Maxwell-Wagner relaxation time, $\tau_{MW}$. In the case of the ceramic test cell, $\tau_{MW}$ is 0.127 µs, which results in a significant smaller trans-membrane potential and shorter effective treatment time, as demonstrated in Section 6.1.1.1. Together with an increase in the applied electric field in order to achieved inactivation of microorganisms, another approach should also be considered to minimise the effect of Maxwell-Wagner field relaxation process. Based on this consideration, a completely new test cell with Titanium dioxide ($TiO_2$) coated electrodes had been designed. Different aspects of design and development of this test cell will be presented in following sections.

### 6.3.1 Selection of Dielectric Material

As demonstrated in Section 6.1.1, short $\tau_{MW}$ can significantly restrict the development of trans-membrane potential. Therefore, the effect of Maxwell-Wagner field relaxation can be limited if $\tau_{MW}$ will be increased, at least by a factor of 10, as compared with the ceramic test cell. According to Equation VI.1, $\tau_{MW}$ is defined by the permittivity of the dielectric material and liquid suspension, by the thickness of the dielectric layer, by the inter-electrode gap, as well as by the conductivity of the liquid suspension. The electrical properties of the liquid suspension and the inter-electrode distance cannot be changed, leaving selection of a dielectric material with different properties the only optimisation option. As can be seen from Equation VI.1, the permittivity and the thickness of the dielectric material affect the Maxwell-Wagner relaxation time. The relationship between the $\tau_{MW}$ and these two factors are plotted in Figure VI.10 and Figure VI.11. It can be found from these figures that

dielectric material with higher permittivity and smaller thickness can lead to a longer Maxwell-Wagner relaxation time. As highlighted in the figures, in order to provide a $\tau_{MW}$ around 1 µs, which equals to the pulse duration, the relative permittivity of the dielectric material needs to be increased to 40000 (with the thickness of the material unchanged, 30 mm) or the thickness of the dielectric material needs to be reduced to 2.6 mm (with the permittivity of the material unchanged, 3500). However, dielectric materials with extremely high permittivity (>10000) are rare. Therefore, reducing the thickness of the dielectric material is the more practical approach to increase the $\tau_{MW}$ of a non-conductive PEF test cell.

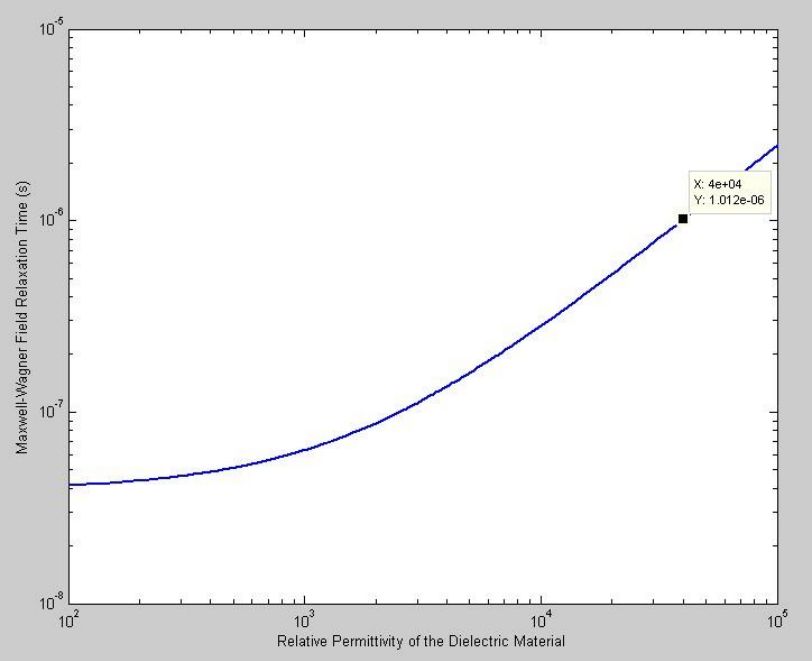


**Figure VI.10** Relationship between the $\tau_{MW}$ and the relative permittivity of the dielectric material.

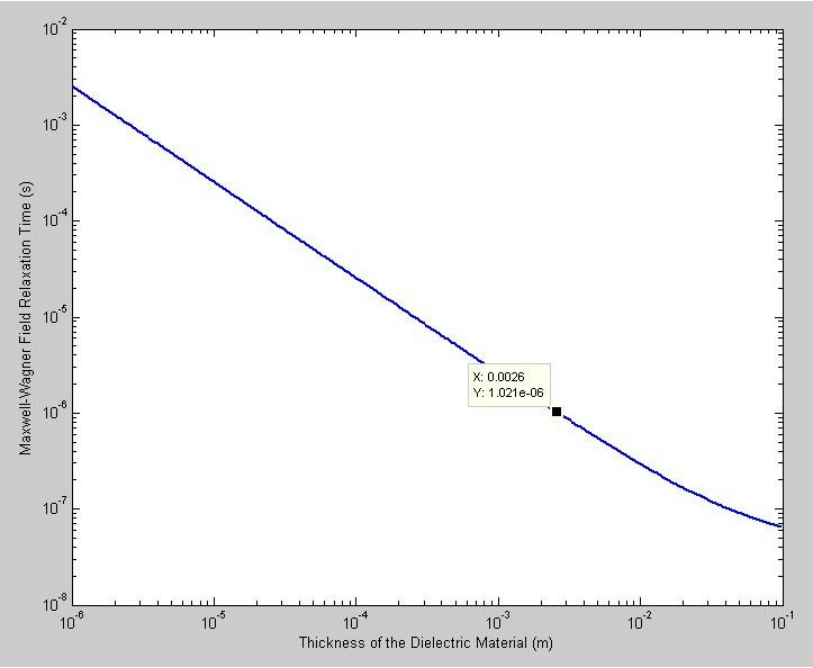


**Figure VI.11** Relationship between the $\tau_{MW}$ and the thickness of the dielectric material.

Based on this consideration, a copper plate coated by a thin film of $TiO_2$ was selected as the electrode material of the new test cell. This $TiO_2$-coated copper plate was processed by sol-gel process, in which sol solution containing $TiO_2$ is sprayed on the surface of the copper plate for several times. The end product is a copper plate coated by a smooth, ultra-thin (2 μm) film, which is consisted of several layers of $TiO_2$, as shown in Figure VI.12. The smooth surface of the $TiO_2$ film provides an even distribution of the electric field and minimises the possibility of field distortion as suggested in Section 6.1.1.2.

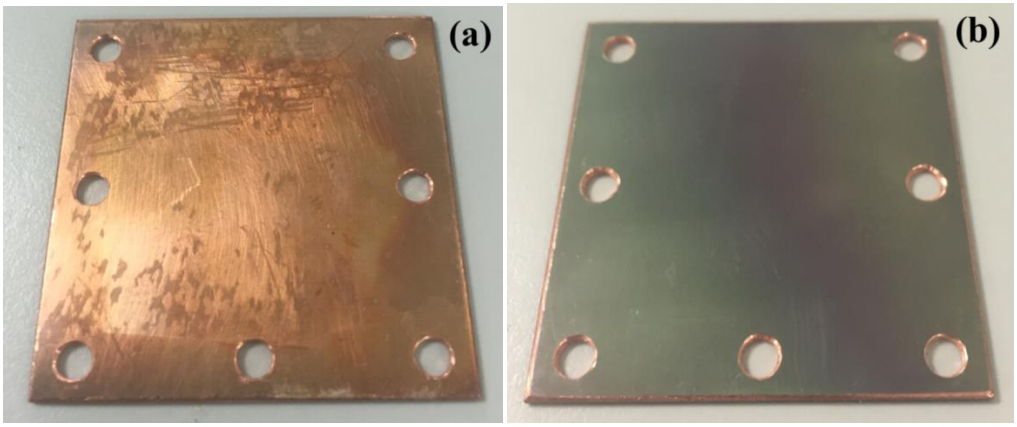


**Figure VI.12** The $TiO_2$-coated copper plate: (a) the un-coated side; (b) the $TiO_2$-coated side.

Titanium dioxide can form a stable dielectric ceramic film in low temperature conditions, [243-246], which is applicable in the temperature condition in the present study. It was shown in [243] that the conductivity of a dry, thin $TiO_2$ film is ~ $5\times10^{-7}$ μS/cm, which suggested a thin layer of $TiO_2$ can be a good insulation in dry condition. It was also reported in [244] that the dielectric constant of $TiO_2$ is ~ 95 at room temperature. As the dielectric constant of $TiO_2$ is higher than the dielectric constant of water (~80), the electric field will be concentrated in the liquid suspension rather than on the $TiO_2$ layer, as demonstrated in Section 4.2.1. Although the relative permittivity of $TiO_2$ is significantly smaller than the permittivity of the ceramic material in the ceramic test cell, the 2 μm ultra-thin $TiO_2$ layer will provide a much longer Maxwell-Wagner relaxation time, ~ 10 μs, as compared with the ceramic test cell (Section 6.1.1.1). In order to evaluate the trans-membrane potential in the microbial membrane treated in the test cell with the $TiO_2$-coated electrodes, the same analytical model described in Section 3.2.1 was used. The obtained results, as shown in Figure VI.13, indicate that the field strength developed across the membrane can reach similar magnitude as in the case of the stainless steel test cell.

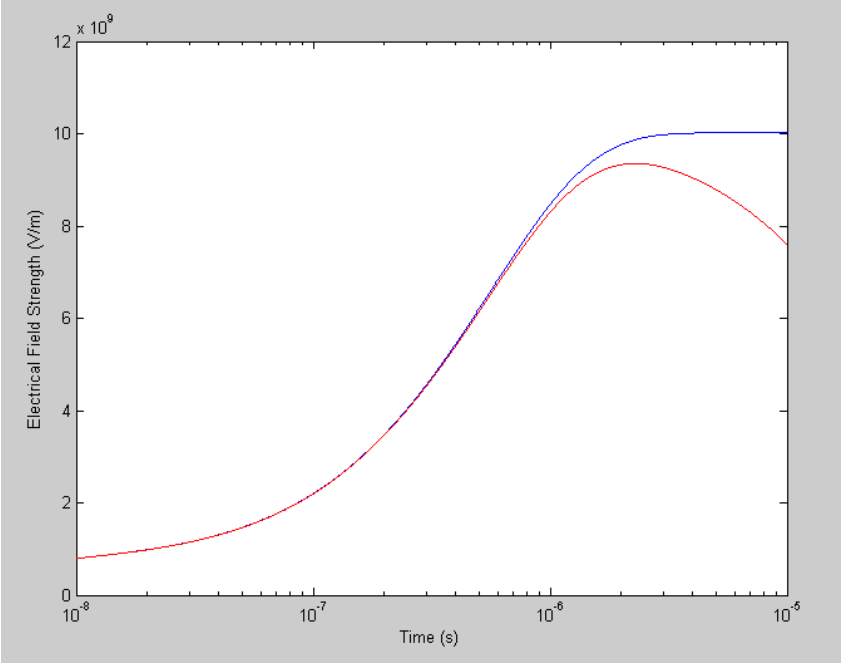


**Figure VI.13** The electric field strength across the microbial membrane treated in the proposed $TiO_2$-coated test cell (red line) and in the stainless steel test cell (blue line).

### 6.3.2 $TiO_2$-Coated Test Cell Topology

In the case of $TiO_2$-coated test cell, it would be beneficial to have a topology similar to the new stainless steel test cell. Therefore, a similar square shaped open-top design was employed, as shown in Figure VI.14(a). Two $TiO_2$-coated electrodes are separated by the Π-shaped PTFE spacer, forming an open-top treatment volume. The thickness of the PTFE spacer is 1 mm, which is identical to the spacer used in the new stainless steel test cell. Therefore, the electric field strength in the $TiO_2$-coated test cell can reach 200 kV/cm.

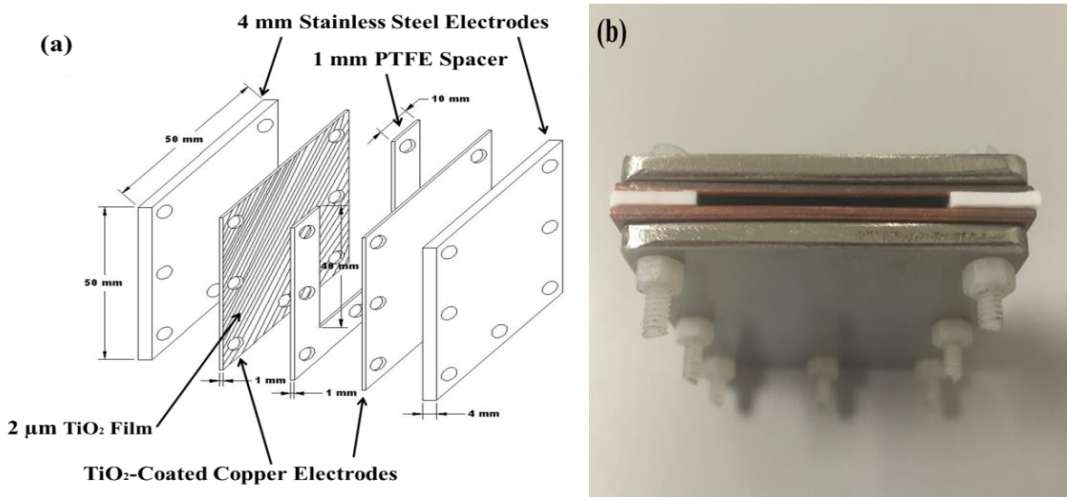


**Figure VI.14** The $TiO_2$-coated PEF test cell. (a) Schematic diagram of the exploded test cell. (b) Fully assembled test cell.

Since $TiO_2$-coated copper plates are relatively thin, with a thickness of 1 mm, two 4 mm stainless steel plates are connected to the un-coated side of each copper plate, as shown in Figure VI.14(b). By doing so, the total thickness of each electrode is extended to 5 mm, which is identical to the new stainless steel test cell. The fully assembled $TiO_2$-coated test cell will also be thick enough to fit into the pressurized chamber, described in Section 6.4.3. The treatment volume of the dielectric cell (1.2 $cm^3$) is slightly smaller than the new stainless steel cell (1.5 $cm^3$), which is due to the smaller dimensions of the $TiO_2$-coated copper plates. However, this volume is still large enough to provide sufficient volume of liquid suspension for post treatment analysis.

### 6.3.3 Ionic Conduction in the $TiO_2$-Coated Test Cell

As reported in [243], in dry condition the thin $TiO_2$ layer is a good insulator. Measurements of the resistance of the $TiO_2$-coated electrodes in dry conditions have also been conducted in the present study using a digital multi-meter. All measurements demonstrated that there is no conduction through the $TiO_2$ dry thin film. However, it was found that the conductivity of the $TiO_2$-coated electrodes increases significantly when this thin film is in contact with water.

The conductivity tests performed during this study revealed that the $TiO_2$-coated electrodes became conductive when in contact with water/water solution. As demonstrated in Figure VI.15, a conduction through the $TiO_2$ film was detected by the digital multi-meter: a drop of water was placed on the surface of the $TiO_2$ film, and the digital multi-meter was used to measure the resistance between two probes, one in contact with the water dropped on the $TiO_2$ surface and another in contact with the bottom (uncoated) side of the electrode. Therefore, during the PEF treatment when the $TiO_2$-coated test cell is filled with liquid suspension, the $TiO_2$ film became conductive and ionic current can flow through the test cell. The mechanisms for this conduction through the $TiO_2$ film may include ionic transport through a thin $TiO_2$ film and requires further investigation using research methods which are beyond the scope of this project.

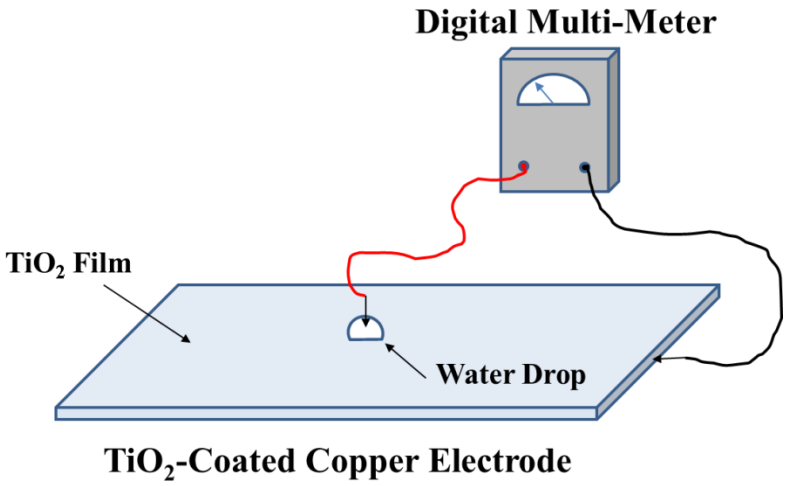


**Figure VI.15** Demonstration of the exploratory experiment about the conductivity characteristic of the $TiO_2$-coated electrode.

Measurements of current in the $TiO_2$-coated test cell during PEF process were conducted in order to obtain conduction current. The current measurements were used for calculations of the specific energy consumption of the PEF process. The results of the current measurements demonstrate that there is an ionic current in the $TiO_2$-coated test cell during PEF process, as shown in Figure VI.16. As can be seen from Figure VI.16(a), the current waveform in the $TiO_2$-coated test cell is very similar to the current waveform obtained in the stainless steel test cell, which suggests the dominant current regime in the $TiO_2$-coated cell is the ionic conduction rather than displacement current obtained in the ceramic test cell, as shown in Figure VI.16(b). This finding confirms that the $TiO_2$-coated electrodes became conductive when the test cell is filled with water solution during the PEF treatment.

Although this result suggests that this $TiO_2$-coated test cell could not be considered as a completely non-conductive test cell filled with liquid, the current measurement indicated that a notable reduction in the conduction current is achieved using this test cell, as shown in Figure VI.16(a). Since the ionic conduction current is the main cause of the energy losses in the PEF test cell, as discussed in Section 5.3.2.4, this notable reduction in the ionic conduction current means significant reduction in the energy consumption of the PEF process can be achieved using this $TiO_2$-coated test cell. Therefore, it was decided to investigate the PEF performance of this low-conductive PEF test cell with $TiO_2$-coated electrodes.

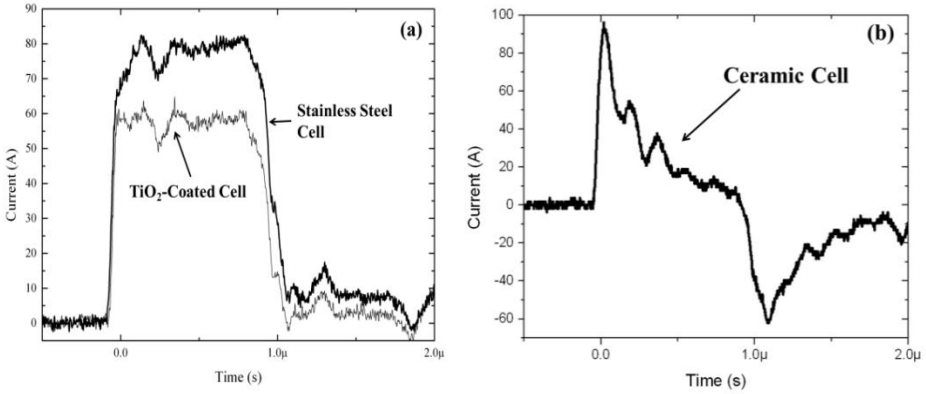


**Figure VI.16** Current waveforms obtained during PEF treatment using square impulse. (a) Dark line: Current waveform in the test cell with stainless steel electrodes; Gray line: Current waveform in the test cell with $TiO_2$-coated electrodes; (b) Current waveform in the test cell with ceramic electrodes.

## 6.4 Pulse Power Systems

As discussed in Section 2.6, one of the main objectives of the project is to investigate the effects of different pulse wave-shape on PEF treatment. Therefore, in addition to the ready-made square impulse generator described in Section 4.3, two more pulse power systems were designed and built for the PEF studies using the re-designed stainless steel PEF test cell and the $TiO_2$-coated PEF test cell.

### 6.4.1 Smooth Exponential Impulse Generator

Apart from the HV square impulse, other types of waveforms were investigated in this project. One of them is the HV impulse with smooth exponential waveshape. To generate impulse with smooth exponential waveshape, a new pulse power system was designed and built during this project.

As discussed in Section 2.4.1, a single exponential impulse can be produced by a simple *RC* circuit, shown in Figure VI.17. When the switch is open, the capacitor is charged through the charging resistor up to the required voltage level. Once the switch is closed, the capacitor discharges through the load. The voltage across the load rises to the supply voltage rapidly and then decays exponentially according to Equation VI.2.

$$v(t) = V_0 \cdot e^{-\frac{t}{(R_L // R_{pro})C}} \qquad \text{(VI.2)}$$

where $v(t)$ is the transient voltage across the load, $V_0$ is the supply voltage, $t$ is the time, $R_L$ is the resistance of the load, $R_{pro}$ is the resistance of the protective resistor and $C$ is the capacitance of the charging capacitor.

An exponential impulse generating system based on this *RC* circuit was designed and built as shown in Figure V.19. The system consists of a high voltage DC charging unit, a charging resistor, a self-breakdown plasma switch, a charging capacitor and a

protective resistor. The detail of each components and the consideration behind the selection are introduced in the following sections.

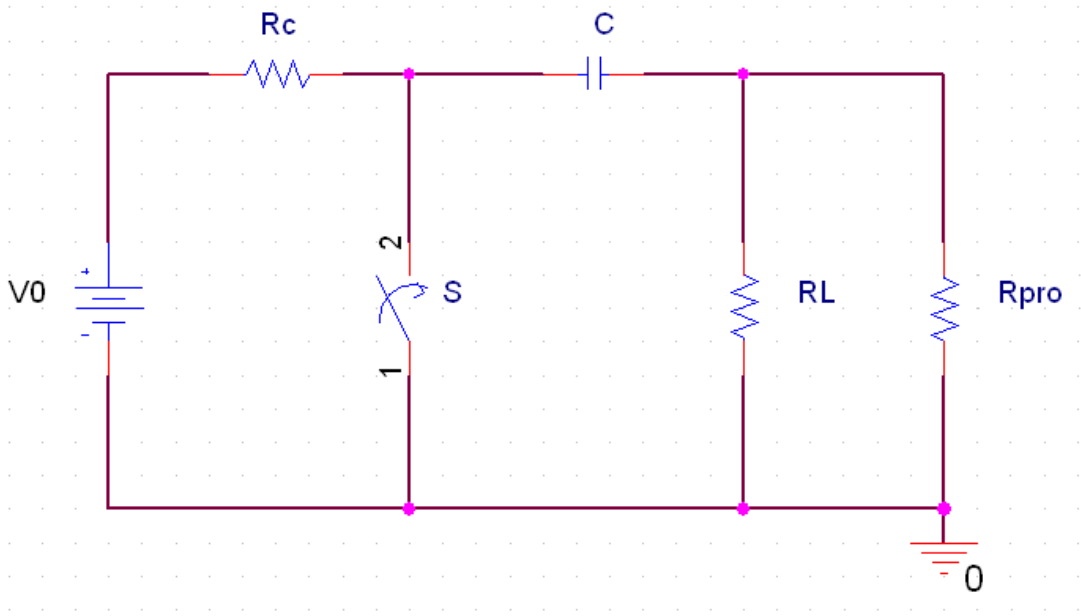


**Figure V.17** Diagram of a simple exponential impulse generating *RC* circuit.

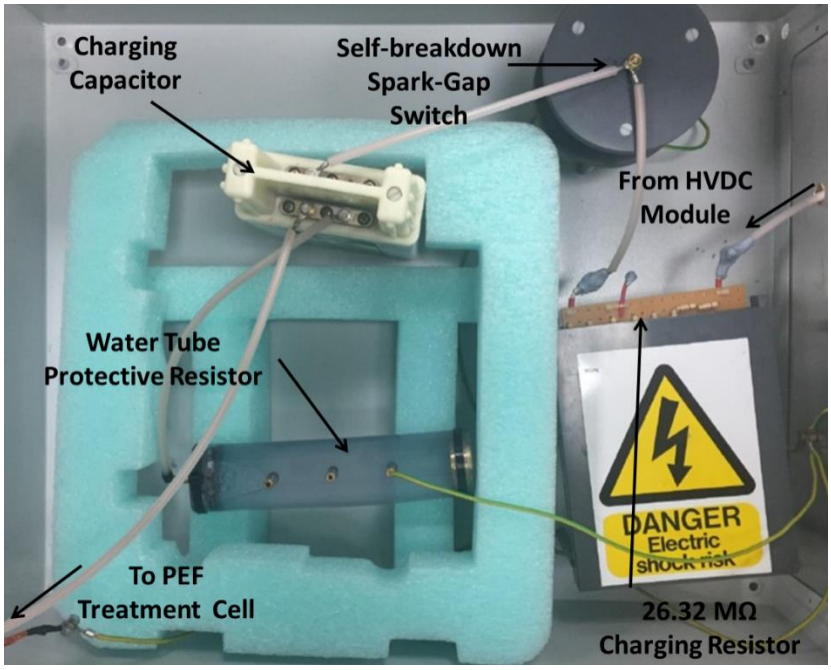


**Figure V.18** Overview of the exponential impulse generation system.

#### 6.4.1.1 High Voltage DC Module

The HVDC module, manufactured by Glassman, type EH50P2, was used to provide HV charging voltage to the RC circuit. In order to be consistent with the square impulse generator, the module has a positive polarity with the maximum output voltage of +50 kV. Therefore, the impulse generated at the output terminal of the charging capacitor, which connects to the PEF test cell, has a negative polarity. This HVDC module has both voltage and current regulators. The voltage regulator controls the magnitude of the charging voltage on the charging capacitor. The current regulator controls the magnitude of the charging current, thereby controls the time required to reach the set charging voltage. Therefore, the pulse repetition rate can be modified by the current regulator.

#### 6.4.1.2 Charging Resistor

The charging resistor, $R_C$, is connected between the HVDC module and the input terminal of the charging capacitor. The resistance of this charging resistor should be relatively high so that the capacitor can be charged gradually through this high resistor to the supply voltage. A resistor module consisting fifty-six 470 kΩ resistors connected in series and having a total resistance of 26.32 MΩ (which satisfies the requirement of the charging resistor) was selected as the charging resistor in this smooth exponential impulse generator.

#### 6.4.1.3 Self-breakdown Spark-Gap Switch

A self-breakdown spark-gap switch, *S*, was used to trigger the generation of exponential impulse in this pulse generating system. As shown in Figure V.19, the switch has a stationary ground spherical electrode and an adjustable HV spherical electrode. The switch is filled with air under atmospheric pressure. The closure mechanism of this type of switch is detailed in Section 2.4.5.1. As the charging voltage on the HV electrodes reaches the self-breakdown voltage, an air breakdown occurs between the two electrodes, allowing the charging capacitor to deliver exponential impulse to the PEF test cell. The distance of the inter-electrode gap can be changed to adjust the voltage magnitude of output impulse.

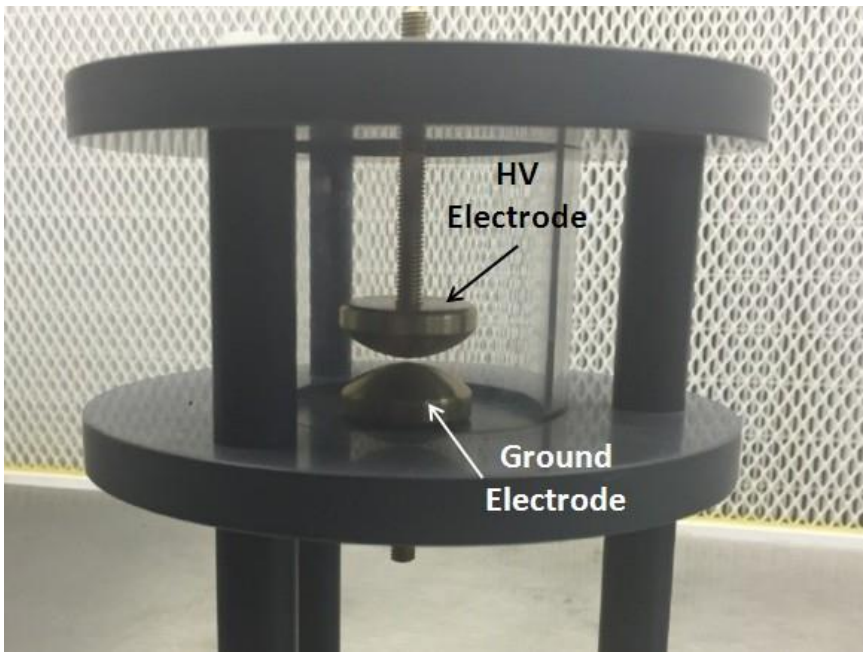


**Figure V.19** Close look of the Self-breakdown spark-gap switch.

#### 6.4.1.4 Charging Capacitor

The charging capacitor is used to deliver exponential impulse with an opposite polarity to the load when the switch is triggered. The capacitance of this capacitor defines the fall time of the impulse, therefore needs to be carefully selected. The following equation can be used for selection of the charging capacitor.

$$\tau = -ln\left(\frac{1}{2}\right) \cdot RC \qquad \text{(VI.2)}$$

where $\tau$ is the fall time of the impulse, during which the voltage across the load falls to 50% of its peak magnitude, $R$ is the resistance of the load and $C$ is the capacitance of the charging capacitor.

In order to be consistent with the square impulse, the fall time should be 1 µs. Therefore, the capacitance of the charging capacitor should be ~ 28.8 nF if a load has an impedance of 50 Ω. Considering the practical impedance of the load, the PEF test cells and 50 Ω matching resistor in parallel, would be slightly smaller than 50 Ω, it would be beneficial to have a capacitor with a higher capacitance value. Therefore, a

40 nF capacitor was selected for this system and the exponential impulse produced by this generator has a falling time ~ 1 µs.

#### 6.4.1.5 Protective Resistor

There is a protective resistor connected between the output terminal of the charging capacitor and ground, as shown in Figure V.16. This protective resistor is a water tube resistor with an approximate resistance of a few hundreds of kΩ. The purpose of using this resistor is to allow capacitor to be charged and to divert current to the ground in the case of open circuit or undesirable high impedance between the charging capacitor and the PEF test cell.

#### 6.4.1.6 Connection HV Cables

There are two main connection cables in this generating system. One connects the HVDC power supply and the other one connects the output terminal and the PEF test cell. Both cables used in this system are URM67 coaxial cables, which have an impedance of 50 Ω. As a result, the impedance of this exponential impulse generator is 50 Ω, which equals the impedance of the square impulse generator. The length of the cables is ~ 2 m each, which produces a propagation delay of ~ 10 ns according to Equation VI.3.

$$PD = \frac{l\sqrt{\mu_r \varepsilon_r}}{c} \tag{VI.3}$$

where *PD* is the propagation delay of the cable, $l$ is the length of the cable, $\varepsilon_r$ is the relative permittivity of the cable, $\mu_r$ is the relative permeability of the cable, and $c$ is the speed of light. For a URM67 cable, relative permittivity $\varepsilon_r$ ~ 2.2 and relative permeability $\mu_r$ ~ 1. Consider that the pulse duration is in the range of few µs, this 10 ns propagation delay should not have any significant effects.

### 6.4.1.7 *PSpice* Simulations

Prior to building the practical pulsed power system, the above design was simulated using *PSpice* software to investigate its feasibility. The components selected above were used in the simulation circuit, as shown in Figure V.20. The result shows a good agreement between exponential impulses produced by the pulsed circuit and the model *PSpice* circuit. The practical smooth exponential waveform generated by this generator during the experiments showed a high degree of similarity with the simulation waveforms, as can be seen in Figure V.21.

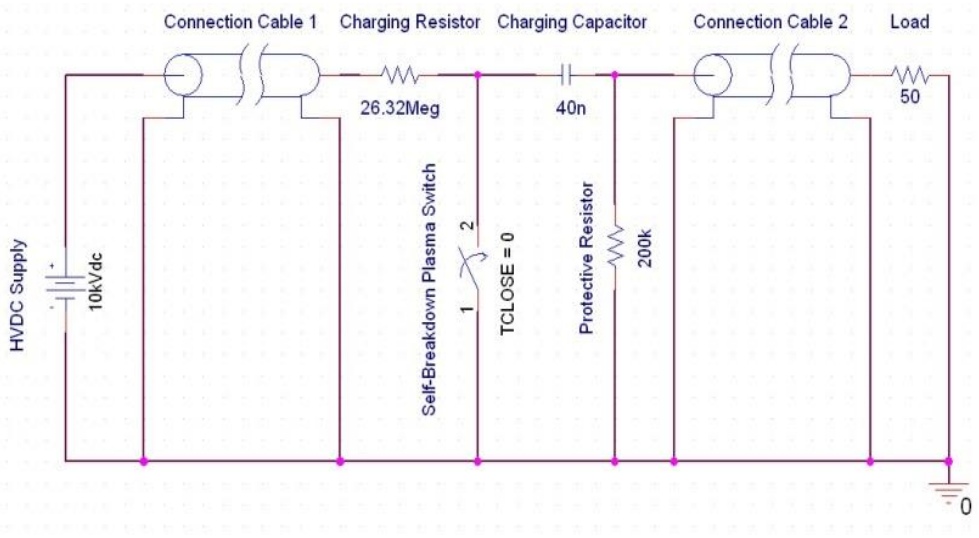


**Figure V.20** Pspice model of the exponential impulse generating circuit.

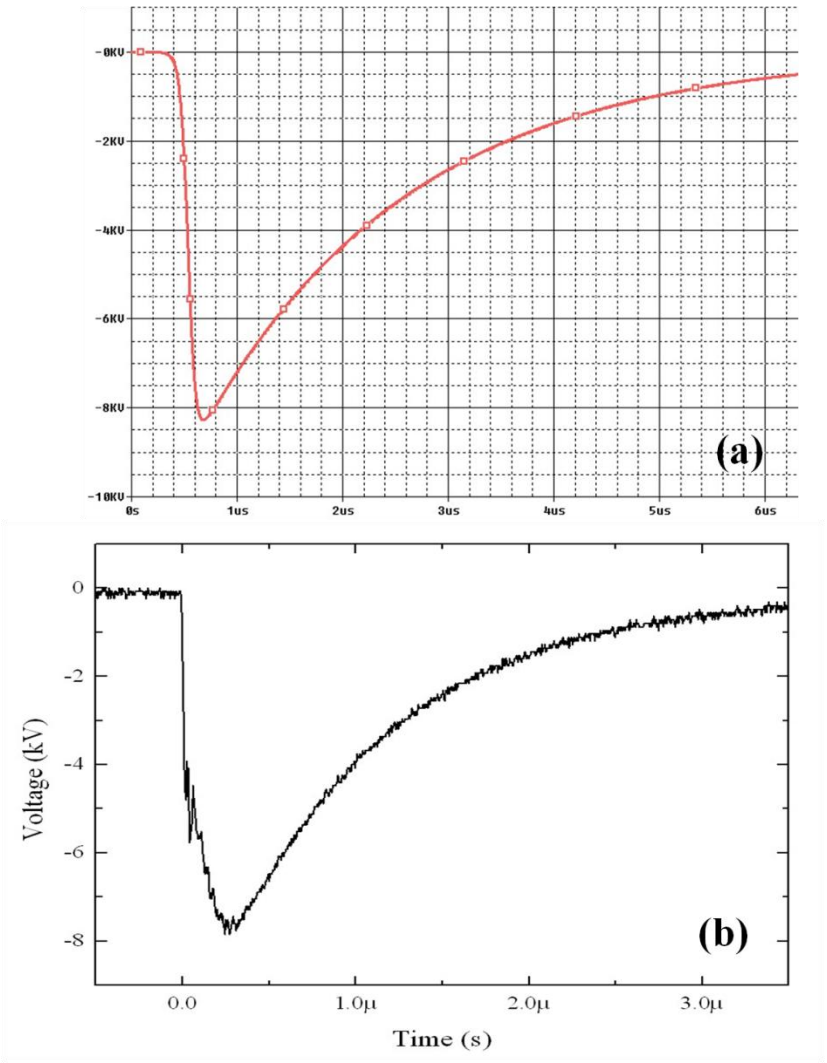


**Figure V.21** (a) *PSpice* simulation result of an exponential waveform generated by the design circuit. (b) Practical smooth exponential impulse waveform generated by the generator during experiment.

### 6.4.2 Oscillating Exponential Impulse Generator

As discussed in Section 3.1.3 and Section 3.2.2, when the biological membrane is exposed to intensive electrical field, the trans-membrane voltage requires a certain time to reach its peak value. According to the 2-dimentional equivalent circuit model developed in Section 3.1 and the transient membrane charging model developed in [6], this charging time required to achieve the maximum voltage across membrane is ~ 1 μs. This simulation result suggested that the trans-membrane potential could not be developed to its peak value when exposed to impulse with a shorter duration or

fast oscillating impulse. As it could be an important factor in practical PEF processes, it was decided to investigate the effect of fast oscillating impulse with oscillating period much shorter than 1 μs.

As demonstrated in Section 2.4.3, a relatively complicated *RLC* circuit is required in order to generate a fast oscillating impulse. However, a fast oscillating impulse can also be generated by introducing an impedance mismatch between the load and the pulsed power system. When the un-matched load is connected to the generator, signal reflection occurs resulting in a fast oscillating signal across the load. As demonstrated in Section 4.4.1, the PEF test cell can be modelled as equivalent *RC* circuit and its equivalent impedance can be calculated by corresponding equations. According to Equation IV.2 ~ IV.5, the equivalent impedance of the re-designed PEF test cell is around 350 Ω. Meanwhile, the impedance of the exponential generator, as mentioned in Section 6.4.1, is 50 Ω. Therefore, an oscillating exponential impulse can be produced if the PEF test cell is directly connected to the generator.

The design of such modified circuit was modelled in *PSpice* as shown in Figure V.22. The load is represented by the equivalent *RC* model of the PEF test cell, the connection wires are represented by respective inductances as well. The results of modelling this pulsed power system in *PSpice* analysis are shown in Figure V.23. As can be seen in this figure, a fast oscillating waveform is generated when the un-matched PEF test cell is connected directly to the output of the pulsed power circuit. The fall time of the impulse is largely increased due to un-matched load at the same time. However, in practical tests, the fall time of the oscillating impulse remains similar to the exponential impulse, as can be seen in Figure V.24. At the same time, the oscillating period is ~ 0.14 μs, which is much shorter than the 1 μs membrane charging time. Therefore, it was decided to use this system to generate an oscillating exponential impulse for the research purposes of the present project.

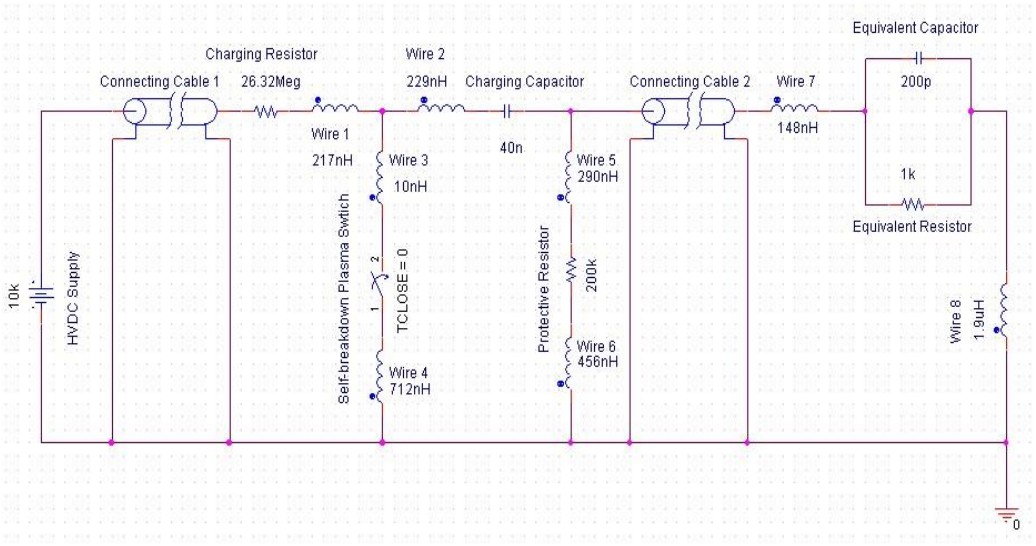


**Figure V.22** *PSpice* model of the oscillating impulse generating circuit.

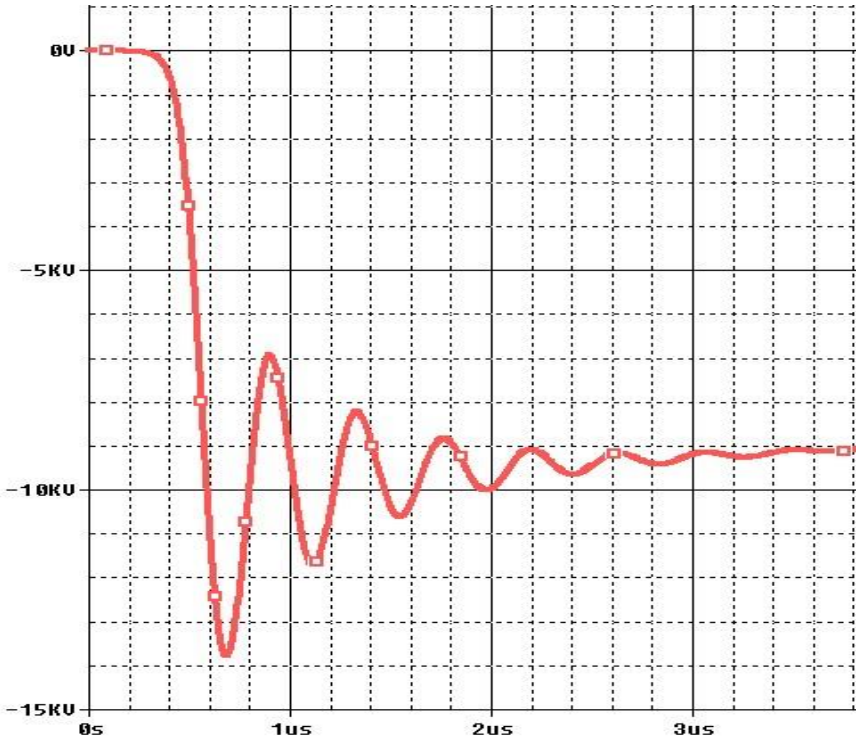


**Figure V.23** *PSpice* simulation result of an oscillating impulse generated by the design circuit.

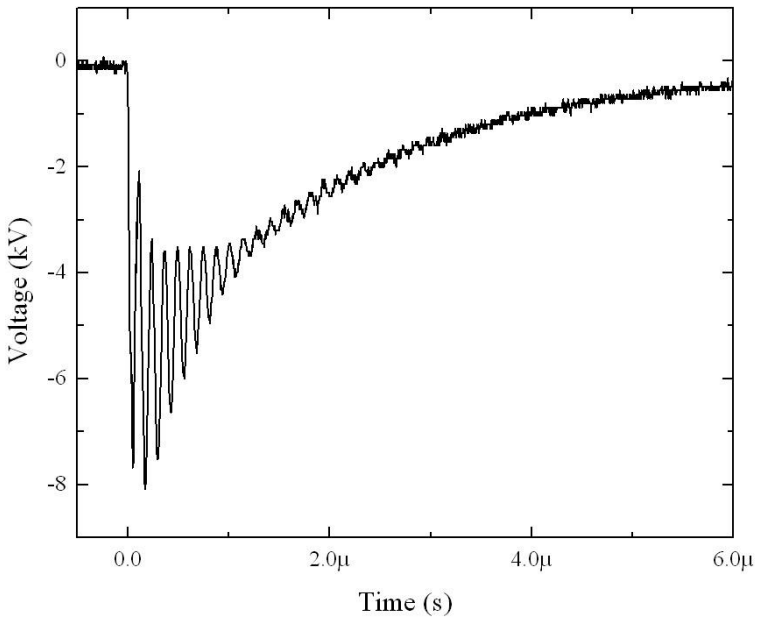


**Figure V.24** Practical impulse with oscillating exponential waveshape generated by the generator during experiment.

## 6.4.3 Other Components of the PEF System

### 6.4.3.1 Pressurised Chamber

As discussed in Section 6.1.2.1, the electrical breakdown inside the test cell due to the presence of air bubbles will damage the electrodes and interrupt the PEF experiment. Therefore, these undesirable breakdowns should be avoided. Although the new design of the PEF test cell aims to remove all the air bubbles completely prior to the PEF process, there is a need to reduce the probability of breakdown even if there will be no air bubbles trapped inside the test cell as gaseous bubble can be generated during PEF process. According to Paschen's curve of air, as shown in Figure V.25, the breakdown voltage of air could be increased by either increasing the gap length or air pressure. In the case of the air bubble breakdown, the gap length is effectively the diameter of the air bubble. Therefore, the only way to increase the breakdown voltage is to put the PEF test cell in a pressurised environment.

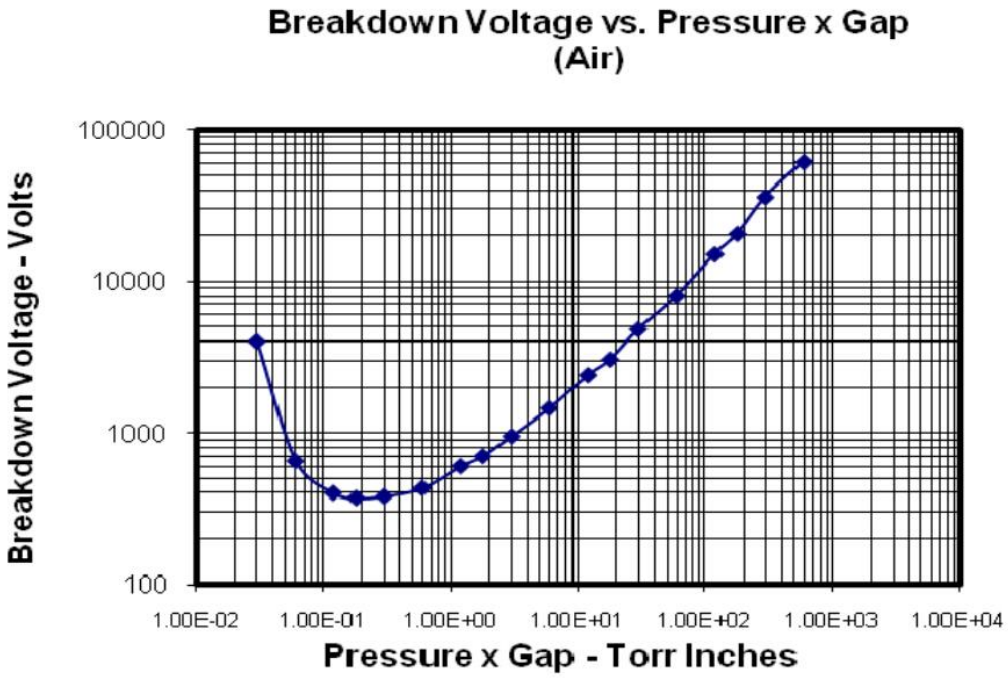


**Figure V.25** Paschen's curve of air, figure taken from [247].

Based on this consideration, a pressurised chamber is used in addition to the redesign of the PEF test cell. The chamber, shown in Figure V.26, has an HV connector, a gas inlet, an HV electrode, a ground electrode, a viewing window and a removable front door. The HV connector is connected to the output cable of the pulse generators. The gas inlet is connected to an air compressor to allow the chamber to be pressurized up to 18 bars (absolute). The HV electrode, which is electrically connected to the HV connector, has a movable metal ball connected to a compressed spring. The distance between the top of the ball and the stationary ground electrode is slightly shorter than the thickness of the test cell. As the test cell is placed between the electrodes, the metal ball is pushed against the spring further, as shown in Figure V.26(b). Therefore, a solid electrical contact between the electrodes and the test cell is provided. A glass viewing window is on top of the chamber, through which the situation inside the chamber can be monitor once the chamber is sealed. The placement and removal of the PEF test cell is done through the removable front door. The removable front door, made of aluminium, can provide reliable sealing in cooperation with an O-ring and 6 sets of screws.

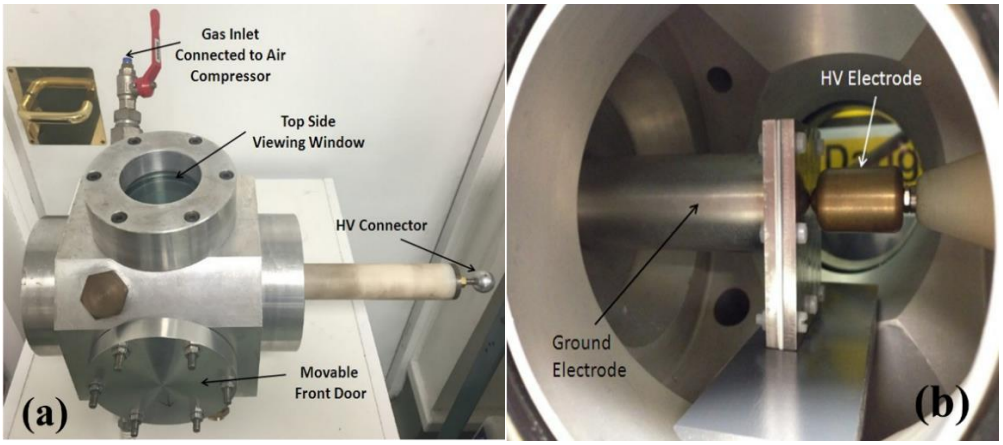


**Figure V.26** The pressurised chamber. (a) Overview of the chamber with the front door closed. (b) Inside view of the chamber with the PEF test cell in place.

### 6.4.3.2 Current Probe

As discussed in Section 6.3.3, the current through the test cell was measured during the PEF treatment. The purpose of the current measurements is to distinguish different current regimes during the PEF treatment when using different test cells, as well as to obtain an accurate estimation of the specific energy consumption of the PEF process.

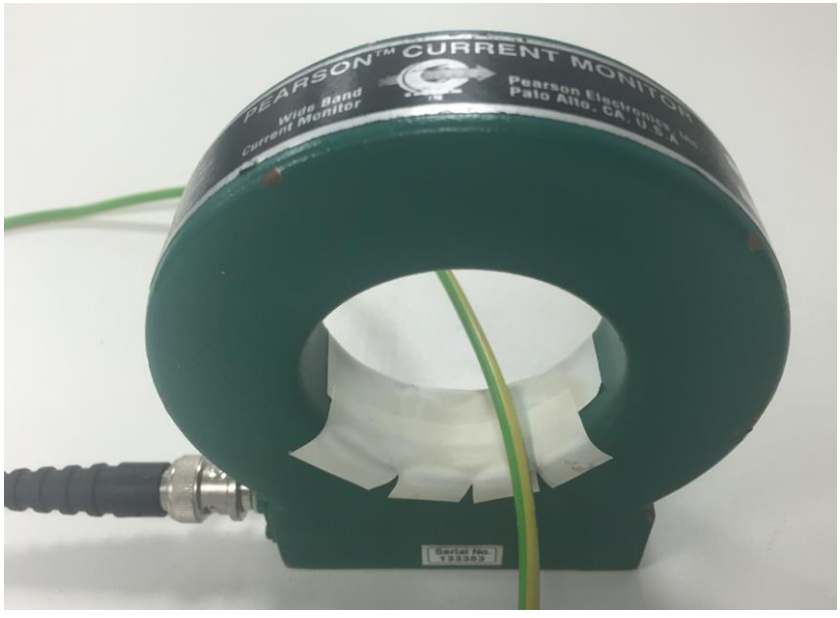


**Figure V.27** Current probe, 6585 from Pearson Electronic.

A current monitor, current transformer 6585 from Pearson Electronic, was used for this purpose, as shown in Figure V.27. This current transformer has a sensitivity of 1 Volt/Ampere, an output resistance of 50 Ω, and is capable to measure a maximum current of 500 A. The length of the BNC cable was also selected so that it was identical to the length of the BNC cable of the voltage probe. By doing so, the propagation delay of both voltage and current signals should be identical and the effect of signal propagation delay can be regarded as negligible in estimation of the specific energy consumption.

## 6.5 Discussion

The potential reasons for the ineffective PEF performance of the ceramic test cell have been analysed in this chapter. Due to the Maxwell-Wagner field relaxation process, the actual field strength inside the ceramic test cell and the trans-membrane potential can be much smaller and the field in the suspension will last only a fraction (30%) of the pulse duration across the test cell before collapsing. In addition, the uneven surface of the ceramic capacitor may also cause a distortion of the field distribution inside the test cell. The results from these analyses and additional experiments suggested that much higher field strength (> 80 kV/cm) may be needed to achieve successful PEF treatment using the ceramic test cell. A new selection of the electrode material with a longer Maxwell-Wagner relaxation time may also be needed in order to achieve successful PEF inactivation using current field strength.

The drawbacks of the initial designed stainless steel test cell have been discussed in this chapter. The geometries design of the original test cell will help to introduce undesirable air bubble inside the cell and there is no reliable method to detect these bubbles after the filling process. The presence of the bubbles will cause undesirable and damaging electrical breakdown. Besides, the use of O-rings and the inlet hole may form some potential dead zones, where microorganism samples are not be treated effectively during PEF treatment. On the other hand, the inter-electrode distance is too large for achieving high field strength required for PEF treatment. These findings suggest the design of the test cell should be improved in order to

eliminate the presence of air bubbles and dead zones, and be capable for higher field PEF treatment.

Based on the findings and suggestions provided by this analysis, a new metallic test cell has been designed and built. The new test cell employed a different topology, which was an open-top rectangular parallel plate to plate electrode with a 1 mm inter-electrode distance. The electrodes of the new metallic cell remained stainless steel and the 1 mm inter-electrode gap was kept by a Π-shaped PTFE layer. The open top design reduced the probability of trapping air bubbles inside the cell and allowed visual inspection for these bubbles. The new design also eliminated necessity of the use of the O-rings and the inlet hole, which helped to remove the potential dead zones. The 1 mm inter-electrode gap allowed PEF treatment with the field strength up to 200 kV/cm to be conducted using the same pulse generator. In order to reduce the probability of air breakdown inside the test cell during PEF treatment further, a pressurized chamber was also employed.

A new $TiO_2$-coated PEF test cell has also been designed based on the analysis presented in this chapter. The topology of this $TiO_2$-coated test cell was the same as the new stainless steel cell, rectangular parallel plate to plate electrodes separated by a 1 mm Π-shape PTFE spacer, which formed an open-top treatment area. The electrodes of the new $TiO_2$-coated cell were made from copper plates coated by a 2-μm $TiO_2$ thin film. In dry condition, $TiO_2$ can be regarded as a good insulation with relatively high permittivity and extremely low conductivity. The ultra-thin film also provided a much longer Maxwell-Wagner relaxation time as compared with the ceramic test cell. However, it was found that the conductivity of the thin $TiO_2$ film changed dramatically when in contact with liquid suspension, resulting in an ionic conduction current through the test cell. However, this ionic conduction current was noticeable lower when compared with the conduction current during PEF treatment with stainless steel test cell, which suggested potential reduction in the specific energy consumption could be achieved using this $TiO_2$-coated cell.

In addition to the square impulse generator used in the preliminary experiments, another two pulse generators were designed and built, these generators will be used

for the subsequent PEF studies. The design process of these two *RC* circuit based generators, the smooth exponential impulse generator and the oscillating exponential impulse generator, was also described in this chapter. The smooth exponential impulse generator can produce negative impulses with a decay time of ~ 1 μs. The maximum output voltage from the generator can reach 50 kV if a matched load is used. On the other hand, the oscillating exponential HV impulses were generated by connecting the un-matched PEF test cell directly to the smooth exponential impulse generator. The result of this un-matched load was a fast oscillating (with oscillating period ~ 0.15 μs) exponential impulse with a similar decay time of ~ 1 μs.

The new PEF test cells and the new pulse generators, described in this chapter, will be used in PEF treatment on microorganisms. The experiment process and the results of these experiments will be introduced and discussed in next chapter.

# Chapter VII

# PEF TREATMENT OF MICROOGANISMS: IMPROVED TEST CELLS

## 7.0 General

As described in Chapter VI, a new stainless steel test cell and a low-conductive $TiO_2$-coated test cell have been designed and built. Two pulsed power systems, which produce impulses with smooth exponential waveshape and oscillating exponential waveshape, were also constructed for the PEF experiments. Both test cells will be used for PEF tests described in Chapter IV. The results from these tests in which re-designed stainless steel test cell was used will be compared with the result obtained using the original stainless steel cell. These results will also provide reference for the PEF inactivation results obtained using $TiO_2$-coated cell. The PEF experiments will also be conducted using the new $TiO_2$-coated test cell to investigate whether this low-conductive PEF test cell can achieve satisfactory inactivation results in practical experiments. The successful inactivation of microorganisms in the $TiO_2$-coated test cell would demonstrate that the PEF treatment with significantly low ionic conduction current can produce satisfactory practical PEF performance.

The comparison between PEF performances obtained using HV impulses with different waveshapes will be conducted in this chapter. The results from this comparison will be compared with literature data and will provide further understanding of the effect of pulse waveshape on the PEF treatment. Specific energy consumption for the PEF treatment process will be obtained in both test cells. It is expected that significant improvement in the specific energy consumption can be achieved by using the low-conductive $TiO_2$-coated PEF test cell. The analysis and discussion of this new test cell design will also be presented in this chapter.

## 7.1 Design of PEF Tests

### 7.1.1 Microorganisms Used in the PEF Tests

The microorganisms used in the PEF tests described in this chapter were *A. platensis* and *S. cerevisiae*. Both types of microorganisms were prepared according to the procedures described in Section 5.1 prior to the PEF experiments.

One of the findings from the experiments described in Chapter V was the 'tailing' effect in the inactivation curves, which was observed in the PEF treatment of the *S. cerevisiae*: during PEF treatments the population of *S. cerevisiae* sample was not further reduced despite increasing the number of HV impulses. Potential reason for this effect was the presence of low field zones in the original stainless steel test cell. However, it would be beneficial to investigate PEF inactivation of *S. cerevisiae* sample with different population densities to investigate if this 'tailing' effect still exists. Therefore, additional procedures were taken to prepare *S. cerevisiae* sample with different cell concentrations.

As verified in Section 5.4, the untreated *S. cerevisiae* suspension, prepared as described in Section 5.1.3, had an initial population density of ~$10^7$ CFU/ml. Therefore, the initial *S. cerevisiae* suspension was serially diluted to prepare suspension with different concentration. To do so, 1 ml of initial suspension was added into 9 ml of Mycological Peptone solution. The mixture of the resulting *S. cerevisiae* suspension had a population density of ~ $10^6$ CFU/ml. Suspensions with population densities of ~ $10^5$ and ~ $10^4$ CFU/ml were also prepared using this method.

### 7.1.2 Assessment of PEF Performance

To investigate the efficiency of the pulsed electric field treatment of *A. platensis*, two established methods, as described in Section 5.2.1, were used. The growth curve of the *A. platensis* sample was measured and the visual inspection of individual cells was conducted using microscope. Both untreated and PEF-treated samples were

assessed using these two methods and their efficiencies were compared to determine the optimal regime of the PEF treatment.

In the experiments with *S. cerevisiae*, the performance of the PEF treatment was assessed by calculating the reduction in the *S. cerevisiae* population density after PEF treatment. Population densities of untreated and PEF-treated samples were counted as described in Section 5.2.2. The reduction in the population density was determined by comparing the results of population counts in CFU/ml.

In addition, the temperature of the liquid suspension was also measured for both *A. platensis* and *S. cerevisiae* experiments to detect any significant thermal effects.

### 7.1.3 Potential Antimicrobial Effects of $TiO_2$

Although $TiO_2$ has long been regarded as a chemically-stable and non-toxic substance, recently it has been reported that $TiO_2$ demonstrates antimicrobial effects when photo-activated with near UV-light, [248-252]. When $TiO_2$ molecule is excited by a photon with sufficient energy, an electron-hole pair will be generated on the $TiO_2$ surface. The hole can react with water ($H_2O$) or hydroxide ions ($OH^-$) to produce hydroxyl radicals (OH•), while the electron can react with oxygen ($O_2$) to produce superoxide ions ($O_2^-$), [248]. These radicals are extremely reactive when contacting with organic compound and eventually inhibiting the DNA cloning process. However, during the PEF treatment procedure, the $TiO_2$-coated electrodes are not exposed to any near-UV light and the total treatment time is relatively short compared to the 1~2 hours exposure time required to achieve noticeable antimicrobial photo effect as reported in [252].

Although it is unlikely that the antimicrobial properties of $TiO_2$ film will affect microorganisms during PEF treatment, it is important to verify this suggestion. Therefore, a control group of microorganism samples has been prepared prior to the PEF experiments. In these control tests a *S. cerevisiae* sample was placed inside the $TiO_2$-coated test cell without the application of HV impulses for the same period of time as duration of the PEF treatment. The surviving population of the *S. cerevisiae*

from this control group was compared with the untreated *S. cerevisiae* sample, which was located in a glass bottle without contact with $TiO_2$ surface, to detect any antimicrobial effect of the $TiO_2$ film. The results of this control group test are shown in Figure VII.1.

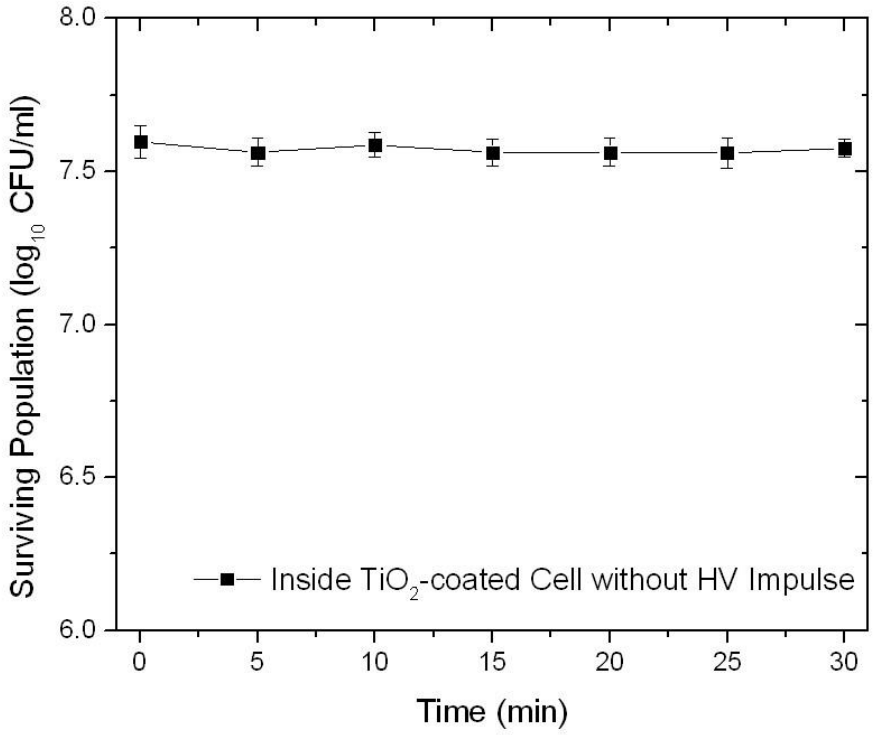


**Figure VII.1** Surviving population of *S. cerevisiae* ($log_{10}$ CFU/ml) as a function of duration of contacting with $TiO_2$-coated electrodes. Error bars show standard deviation for 3 independent tests (n=3).

As can be seen from Figure VII.1, no reduction in *S. cerevisiae* population of the sample placed in $TiO_2$-coated test cell was observed after 30 minutes, which was slightly longer than the maximum time required for the PEF experiment. Therefore, it can be concluded that there was no observable antimicrobial effect induced by the $TiO_2$-coated electrodes. Any inactivation of microorganisms during the PEF experiment using this $TiO_2$-coated test cell should be considered as the direct result of the PEF treatment.

### 7.1.4 Field Magnitude in the PEF Test Cells

In the PEF tests with the original test cells (described in Chapter V), two levels of field strengths (33 kV/cm and 67 kV/cm) were used. To make direct comparison with these results, the PEF process in which the new test cells were employed should also be conducted using the same field magnitudes. Therefore, comparison of the PEF efficiency could be made between the original and re-designed test cells. As the inter-electrode distance in the re-designed cells was reduced to 1 mm, the required voltage which will provide 33 kV/cm and 67 kV/cm field magnitudes was 3.3 kV and 6.7 kV respectively. However, as shown in Figure IV.14, the lowest stable voltage output from the square impulse generator was ~ 5 kV. Therefore, the field magnitude of 33 kV/cm cannot be achieved in the PEF treatment using the re-designed test cells.

On the other hand, the maximum achievable field strength was also limited. It was aimed to achieve a field magnitude of 200 kV/cm using the re-designed PEF test cells, as discussed in Section 6.5. Several attempts have been made to produce this level of electric field. The reduced inter-electrode gap in the new test cells allowed such field magnitude to be developed using the same square impulse generator. The open-top design also reduced the probability of air bubbles being trapped inside the test cell during the filling process, which minimised the probability of an electrical breakdown under such high electric field. In addition, a pressurised chamber was also used to elevate the air pressure in order to minimise the probability of electrical breakdown if an air bubble is developed inside the test cell during the PEF process. Although these efforts proved to be effective in reducing the numbers of undesirable breakdowns, the maximum field strength was still limited by another type of breakdown. As the field strength increased, electrical breakdown started to occur at the ‘triple point’ at the opened top, which was the junction of liquid suspension, electrode and the air. As a result, it was established that a maximum field strength which can be applied to the PEF test cell without breakdown was 80 kV/cm.

Therefore, two field magnitudes were used in the PEF experiments with the new test cells. One field magnitude was 67 kV/cm, which was identical to the field strength

used in the PEF experiments with original test cell. The other field magnitude was 80 kV/cm, which was the maximum field strength achievable in the current configuration of the PEF system.

## 7.2 PEF Treatment of *A. platensis*

### 7.2.1 Experimental Procedures

In the present experimental procedure, liquid suspensions of *A. platensis*, prepared as described in Section 5.1.2, were transferred into the PEF test cells by a syringe. The visual inspection of the test cell was conducted to detect any trapped air bubbles. Air bubbles trapped in the test cell were removed prior to the test cell being placed inside the pressurised chamber. The chamber was then sealed and pressurised to 8 bars (absolute), which was the maximum safe pressure output from the air compressor, Fiac FX95. HV impulses with square waveshape were used to treat *A. platensis*. Two levels of the field strengths, 67 kV/cm and 80 kV/cm, were used in the tests. The *A. platensis* samples were subjected to 50, 100, 500 and 1000 HV impulses, as in the experiments described in Section 5.3.1. The liquid suspension containing the *A. platensis* sample was mixed after every 250 impulses in the tests in which the number of impulses exceeded 250, in order to compensate the sedimentation effect.

After the PEF treatment, the liquid suspensions were taken out from the test cell for assessment. The obtained results from the assessments were compared with untreated sample. As discussed in Section 5.3.2, the centrifugation process introduced considerable mechanical effects to the *A. platensis* cell. Therefore, the same assessment was also conducted for *A. platensis* samples which were centrifuged but not subjected to HV impulses, in order to investigate the effect of centrifugation process. All PEF experiments were conducted in triplicate (n=3). The assessment results obtained from both the stainless steel and $TiO_2$-coated test cells will be presented and discussed in the following sections.

### 7.2.2 Visual Inspection of *A. platensis*

Figure VII.2 shows the images of individual *A. platensis* cells of untreated, centrifuged and PEF treated samples. As can be seen in Figure VII.2, the visual appearances of the centrifuged and PEF treated *A. platensis* cells, both in stainless steel and $TiO_2$-coated test cells, were significantly different from that of the untreated sample. However, the difference between the centrifuged and PEF treated samples was not so obvious. It is worth to notice that, unlike in the case of the ceramic cell, the *A. platensis* cells treated in the $TiO_2$-coated test cell showed a slight difference from the centrifuged sample, as in the case of stainless steel cell. This visual difference indicated that PEF impulses in the $TiO_2$-coated and re-designed stainless steel test cells produce an impact on the inner structure of *A. platensis* cell.

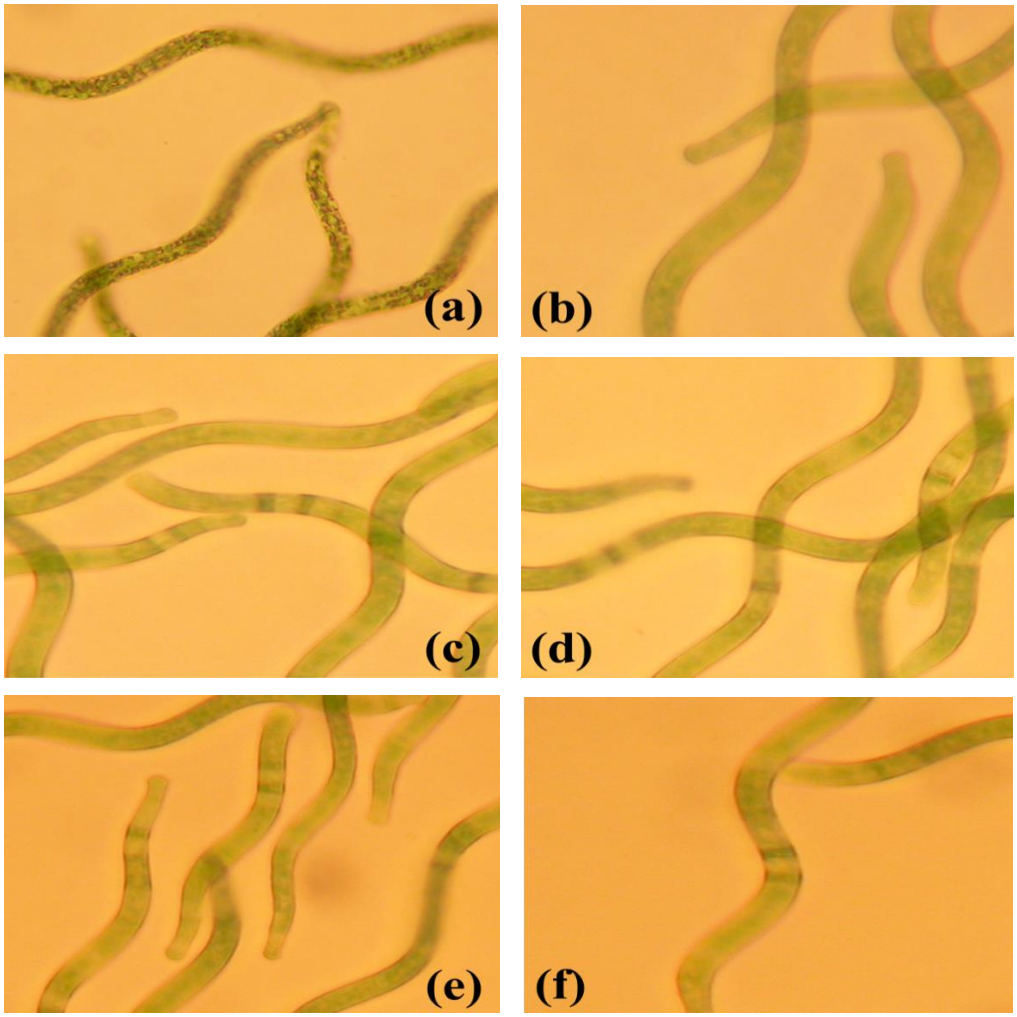


**Figure VII.2** *A. platensis* cells under microscope (×400 magnification) (a) Untreated sample; (b) Centrifuged sample; (c) PEF treated sample (Stainless steel test cell, 67 kV/cm,

500 pulses); (d) PEF treated sample (Stainless steel test cell, 80 kV/cm, 500 pulses); (e) PEF treated sample ($TiO_2$-coated test cell, 67 kV/cm, 500 pulses); (f) PEF treated sample ($TiO_2$-coated test cell, 80 kV/cm, 500 pulses).

The obtained visual inspection results from both re-designed stainless steel and $TiO_2$-coated test cells are similar with the visual observation of *A. platensis* sample treated by the original stainless steel test cell, as shown in Section 5.3.2.1. It suggested that any potential internal structural changes may be caused by the mechanical force induced by the centrifuge process. However, this mechanical force was not strong enough to cause any rupture or external damage as reported in other literature, [240]. In contrast, PEF treatment induced internal damage to the *A. platensis* cells, which was invisible at this scale of magnification, but resulted in inactivation of *A. platensis*. It can also be noticed from the figure that there was no significant difference in visual appearances between the samples treated with 67 kV/cm and 80 kV/cm impulses. In both cases, *A. platensis* treated in stainless steel and $TiO_2$-coated test cells, the visual appearances of the individual *A. platensis* cells were very similar regardless of the field strength.

In order to visualise potential physical damage induced by the PEF process, significantly higher magnification will be required. For example, transmission electron microscope (TEM) and scanning electron microscope (SEM) are capable of producing images of surfaces of microbial cells and their internal structure with magnification factor of a few tens of thousands. The other approach to visualise the damage to the cell is to use specific dyes for monitoring of the morphological changes in the cells and production of free radicals, as was used in other microbiological studies, [71, 253-254].

### 7.2.3 Assessment of PEF Efficiency: Growth Curves

The results of *A. platensis* growth curve measurements are shown in Figure VII.3-VII.6. The growth curves of the *A. platensis* samples treated in the stainless steel test cell are shown in Figure VII.3 and Figure VII.4. As can be seen in these figures, no growth was observed after 15 days in all groups. This result indicated that

*A. platensis* were inactivated by PEF treatment using the re-designed stainless steel test cell. Similar to the experiment with the original stainless steel test cell, complete inactivation was achieved by 50 HV impulses at 67 kV/cm.

The same PEF performance was also achieved in the new $TiO_2$-coated test cell, as shown in Figure VII.5 and Figure VII.6. It can be seen from the figures that growth of *A. platensis* has been halted by the PEF treatment. In both 67 kV/cm and 80 kV/cm groups, no growth of *A. platensis* was detected after 15 days regardless of the number of the HV impulses. These results demonstrated that complete inactivation of *A. platensis* was achieved by 50 HV impulses with magnitude of 67 kV/cm in the new $TiO_2$-coated test cell.

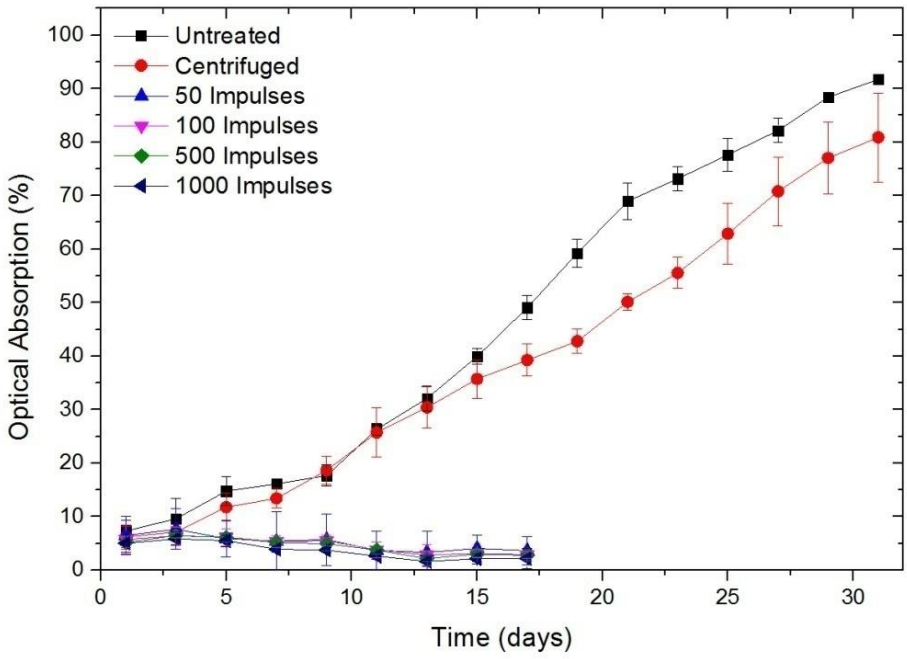


**Figure VII.3** Growth curves for untreated, centrifuged and PEF treated (67 kV/cm, re-designed stainless steel test cell) *A. platensis* sample. Data points are the average value of triplicate tests, error bars show standard deviation (n=3).

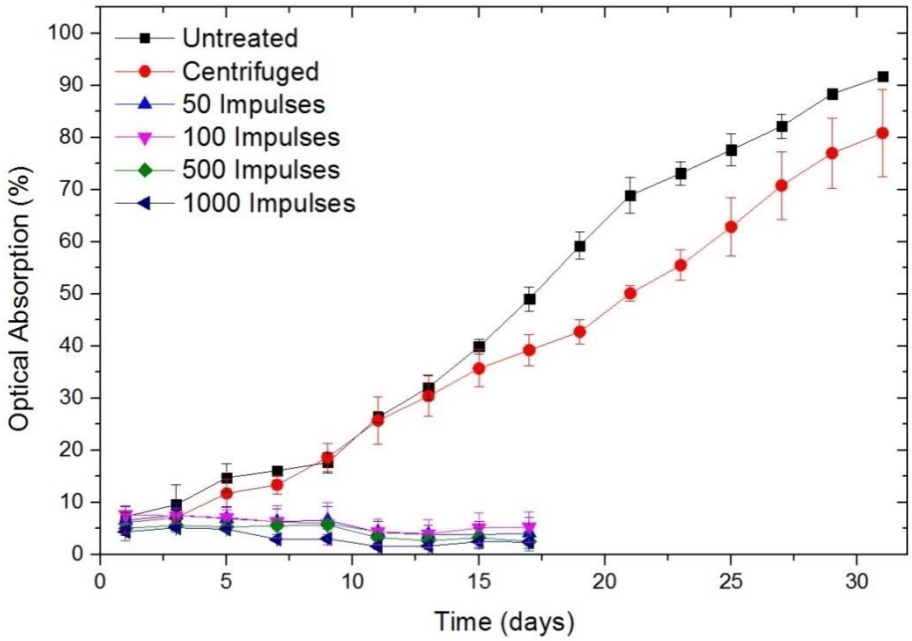


**Figure VII.4** Growth curves for untreated, centrifuged and PEF treated (80 kV/cm, re-designed stainless steel test cell) *A. platensis* sample. Data points are the average value of triplicate tests, error bars show standard deviation (n=3).

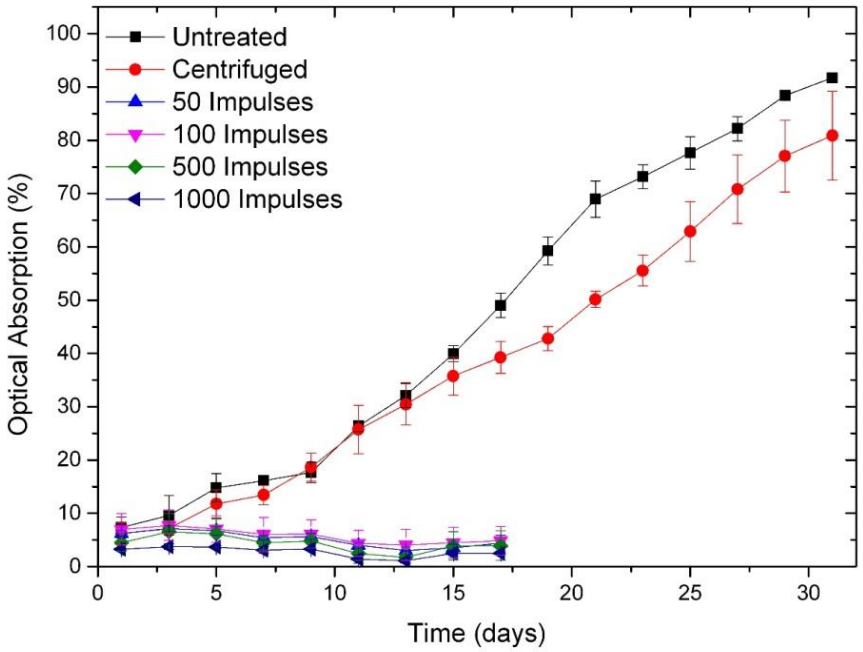


**Figure VII.5** Growth curves for untreated, centrifuged and PEF treated (67 kV/cm, $TiO_2$-coated test cell) *A. platensis* sample. Data points are the average value of triplicate tests, error bars show standard deviation (n=3).

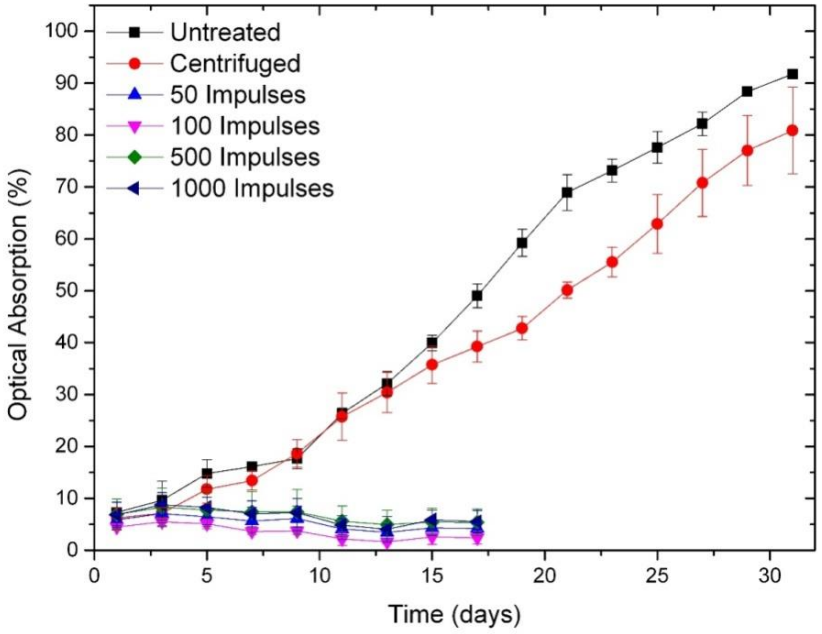


**Figure VII.6** Growth curves for untreated, centrifuged and PEF treated (80 kV/cm, $TiO_2$-coated test cell) *A. platensis* sample. Data points are the average value of triplicate tests, error bars show standard deviation (n=3).

### 7.2.4 Temperature Measurements

As mentioned in Section 7.1.2, the temperature of liquid suspensions was measured before and after PEF treatment in order to detect any significant thermal effects. The results of these measurements indicate that no significant heating had occurred during the PEF treatment as the maximum increase in temperature of liquid suspension was less than 1 °C.

In the case of PEF treatments in the stainless steel test cell, the reason for this insignificant heating effect is the same as observed in the PEF tests sing the original stainless steel cell, as discussed in Section 5.3.2.3. The Joule heating of the liquid suspensions, which is due to ionic conduction through the sample, is significantly reduced by the use of low conductive suspension. In the case of the $TiO_2$-coated test cell, the ionic conduction is reduced further due to low-conductive coating. The Joule heating of the liquid suspension was further reduced during the PEF treatment in the $TiO_2$-coated cell.

However, in the PEF treatment with the new test cells, the temperature measurement could only be conducted after the depressurisation of the chamber and removal of the treated samples from the chamber. This process takes ~ 2 minutes, during which the liquid suspension could be cooled down due to its small volume. Therefore, the observed insignificant increase in temperature could also be the result of this process.

### 7.2.5 Summary of the Results of PEF Treatment of *A. platensis*

In this section a summary of the results of the PEF experiment of *A. platensis* in the new test cells is provided. The main findings can be summarised as follow:

- PEF inactivation of *A. platensis* was realised in the re-designed stainless steel test cell. Similar to PEF inactivation in the original stainless steel test cell, complete inactivation was achieved by 50 HV impulses with square waveshape with a field magnitude of 67 kV/cm.

- PEF inactivation of *A. platensis* was achieved in the new $TiO_2$-coated test cell. As in the case of the re-designed stainless steel test cell, complete inactivation was achieved by application of 50 HV impulses with square waveshape with a field magnitude of 67 kV/cm.

- No damage of the external structure of the *A. platensis* cells was observed under optical microscope with ×400 magnification. However, inactivation of the *A. platensis* confirmed that internal structural damage and cell dysfunction were induced by PEF.

- Heating effects were not significant during the PEF process in both stainless steel and $TiO_2$-coated test cells. Maximum increase in temperature recorded during the PEF tests was ~ 1°C. In the case of stainless steel test cell, the heating was limited by the use of low conductive sample suspension. In the case of $TiO_2$-coated test cell, the ionic conduction was reduced by the use of low-conductive electrodes and the Joule heating was reduced further. However, the delay in measurement of the sample suspension temperature

after PEF treatment due to the depressurisation process could introduce some uncertainty in temperature measurement.

## 7.3 PEF Treatment of *S. cerevisiae*

### 7.3.1 Experimental Procedures

Before the PEF treatment, liquid suspensions of yeast *S. cerevisiae*, prepared as described in Section 5.1.3 and Section 7.1.1, was transferred into the PEF test cells by a syringe. As with the *A. platensis* PEF tests, visual inspection of the test cells was then conducted in order to detect and remove any trapped air bubbles prior to placing the test cell inside the pressurised chamber. The chamber was then sealed and pressurised to 8 bars (absolute), the same pressure as used in the *A. platensis* experiments.

HV impulses with three types of waveshapes, the square, smooth exponential and oscillating exponential, were used in the *S. cerevisiae* PEF experiments in which the effects of different pulse waveshapes on PEF efficiency were investigated. In the tests using impulses with square and smooth exponential waveshapes, the 50 Ω matching resistor was connected in parallel with the test cell outside the pressurised chamber in order to match the impedance of the pulse generators. In the PEF experiments in which oscillating exponential impulses were used, the matching resistor was removed to obtain the desirable waveshape, as discussed in Section 6.4.2. The field magnitude of 67 kV/cm and 80 kV/cm were used in these tests and the *S. cerevisiae* samples were subject to 25, 50 and 100 PEF impulses.

After the PEF treatment, the liquid suspension was taken from the test cell for assessment. The surviving population of the PEF treated *S. cerevisiae* was compared with untreated *S. cerevisiae* sample. All experiments were conducted in triplicate (n=3). The results obtained using the re-designed stainless steel and $TiO_2$-coated test cells will be presented and discussed in the following sections.

### 7.3.2 Characterisation of the Waveforms

As introduced in Section 7.3.1, in addition to the HV impulse with square waveshape, HV impulses with smooth and oscillating exponential waveshapes were used in the PEF treatment of yeast with the new test cells. In order to compare the PEF performance of different impulses directly, the voltage output from all impulse generators should be the same for a required field magnitude. Due to the difference in waveshapes of the HV impulses, as shown in Figure VII.7, it was necessary to define what voltage output should be for each impulse waveshape. It was decided that, in the case of impulse with smooth and oscillating exponential waveshape, the corresponding field strength was defined by the peak voltage of these impulses. For example, to provide an 80 kV/cm impulse, the peak voltage from the impulse generators should reach 8 kV, given that the inter-electrode distance is 1 mm. However, in the case of impulse with square waveshape, the voltage over-shot occurred frequently at the beginning of the impulse, as demonstrated in Figure VII.7(a). Then the voltage magnitude was stabilised to form a 'flat top' over majority time of the pulse duration. Therefore, it was decided that the corresponding field strength was defined by the voltage magnitude of this stabilised 'flat top' in the impulse with square waveshape.

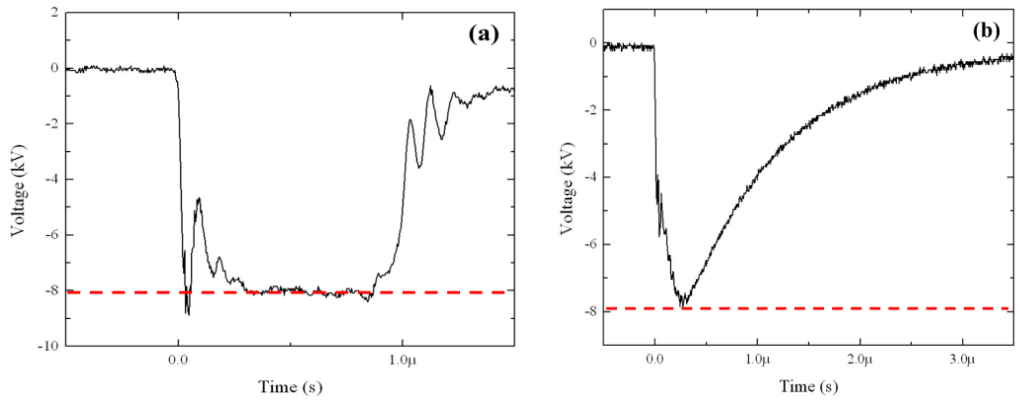

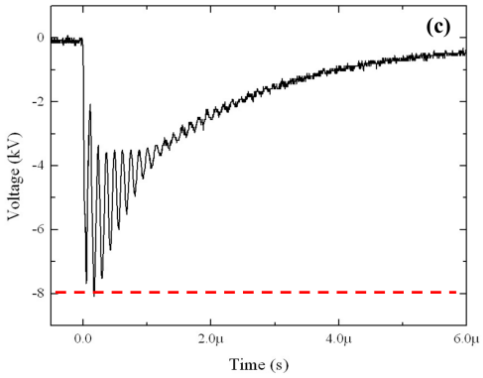


**Figure VII.7** Voltage waveform of different impulses during PEF experiment: (a) impulse with square waveshape; (b) impulse with smooth exponential waveshape; (c) impulse with oscillating exponential waveshape. The red dashed lines in the figures indicate the defined peak voltage level.

## 7.3.3 PEF Treatment in Stainless Steel Test cell

### 7.3.3.1 Temperature Measurement

As discussed in Section 7.1.2, the temperature of the liquid suspensions was measured before and after the PEF treatment to detect any variations of the temperature induced by the PEF impulses. The obtained results of these measurements showed that the maximum increase in the temperature after PEF treatment in stainless steel test cell was ~ 1.5 °C.

As explained in Section 5.4.2.1, this insignificant thermal effect was likely to be the result of the use of low conductive suspension. The ionic conduction current through the suspension was limited in low conductive suspension and therefore the Joule heating of the liquid sample was restricted. However, as indicated in Section 7.2.4, the process of depressurisation of the host chamber and removal of the test cell could delay the temperature measurement by up to 2 minutes. This delay allowed the liquid suspension to cool down due to its small volume. Therefore, the insignificant increase in sample temperature could be a result of both factors.

In the PEF experiments of *S. cerevisiae*, the current through the test cell was measured during the PEF tests, which allowed the estimation of the specific energy consumption of the PEF process. A correlation between the calculated specific energy consumption and the change in the temperature of the liquid suspension was established, which will be discussed in Section 7.3.4.3.1.

### 7.3.3.2 PEF Treatment with Square Impulses

The results of the PEF treatment of *S. cerevisiae* by impulses with square waveshape are shown in Figure VII.8 and Figure VII.9. These figures show the results of PEF tests with impulses with the field magnitudes of 67 kV/cm and 80 kV/cm respectively. As can be seen from the figures, the surviving population of the *S. cerevisiae* reduced as the number of impulses increased, which indicated that the *S. cerevisiae* were effectively inactivated by the HV impulses with square waveshape in the re-designed stainless steel test cell.

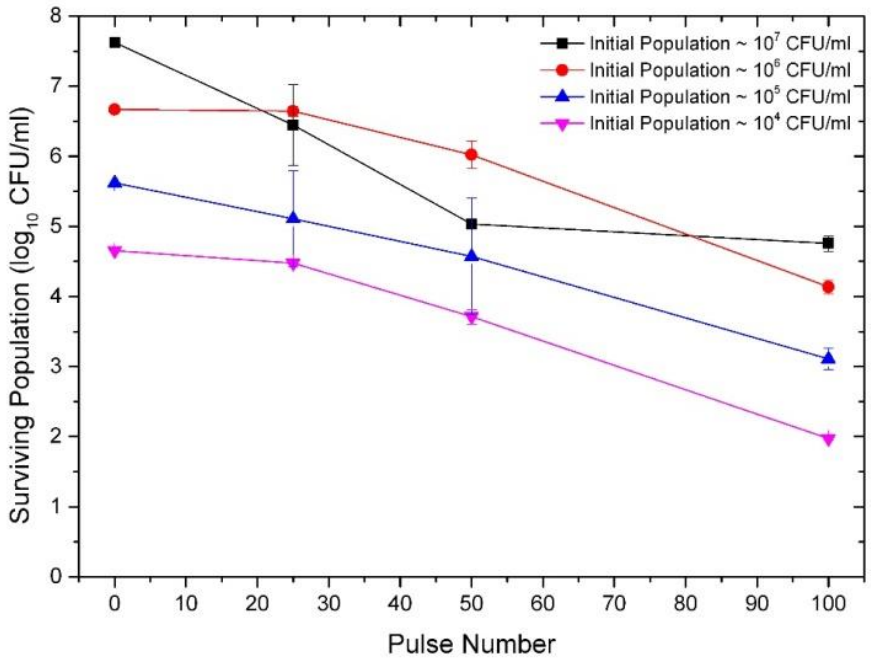


**Figure VII.8** Surviving population of *S. cerevisiae* ($log_{10}$ CFU/ml) as a function of number of impulses. PEF treatment with square waveform of different initial populations. Field strength was 67 kV/cm. Error bars show standard deviation (n=3).

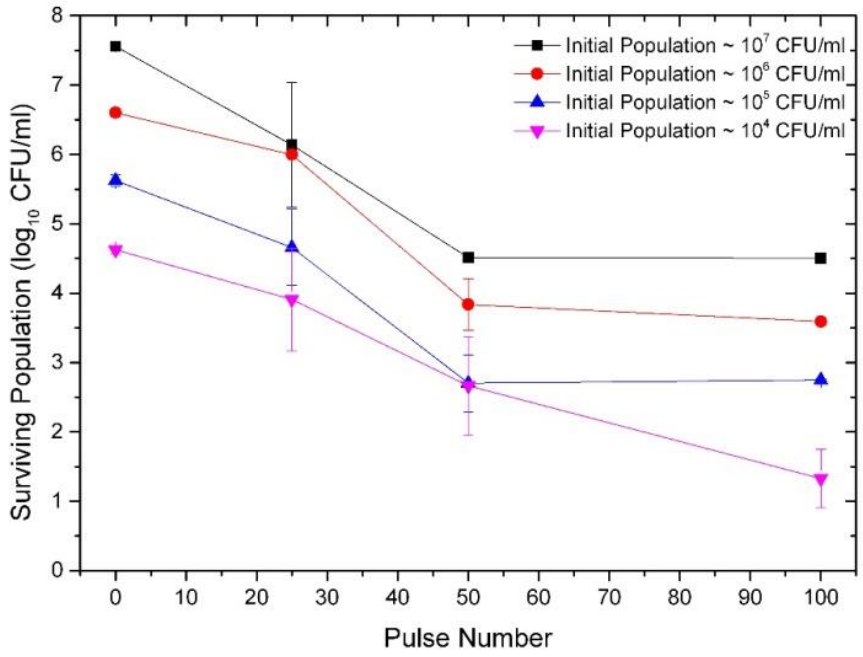


**Figure VII.9** Surviving population of *S. cerevisiae* ($log_{10}$ CFU/ml) as a function of number of impulses. PEF treatment with square waveform of different initial populations. Field strength was 80 kV/cm. Error bars show standard deviation (n=3).

As shown in Figure VII.8, 2-$log_{10}$ reduction was achieved after 100 impulses with field magnitude of 67 kV/cm regardless of the initial populations. The inactivation tendencies obtained for samples with different initial populations were very similar except for the $10^7$ CFU/ml initial population. In this case, less impulses were needed to achieve the same $log_{10}$ reduction as in the case of other initial populations. PEF tests with this particular initial population can be used to compare the PEF inactivation efficiency between the re-designed and original test cells, as shown in Figure VII.10. When subjected to 50 HV square impulses with field magnitude of 67 kV/cm, the population of the *S. cerevisiae* was reduced by only 1-$log_{10}$ in the original test cell while 2-$log_{10}$ reduction was observed in the re-designed test cell. This result suggested that the PEF inactivation performance was improved by the use of the re-designed stainless steel test cell. Some of potential low field zones, as identified in Section 6.1.2.2, may be eliminated in the new test cell. However, the 'tailing' effect in the inactivation curve still existed, as shown in Figure VII.9.

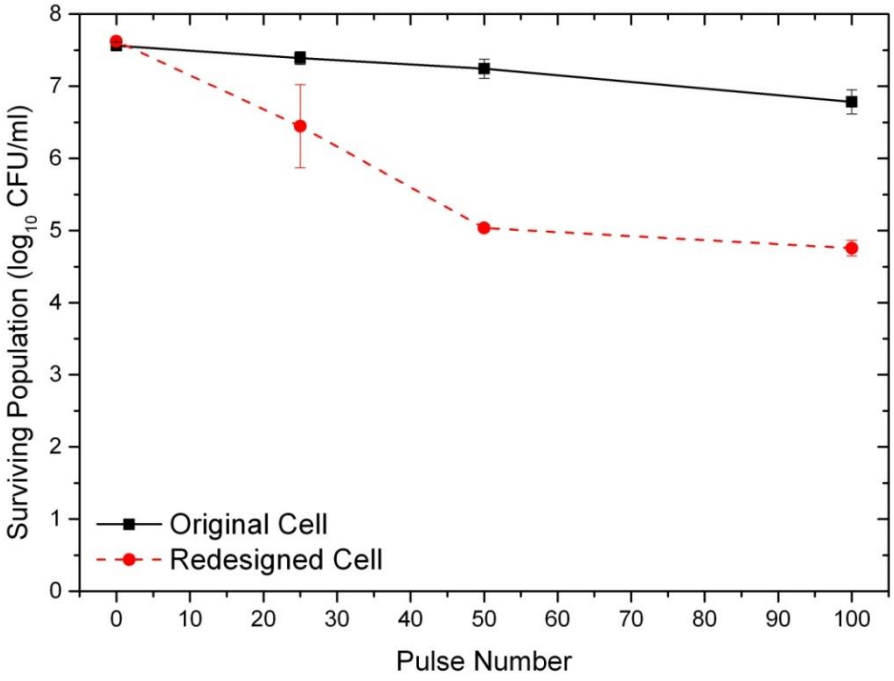


**Figure VII.10** Surviving population of *S. cerevisiae* ($log_{10}$ CFU/ml) as a function of number of impulses. PEF treatment with square waveform of 67 kV/cm. Solid line, the original test cell; Dash line, the re-designed test cell. Error bars show standard deviation (n=3).

When *S. cerevisiae* sample was treated with pulsed electric field with magnitude of 80 kV/cm, 3-$log_{10}$ reduction in surviving population was achieved after application of 100 square impulses regardless of the initial population, as shown in Figure VII.9. As in the case of the 67 kV/cm tests, inactivation tendencies of *S. cerevisiae* samples with different initial populations were similar. However it was shown that, 80 kV/cm impulses resulted in better inactivation efficiency as compared with the 67 kV/cm impulses. This was demonstrated using direct comparison of the PEF results, as shown in Figure VII.11. The PEF results for only two initial populations, the highest, ~ $10^7$ CFU/ml, and the lowest, ~ $10^4$ CFU/ml, were shown in the figure in order to provide clear representation of the inactivation curves. As there was no significant difference in the inactivation tendencies for other two initial populations used in these tests, $10^6$ CFU/ml and $10^5$ CFU/ml, they were not shown in the figure. It could be seen from Figure VII.11 that the PEF treatment with the higher field strength provided superior inactivation performance. In both $10^7$ CFU/ml and $10^4$ CFU/ml

groups, the PEF treatment with field magnitude of 80 kV/cm provided ~ 1-$\log_{10}$ more reduction in *S. cerevisiae* population as compared with PEF treatment with 67 kV/cm impulses using the same number of impulses.

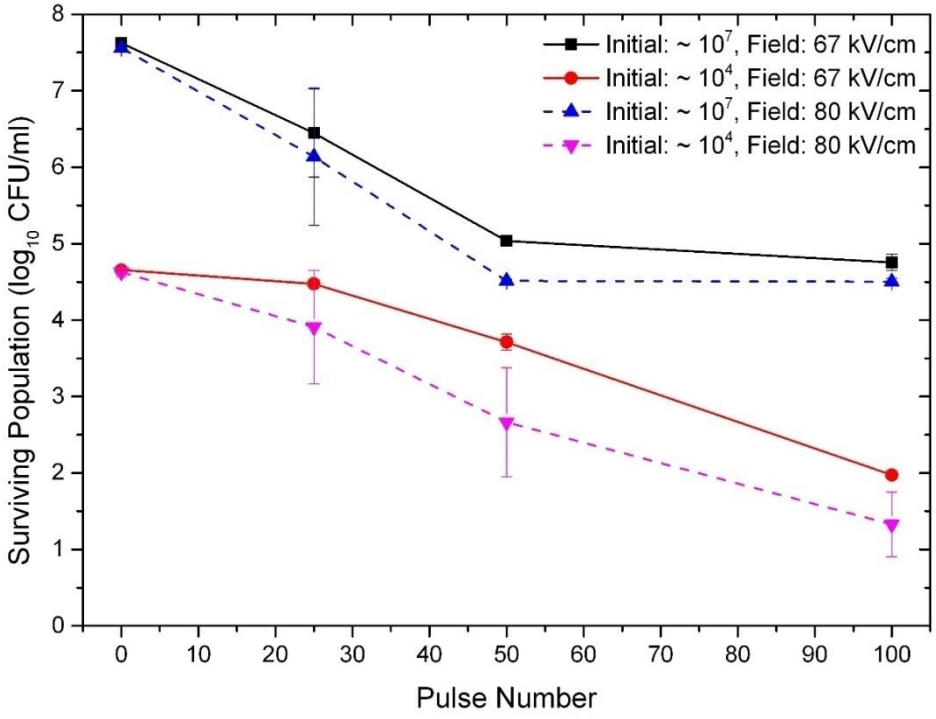


**Figure VII.11** Surviving population of *S. cerevisiae* ($\log_{10}$ CFU/ml) as a function of number of impulses. PEF treatment with square waveform of different initial populations. Solid lines, 67 kV/cm; Dash lines, 80 kV/cm. Error bars show standard deviation (n=3).

#### 7.3.3.3 PEF Treatment with Smooth Exponential Impulses

Figure VII.12-VII.13 show the results obtained from the PEF treatment of *S. cerevisiae* by HV impulses with smooth exponential waveshape. The obtained results from PEF tests with impulses magnitudes of 67 kV/cm and 80 kV/cm are shown in Figure VII.12 and Figure VII.13 respectively. As demonstrated in these figures, the surviving population of the *S. cerevisiae* sample reduced as the number of impulse increased, which indicated that *S. cerevisiae* were effectively inactivated by PEF treatment using HV impulses with smooth exponential waveshape in the re-designed stainless steel test cell.

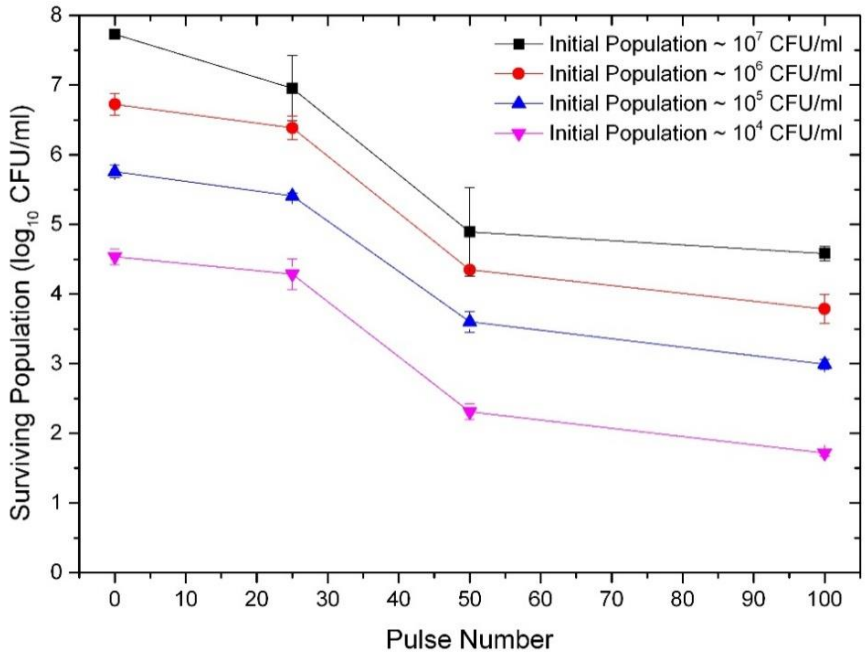


**Figure VII.12** Surviving population of *S. cerevisiae* ($log_{10}$ CFU/ml) as a function of number of impulses. PEF treatment with smooth exponential waveform of different initial populations. Field strength was 67 kV/cm. Error bars show standard deviation (n=3).

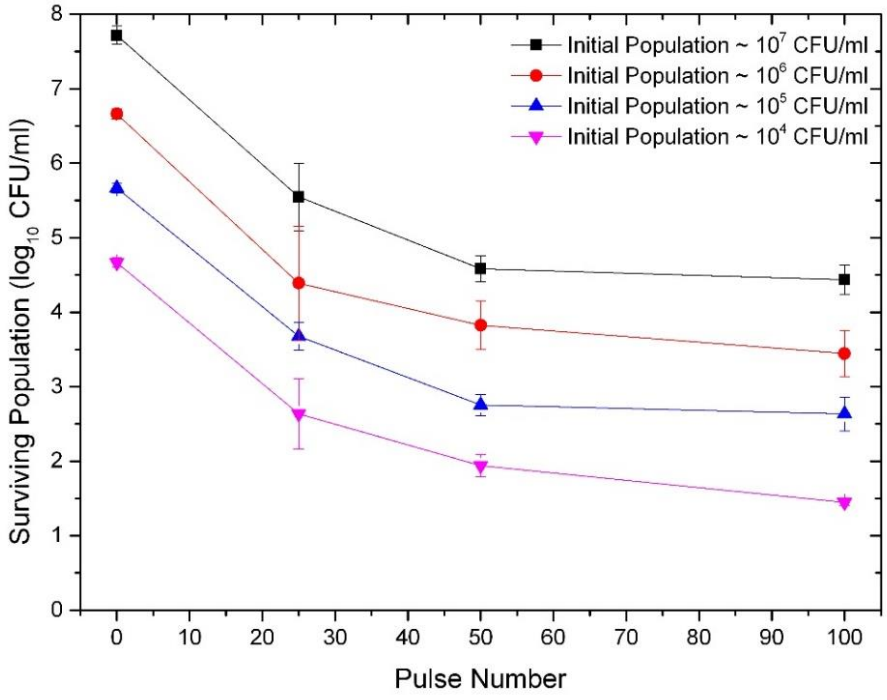


**Figure VII.13** Surviving population of *S. cerevisiae* ($log_{10}$ CFU/ml) as a function of number of impulses. PEF treatment with smooth exponential waveform of different initial populations. Field strength was 80 kV/cm. Error bars show standard deviation (n=3).

It can be seen from Figure VII.12 that, 3-$\log_{10}$ reduction in the surviving *S. cerevisiae* population was achieved after the application of 100 impulses with field magnitude of 67 kV/cm regardless of the initial population. However, in the case of PEF treatment with 80 kV/cm impulses, the same 3-$\log_{10}$ reduction of *S. cerevisiae* population was achieved after the application of 50 impulses in all initial population groups, as demonstrated in Figure VII.13. In both cases, for PEF tests with 67 kV/cm and 80 kV/cm impulses, the inactivation tendencies of *S. cerevisiae* sample with different initial populations were very similar. However, the 'tailing' effect of the inactivation curves was still observed, especially in the 80 kV/cm group as shown in Figure VII.13, where no further inactivation was observed after 50 impulses. In general, the PEF performance of impulses with 80 kV/cm field magnitude was superior to that of 67 kV/cm impulses, as shown in Figure VII.14 where direct comparison between the impulses with two levels of field magnitudes was made. Again, only two initial populations, $10^7$ CFU/ml and $10^4$ CFU/ml, are shown in the figure for a clear observation of the inactivation curves. The inactivation curves of other two initial population demonstrated very similar inactivation tendencies and therefore not shown in Figure VII.14. It can be seen in the figure that a higher degree of reduction in *S. cerevisiae* population was achieved by the impulses with higher field strength using the same number of impulses.

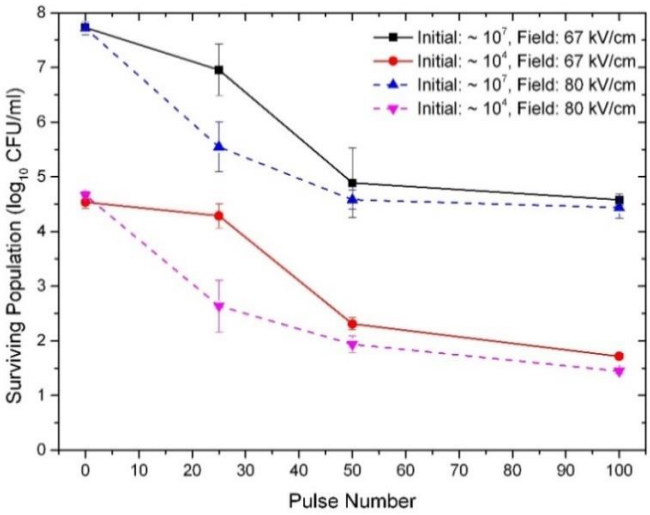


**Figure VII.14** Surviving population of *S. cerevisiae* ($\log_{10}$ CFU/ml) as a function of number of impulses. PEF treatment with smooth exponential waveform of different initial populations. Solid lines: 67 kV/cm; Dash lines: 80 kV/cm. Error bars show standard deviation (n=3).

It can be noted from Figure VII.12 and Figure VII.14, ‘shoulders’ in the inactivation curves of *S. cerevisiae* appeared at 25 impulses with the electric field strength of 67 kV/cm. The ‘shoulder’ effect was also observed in other inactivation studies [255-256]. The potential reason for this ‘shoulder’ effect is that the microorganisms are adjusting to the external stress and a sub-population of microorganisms remain viable after the treatment. However, it was demonstrated in [255] using real-time monitoring method that the damage had been done to *C. albicans* treated by pulsed UV light at the ‘shoulder’ points of the inactivation curves. In [255], real-time monitor of the changing substances in *C. albicans* suspension indicated that substance’s content in the suspension starts to change at the ‘shoulder’ points. Further investigation of the ‘shoulder’ effect using lower electric fields or lower number of pulses could be beneficial for better understanding of the mechanisms of microbial cell adjustment to external stresses.

#### 7.3.3.4 PEF Treatment with Oscillating Exponential Impulses

The results obtained from PEF treatment of *S. cerevisiae* using HV impulses with oscillating exponential waveshape are shown in Figure VII.15 and Figure VII.16. These figures demonstrated the results of for PEF tests with field magnitude of 67 kV/cm and 80 kV/cm respectively. Similar to PEF tests using impulses with the other two waveshapes, the surviving population of the *S. cerevisiae* sample reduced as the number of impulse increased, which indicated that *S. cerevisiae* were inactivated by PEF treatment using impulses with oscillating exponential waveshape in the re-designed stainless steel test cell.

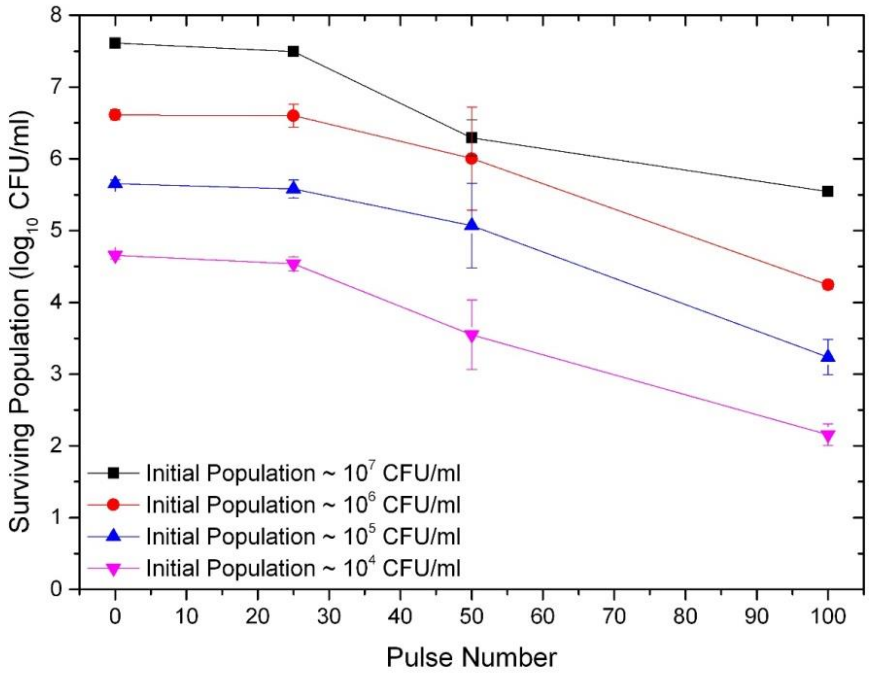


**Figure VII.15** Surviving population of *S. cerevisiae* ($log_{10}$ CFU/ml) as a function of number of impulses. PEF treatment with oscillating exponential waveform of different initial populations. Field strength was 67 kV/cm. Error bars show standard deviation (n=3).

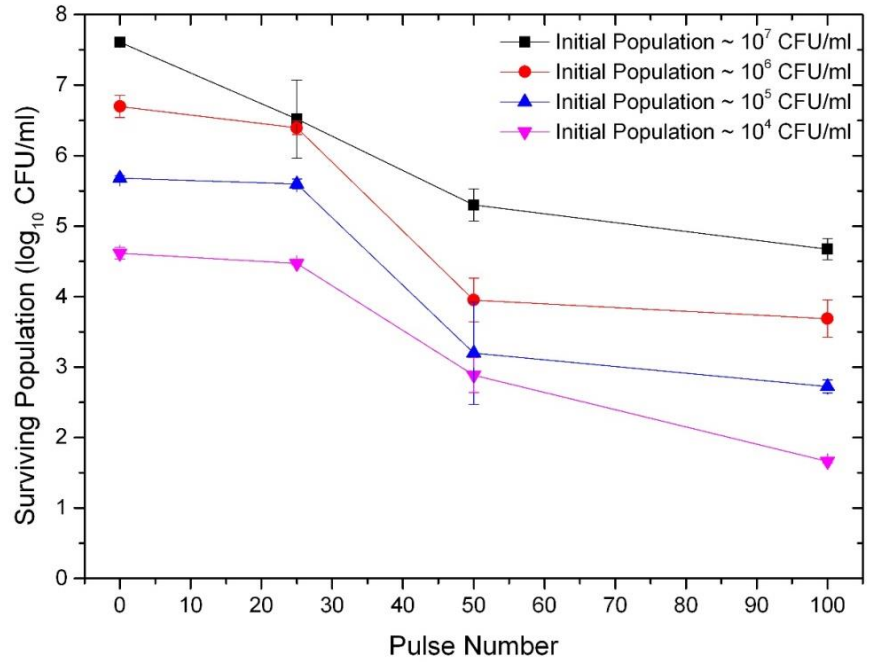


**Figure VII.16** Surviving population of *S. cerevisiae* ($log_{10}$ CFU/ml) as a function of number of impulses. PEF treatment with oscillating exponential waveform of different initial populations. Field strength was 80 kV/cm. Error bars show standard deviation (n=3).

In the PEF treatment using impulses with field magnitude of 67 kV/cm, 2-$\log_{10}$ reduction in surviving *S. cerevisiae* population was achieved after 100 impulses regardless of the initial populations, as shown in Figure VII.15. It can also be seen that the inactivation tendencies of *S. cerevisiae* samples with different initial populations were similar in the 67 kV/cm group. While in the PEF treatment with 80 kV/cm field magnitude, 3-$\log_{10}$ reduction in *S. cerevisiae* population was achieved after 100 impulses in all initial population groups. The inactivation tendencies were slightly different among different initial populations when *S. cerevisiae* samples were treated by impulses with 80 kV/cm field magnitude, but the general tendencies were similar. The inactivation performance obtained using impulses with 80 kV/cm magnitude was superior to that obtained using 67 kV/cm field strength, as displayed in Figure VII.17 and Figure VII.18 where direct comparison between the two groups has been made. Comparison between all initial populations groups have been made in separate figures (Figure VII.17 and Figure VII.18) for clear viewing. It can be seen in the figure that higher level of reduction in *S. cerevisiae* population was achieved using higher field strength with the same number of impulses. The 'shoulder' effect was also observed in the inactivation curves of the PEF treatment using 80 kV/cm impulses with initial *S. cerevisiae* population of $10^4$-$10^6$ CFU/ml.

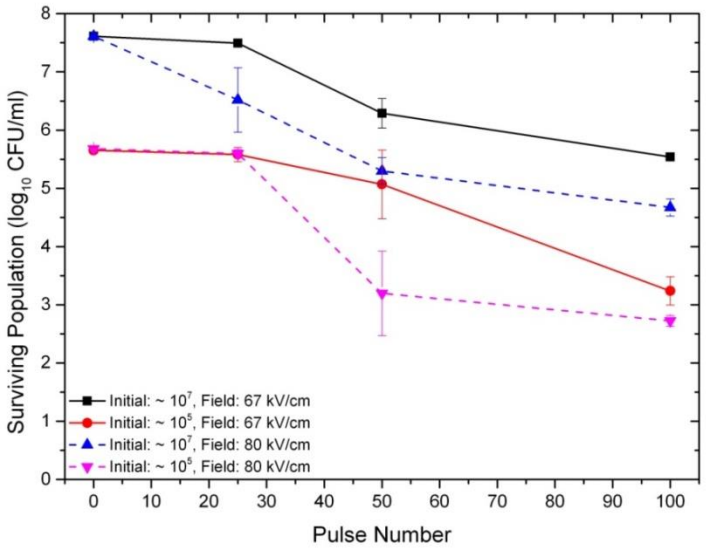


**Figure VII.17** Surviving population of *S. cerevisiae* ($\log_{10}$ CFU/ml) as a function of number of impulses. PEF treatment with oscillating exponential waveform of different initial populations. Solid lines, 67 kV/cm; Dash lines, 80 kV/cm. Error bars show standard deviation (n=3).

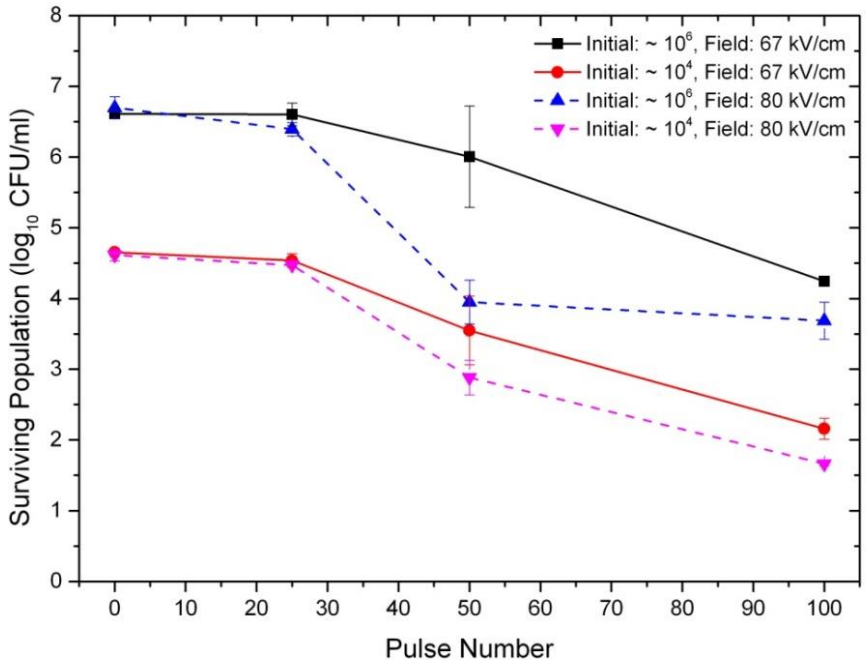


**Figure VII.18** Surviving population of *S. cerevisiae* ($log_{10}$ CFU/ml) as a function of number of impulses. PEF treatment with oscillating waveform of different initial populations. Solid lines, 67 kV/cm; Dash lines, 80 kV/cm. Error bars show standard deviation (n=3).

#### 7.3.3.5 Summary of PEF Results: Stainless Steel Test Cell

A summary of the obtained results of the PEF inactivation of *S. cerevisiae* in the re-designed stainless steel test cell is provided in this section. The main conclusions which can be made based on the conducted experiments and the comparison of PEF performance obtained using impulses with different waveshapes will be discussed in Section 7.3.4.

- Successful inactivation of *S. cerevisiae* was achieved by PEF impulses in the re-designed stainless steel test cell. PEF impulses with the three different waveshapes, the square, smooth exponential and oscillating exponential waveshapes, demonstrated successful inactivation of *S. cerevisiae* in this test cell.

- PEF tests with all impulse waveshapes demonstrated that the inactivation tendencies were very similar for different initial concentrations of

*S. cerevisiae* in suspension. A similar $\log_{10}$ reduction was achieved by the same number of impulse regardless of initial yeast population.

- After application of 100 impulses, 2-$\log_{10}$ reduction in surviving *S. cerevisiae* population was achieved by 67 kV/cm impulses with square and oscillating exponential waveshapes, while 3-$\log_{10}$ reduction was achieved by using impulses with 67 kV/cm field magnitude and smooth exponential waveshape.

- 3-$\log_{10}$ reduction in surviving *S. cerevisiae* population was achieved using 100 impulses of all the waveshapes with the peak field of 80 kV/cm.

- PEF impulses with a higher magnitude (80 kV/cm) demonstrated better performance than impulses with lower magnitude (67 kV/cm). This tendency was observed in PEF tests using impulses with all three types of waveshapes. Greater reduction in surviving *S. cerevisiae* population was achieved using same number of PEF impulses with higher field strength.

- PEF process in the re-designed test cell showed a better inactivation performance than in the original test cell, as demonstrated by the experiment results using 67 kV/cm square impulses. One extra $\log_{10}$ reduction was achieved after 50 impulses using the re-designed test cell. This result demonstrated that the PEF performance has been improved in the new stainless steel test cell.

- It was shown that the 'tailing' effect in the inactivation curves existed in most of the PEF experiments: no further reduction in surviving population of *S. cerevisiae* was achieved by increasing the number of impulses. Investigation of the potential reasons for the 'tailing' effect will be discussed in Section 7.3.5.4.

- The 'shoulder' effect in the inactivation curves was also observed in several PEF experiments. The presence of the 'shoulder' in the inactivation curves suggested that damage has been done to the *S. cerevisiae* cells but sub-

population of the *S. cerevisiae* sample was adjusting to the stress produced by the PEF process.

- Heating effect was not significant in the PEF treatment in the re-designed stainless steel test cell: the maximum increase in temperature recorded during the experiments was ~ 1.5 °C. The heating effect was limited by the use of low conductive sample suspension. However, the measurements of temperature were also delayed due to the depressurisation process, which could allow the sample to be cooled down during this process.

### 7.3.4 PEF Treatment in $TiO_2$-Coated Test cell

#### 7.3.4.1 Temperature Measurements

The potential thermal effects of the PEF process were monitored by measuring the temperature of the sample suspensions after the treatments, as mentioned in Section 7.1.2. The results obtained from these measurements showed that the maximum increase in temperature after PEF treatment in the $TiO_2$-coated test cell was ~ 0.5 °C.

As explained in Section 7.2.4, this insignificant increase in temperature was likely to be the result of the use of low conductive sample suspension and low-conductive $TiO_2$-coated electrodes. However, as highlighted in Section 7.2.4, the depressurisation process of the pressurised chamber and the removal of the test cell could also affect the temperature measurements. The delay in measurement potentially allowed the sample suspension to cool down before the temperature measuring process. Therefore, the insignificant increase in sample suspension temperature could be the combined result of both factors.

#### 7.3.4.2 PEF Treatment with Square Impulses

The *S. cerevisiae* samples were treated in the $TiO_2$-coated test cell using HV impulses with square waveshape. Figure VII.19-VII.20 show the results obtained from these PEF tests using field magnitudes of 67 kV/cm and 80 kV/cm respectively. As can be seen from these figures, the population of the *S. cerevisiae* sample was

reduced through the application of PEF impulses, which indicated that *S. cerevisiae* were effectively inactivated by HV impulses with square waveshape in the $TiO_2$-coated test cell.

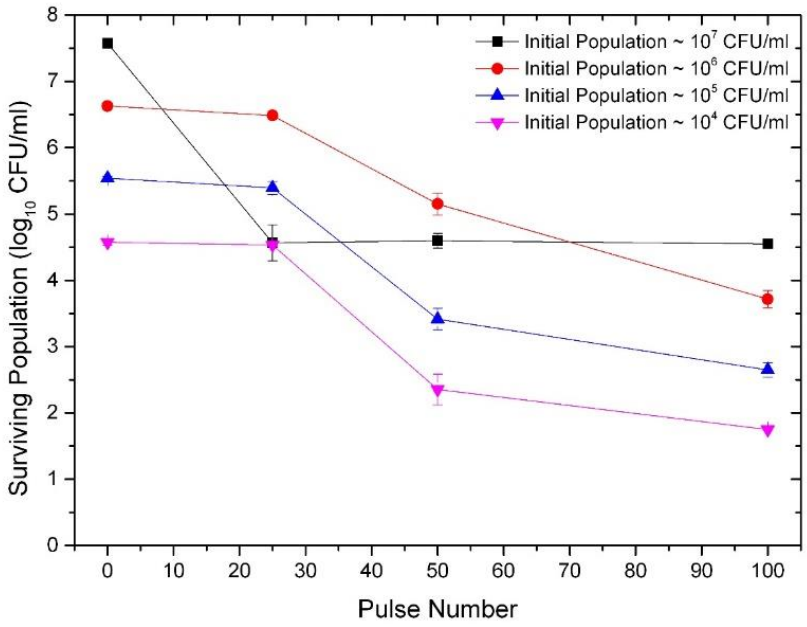


**Figure VII.19** Surviving population of *S. cerevisiae* ($log_{10}$ CFU/ml) as a function of number of impulses. PEF treatment with square waveform of different initial populations. Field strength was 67 kV/cm. Error bars show standard deviation (n=3).

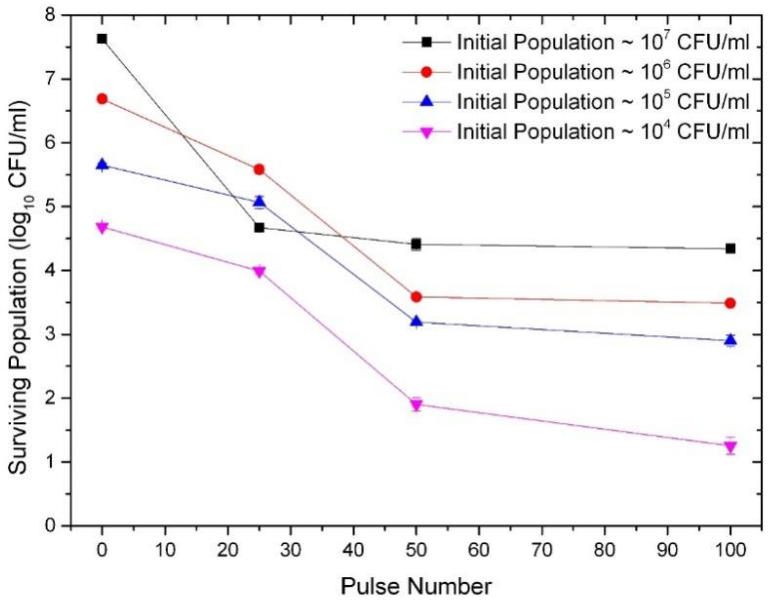


**Figure VII.20** Surviving population of *S. cerevisiae* ($log_{10}$ CFU/ml) as a function of number of impulses. PEF treatment with square waveform of different initial populations. Field strength was 80 kV/cm. Error bars show standard deviation (n=3).

As can be seen from Figure VII.19, 3-$\log_{10}$ reduction in *S. cerevisiae* surviving population was achieved after the application of 100 impulses with field magnitude of 67 kV/cm regardless of the initial sample concentration. However in the case of 80 kV/cm field magnitude, only 50 impulses were required to achieve the same 3-$\log_{10}$ reduction in *S. cerevisiae* population. It can also be seen from both figures that the inactivation tendencies for different sample concentrations were very similar except for the $10^7$ CFU/ml group, where 3-$\log_{10}$ reduction was achieved after only 25 impulses using both 67 kV/cm and 80 kV/cm field magnitudes. Generally speaking, PEF treatment using 80 kV/cm impulses produced better inactivation performance when compared with impulses with 67 kV/cm field magnitude. Figure VII.21 demonstrates a direct comparison between two inactivation curves from PEF treatments of *S. cerevisiae* sample with $10^7$ CFU/ml and $10^4$ CFU/ml initial concentrations. The other two initial concentrations are not shown in the figure to provide a clear presentation. The inactivation tendencies of these two non-presented groups were very similar to the $10^4$ CFU/ml group, as can be seen from Figure VII.19-VII.20. It should also be noticed that the 'tailing' effect can be clearly seen in all the inactivation curves. The 'shoulder' effect can also be observed in the inactivation curves of the PEF treatment using *S. cerevisiae* samples with initial population of $10^4$-$10^6$ CFU/ml.

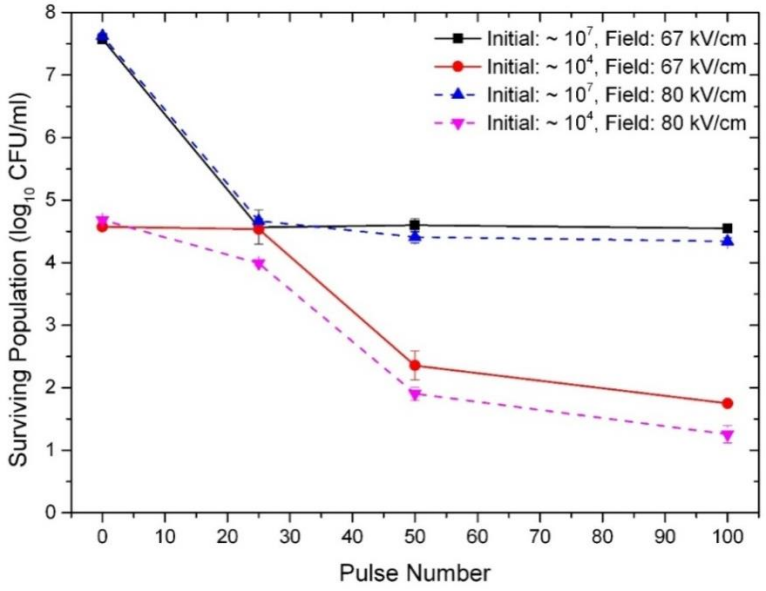


**Figure VII.21** Surviving population of *S. cerevisiae* ($\log_{10}$ CFU/ml) as a function of number of impulses. PEF treatment with square waveform of different initial populations. Solid lines, 67 kV/cm; Dash lines, 80 kV/cm. Error bars show standard deviation (n=3).

### 7.3.4.3 PEF Treatment with Smooth Exponential Impulses

The results obtained using PEF impulses with smooth exponential waveshape are shown in Figure VII.22-VII.23, for the field level of 67 kV/cm and 80 kV/cm respectively. As the two figures demonstrate, population of the *S. cerevisiae* reduced with an increase in the PEF impulses. These results suggested that effective inactivation of *S. cerevisiae* was achieved by PEF process in the $TiO_2$-coated test cell using impulses with smooth exponential waveshape.

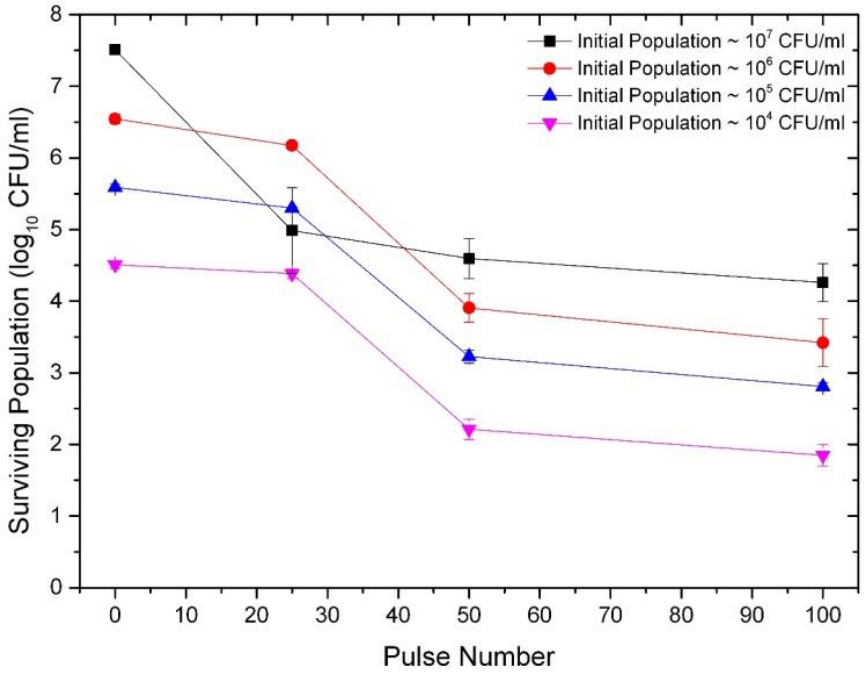


**Figure VII.22** Surviving population of *S. cerevisiae* ($log_{10}$ CFU/ml) as a function of number of impulses. PEF treatment with smooth exponential waveform of different initial populations. Field strength was 67 kV/cm. Error bars show standard deviation (n=3).

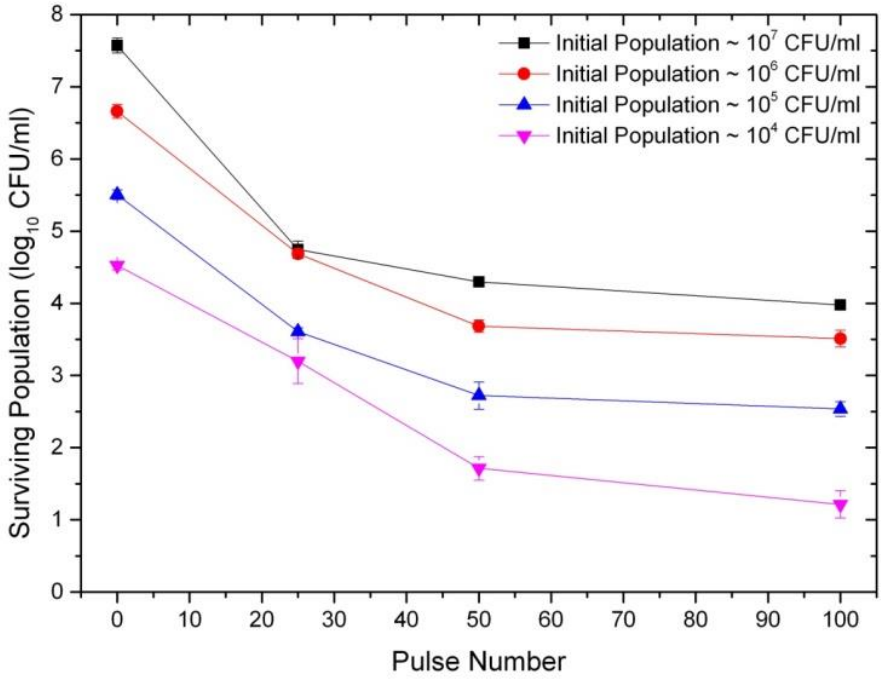


**Figure VII.23** Surviving population of *S. cerevisiae* ($log_{10}$ CFU/ml) as a function of number of impulses. PEF treatment with smooth exponential waveform of different initial populations. Field strength was 80 kV/cm. Error bars show standard deviation (n=3).

Regardless of the initial *S. cerevisiae* cell density and the levels of field magnitude, 3-$log_{10}$ reduction in viable cells was achieved after the application of 50 impulses, as demonstrated in Figure VII.22-VII.23. It can also be seen that the inactivation tendencies of PEF tests with $10^7$ CFU/ml initial sample concentration were more pronounced than the tests with other initial yeast populations, as 3-$log_{10}$ reduction in population was achieved by only 25 impulses when the initial populations were $10^7$ CFU/ml. However, inactivation tendencies of the other groups, with initial sample populations of $10^6$ CFU/ml, $10^5$ CFU/ml and $10^4$ CFU/ml, were very similar. Comparison between the PEF inactivation curves ($10^7$ CFU/ml and $10^4$ CFU/ml groups) using different field magnitudes has been made and shown in Figure VII.24. It was showed in this figure that PEF process with the 80 kV/cm field magnitude had a slightly better performance than with the 67 kV/cm magnitude. Again, the 'tailing' effect in the inactivation curves was observed clearly in all the obtained results. The 'shoulder' effect can be seen in the inactivation curves of the 67 kV/cm PEF treatment using *S. cerevisiae* samples with initial population of $10^4$-$10^6$ CFU/ml.

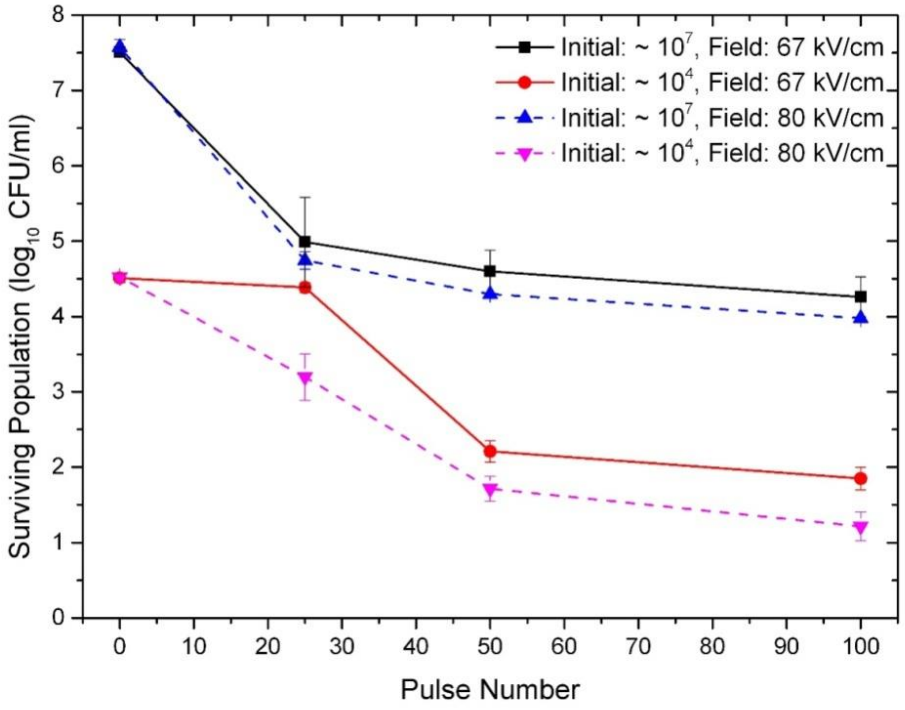


**Figure VII.24** Surviving population of *S. cerevisiae* ($log_{10}$ CFU/ml) as a function of number of impulses. PEF treatment with smooth exponential waveform of different initial populations. Solid lines, 67 kV/cm; Dash lines, 80 kV/cm. Error bars show standard deviation (n=3).

#### 7.3.4.4 PEF Treatment with Oscillating Exponential Impulses

Figure VII.25-VII.26 show the inactivation curves of *S. cerevisiae* treated using oscillating exponential PEF impulses. The results obtained from PEF tests with the field magnitudes of 67 kV/cm and 80 kV/cm are presented in Figure VII.25 and Figure VII.26 respectively. As shown in both figures, population of the *S. cerevisiae* was reduced by the PEF process, which indicated the *S. cerevisiae* were inactivated by PEF impulses with oscillating exponential waveshape in the $TiO_2$-coated test cell.

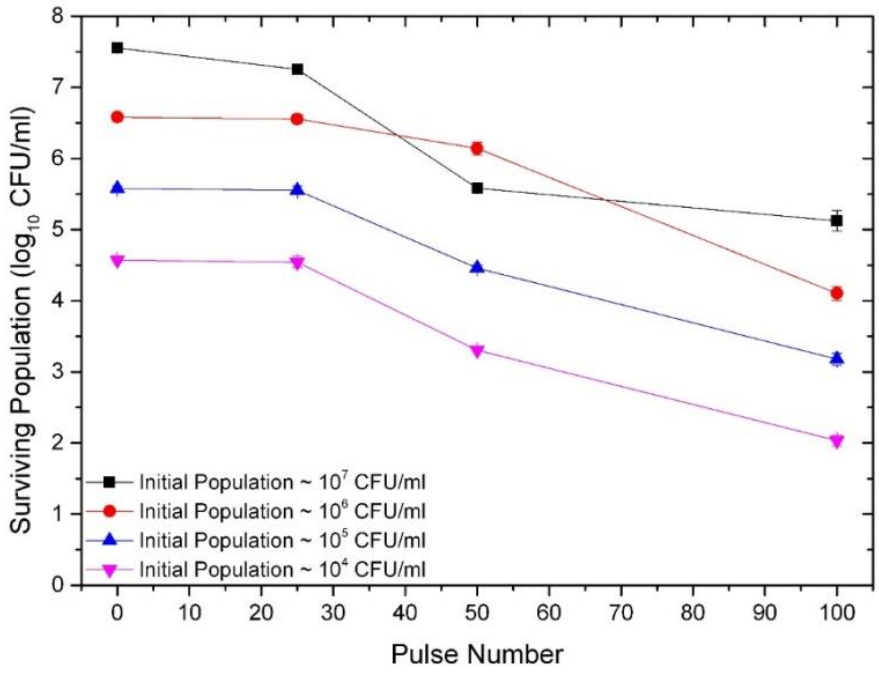


**Figure VII.25** Surviving population of *S. cerevisiae* ($log_{10}$ CFU/ml) as a function of number of impulses. PEF treatment with oscillating exponential waveform of different initial populations. Field strength was 67 kV/cm. Error bars show standard deviation (n=3).

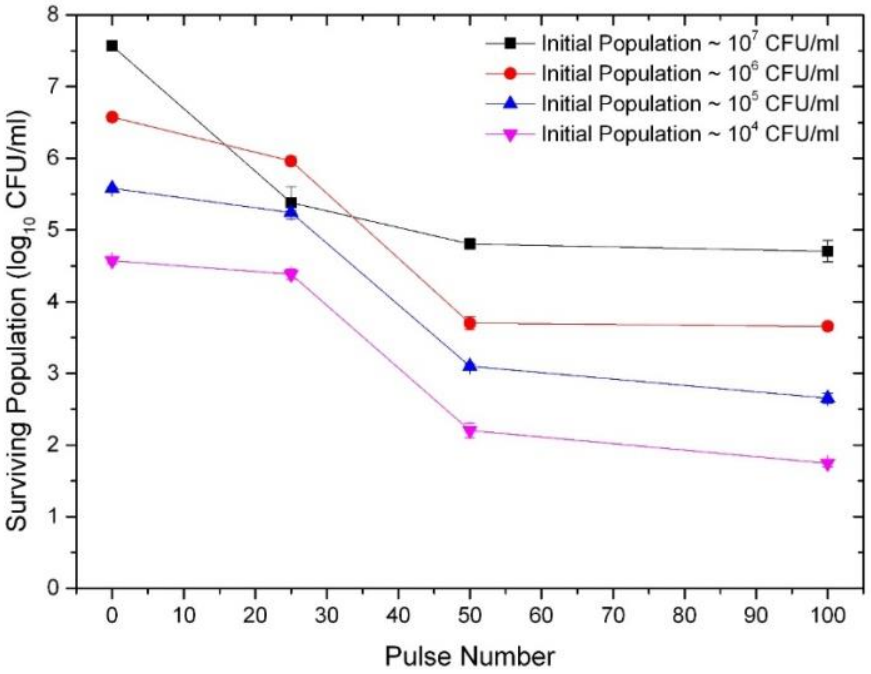


**Figure VII.26** Surviving population of *S. cerevisiae* ($log_{10}$ CFU/ml) as a function of number of impulses. PEF treatment with oscillating exponential waveform of different initial populations. Field strength was 80 kV/cm. Error bars show standard deviation (n=3).

It can be seen from Figure VII.25 that, a 2-$\log_{10}$ reduction in *S. cerevisiae* population was achieved by the application of 100 impulses with the field magnitude of 67 kV/cm, regardless of the initial population of the sample. However, as demonstrated in Figure VII.26, 3-$\log_{10}$ reduction in the *S. cerevisiae* population was achieved when the field magnitude was increased to 80 kV/cm. The inactivation tendencies of PEF treatment of *S. cerevisiae* sample with different initial concentrations were very similar except for the $10^7$ CFU/ml group, which were more pronounced than the other groups. Figure VII.27 shows the direct comparison between the inactivation curves of PEF treatment using different field magnitudes. As the figure demonstrates, PEF treatment with 80 kV/cm impulses provided better inactivation performance than PEF treatment using impulses with lower magnitude. The 'tailing' and 'shoulder' effects were also observed in *S. cerevisiae* inactivation curves.

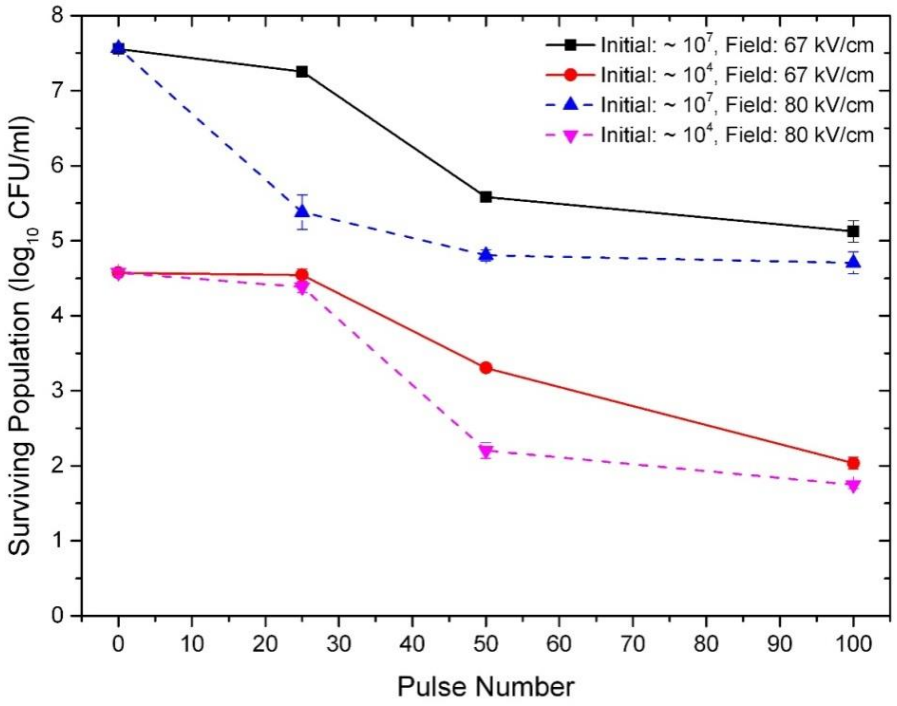


**Figure VII.27** Surviving population of *S. cerevisiae* ($\log_{10}$ CFU/ml) as a function of number of impulses. PEF treatment with oscillating exponential waveform of different initial populations. Solid lines, 67 kV/cm; Dash lines, 80 kV/cm. Error bars show standard deviation (n=3).

### 7.3.4.5 Summary of PEF Results in $TiO_2$-Coated Test Cell

A summary of the results obtain in the PEF experiments in which *S. cerevisiae* was treated in the $TiO_2$-coated test cell is provided in this section. The main findings and the comparison of PEF inactivation efficiencies between different pulse waveshapes and different test cells will be discussed in Section 7.3.4.

- It was demonstrated that *S. cerevisiae* can be inactivated HV impulses in the $TiO_2$-coated test cell. PEF treatment using impulse with three different waveshapes, the square, smooth exponential and oscillating exponential, demonstrated successful inactivation of *S. cerevisiae* was achieved.

- It has been shown that when the initial concentration of *S. cerevisiae* cells was in the range of $10^4$-$10^7$ CFU/ml, the inactivation tendencies were similar and did not depend on the initial concentration of microorganisms. However, it was observed that the 'tailing' effect in the inactivation curves appeared faster (with application of fewer impulses) for a higher concentration of *S. cerevisiae* in suspension, with initial population of $10^7$ CFU/ml.

- It was shown that when the field magnitude was 67 kV/cm, 2-$\log_{10}$ reduction in *S. cerevisiae* population was achieved after the application of 100 impulses with oscillating exponential waveshape. However, application of 100 impulses with square and smooth exponential waveshapes resulted in 3-$\log_{10}$ reduction in *S. cerevisiae* population.

- When the *S. cerevisiae* samples were treated by PEF impulses with field magnitude of 80 kV/cm, 3-$\log_{10}$ reduction in surviving population was achieved using all the pulse waveshapes by the application of 100 impulses.

- It was established that impulses with higher field magnitude (80kV/cm) demonstrated better PEF inactivation performance as compared with impulses with lower field magnitude (67 kV/cm). This tendency was observed in PEF experiments using impulses with all three types of waveshapes. A higher

degree of inactivation ($log_{10}$ reduction in surviving population) was achieved in the case when higher field strength was used.

- The 'tailing' effect in the inactivation curves was observed in most of the experiments: no further reduction in *S. cerevisiae* population was observed by increasing the number of HV impulses. Additional PEF experiments were conducted in the present study to investigate the potential reason for this effect and the obtained results will be discussed in Section 7.3.5.4. The 'shoulder' effect in the inactivation curves was also observed in several PEF tests, especially with initial concentration of $10^4$-$10^6$ CFU/ml.

- It was established that heating of the liquid suspension during PEF treatment in $TiO_2$-coated test cell was not significant. The recorded maximum increase in temperature after the PEF test was ~ 0.5 °C. This increase in temperature was even lower than the temperature increase obtained in the PEF experiments using stainless steel test cell. This result was likely to be explained by the combined factors of low conductive liquid suspension, low-conductive $TiO_2$-coated electrodes, and the depressurised process. A correlation between the specific energy consumption and the temperature change was established and will be discussed in Section 7.3.5.3.1.

### 7.3.5 PEF Treatment of *S. cerevisiae*: Main findings

As demonstrated in the previous sections, PEF treatment of *S. cerevisiae* have been conducted using both re-designed stainless steel and $TiO_2$-coated test cells using impulses with three different types of waveshape. The results obtained from the experiments indicate that inactivation of the *S. cerevisiae* sample was successfully achieved using both test cells and impulse with all three waveshapes. It would be interesting to compare the PEF inactivation performance between different impulse waveshapes and different test cells directly. On the other hand, the 'tailing' effect in the inactivation curves was observed despite improvement in PEF performance has been achieved using the re-designed test cell. Therefore, the potential cause of this 'tailing' effect should be reconsidered.

In this section, direct comparisons of the PEF performance using impulse with different waveshapes and different test cells will be made and discussed. The specific energy consumption corresponding to each type of impulse and test cell will be estimated and discussed. Correlation between these estimated energy consumption and the change in suspension temperature will be established. The potential reason of the 'tailing' effect observed in inactivation curves will also be investigated and discussed in this section.

#### 7.3.5.1 Comparison between Different Waveforms

Comparison between the PEF inactivation performances using impulses with three types of waveshape are shown in Figure VII.28-VII.31. In all figures, two initial concentrations of *S. cerevisiae*, the highest, $10^7$ CFU/ml, and the lowest, $10^4$ CFU/ml, are shown in order to provide clear representation of the inactivation curves. The inactivation curves for initial population of $10^5$ CFU/ml and $10^6$ CFU/ml are not showed in these figures as their inactivation tendencies were similar to the curves presented, as demonstrated in the previous sections. Figure VII.28 and Figure VII.29 show the results obtained from PEF tests in stainless steel test cell using field magnitudes of 67 kV/cm and 80 kV/cm respectively. Figure VII.30 and Figure VII.31 demonstrate the respective results using the $TiO_2$-coated test cell.

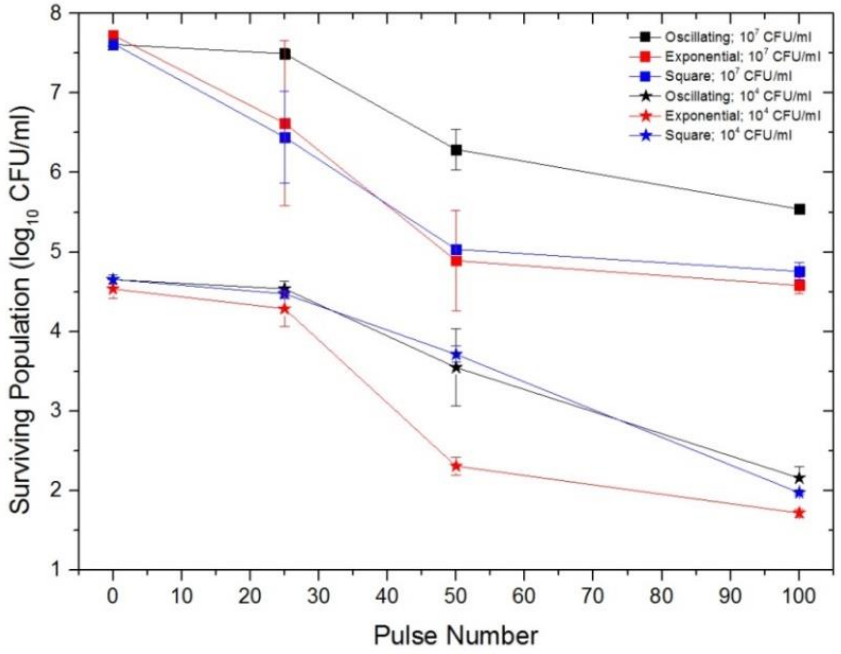


**Figure VII.28** Surviving population of *S. cerevisiae* ($log_{10}$ CFU/ml) treated in stainless steel test cell as a function of pulse number for 67 kV/cm impulses: square waveshape (blue), smooth exponential waveshape (red) and oscillating exponential waveshape (black). Square symbol: $10^7$ CFU/ml initial population; Star symbol: $10^4$ CFU/ml initial population. Error bars show standard deviation (n=3).

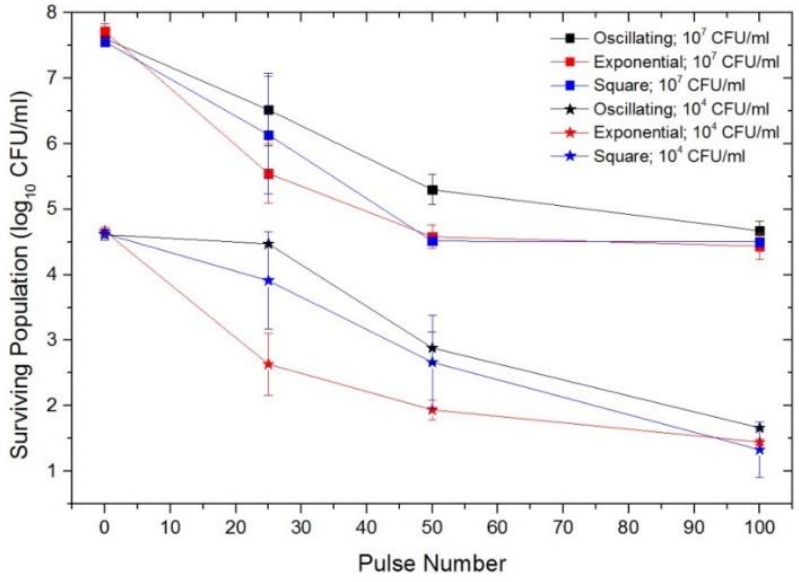


**Figure VII.29** Surviving population of *S. cerevisiae* ($log_{10}$ CFU/ml) treated in stainless steel test cell as a function of pulse number for 80 kV/cm impulses: square waveshape (blue), smooth exponential waveshape (red) and oscillating exponential waveshape (black). Square symbol: $10^7$ CFU/ml initial population; Star symbol: $10^4$ CFU/ml initial population. Error bars show standard deviation (n=3).

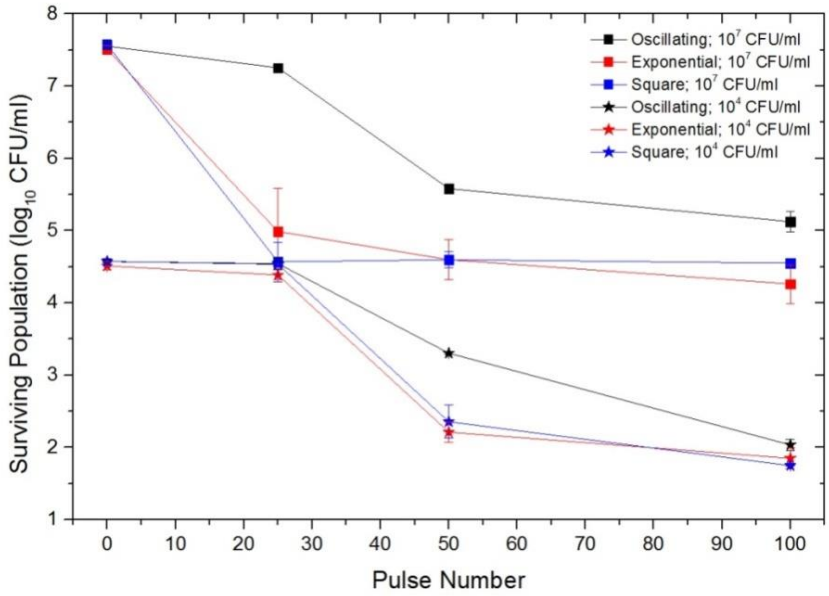


**Figure VII.30** Surviving population of *S. cerevisiae* ($log_{10}$ CFU/ml) treated in $TiO_2$-coated test cell as a function of pulse number for 67 kV/cm impulses: square waveshape (blue), smooth exponential waveshape (red) and oscillating exponential waveshape (black). Square symbol: $10^7$ CFU/ml initial population; Star symbol: $10^4$ CFU/ml initial population. Error bars show standard deviation (n=3).

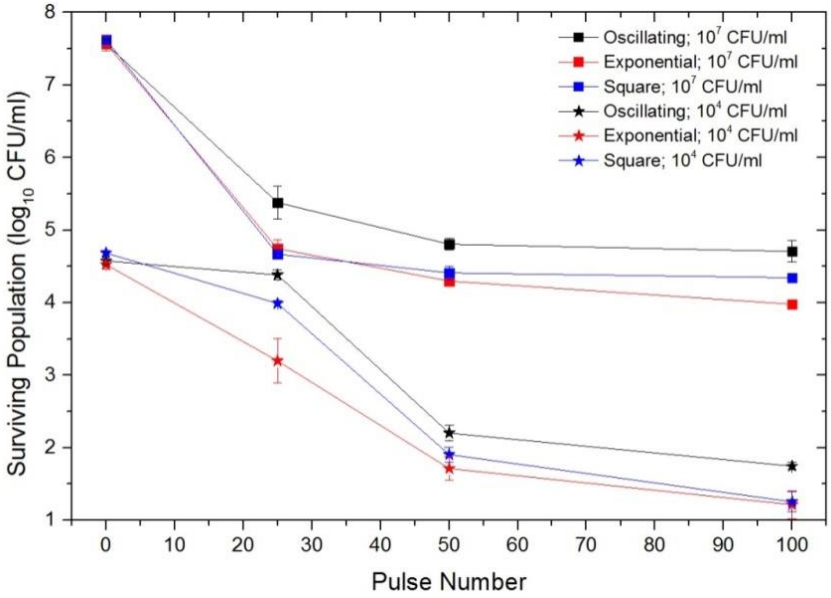


**Figure VII.31** Surviving population of *S. cerevisiae* ($log_{10}$ CFU/ml) treated in $TiO_2$-coated test cell as a function of pulse number for 80 kV/cm impulses: square waveshape (blue), smooth exponential waveshape (red) and oscillating exponential waveshape (black). Square symbol: $10^7$ CFU/ml initial population; Star symbol: $10^4$ CFU/ml initial population. Error bars show standard deviation (n=3).

As can be seen from Figure VII.28-VII.31, regardless of the field magnitude and the test cell used in the PEF treatment, the best PEF inactivation performance was achieved when HV impulses with smooth exponential waveshape were used. On the other hand, impulses with oscillating exponential waveshape produced the worst PEF inactivation performance as compared with other types of impulses.

According to [7], in which PEF treatment with square and exponential decay impulses was studied, square impulses were more energy efficient than exponential decaying impulses. In [7], both impulses with the same peak field magnitude delivered the same amount of energy to the sample. It was reported that the PEF treatment in which square impulses were used required a lower number of impulses to achieve the same inactivation result. However, in the present study, it was shown that the PEF treatment using impulses with smooth exponential waveshape required lower pulse number to achieve the same inactivation result. Although the peak field magnitude was the same for all pulse waveshapes, the specific energy delivered by each type of impulse was not identical in the present study. Therefore, it is important to compare the PEF performance of impulses with different waveshapes in terms of energy efficacy, which will be conducted in Section 7.3.5.3.

The PEF treatment with oscillating exponential impulses demonstrated a relatively poor inactivation performance. This can be explained by the nature of the fast oscillations which should restrict the development of trans-membrane potential according to the analysis in Section 3.1.3 and Section 3.2.2. However, it should be noticed that while the peak field magnitude of these three impulses was the same, the average field strength of the oscillating exponential impulse was significantly lower than the other two due to the fast oscillations. As can be seen in Figure VII.32, where the voltage waveforms of the oscillating exponential impulses were processed by an adjacent-averaging function in the *Origin Pro 9* software package, the average peak field strength were only 47 kV/cm and 59 kV/cm when the actual peak field strength reached 67 kV/cm and 80 kV/cm respectively. This significant lower average field means lower specific energy was delivered to the sample by each oscillating exponential impulse. Therefore, it would be necessary to compare the oscillating exponential impulse with the other two impulses in terms of energy efficacy.

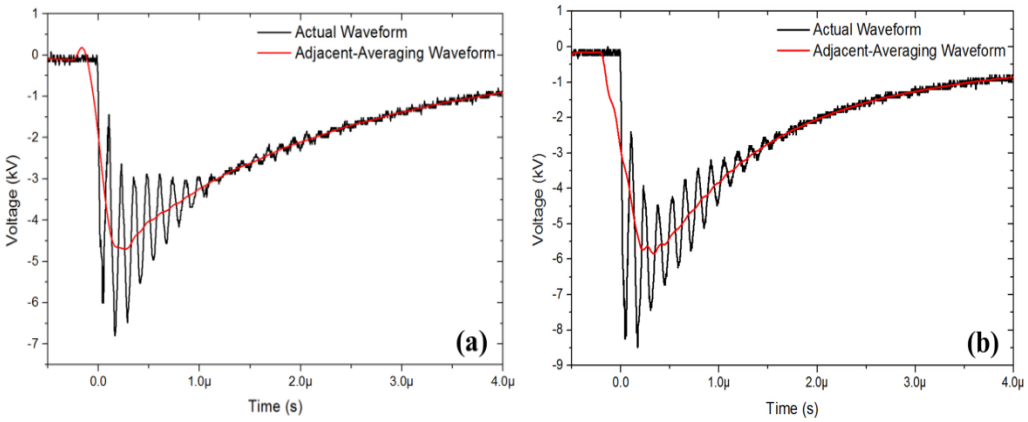


**Figure VII.32** Voltage waveforms of oscillating exponential impulses showing the adjacent-averaging voltage processed by *Origin Pro 9* software package: (a) voltage waveform corresponding to 67 kV/cm field strength; (b) voltage waveform corresponding to 80 kV/cm field strength.

### 7.3.5.2 Comparison between Different Test Cells

The comparison between the PEF inactivation of *S. cerevisiae* conducted in the conductive stainless steel test cell and the low-conductive $TiO_2$-coated test cell is presented in this section. Figure VII.33-VII.34 show the surviving population of *S. cerevisiae* treated with square impulses in both test cells, Figure VII.35-VII.36 show the inactivation curves of *S. cerevisiae* treated with smooth exponential impulses and Figure VII.37-VII.38 show the inactivation results of PEF treatment with oscillating exponential impulses in both test cells. Inactivation curves of *S. cerevisiae* sample with two initial concentrations, $10^7$ CFU/ml and $10^4$ CFU/ml, are presented in these figures in order to provide clear representation.

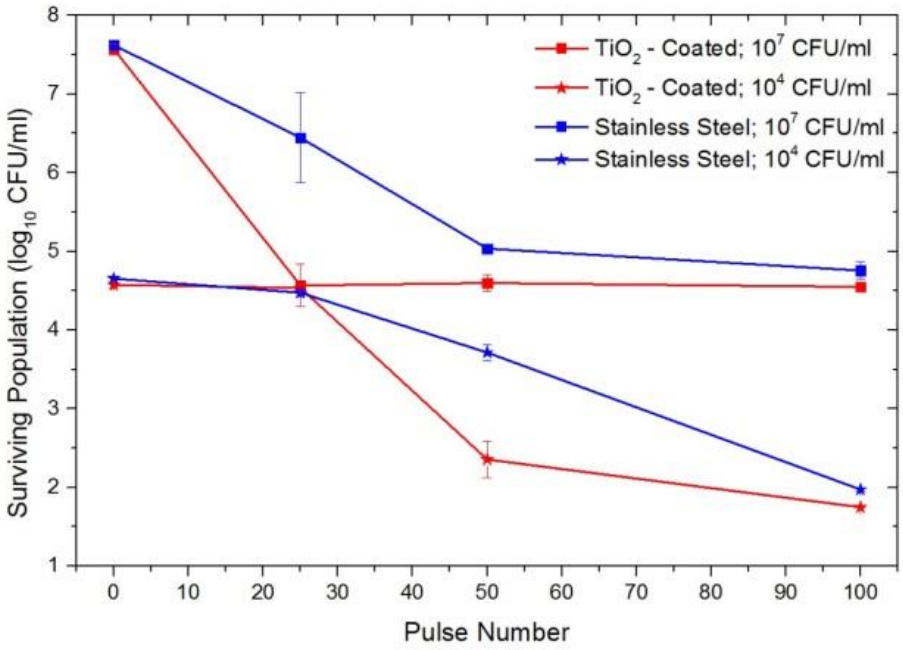


**Figure VII.33** Surviving populations of *S. cerevisiae* ($log_{10}$ CFU/ml) as a function of pulse number for 67 kV/cm square impulse: stainless test cell (blue); $TiO_2$-coated test cell (red); square symbol represent $10^7$ CFU/ml initial population; star symbol represent $10^4$ CFU/ml initial population. Error bars show standard deviation (n=3).

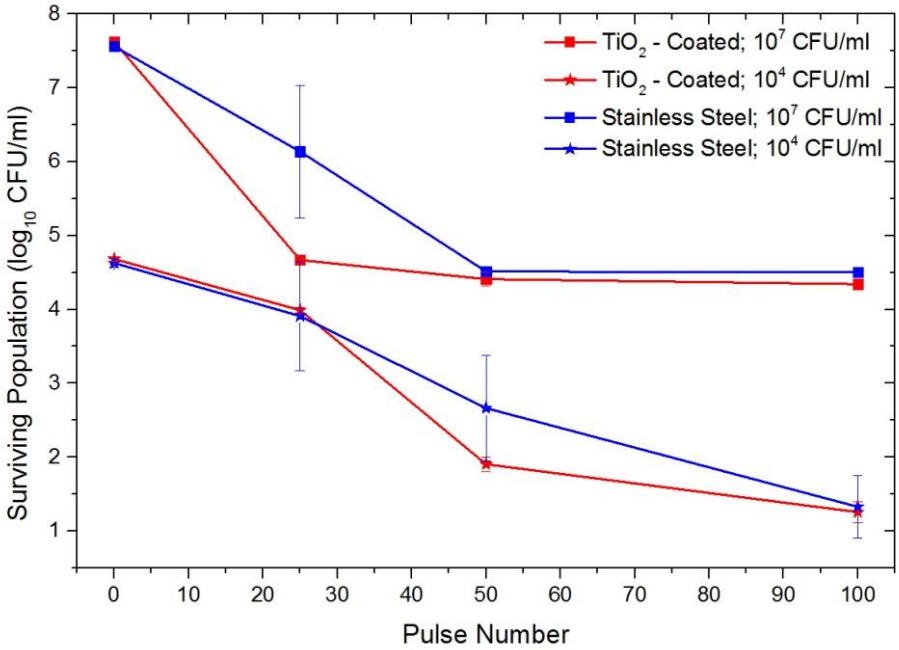


**Figure VII.34** Surviving populations of *S. cerevisiae* ($log_{10}$ CFU/ml) as a function of pulse number for 80 kV/cm square impulse: stainless test cell (blue); $TiO_2$-coated test cell (red); square symbol represent $10^7$ CFU/ml initial population; star symbol represent $10^4$ CFU/ml initial population. Error bars show standard deviation (n=3).

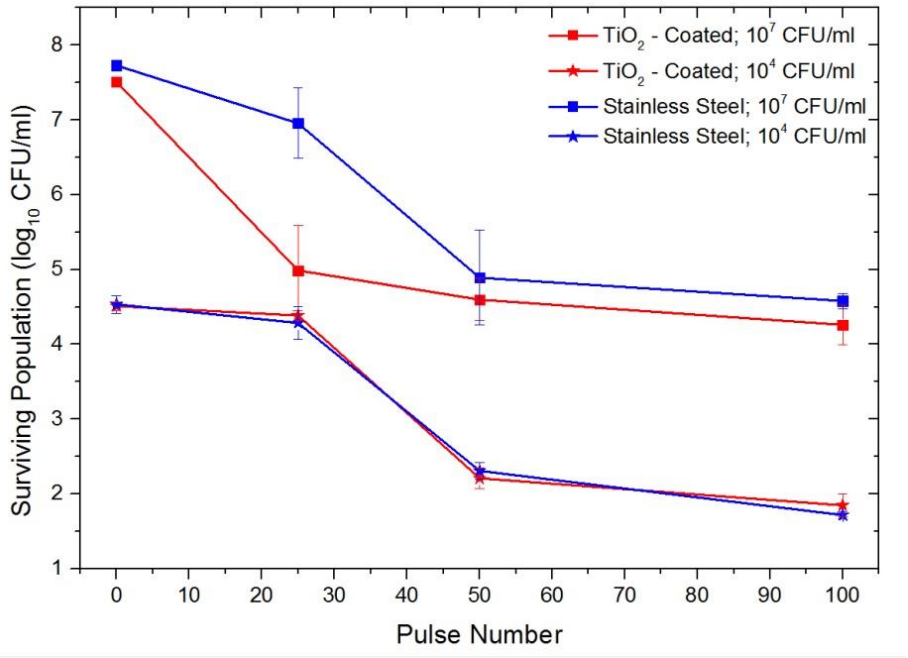


**Figure VII.35** Surviving populations of *S. cerevisiae* ($log_{10}$ CFU/ml) as a function of pulse number for 67 kV/cm smooth exponential impulse: stainless test cell (blue); $TiO_2$-coated test cell (red); square symbol represent $10^7$ CFU/ml initial population; star symbol represent $10^4$ CFU/ml initial population. Error bars show standard deviation (n=3).

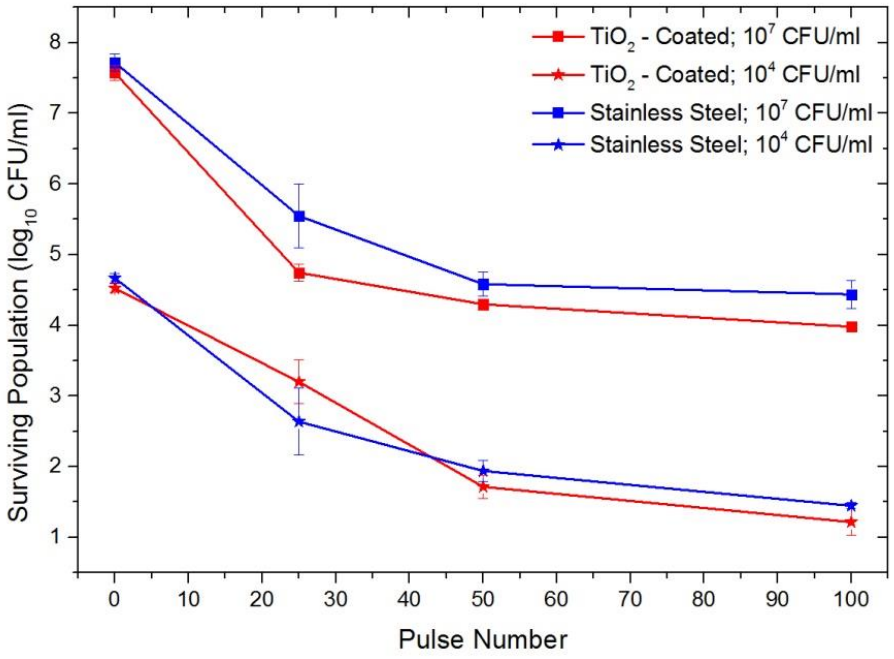


**Figure VII.36** Surviving populations of *S. cerevisiae* ($log_{10}$ CFU/ml) as a function of pulse number for 80 kV/cm smooth exponential impulse: stainless test cell (blue); $TiO_2$-coated test cell (red); square symbol represent $10^7$ CFU/ml initial population; star symbol represent $10^4$ CFU/ml initial population. Error bars show standard deviation (n=3).

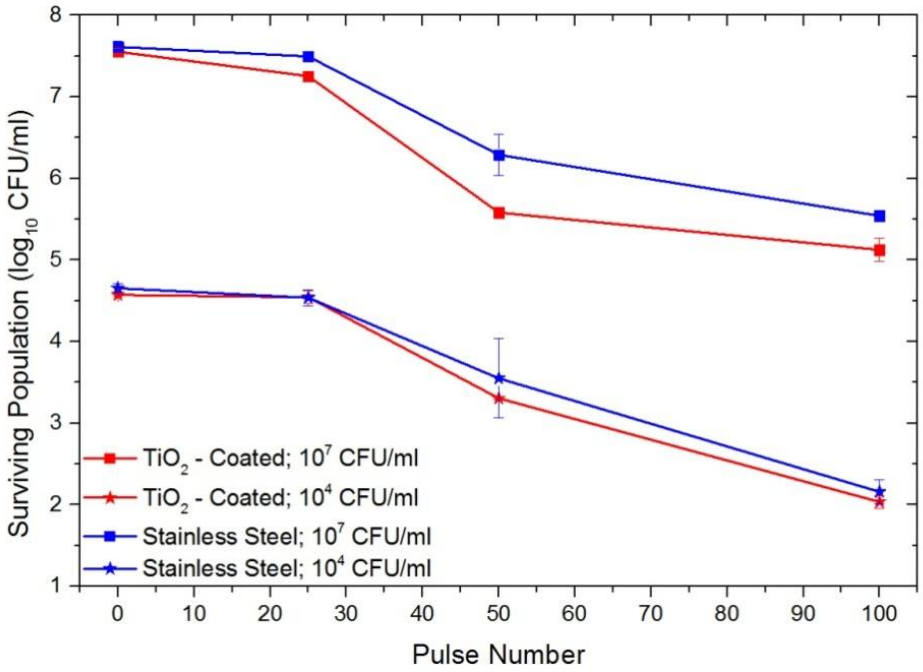


**Figure VII.37** Surviving populations of *S. cerevisiae* ($log_{10}$ CFU/ml) as a function of pulse number for 67 kV/cm oscillating exponential impulse: stainless test cell (blue); $TiO_2$-coated test cell (red); square symbol represent $10^7$ CFU/ml initial population; star symbol represent $10^4$ CFU/ml initial population. Error bars show standard deviation (n=3).

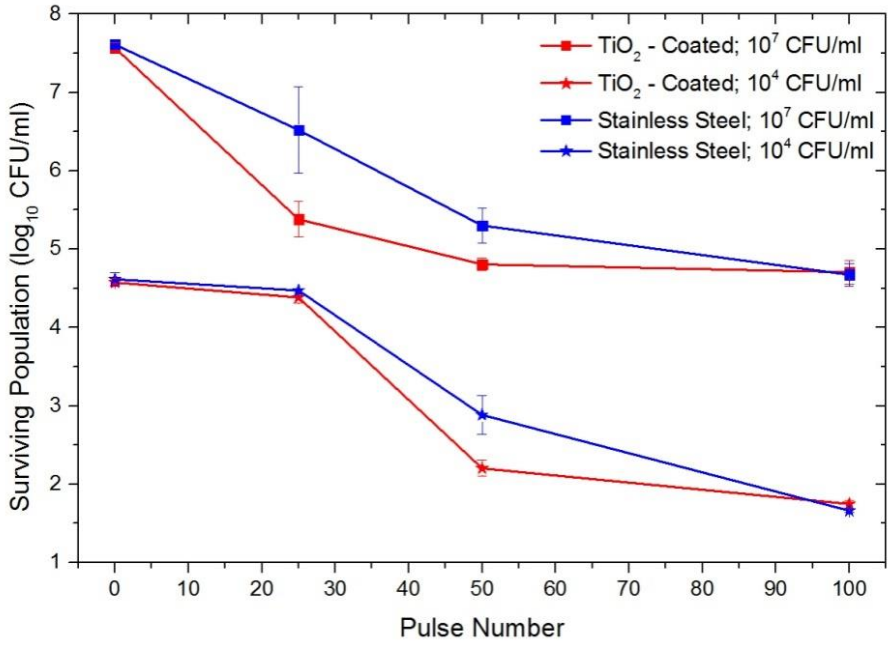


**Figure VII.38** Surviving populations of *S. cerevisiae* ($log_{10}$ CFU/ml) as a function of pulse number for 80 kV/cm oscillating exponential impulse: stainless test cell (blue); $TiO_2$-coated test cell (red); square symbol represent $10^7$ CFU/ml initial population; star symbol represent $10^4$ CFU/ml initial population. Error bars show standard deviation (n=3).

As can be seen from these figures, PEF treatment in the $TiO_2$-coated test cell demonstrated an improved inactivation performance as compared with the stainless steel test cell. In most cases, more $\log_{10}$ reduction in *S. cerevisiae* population was achieved by the application of the same number of impulses using the $TiO_2$-coated test cell. In addition, as the current measurement revealed, the ionic conduction current in the $TiO_2$-coated test cell was significantly lower than that in the stainless steel test cell, as shown in Figure VII.39. The peak magnitude of the ionic conduction current was reduced by ~ 30% on average as compared with the stainless steel test cell in all cases. This significant reduction in the ionic conduction current suggested that even better PEF performance in terms of energy efficacy can be achieved in the $TiO_2$-coated test cell, as ionic conduction is the major contributor to the specific energy consumption of the PEF process. Therefore, comparison between two test cells (stainless steel and $TiO_2$-coated) in terms of energy efficacy will be made and discussed in the following section.

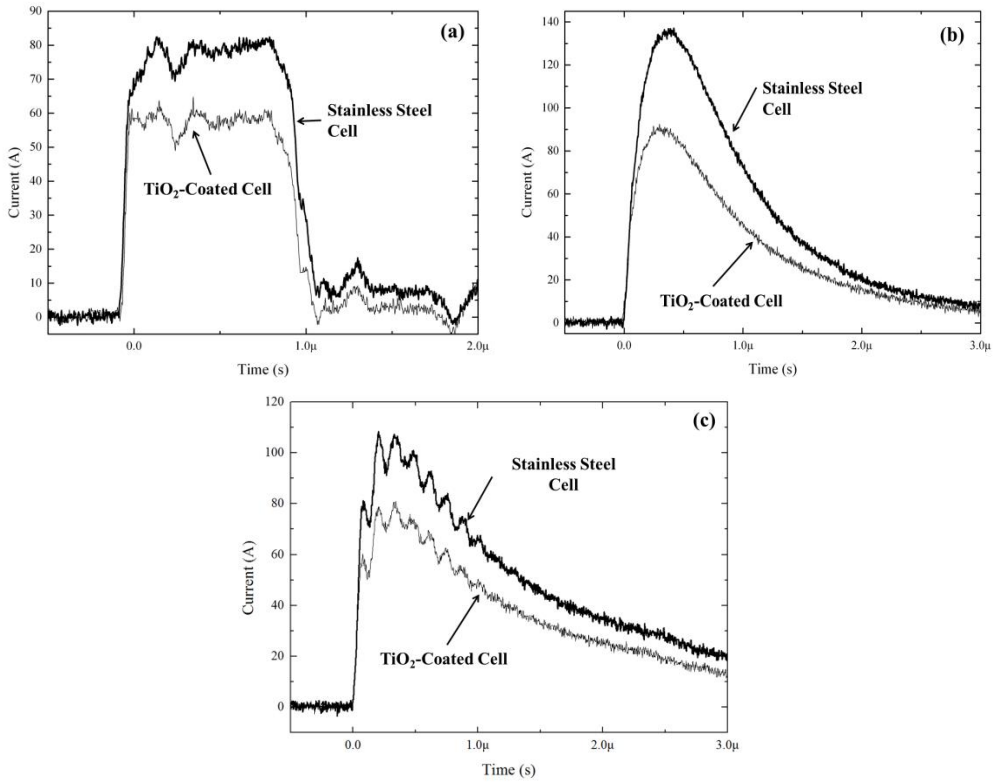


**Figure VII.39** Current waveforms obtained during PEF treatment using stainless steel test cell (dark line) and $TiO_2$-coated test cell (grey line): (a) square impulse; (b) smooth exponential impulse; (c) oscillating exponential impulse.

#### 7.3.5.3 Specific Energy Consumption

As discussed in the previous sections, it is necessary to evaluate the specific energy consumption during the PEF treatment and to compare energy consumption for impulses with three different waveshapes and different test cells used in the present study. As the current measurement indicated, continuous ionic conduction current existed in both stainless steel and $TiO_2$-coated test cells during PEF process. As a result, the specific energy consumption in both test cells was associated with two transient processes: the polarisation process which is manifested by the appearance of the displacement current, $E_{pol}$, and the ionic conduction process which results the Joule energy loss in the treated samples, $E_J$. It was demonstrated in Section 5.3.2.4 that, ~ 99.9% of the energy dissipated in the liquid suspension during PEF treatment was associated with the ionic conduction process.

In the PEF treatment experiments using the re-designed stainless steel and the new $TiO_2$-coated test cells, the direct measurement of current was taken, allowing the total energy consumption (combination of $E_{pol}$ and $E_J$ ) to be obtained using the following equation:

$$E_{total} = \int V(t) \cdot I(t) \cdot dt \qquad \text{(VII.1)}$$

where *V(t)* is the transient voltage across the test cell and *I(t)* is the transient current through the test cell. The total energy losses were calculated using the experimental voltage and current waveforms during PEF treatments and these losses are shown in the following tables.

**Table VII.1** Specific Energy Delivered per Pulse in PEF Treatment Using Stainless Steel Test cell.

| **Waveform** | **Field Strength (kV/cm)** | **Initial Population ($log_{10}$ CFU/ml)** | |
|---|---|---|---|
| | | **~ $10^4$** | **~ $10^7$** |
| Square | 67 | 0.527 J | 0.626 J |
| | 80 | 0.821 J | 0.945 J |
| Exponential | 67 | 0.400 J | 0.600 J |
| | 80 | 0.628 J | 0.832 J |
| Oscillating | 67 | 0.445 J | 0.514 J |
| | 80 | 0.598 J | 0.664 J |

**Table VII.2** Specific Energy Delivered per Pulse in PEF Treatment Using $TiO_2$-Coated Test cell.

| Waveform | Field Strength (kV/cm) | Initial Population ($log_{10}$ CFU/ml) | |
|---|---|---|---|
| | | ~ $10^4$ | ~ $10^7$ |
| Square | 67 | 0.327 J | 0.394 J |
| | 80 | 0.459 J | 0.641 J |
| Exponential | 67 | 0.299 J | 0.401 J |
| | 80 | 0.409 J | 0.544 J |
| Oscillating | 67 | 0.262 J | 0.352 J |
| | 80 | 0.387 J | 0.526 J |

As can be seen from Table VII.1 and Table VII.2, the energy losses are higher for impulses with higher electric field. The tables also demonstrated that the energy delivered by a single impulse increases with an increase in the initial population of the yeast sample. This was due to the difference between the conductivity of the *S. cerevisiae* suspension: the conductivity of the $10^7$ CFU/ml samples was ~ 182 μS/cm while the conductivity of the $10^4$ CFU/ml samples was ~ 124 μS/cm. As a result, the ionic conduction current was higher in the case of $10^7$ CFU/ml samples than that of the samples with initial population of $10^4$ CFU/ml. Therefore, the energy losses due to the conduction current were higher in the case of higher *S. cerevisiae* concentrations.

It should also be noticed that the largest amount of energy was delivered by a single square impulse, while the minimum amount of energy was delivered by a single oscillating exponential impulse. Comparison between Tables VII.1 and Table VII.2 also showed that specific energy consumption in the $TiO_2$-coated test cell was significantly lower than that in the stainless steel test cell. These calculations confirmed that the energy losses vary between different waveforms and test cells. Therefore, the inactivation results from PEF experiments should be re-presented in order to have a better understanding of the energy efficacy of the pulse waveshapes and the electrode materials.

#### 7.3.5.3.1 Correlation between Energy and Temperature

Assuming all energy delivered to the liquid suspension was converted into heat, Equation VII.2 can be used to establish the correlation between the energy consumption and the change in suspension temperature:

$$\Delta T = \frac{E_{total}}{c \cdot M} \quad \text{(VII.2)}$$

Where $\Delta T$ is the change in temperature in °C, $E_{total}$ is the energy absorbed by the liquid suspension, $c$ is the specific heat capacity of water and $M$ is the mass of the liquid suspension. As can be seen from Table VII.1-VII.2, the maximum calculated specific energy consumptions were 0.641 J per pulse and 0.945 J per pulse in the case of $TiO_2$-coated test cell and the stainless steel test cell respectively. According to the equation, the expected increase in temperature would be ~ 0.13°C and ~ 0.15°C after a single impulse in the $TiO_2$-coated and stainless steel test cells respectively. At this rate, temperature of the liquid suspension in the two test cells would be increased by ~ 13°C and ~ 15°C respectively after the application of 100 HV impulses, which was the largest number of impulse used in the present study.

However, as discussed in Section 7.3.2.1 and Section 7.3.3.1, the maximum increase in suspension temperature after PEF treatment was measured at ~ 0.5°C and ~ 1.5°C when using $TiO_2$-coated and stainless steel test cells respectively. Therefore, the temperature of the liquid suspension can potentially be cooled during the depressurisation process or even in between the application of each impulse. A heat transfer model developed in [257] was used to investigate this possibility. The results show that the ~ 0.13°C/0.15°C heat, which was induced by one impulse, would be dissipated into surrounding environment (the electrodes and air) within 1 second. Therefore, as the pulse repetition rate used in the present study was 1 pulse per second, the heat can hardly be accumulated between impulses. Therefore, it is reasonable that the maximum measured increase in temperature in the present study was only ~ 1.5°C.

However, as a comparison, few tens of °C increase in temperature has been reported in literatures [7, 67, and 241], which suggested much higher energy was delivered by a single impulse in those works. The insignificant of the heating effect observed in the present study is likely to be the effect of using the low-conductive liquid suspension and low-conductive $TiO_2$-coated electrodes.

#### 7.3.5.3.2 Comparison between Electric Field Magnitudes

Using the obtained experimental data on PEF inactivation and the specific energy per pulse, the surviving population of *S. cerevisiae* can be re-presented as a function of the specific energy delivered to the test cell during PEF treatment. Figure VII.40-VII.43 show the surviving population of *S. cerevisiae* for different electric field magnitudes. It should be noted that only the energy efficacy of the PEF treatment of $10^7$ CFU/ml yeast sample is shown in the following figures. As demonstrated from Section 7.3.2.2 to Section 7.3.3.4, the inactivation tendencies of samples with different concentrations were similar; therefore energy efficacies of PEF treatments of *S. cerevisiae* with other initial populations had similar tendencies and were not presented in the figures.

In order to provide a quantitative analysis of the inactivation tendencies in terms of energy efficacy, the inactivation data were fitted with analytical fitting curves, as shown in Figure VII.40-VII.43. However, as demonstrated in Section 7.3.3 and Section 7.3.4, the 'tailing' effect in the inactivation curves was obvious, which suggested that increase in the energy cannot result in further inactivation. Therefore, only experimental data prior to the start of 'tailing' effect were used for the fitting. A fitting procedure requires at least three data points, however in the case of PEF treatment using the $TiO_2$-coated test cell with square and smooth exponential impulses, 3-$\log_{10}$ reduction in *S. cerevisiae* population was achieved after 25 impulses, which means only 2 data points were available for the fitting. Therefore, no comparison between the field magnitudes was made in these two groups.

The fitting was done by *Origin Pro 9* software package. The fitting function was a two parameter exponential function, as shown in Equation VII.3.

$$y = A \cdot e^{-Bx} \tag{VII.3}$$

where $y$ represents the surviving population in $\log_{10}$ CFU/ml, and $x$ represents the specific energy consumption in kJ/liter. Two coefficients can be obtained by this fitting process. Coefficient $A$ relates to the initial population of microorganism. Coefficient $B$ describes the kinetic process of inactivation (liter/kJ). Larger value of $B$ indicates better energy efficacy of the PEF process. The obtained values of coefficient $B$ are listed in Table VII.3.

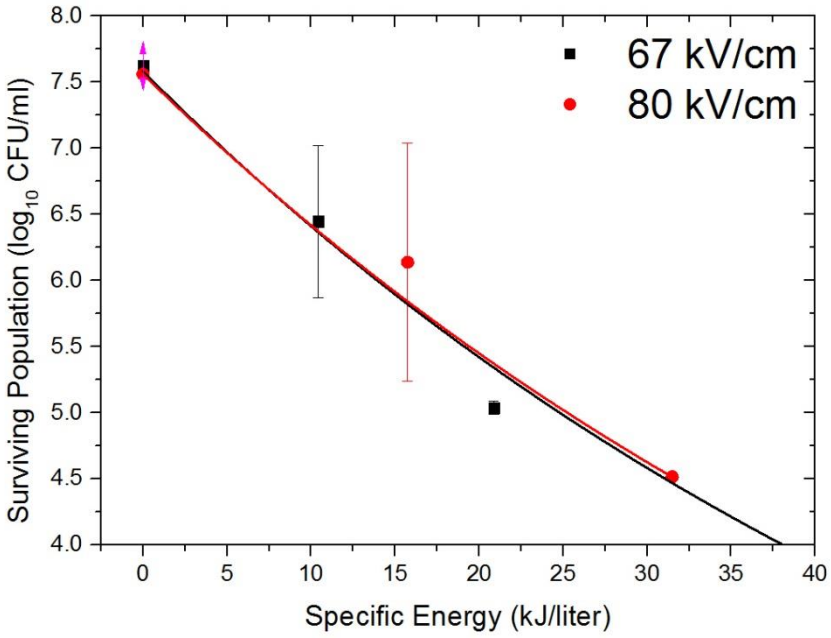


**Figure VII.40** Energy efficacy of PEF treatment (stainless steel test cell, square impulse) using field magnitude of 67 kV/cm (black) and 80 kV/cm (red). Initial population of *S. cerevisiae* was $10^7$ CFU/ml. Error bars show standard deviation (n=3).

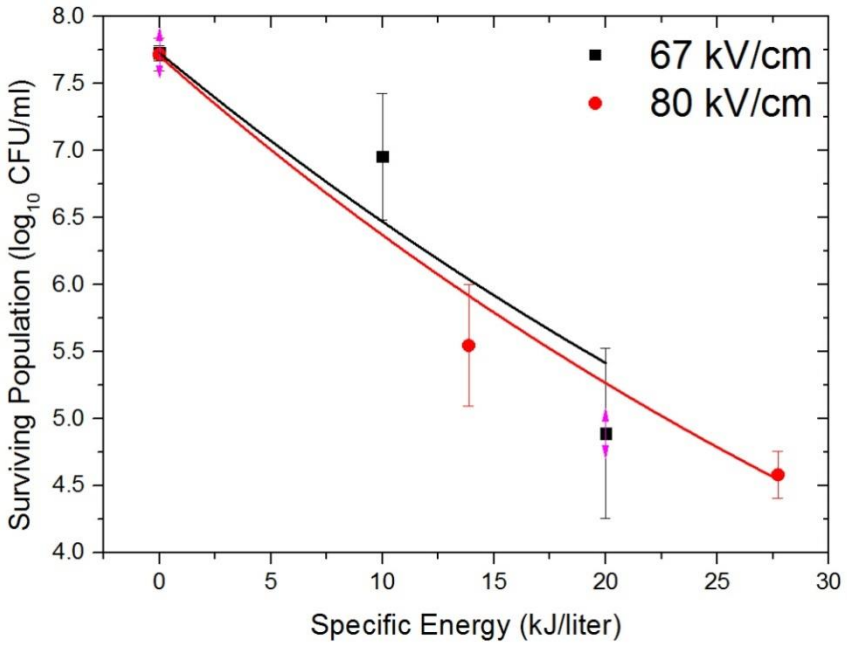


**Figure VII.41** Energy efficacy of PEF treatment (stainless steel test cell, smooth exponential impulse) using field magnitude of 67 kV/cm (black) and 80 kV/cm (red). Initial population of *S. cerevisiae* was $10^7$ CFU/ml. Error bars show standard deviation (n=3).

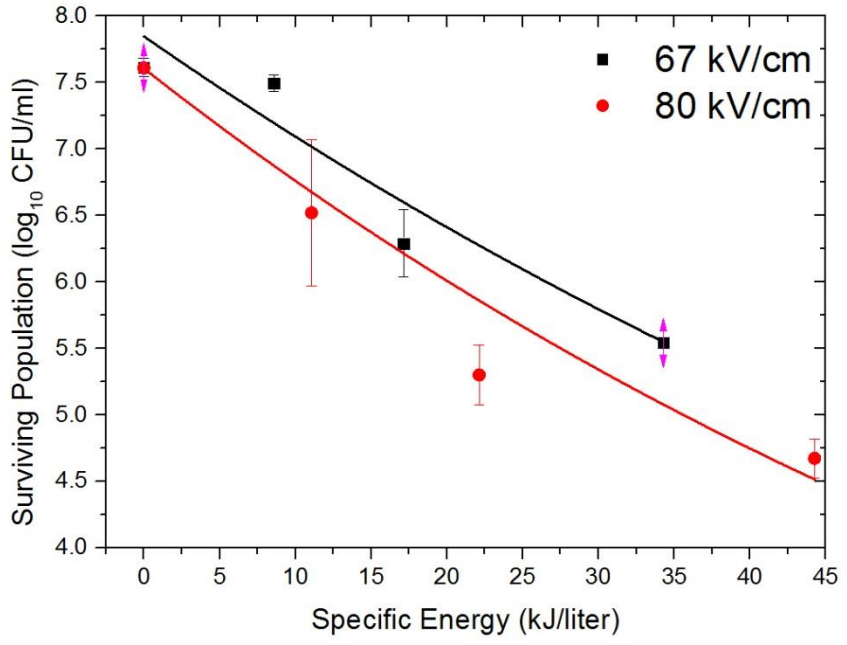


**Figure VII.42** Energy efficacy of PEF treatment (stainless steel test cell, oscillating exponential impulse) using field magnitude of 67 kV/cm (black) and 80 kV/cm (red). Initial population of *S. cerevisiae* was $10^7$ CFU/ml. Error bars show standard deviation (n=3).

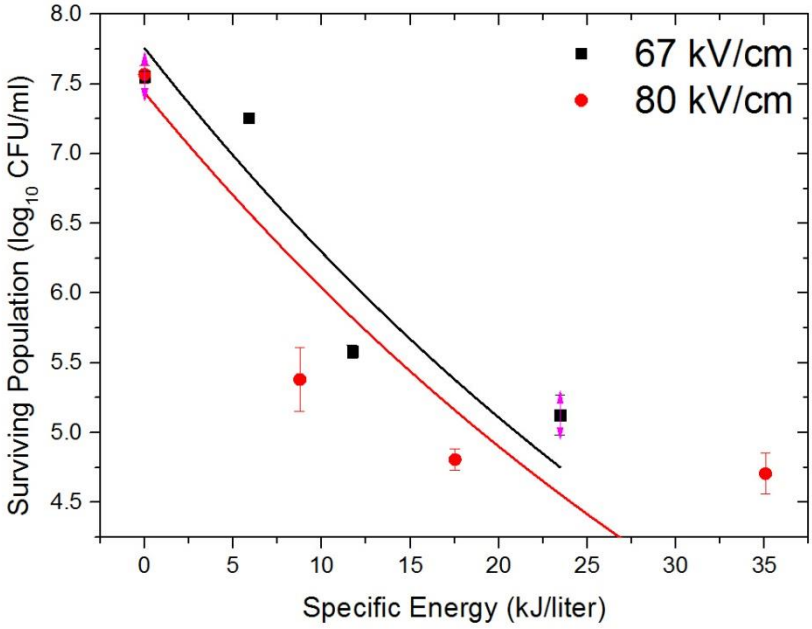


**Figure VII.43** Energy efficacy of PEF treatment ($TiO_2$-coated test cell, oscillating exponential impulse) using field magnitude of 67 kV/cm (black) and 80 kV/cm (red). Initial population of *S. cerevisiae* was $10^7$ CFU/ml. Error bars show standard deviation (n=3).

**Table VII.3** Obtained Value of Coefficient *B* in the Fitting.

| **Test Cell** | | **Stainless Steel Test Cell** | | | **$TiO_2$-coated Test Cell** | | |
|---|---|---|---|---|---|---|---|
| **Impulse Waveshape** | | Square | Smooth Exponential | Oscillating Exponential | Square | Smooth Exponential | Oscillating Exponential |
| **Field Magnitude (kV/cm)** | **67** | **0.017** (0.014-0.020) | **0.018** (0.012-0.024) | **0.010** (0.008-0.012) | N/A | N/A | **0.021** (0.013-0.029) |
| | **80** | **0.016** (0.016-0.016) | **0.019** (0.017-0.021) | **0.011** (0.009-0.013) | N/A | N/A | **0.021** (0.015-0.027) |

Note: Values in the brackets indicate the range of value of coefficient *B* with 95% confidence based on the standard error from the fitting and Student coefficient table.

It can be seen from all the figures that PEF inactivation tendencies are very similar when using both field magnitudes of 67 kV/cm and 80 kV/cm: the surviving population of *S. cerevisiae* sample reduced gradually as the specific energy delivered to the sample increased. It can also be learned from Table VII.3 that field magnitude had minimal impact on the energy efficacy of the PEF process. The value of coefficient *B*, which describes the inactivation kinetic, showed little variation (maximum ~ 9%) between the two levels of field magnitude. Therefore, it can be

concluded that the magnitude of field strength did not have significant impact of on the energy efficacy of the PEF treatments at the field level being investigated (67 kV/cm and 80 kV/cm).

#### 7.3.5.3.3 Comparison between Pulse Waveshapes

The same fitting procedure was applied to compare the effect of the pulse waveshape on the energy efficacy of PEF treatment. As demonstrated in Section 7.3.5.3.2, the magnitude of field strength had minimal impact on the energy efficacy. Therefore, PEF treatment data for different field strengths (but for the same pulse waveshape and the same test cell) were combined for the following analysis. By doing so, the analytical fitting procedure and analysis can now be conducted for the results of the PEF treatment in the $TiO_2$-coated test cell as the number of data points for each inactivation curve was at least three.

Figure VII.44-VII.45 show the surviving population of the *S. cerevisiae* as a function of the specific energy delivered to the test cell using impulses with different waveshapes. Figure VII.44 shows the inactivation kinetic obtained when the *S. cerevisiae* suspension was treated in the stainless steel test cell, while Figure VII.45 shows the inactivation kinetic when the PEF treatment was conducted using the $TiO_2$-coated test cell. The obtained values of coefficient *B* for the analytical fitting are listed in Table VII.4.

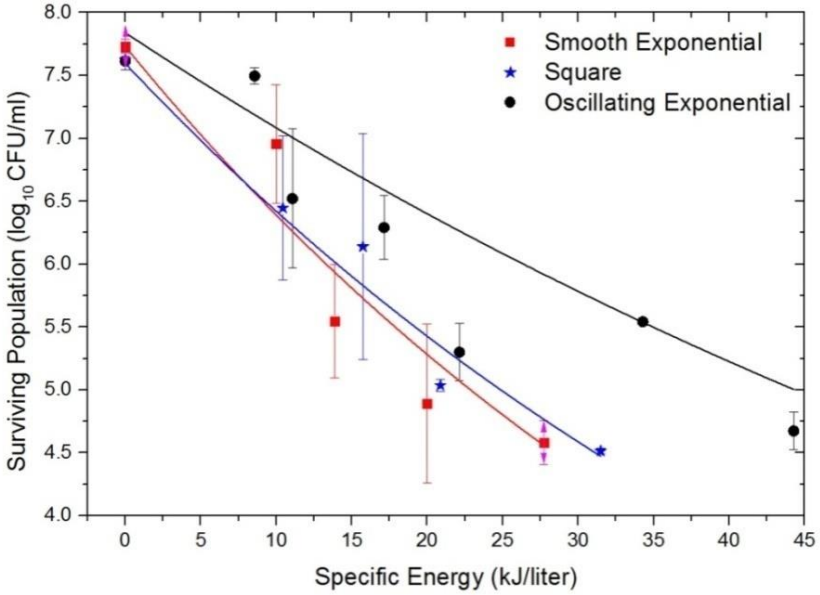


**Figure VII.44** Energy efficacy of PEF treatment (stainless steel cell) using smooth exponential (red), square (blue) and Oscillating exponential (black) impulses. Initial population of *S. cerevisiae* was $10^7$ CFU/ml. Error bars show standard deviation (n=3).

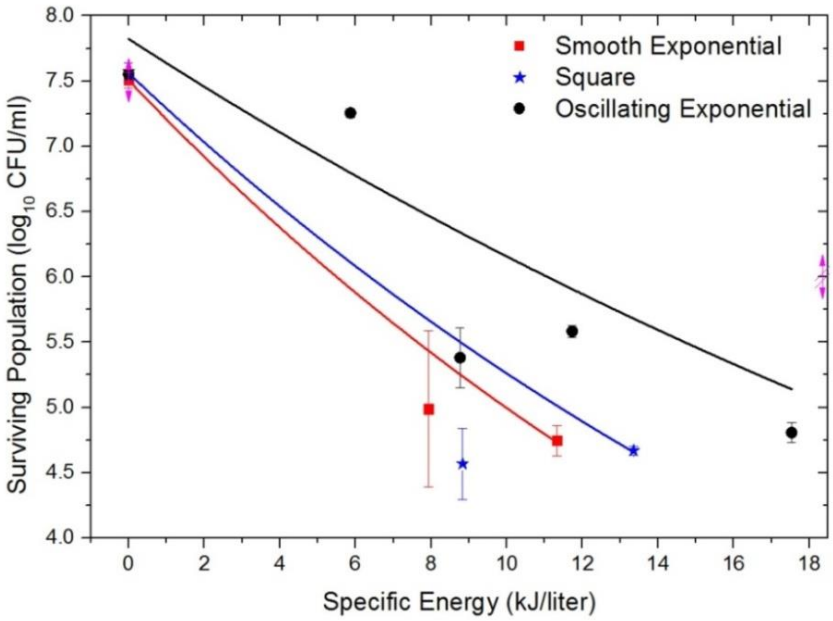


**Figure VII.45** Energy efficacy of PEF treatment ($TiO_2$-coated cell) using smooth exponential (red), square (blue) and Oscillating exponential (black) impulses. Initial population of *S. cerevisiae* was $10^7$ CFU/ml. Error bars show standard deviation (n=3).

**Table VII.4** Obtained Value of Coefficient *B* in the Fitting.

| Impulse Waveshape | | Square | Smooth Exponential | Oscillating Exponential |
|---|---|---|---|---|
| **Test Cell** | Stainless Steel | **0.017** (0.016-0.018) | **0.019** (0.017-0.021) | **0.010** (0.008-0.012) |
| | $TiO_2$-coated | **0.036** (0.030-0.042) | **0.041** (0.037-0.045) | **0.023** (0.017-0.029) |

Note: Values in the brackets indicate the range of value of coefficient *B* with 95% confidence based on the standard error from the fitting and Student coefficient table.

It can be seen from the two figures that all three types of waveforms provided similar PEF inactivation tendencies in the experiments in which both stainless steel and $TiO_2$-coated cells were used. In all cases, the surviving population of *S. cerevisiae* reduced gradually as the specific energy delivered to the sample increased. However, as shown in Table VII.4, the pulse waveshape had a significant impact on the energy efficacy of the PEF process, as the coefficient *B* describing the inactivation kinetic varied among the pulse waveshape being investigated. As shown in Table VII.4, impulses with smooth exponential waveshape demonstrated the best energy efficacy: their value of coefficient *B* was ~ 13% greater than square impulses and ~ 84% greater than the oscillating exponential impulses. On the other hand, oscillating exponential impulse showed the worst energy efficacy: their value of coefficient *B* was ~ 84% lower than the smooth exponential impulse and ~ 63% lower than the square impulse. Using the obtained values of coefficient *B*, the $\log_{10}$ reduction in *S. cerevisiae* population can be estimated for a fixed amount energy input in the PEF system described in the present study. For example, the expected $\log_{10}$ reduction in *S. cerevisiae* population for an energy input of 10 kJ/liter is listed in Table VII.5. As can be seen from the table, more $\log_{10}$ reduction in *S. cerevisiae* population is expected when the *S. cerevisiae* suspension is subjected to PEF impulses with smooth exponential waveform as compared with PEF impulses with the other two waveforms.

**Table VII.5** Estimated $\log_{10}$ reduction in *S. cerevisiae* population for an energy input of 10 kJ/liter.

| Impulse Waveshape | | Square | Smooth Exponential | Oscillating Exponential |
|---|---|---|---|---|
| **Test Cell** | Stainless Steel | 1.1 | 1.2 | 0.7 |
| | $TiO_2$-coated | 2.1 | 2.4 | 1.4 |

As mentioned in Section 2.5.4.2, limited results have been reported in the literature on the comparison of the PEF performance using impulses with different waveshapes except for the study conducted in [7, 8]. It was reported in [7] that impulses with square waveshape were more energy efficient than exponentially decaying impulses, which is opposite to the findings of the present study. However, the field strength used in [7] for the PEF treatment was only 12 kV/cm, which is just above the 10 kV/cm critical level which is required, as discussed in Section 2.5.4.1, for the effective irreversible electroporation process to take place. For the waveshapes reported in [7], the field strength was above 10 kV/cm for only ~20 μs in the case of a single exponential impulse, while in the case of a single square impulse the field strength was above 10 kV/cm for ~50 μs. This suggested the long decaying tail of the exponential impulse could be ineffectual for inducing lethal electroporation. Therefore, the square impulses were more energy efficient than the exponential decaying impulses in the case of [7]. However, in the present study, the field strength used was much higher than the 10 kV/cm critical field strength. This suggested that the long decaying tail of the smooth exponential impulse could still induce lethal electroporation using this relatively high field strength. The duration of parts of the smooth exponential and square impulses which exceeded 10 kV/cm were 2.5 μs and 1 μs respectively. Therefore, it was found that the smooth exponential impulse was more energy efficient in the present study. Based on this analysis, a correlation between the effective impulse duration (period where the field strength is above the critical field strength) and the PEF performance can be established according to the results reported in [7] and the present study. Thus, the difference in time during which the field exceeded the critical value may explain the advantage of one impulse

over the other impulse. The pulse waveshape with the longer effective duration results in a better PEF performance in terms of energy efficacy.

In the case of the oscillating exponential impulse, despite having a similar effective duration to the smooth exponential impulse, energy efficacy of this fast oscillating impulse was the worst as compared to the other impulses. This can be explained by the lower average peak fields and deep oscillations at the peak of the waveform. The average peak field strengths of the oscillating exponential impulse are 47 kV/cm and 59 kV/cm for the two levels of charging voltage respectively, as shown in Figure VII.32. Both values were below the 60 kV/cm threshold identified in [164], above which the HV impulses demonstrated noticeably better PEF performance. On the other hand, the oscillating exponential impulse had deep oscillations at its peak, duration of the 1/4 period of these oscillations was ~ 30 ns. According to the transient membrane charging model described in Section 3.1 and Section 3.2, time required to achieve the maximum potential across microbial membrane is ~ 1 μs and during the 30 ns period the field across the membrane can reach only ~ 10% of its potential maximum value. This result was in line with the experimental result reported in [7], where an oscillatory impulse was also used for PEF treatment and demonstrated least efficient.

Based on the discussions above it can be stated that, in order to achieve high energy efficacy in the PEF inactivation process, it is desirable to increase duration of exposure to the critical field and to avoid field oscillation. However, it is not clear which of these two factors play a dominant role and further investigation is required to clarify their contribution to pulsed electric field inactivation.

#### 7.3.5.3.4 Comparison between Test Cells

It can also be seen from Table VII.4 and Table VII.5 that there was a significant difference in the energy efficacy for the PEF process in the two test cells. Therefore, it is important to present the direct comparison between the inactivation kinetic in the stainless steel and $TiO_2$-coated test cells. Figure VII.46-VII.48 show the inactivation

kinetic obtained using the square, smooth exponential and oscillating exponential impulses respectively.

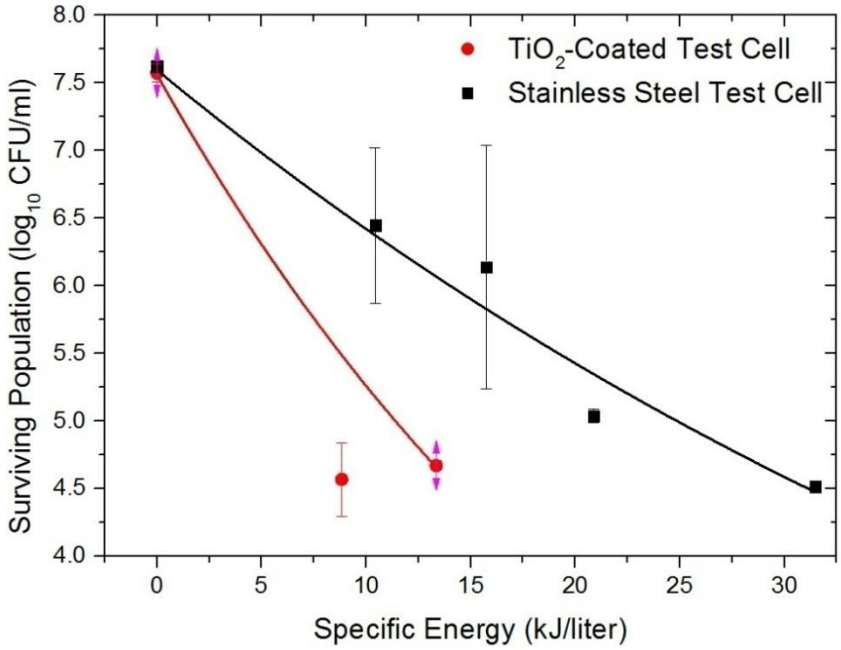


**Figure VII.46** Energy efficacy of PEF treatment (square impulse) using $TiO_2$-coated cell (red) and stainless steel cell (black). Initial population of *S. cerevisiae* was $10^7$ CFU/ml. Error bars show standard deviation (n=3).

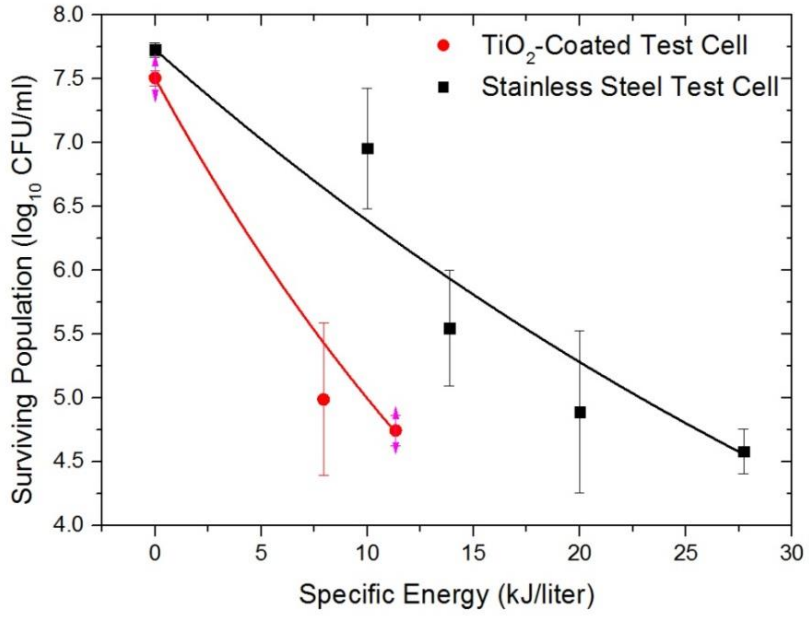


**Figure VII.47** Energy efficacy of PEF treatment (smooth exponential impulse) using $TiO_2$-coated cell (red) and stainless steel cell (black). Initial population of *S. cerevisiae* was $10^7$ CFU/ml. Error bars show standard deviation (n=3).

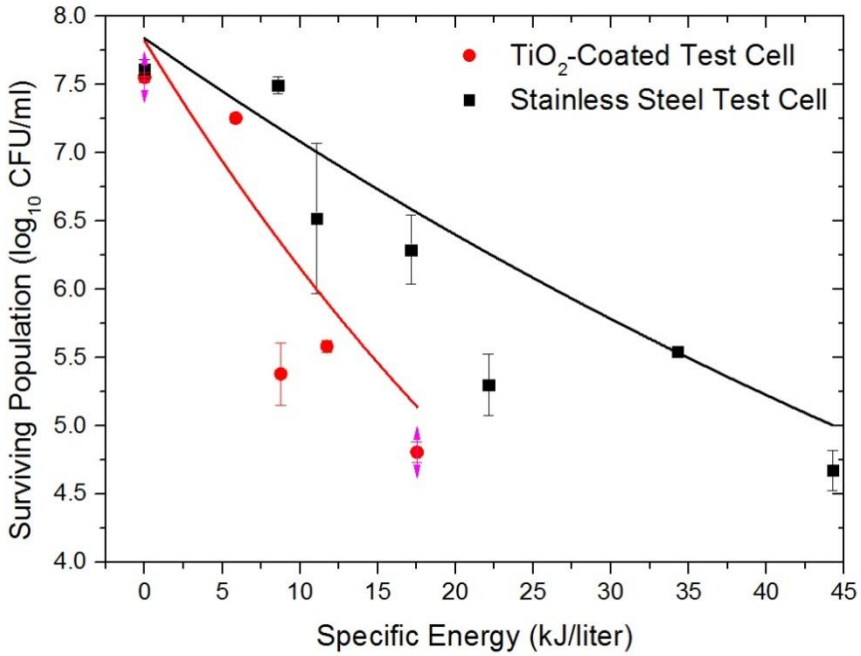


**Figure VII.48** Energy efficacy of PEF treatment (oscillating exponential impulse) using $TiO_2$-coated cell (red) and stainless steel cell (black). Initial population of *S. cerevisiae* was $10^7$ CFU/ml. Error bars show standard deviation (n=3).

It can be concluded from these figures that the energy efficacies of the PEF treatment using the stainless steel and $TiO_2$-coated test cells were significantly different: the specific energy losses in the $TiO_2$-coated test cell which were associated with the same $\log_{10}$ reduction in the *S. cerevisiae* population were significantly lower as compared with the stainless steel test cell. The analysis of the inactivation kinetic confirmed this tendency, as shown in Table VII.4. In the case of square, smooth exponential and oscillating exponential impulses, the values of coefficient *B* of the PEF process in the $TiO_2$-coated test cell were 112%, 116% and 130% greater respectively as compared with the PEF process in the stainless steel test cell. It can also be seen from Table VII.5 that more $\log_{10}$ reduction in *S. cerevisiae* population was expected by the PEF treatment in the $TiO_2$-coated test cell.

The main reason for the reduction in specific energy consumption was the lower ionic conduction current though the *S. cerevisiae* suspension in the test cell with $TiO_2$-coated electrodes, as ionic conduction current results in Joule heating and accounts for the majority of specific energy consumption. Therefore, the obtained

results showed that using the low-conductive test cell can result in similar inactivation performance and improve the energy efficacy of the PEF process significantly.

The result also confirmed the main mechanism of PEF inactivation is the non-thermal process, which is the irreversible electroporation involves electro-mechanical disruption of the microbial membrane. The presence of ionic conduction through the liquid suspension during the PEF process had a minimum impact in terms of inactivation performance, but worsened the energy efficacy of the PEF process. Potentially further reduction in the specific energy consumption could be achieved if completely non-conductive electrodes are used. However, as demonstrated in Section 6.1.1, this non-conductive design of the PEF test cell will be accompanied by the Maxwell-Wagner field relaxation process. To compensate for this Maxwell-Wagner reduction in field, either the field strength or the Maxwell-Wagner relaxation time constant should be increased. Such PEF process was implemented in [176], where inactivation of *E. coli* was successfully achieved by using a high field magnitude (up to 200 kV/cm). A similar approach was used in the present study however inactivation of microorganisms was not achieved in the ceramic test cell with field strength up to 80 kV/cm.

#### 7.3.5.4 Tailing Effect

In the PEF experiments using the new test cells, the 'tailing' effect in the inactivation curves was observed despite the removal of the potential dead zones identified in the original test cell design. The results for all experiments conducted during the present study showed that the inactivation curves for the *S. cerevisiae* samples with an initial population of $10^7$ CFU/ml would eventually saturated at ~ $10^4$ CFU/ml. However, fresh *S. cerevisiae* samples with an initial population of $10^4$ CFU/ml can also be reduced to ~ $10^1$ CFU/ml using the same experiment parameters.

During the PEF experiments, it was observed that there was significant sedimentation of the *S. cerevisiae* cells during the time (~20 minutes) associated with pressurising/depressurising of the test chamber and applying PEF impulses.

Therefore, an additional test was designed to investigate the effect of the sample sedimentation. In this test, *S. cerevisiae* suspension was first subjected to 100 HV impulses before a mixing procedure was introduced. The sample inside the test cell would be re-mixed to a homogeneous state after the first 100 HV impulses in order to minimise the sedimentation, and the re-mixed suspension was then subjected to another 100 HV impulses. The surviving population of this re-mixed sample was compared with the surviving population of the sample which was subjected to 200 HV impulses without re-mixing procedure. This PEF test was conducted in both stainless steel and $TiO_2$-coated test cells and the results are shown in Figure VII.49 and Figure VII.50 respectively. It can be seen from both figures that further reduction in the surviving *S. cerevisiae* population was achieved by introducing the re-mixing process. This result suggested that the sedimentation of the microorganism cells could be the cause of the 'tailing' effect and the re-mixing procedure could be used to eliminate the 'tailing' effect.

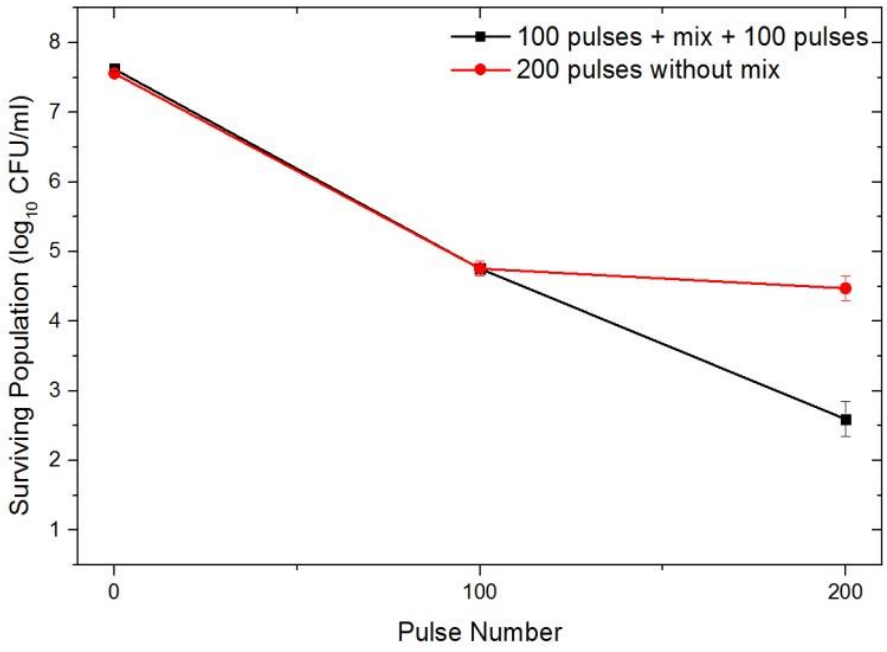


**Figure VII.49** Comparison of the PEF performance between treatments in the stainless steel test cell with and without sample mixing after 100 pulses. Black line represents the PEF treatment with mix process; Red line represents PEF treatment without mix process. Error bars show standard deviation (n=3).

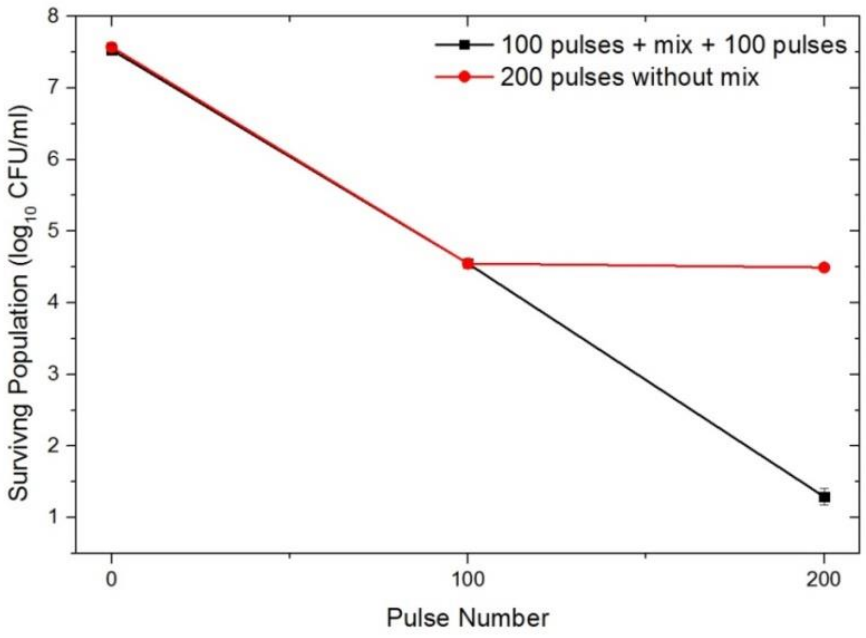


**Figure VII.50** Comparison of the PEF performance between treatments in the $TiO_2$-coated cell with and without sample mixing after 100 pulses. Black line represents the PEF treatment with mix process; Red line represents PEF treatment without mix process. Error bars show standard deviation (n=3).

The 'tailing' effect was also observed in [7-8, 258] and an attempt to investigate the cause of this undesirable phenomenon was made in [258]. It was suggested in [258] that the cell clumps and inherent resistance to PEF treatment of sub-population of cells could be the cause of the 'tailing' effect. However, the experimental results strongly suggested that the occurrence of the 'tailing' effect was not the consequence of neither factors. In the present study, there are other potential reasons for the presence of the 'tailing' effect apart from cell sedimentation. Firstly, there could be low field areas (dead zones) in the PEF test cells. Secondly, the *S. cerevisiae* samples were incubated overnight for reproduction prior to the PEF treatment, which suggested that the sample suspension consisted of *S. cerevisiae* cells with different ages. As discussed in Section 2.5.4.4, microorganisms with different growing phases have different susceptibility to the PEF process. Therefore, it could be possible that sub-population of the *S. cerevisiae* samples was less-susceptible to the PEF process and the cells in this sub-population were dying at a slower rate. The introduction of the mixing procedure not only minimised the sedimentation effect but also changed

the location of *S. cerevisiae* cells in the test cell and unified the distribution of the cells with different ages. Therefore, the effect of those two potential causes of the 'tailing' effect were also minimised by the mixing procedure.

In [7-8, 258] and the present study where 'tailing' effect was observed, batch PEF treatment process was used, during which the liquid suspension was stationary without the mixing procedure. However, in several other studies where continuous PEF treatments were employed and the microorganism samples were mixed continuously, the 'tailing' effect was less pronounced [182-183, 232, 259]. It was also reported in [232] that continuous flowing chamber was more effective in microorganism inactivation than the static systems. The results from these reports were in line with the finding from the additional test conducted in the present study.

These findings suggested that measures which unify the distribution of microorganism samples during the PEF treatment, either by using continuous flow PEF system or by applying a mixing procedure, can be used to eliminate the 'tailing' effect and to improve PEF performance. However, the exact causes of the 'tailing' effect in the inactivation process require further investigation.

## 7.4 Discussion

In this chapter, the results of investigation into PEF treatment of *A. platensis* and *S. cerevisiae* in the re-designed stainless steel and the low-conductive $TiO_2$-coated test cells were presented and discussed. It was found that both test cells can be used for successful PEF inactivation of *A. platensis* and *S. cerevisiae* in liquid suspension.

It was established that the *A. platensis* were inactivated by application of 50 square impulses with magnitude of 67 kV/cm and 80 kV/cm in both test cells. Although the *A. platensis* was successfully inactivated by the PEF impulses, the visual inspection (under optical microscope with ×400 magnification) of the individual *A. platensis* cells revealed that no visible external structural damage, such as visually detected cell rupture or lysis, has been introduced by the HV impulses. This finding suggested that PEF impulses only induced internal damage and dysfunction to the

microorganism cells. Significant degree of rupture of the *A. platensis* cells (which would be noted under optical microscope) could not be achieved by PEF treatment only.

It was established that, the population of *S. cerevisiae* was reduced by 3-$\log_{10}$ after application of 100 HV impulses regardless of test cell, field magnitude, initial *S. cerevisiae* population and pulse waveshapes. Moreover, in most cases, this 3-$\log_{10}$ reduction in the *S. cerevisiae* population was achieved after application of 50 HV impulses. However, further increase in the number of impulses did not lead to additional reduction in surviving population of the *S. cerevisiae*. Thus, it was shown that the 'tailing' effect of the inactivation curve was also observed during PEF treatment in the re-designed test cells. However, comparison of the PEF performance of the original and re-designed stainless steel cells demonstrated that improvement in the PEF performance has been achieved in the re-designed cell: when subjected to 50 HV square impulses with field magnitude of 67 kV/cm, the population of the *S. cerevisiae* was reduced by 1-$\log_{10}$ in the original test cell while 2-$\log_{10}$ reduction was observed in the re-designed stainless steel test cell. Therefore, some of the potential low field zones which were presented in the original test cell design have been eliminated in the re-designed test cell.

Specific energy consumption of the PEF treatment of *S. cerevisiae* has been obtained. The PEF performance in terms of energy efficacy using different field magnitudes, pulse waveshapes and test cells has also been analysed and discussed in this chapter. It was established that the field magnitude has minimal impact on the energy efficacy of the PEF process: the difference in the values of coefficient *B*, which reflects the inactivation kinetic, was less than ~ 9% using the two field magnitudes (67 kV/cm and 80 kV/cm). It was also established that HV impulses with smooth exponential waveshape demonstrated the best energy efficacy: the value of coefficient *B* was ~ 13% greater than square impulses and was ~ 84% greater than the oscillating exponential impulses. HV impulses with oscillating exponential waveshape showed the worst energy efficacy: the value of coefficient *B* was ~ 84% lower than the smooth exponential impulses and ~ 63% lower than the square impulses. Based on this result obtained in the present study and limited literature data, important

conclusions can be made. In order to achieve high efficacy in the PEF inactivation process, it is desirable to increase duration of exposure of microorganisms to the critical field and to avoid fast field oscillations. However, it is not clear which of these two factors play a dominant role in determination of PEF efficiency and further investigation is required to clarify their contribution to pulsed electric field inactivation.

It was established that significant improvement in energy efficacy can be achieved by using the low-conductive $TiO_2$-coated test cell: the values of coefficient *B* of the PEF process using $TiO_2$-coated test cell were 112%, 116% and 130% greater when using the square, smooth exponential and oscillating exponential impulses respectively as compared with the same waveforms in the stainless steel test cell. The main reason for this reduction in energy consumption was the lower ionic conduction current though the *S. cerevisiae* suspension in the test cell with $TiO_2$-coated electrodes. The result also suggested the main inactivation mechanism of the PEF process was the non-thermal irreversible electroporation, which involves electro-mechanical disruption of the microbial membrane. The ionic conduction process had insignificant impact in terms of inactivation performance, but impaired the energy efficacy of the PEF process significantly. Therefore, potentially further reduction in the specific energy consumption could be achieved if completely non-conductive electrodes will be used.

The cause of the 'tailing' effect in the inactivation curve was also discussed in this chapter. It was found that the sedimentation of *S. cerevisiae* cells during the PEF treatment could potentially be one of the reasons for this 'tailing' effect. Therefore, the measures which unify the distribution of microorganisms during the PEF treatment can be used to improve PEF performance: for example, through application of a mixing procedure as demonstrated in the present study or by using continuous flow PEF system as reported in several studies. The 'shoulder' effect also appeared on the several inactivation curves of the *S. cerevisiae* samples, especially with initial population of $10^4$~$10^6$ CFU/ml. The potential reason for this 'shoulder' effect is that the microorganisms are adjusting to the external stress and sub-population of the microorganisms remain viable despite damage has been done. Further investigation

of the ‘shoulder’ effect using lower electric field strength or lower number of pulses could be beneficial for better understanding of the mechanisms of microbial cell adjustment to external stresses.

The obtained results from temperature measurements before and after the PEF experiments indicated that the heating effect was not significant. It was shown that the maximum increase in temperature recorded during the experiments in both test cells (stainless steel and $TiO_2$-coated) was ~ 1.5 °C. A correlation between the delivered specific energy and the increase in suspension temperature was established in this chapter. It was shown that the suspension temperature should be increase by a maximum of 15 °C (in the case of application of 100 square impulses in the stainless steel test cell) after the PEF treatment. However, it was also demonstrated that the 0.15 °C of heat, which is generated by the energy dissipated into the liquid suspension after each impulse, will dissipate into surrounding environment in the time interval between impulses (1 s). This fast dissipation of heat can be the reason for the insignificant increase in suspension temperature in the present study. Nevertheless, the thermal effect induced by the PEF process in the present study is significantly smaller as compared to other PEF studies reported in literature, in which few tens of °C increase in temperature was observed. It suggests that significantly less energy is delivered by the HV impulse in the present study. The heating of liquid suspension and specific energy consumption are limited by the low conductivity of the liquid suspension, which significantly reduced the ionic conduction through the suspension during PEF treatment. The use of low-conductive $TiO_2$-coated electrodes results in even lower increase in suspension temperature. This founding also suggests that PEF treatment in completely non-conductive test cell will be beneficial as thermal effects will be reduced significantly in such scenario.

# Chapter VIII

# CONCLUSIONS AND FUTURE WORKS

## 8.0 General Conclusions

In the present study the PEF treatment of two species of microorganisms, *A. platensis* and *S. cerevisiae* has been conducted and investigated. The objectives of the present study were made clear through the comprehensive literature review in ***Chapter II***, in which the gaps in the current knowledge in the field of the PEF treatment of microorganisms were identified. These objectives have been achieved in the course of this project, which provided valuable information in the field of PEF treatment of microorganisms. The main goals achieved in the course of the present study are highlighted below and will be discussed in detail in the following sections.

- The lumped element circuit models of the PEF process have been developed, which included the pulse generating system, PEF test cell and the microbial cell.

- Novel non-conductive ceramic PEF test cell has been designed and developed. Investigation of the PEF process in this ceramic test cell has been conducted.

- Novel low-conductive $TiO_2$-coated PEF test cell has been designed and constructed. PEF inactivation performance in this $TiO_2$-coated test cell has been studied.

- Investigation of the effect of the pulse waveshapes (squre, smooth exponential and oscillating exponential) on the inactivation performance and energy efficacy during the PEF treatment has been conducted.

- The effect of the electrical conductivity of the suspension on the energy consumption has been investigated.

- The potential cause of the tailing effect in the inactivation curves obtained during the PEF experiment has been investigated and the recommendations for minimising this undesirable effect have been made.

- Investigation of PEF inactivation and lysis of *A. platensis* has been conducted.

## 8.1 Equivalent Circuit Models of PEF Process

The equivalent lumped element circuit models of the PEF process, which include the pulse generators, PEF test cells and the microbial cell, were developed over the course of the present study. The development of equivalent circuit models of three pulse generating systems, which generate square, smooth exponential and oscillating exponential impulses, were presented in ***Chapter IV*** and ***Chapter VI***. Simulations conducted in the *OrCAD® PSpice* environment using the developed models showed a good agreement with the practical waveforms produced by the pulse generating systems.

The equivalent circuit models of the PEF test cells designed in the present study were also developed, as described in ***Chapter IV*** and ***Chapter VI***. These models were used to evaluate the equivalent impedance of the PEF test cells, which provides valuable information for the design of the PEF system. The model describing the ceramic test cell was used to analyse the transient electric field in the treatment region in the ceramic test cell, which is in good agreement with the analytical model developed in [4].

A 2-dimentional equivalent model of the microbial cell was also developed, as described in ***Chapter III***. The response of this model cell to an external electric field was simulated using the *OrCAD® PSpice* software in order to investigate the effect of cell wall on the development of trans-membrane potential. The obtained results show that the presence of cell wall has minimal effect on the dynamic of the induced voltage across the membrane. The unique electrical characteristics of the cell wall, which act as an ions exchanger, make its electrical properties very similar to that of

the surrounding suspension. As a result, from the electrical point of view, the cell wall is effectively an extended layer of the surrounding suspension.

Apart from the lumped element circuit models, an analytical model developed in [4] was also introduced and analysed in ***Chapter III*** and ***Chapter VI***. This model allowed estimation of field relaxation time and the transient behaviour of the field across the membrane in a non-conductive ceramic PEF test cell. In ***Chapter III***, the effects of different microbial cell properties and suspension properties on the transient development of the field across the membrane were investigated based on this model. The obtained results indicated that the size of the microbial cell and the electrical conductivity of the liquid suspension are two main factors which affect the transient process. The effects of these parameters are useful for optimisation of the PEF process. For example, liquid suspension with conductivity in the range of $10^{-3}$-$10^{-2}$ S/m was recommended to be used in the practical PEF studies for the optimal development of trans-membrane potential.

## 8.2 Non-Conductive Ceramic and Low-Conductive $TiO_2$-Coated Test Cells

A novel non-conductive ceramic PEF test cell was designed and constructed, as presented in ***Chapter IV.*** This ceramic PEF test cell implements the novel concept proposed in [6]. In ***Chapter V,*** PEF treatment of *A. platensis* and *S. cerevisiae* was conducted using this ceramic test cell. The results obtained from these experiments confirm that the effective PEF inactivation of microorganisms was not achieved in the developed ceramic test cell using PEF impulses with the field magnitudes of 33 kV/cm and 67 kV/cm.

The reason for the ineffective PEF performance in the developed ceramic test cell were analysed in ***Chapter VI***. It was established that the main reason is the field relaxation due to the Maxwell-Wagner field relaxation process in the liquid suspension between the two ceramic electrodes. According to the analytical model of transient trans-membrane potential developed in ***Chapter III***, the actual electric field

in the treatment region and the induced potential across the microbial membrane are much smaller, which is only ~10% as compared with the case of stainless steel test cell. In addition, the field and the induced trans-membrane potential last only ~ 13% of the total pulse duration across the electrode before collapsing.

These analytical results and further experiment suggest that the electric field with much higher magnitude (> 80 kV/cm) is required to achieve successful PEF treatment using the developed ceramic test cell, as demonstrated in [189] where successful inactivation of *E. coli* was achieved in a similar ceramic PEF test cell using the field magnitude of at least 130 kV/cm. The other approach to achieve effective PEF inactivation at a relatively low field magnitude in the non-conductive test cell is to select dielectric material with much longer Maxwell-Wagner characteristic time. This can be achieved either by using dielectric material with a significantly high permittivity or by using dielectric layer with significantly small thickness.

The latter approach was implemented in the present study and a PEF test cell with $TiO_2$-coated electrodes was designed and constructed, as presented in ***Chapter VI***. The electrodes of this test cell were made of copper plates coated with a 2 μm-thick $TiO_2$ film. The test cell was designed in such a way that the Maxwell-Wagner characteristic time of this test cell would be significantly longer (~ 1 μs) as compared with the ceramic test cell (~ 0.1 μs), which allows the trans-membrane potential to develop to the same level as in the case of the stainless steel test cell. However, the non-zero conductivity of the $TiO_2$ film was observed when these electrodes were in contact with liquid suspension, which allows the conduction current to flow during the PEF process. Although the $TiO_2$-coated test cell was not completely non-conductive, the magnitude of the ionic conduction current was reduced by ~ 30% as compared with the conductive stainless steel test cell, which resulted in significant reduction in the energy consumption.

The PEF treatment of *A. platensis* and *S. cerevisiae* was conducted using this low-conductive $TiO_2$-coated test cell, as presented in ***Chapter VII***. The results obtained from these experiments show that effective PEF inactivation of both *A. platensis* and

*S. cerevisiae* was achieved in the $TiO_2$-coated test cell. The PEF inactivation performance in the $TiO_2$-coated test cell was similar to the case of stainless steel test cell, which suggests the main inactivation mechanism of the PEF process is the non-thermal irreversible electroporation, while the ionic conduction process has insignificant impact in terms of inactivation performance.

Evaluation of specific energy consumption of the PEF treatment of *S. cerevisiae* was conducted in ***Chapter VII***. The obtained results indicated that the energy efficacy of the PEF process can be improved significantly in the low-conductive $TiO_2$-coated test cell as compared with stainless steel test cell, which indicates further reduction in the specific energy consumption could be achieved if completely non-conductive electrodes are used.

## 8.3 Effect of Pulse Waveshape and Field Magnitude

In addition to the square impulse generator, another two pulsed power systems which generate HV impulses with smooth exponential and oscillating exponential waveshapes were built in the present study, as described in ***Chapter VI***. PEF treatment on *S. cerevisiae* using these three types of impulses was conducted and their energy efficacies were compared in ***Chapter VII***. Although successful inactivation of *S. cerevisiae* was achieved using impulses with all the waveshapes, the best energy efficacy of the PEF treatment was obtained using the smooth exponential impulses, while PEF treatment using the oscillating exponential impulses demonstrated the worst energy efficacy.

The obtained results from the present study are partially different from the PEF study in [7], in which the PEF performances of square, exponential decaying and oscillatory decaying impulses were compared. In [7], PEF treatment using the square impulse demonstrated better energy efficient as compared with PEF treatment using the exponential decaying impulse. However, different field magnitudes are used in the present study (67 kV/cm and 80 kV/cm) and in [7] (12 kV/cm). A correlation between the effective impulse duration (period where the field strength is above the

critical field strength) and the PEF performance is established. The pulse waveshape with the longer effective duration, during which the magnitude of the field exceeds the critical field strength $E_C$ (~ 10 kV/cm), results in a better PEF performance in terms of energy efficacy.

Both the present study and the PEF study reported in [7] show that impulses with fast oscillations demonstrated the worst energy efficacy. The fast oscillations impede the development of the trans-membrane potential according to the transient membrane charging model described ***Chapter III***. Therefore, in order to achieve high energy efficacy in the PEF inactivation process, it is desirable to increase duration of exposure of microorganisms to the critical field and to avoid fast field oscillations.

In the present study, the effect of the field magnitude on the energy efficacy of the PEF process was also investigated, as discussed in ***Chapter VII***. The obtained results indicate that the magnitude of the applied electric field has a minimal impact on the energy efficacy of the PEF treatment for the field level being investigated (67 kV/cm and 80 kV/cm). It should be noted that these field levels are much higher than the critical field strength, which is ~ 10 kV/cm. Therefore, this conclusion should only be applied to the PEF process using PEF impulses with a relatively high field magnitude.

## 8.4 Low Conductive Suspension for Energy Reduction

In the present study, the liquid suspension used for the PEF treatment was prepared to have conductivity in the range of $10^{-3}$-$10^{-2}$ S/m. These values were selected based on the results of the transient analytical analysis, as described in ***Chapter III***. The use of low conductive suspension reduced the specific energy consumption of the PEF process significantly, as demonstrated in ***Chapter V***. In the PEF experiment with *A. platensis* in the conductive stainless steel test cell, the specific energy consumption is significantly lower than the values reported in the literature. It was calculated that the specific energy consumption in present study for reliable inactivation of *A. platensis* was as low as 0.35 MJ/kg. It was significantly lower than

the energy consumption of PEF treatment of microalgae reported in [67-68], where the same material (stainless steel) was used for the PEF test cell electrodes, the reported specific energy consumption in these studies was 26 MJ/kg and 2 MJ/kg respectively.

In addition, the use of the relatively low conductive liquid suspension reduced the thermal effect during the PEF process. In all the PEF experiments conducted in the present study, the maximum increase in suspension temperature after the PEF treatment was ~ 3°C. As a comparison, few 10's of °C increase in temperature has been reported in literatures [7, 67, 241].

## 8.5 Potential Cause of the Tailing Effect

In the PEF treatment of *S. cerevisiae* conducted in ***Chapter V*** and ***Chapter VII***, the tailing effect on the inactivation curves was observed. It was observed that the inactivation curves for the *S. cerevisiae* samples saturated after 3-$\log_{10}$ reduction regardless of the initial *S. cerevisiae* cells' concentrations, the impulse waveshapes and the test cells. No further reduction in the viable population was observed despite the increase in the pulse number. Further PEF experiments were conducted to identify the potential cause of this undesirable tailing effect and it was found that the sedimentation of *S. cerevisiae* cells during the PEF treatment could potentially be the reason. Further reduction in the surviving *S. cerevisiae* population was achieved by introducing a mixing procedure during the PEF treatment, which unified the distribution of the *S. cerevisiae* cells. Therefore, it was suggested that measures which unify the distribution of microorganisms during the PEF treatment can be used to improve PEF performance: for example, through application of a mixing procedure as demonstrated in present study or by using continuous flow PEF system as reported in several literature [182-183, 259]. The exact causes for the 'tailing' effect require further investigation.

## 8.6 Potential PEF Stimulated Lysis

Investigation into the possibility of PEF inactivation and lysis of *A. platensis* was conducted in the present study, as presented in ***Chapter V*** and ***Chapter VII***. The obtained results showed that the growth of the *A. platensis* was stopped by the PEF treatment in the stainless steel and $TiO_2$-coated test cells, which suggested that effective PEF inactivation of *A. platensis* can be achieved. However, the visual inspection of the individual *A. platensis* cells using optical microscope with ×400 magnification revealed that no visible external structural damage, such as cell rupture, has been introduced by the PEF process. This finding suggested that the PEF treatment (with parameters used in the present study) can induce critical internal damage and dysfunction to the microorganism cells. Significant degree of rupture of the *A. platensis* cells (which would be noted under optical microscope) was not detected in the present study. Visualisation of the induced damage requires other approaches: using powerful TEM or SEM microscopes or using specific dyes to monitor cell changes and free radicals production.

## 8.7 Recommendations for Future Work

Based on the results and significant finding obtained over the course of the present study, recommendations for future investigation and potential scale-up product development directions can be made.

As demonstrated in the present study, the PEF treatment using a low-conductive $TiO_2$-coated PEF test cell results in significant improvement in the energy efficacy and suggests that further improvement can be achieved using a completely non-conductive PEF test cell. On the other hand, due to the Maxwell-Wagner field relaxation process, significantly higher field magnitude, > 130 kV/cm, is required to achieve PEF inactivation using the non-conductive ceramic test cell, [189]. Such high field magnitude would raise technical difficulties in the pulsed power system design and in the potential scale-up process in the future. Therefore, optimisation of the test cell design is required in order to achieve effective PEF inactivation at a

lower field magnitude. One of the directions is to design a non-conductive PEF test cell with longer Maxwell-Wagner characteristic time, which will require novel dielectric materials with high permittivity or ultra-thin thickness.

On the other hand, in the PEF experiments using stainless steel and $TiO_2$-coated test cells (in which microorganisms were successfully inactivated), the 'tailing' of the inactivation curves was observed. Further investigation suggested that this undesirable effect could be eliminated by unifying the distribution of the microorganisms in the PEF test cell. Therefore, continuous flow PEF systems or PEF test cells with a mixing function should be developed for future scale-up applications in order to improve the PEF performance. The exact reasons for this 'tailing' effect are unknown and further investigation is required for better understanding of microbial cell response during the PEF process. These potential causes include microbial cell sedimentation, microbial cell clumping, inherent resistance of cells to the PEF treatment, dead zones in the PEF test cell, and microbial cells in different growing phases.

In addition to the 'tailing' effect, the 'shoulder' effect was also observed in some inactivation curves, which suggested that the damage to the cells has been done and the microbial cells were adjusting to the stress induced by the PEF process. Further investigation of the 'shoulder' effect should be conducted in order to understand the mechanisms of microbial cell adjustment to external stress and ultimately to understand the exact inactivation mechanisms of the PEF process. For example, when microbial cells are treated by PEF impulses with lower field strength or shorter duration, the formation of the pores in their membranes could still be reversed or may not be started. However, the damage could also be induced through other mechanisms, which could result in dysfunction of the microbial cells and their inactivation.

Although the *A. platensis* were successfully inactivated by the PEF treatment, significant degree of rupture of the *A. platensis* cells was not detected in the present study. However, critical internal damage which results in cell death is induced to the *A. platensis* cells by the PEF process, which suggested that the structure of the cells

could potentially be weakened after the PEF treatment. Therefore, it will be interesting to combine the PEF treatment with other established extraction methods to investigate whether this combination can improve the efficiency of extraction of oily content from cyanobacteria and microalgae.

For future scale-up PEF systems, the following development directions and considerations could be suggested:

- Real-time monitoring of the inactivation process: especially for applications using lower electric field strength.
- Possible development of biofilms within the PEF treatment chamber: especially in the case of continuous flow systems.
- Potential combination of the PEF treatment and other microbial control technologies including pulsed UV, spark discharge and non-thermal plasma.
- Evaluation of the overall energy consumption and operational cost of scale-up PEF systems.

# REFERENCES


[1] T. M. Mata, A. A. Martins, and N. S. Caetano, “Microalgae for Biodiesel Production and Other Applications: A Review,” *Renewable and Sustainable Energy Reviews*, Vol. 14, No. 1, pp. 217-232, 2010.

[2] A. J. H. Sale, and W. A. Hamilton, “Effects of High Electric Fields on Microorganisms: I. Killing of Bacteria and Yeasts,” *Biochim. Biophys. Acta*, Vol. 148, No. 3, pp. 781-788, 1967.

[3] W. A. Hamilton, and A. J. H. Sale, “Effects of High Electric Fields on Microorganisms: II. Mechanism of Action of the Lethal Effect,” *Biochim. Biophys. Acta*, Vol. 148, No. 3, pp. 789-800, 1967.

[4] A. J. H. Sale, and W. A. Hamilton, “Effects of High Electric Fields on Microorganisms: III. Lysis of Erythrocytes and Protoplasts,” *Biochim. Biophys. Acta*, Vol. 163, No. 1, pp. 37-43, 1968.

[5] U. Zimmermann, and G. A. Neil, *Electromanipulation of Cells*, Boca Raton: CRC Press, 1996.

[6] I. Timoshkin, S. MacGregor, R. Fouracre, B. Crichton, and J. Anderson, "Transient Electrical Field across Cellular Membranes: Pulsed Electric Field Treatment of Microbial Cells", *J. Phys. D: Appl. Phys.*, Vol. 39, pp. 569-603, 2006.

[7] B. L. Qin, Q. Zhang, G. V. Barbosa-Canovas, B. G. Swanson, and P. D. Pedrow, “Inactivation of Microorganisms by Pulsed Electric Fields of Different Voltage Waveforms,” *IEEE Trans. Dielectr. Electr. Insul.*, Vol. 1, No. 6, pp. 1047-1057, 1994.

[8] J. R. Beveridge, S. J. MacGregor, L. Marsili, J. G. Anderson, N. J. Rowan, and O. Farish, “Comparison of the Effectiveness of Biphase and Monophase Rectangular Pulses for the Inactivation of Microorganisms Using Pulsed Electric Fields,” *IEEE Trans. Plasma Sci.*, Vol. 30, No. 4, pp. 1525–1531, 2002.

[9] H. P. Schwan, "Electrical Properties of Tissue and Cell Suspensions," *Adv. Biol. Med. Phys.*, Vol. 5, pp. 147-209, 1957.

[10] D. Hawksworth, 1992. Microorganisms. In: B. Groombridge ed. *Global Biodiversity: Status of the Earth's Living Resources.* New York: Chapman & Hall, pp: 47-54.

[11] M. Madigan, J. Martinko, K. Bender, D. Buckley, and D. Stahl, *Brock Biology of Microorganisms, 14th ed. Globe ed.* San Francisco: Pearson Education, 2014.

[12] J. Schopf, "Fossil Evidence of Archaean Life," *Philosophical Transactions of the Royal Society, B,* 361 (2006), pp. 869–885.

[13] W. Altermanna, and J. Kazmierczak, "Archean Microfossils: A Reappraisal of Early Life on Earth," *Research in Microbiology*, Vol. 154, No. 9, pp. 611–617, 2003.

[14] T. Cavalier-Smith, "Cell Evolution and Earth History: Stasis and Revolution," *Philosophical Transactions of the Royal Society, B,* 361 (2006), pp. 969–1006.

[15] S. Stanley, "An Ecological Theory for the Sudden Origin of Multicellular Life in the Late Precambrian". *Proceedings of the National Academy of Sciences of the USA*, Vol. 70, No. 5, pp. 1486-1489, 1973.

[16] J. Fuerst. (2010) Beyond Prokaryotes and Eukaryotes: Planctomycetes and Cell Organization. [Online] Available at: http://www.nature.com/scitable/topicpage/beyond-prokaryotes-and-eukaryotes-planctomycetes-and-cell-14158971 [Assessed 16 March 2016].

[17] J. L. Howland, *The Surprising Archaea: Discovering Another Domain of Life,* New York: Oxford University Press, 2000.

[18] A. L. Koch, "Bacterial Wall as Target for Attack: Past, Present and Future Research," *Clinical Microbiology Reviews*, Vol. 16, No. 4, pp. 673-687, 2003.

[19] D. White, *The Physiology and Biochemistry of Prokaryotes,* New York: Oxford University Press, 1995.

[20] J. Webster, and R. Weber, *Introduction to Fungi, 2nd ed.,* New York: Cambridge University Press, 1980.

[21] D. S. Domozych, M. Ciancia, J. U. Fangel, M. D. Mikkelsen, P. Ulvskov, and W. G. T. Willats, "The Cell Walls of Green Algae: A Journey through Evolution and Diversity," *Front Plant Sci*., Vol. 3, No. 82, 2012.

[22] P. Singleton, *Bacteria in Biology, Biotechnology, and Medicine, 4th ed.,* New York : J. Wiley & Sons, 1997.

[23] B. Alberts, A. Johnson, J. Lewis, M. Raff, K. Roberts, and P. Walter, *Molecular Biology of the Cell, 4th ed.*, New York: Garland Science, 2002.

[24] Plasma Membrane. [Online] Available at: http://biology.tutorvista.com/animal-and-plant-cells/plasma-membrane.html [Assessed 25 March 2016].

[25] J. F. Naglea, and S. Tristram-Nagle, "Structure of Lipid Bilayers," *Biochim. Biophys. Acta,* Vol. 1469, No. 3, pp. 159-195, 2000.

[26] Phospholipids. [Online] Available at: https://www.boundless.com/biology/textbooks/boundless-biology-textbook/biological-macromolecules-3/lipids-55/ phospholipids-300-11433/images/phospholipid-bilayer/ [Assessed 25 March 2016].

[27] W. Weckwerth, "Metabolomics in Systems Biology," *Annual Review of Plant Biology*, Vol. 54, pp. 669-689, 2003.

[28] J. S. Clegg, "Properties and Metabolism of the Aqueous Cytoplasm and Its Boundaries," *Am. J. Physiol.* Vol. 246, pp. 133-151, 1984.

[29] S. Naeem, D. R. Hahn, and G. Schuurman, "Producer–Decomposer Co-dependency Influences Biodiversity Effects," Nature, Vol.403, pp. 762-764, 2000.

[30] J. Rousk, P. C. Brookes, and E. Bååth, "Contrasting Soil pH Effects on Fungal and Bacterial Growth Suggest Functional Redundancy in Carbon Mineralization," *Applied and Environmental Microbiology*, Vol. 75, No. 6, pp. 1589-1596, 2009.

[31] M. A. Altieri, “The Ecological Role of Biodiversity in Agroecosystems,” *Agriculture, Ecosystems & Environment,* Vol. 74, Issues. 1–3, pp. 19-31, 1999.

[32] S. Naeem, and S. Li, “Biodiversity Enhances Ecosystem Reliability,” *Nature*, Vol. 390, pp. 507-509, 1997.

[33] W. B. Whitman, D. C. Coleman, and W. J. Wiebe, “Prokaryotes: The Unseen Majority,” *Proc. Natl. Acad. Sci. USA*, Vol. 95, pp. 6578–6583, 1998.

[34] N. Latysheva1, V. L. Junker1, W. J. Palmer, G. A. Codd, and D. Barker, “The Evolution of Nitrogen Fixation in Cyanobacteria,” *Bioinformatics*, Vol. 28, No. 5, pp. 603-606, 2012.

[35] M. Alexander, *Introduction to Soil Microbiology, 2nd ed.* New York: John Wiley & Sons, 1977.

[36] M. Hayatsu, K. Tago, and M. Saito, “Various Players in the Nitrogen Cycle: Diversity and Functions of the Microorganisms Involved in Nitrification and Denitrification,” *Soil Science and Plant Nutrition*, Vol. 54, No. 1, pp. 33-45, 2008.

[37] D. E. Canfield, A. N. Glazer, and P. G. Falkowski, “The Evolution and Future of Earth’s Nitrogen Cycle,” *Science*, Vol. 330, pp. 192-196, 2010.

[38] P. E. McGovern, J. Zhang, J. Tang, Z. Zhang, G. R. Hall, R. A. Moreau, A. Nunez, E. D. Butrym, M. P. Richards, C.Wang, G. Cheng, Z. Zhao, and C. Wang, “Fermented Beverages of Pre- and Proto-historic China,” *Proceedings of the National Academy of Sciences of the USA*, Vol. 101, No. 51, pp. 17593-17598, 2004.

[39] D. Cavalieri, P. E. McGovern, D. L. Hartl, R. Mortimer, and M. Polsinelli, “Evidence for S. cerevisiae Fermentation in Ancient Wine,” *Journal of Molecular Evolution*, Vol. 57, No. 1, pp. S226-S232, 2003.

[40] C. Boulton, and D. Quain, *Brewing Yeast and Fermentation,* Oxford: Blackwell Science, 2001.

[41] E. R. Farnworth, *Handbook of Fermented Functional Foods*, Boca Raton: CRC Press, 2003.

[42] J. C. Kolars, M. D. Levitt, M. Aouji, and D. A. Savaiano, "Yogurt — An Autodigesting Source of Lactose," *N Engl J Med*, Vol. 310, pp. 1-3, 1984.

[43] P. Deetae, P. Bonnarme, H. E. Spinnler, and S. Helinck, "Production of Volatile Aroma Compounds by Bacterial Strains Isolated from Different Surface-Ripened French Cheeses," *Applied Microbiology and Biotechnology*, Vol. 76, No. 5, pp. 1161-1171, 2007.

[44] P. R. Murray, K. S. Rosenthal, and M. A. Pfaller, *Medical Microbiology, 8th ed.* Philadelphia: Elsevier, 2016.

[45] R. I. Aminov, "A Brief History of the Antibiotic Era: Lessons Learned and Challenges for the Future," *Frontiers in Microbiology*, Vol. 1, p. 134, 2010.

[46] R. Simon, U. Priefer, and A. Pühler, "A Broad Host Range Mobilization System for Invivo Genetic-Engineering-Transposon Mutagenesis in Gram-Negative Bacteria", *Bio-Technology*, Vol. 1, pp. 784-791, 1983.

[47] H. Daniell, M. S. Khan, and L. Allison, "Milestones in Chloroplast Genetic Engineering: An Environmentally Friendly Era in Biotechnology," *Trends in Plant Science*, Vol. 7, No. 2, pp. 84-91, 2002.

[48] L. O. Ingram, T. Conway, D. P. Clark, G. W. Sewell, and J. F. Preston, "Genetic Engineering of Ethanol Production in Escherichia Coli," *Applied and Environmental Microbiology*, Vol. 53, No. 10, pp. 2420-2425, 1987.

[49] P. Spolaore, C. Joannis-Cassan, E. Duran, and A. Isambert, "Commercial Applications of Microalgae," *Journal of Bioscience and Bioengineering*, Vol. 101, No. 2, pp. 87–96, 2006.

[50] D. Solettoa, L. Binaghia, A. Lodia, J. C. M. Carvalhob, and A. Convertia, "Batch and Fed-batch Cultivations of *Spirulina Platensis* Using Ammonium Sulphate and Urea as Nitrogen Sources," *Aquaculture*, Vol. 243, pp. 217–224, 2005.

[51] R. J. Radmer, “Algal Diversity and Commercial Algal Products,” *Bioscience*, Vol. 46, No. 4, pp. 263–270, 1996.

[52] H. Desmorieux, and N. Decaen, “Convective Drying of *Spirulina* in Thin Layer,” *J. Food Eng.*, Vol. 66, No. 4, pp. 497–503, 2005.

[53] C. O. Rangel-Yagui, E. D. G. Danesi, J. C. M. Carvalho, and S. Sato, “Chlorophyll Production from *Spirulina Platensis*: Cultivation with Urea Addition by Fed-batch Process,” *Bioresource Technology*, Vol. 92, No. 2, pp. 133–141, 2004.

[54] A. Muller-Feuga, “The Role of Microalgae in Aquaculture: Situation and Trends,” *Journal of Applied Phycology*, Vol. 12, No. 3, pp. 527–534, 2000.

[55] M. Servel, C. Claire, A. Derrien, L. Coiffard, and Y. Roeck-Holtzhauer, “Fatty Acid Composition of Some Marine Microalgae,” *Phytochemistry*, Vol. 36, No. 3, pp. 691-693, 1994.

[56] J. A. D. Campo, J. Moreno, H. Rodríguez, M. A. Vargas, J. Rivas, and M. G. Guerrero, “Carotenoid Content of Chlorophycean Microalgae: Factors Determining Lutein Accumulation in *Muriellopsis sp.* (*Chlorophyta*),” *Journal of Biotechnology*, Vol. 76, No. 1, pp. 51–59, 2000.

[57] A. R. Medina, E. M. Grima, A. G. Giménez, and M. J. I. González, “Downstream Processing of Algal Polyunsaturated Fatty Acids,” *Biotechnology Advances*, Vol. 16, No. 3, pp. 517–580, 1998.

[58] J. Yue, C. Feng, and S. Liang, “Production Potential of Docosahexaenoic Acid by the Heterotrophic Marine Dinoflagellate *Crypthecodinium cohnii*,” *Process Biochemistry*, Vol. 34, No. 6–7, pp. 633–637, 1999.

[59] E. M. Grima, E. H. Belarbi, F. G. A. Fernández, A. R. Medina, and Y. Chisti, “Recovery of Microalgal Biomass and Metabolites: Process Options and Economics,” *Biotechnology Advances*, Vol. 20, No. 7-8, pp. 491–515, 2003.

[60] Z. Wen, and F. Chen, “Heterotrophic Production of Eicosapentaenoic Acid by Microalgae,” *Biotechnology Advances*, Vol. 21, No. 4, pp. 273–294, 2003.

[61] Y. Chisti, “Biodiesel from Microalgae,” *Biotechnology Advances*, Vol. 25, No. 3, pp. 294–306, 2007.

[62] L. Brennana, and P. Owendea, “Biofuels from Microalgae—A Review of Technologies for Production, Processing, and Extractions of Biofuels and Co-products,” *Renewable and Sustainable Energy Reviews*, Vol. 14, No. 2, pp. 557–577, 2010.

[63] Y. Ghasemi, S. Rasoul-Amini, A. T. Naseri, N. Montazeri-Najafabady, M. A. Mobasher, and F. Dabbagh, “Microalgae Biofuel Potentials (Review),” *Applied Biochemistry and Microbiology*, Vol. 48, No. 2, pp. 126-144, 2012.

[64] Q. Hu, M. Sommerfeld, E. Jarvis, M. Ghirardi, M. Posewitz, M. Seibert, and A. Darzins, “Microalgal *Triacylglycerols* as Feedstocks for Biofuel Production: Perspectives and Advances,” *The Planet Journal*, Vol. 54, No. 4, pp. 621–639, 2008.

[65] B. Sialve, N. Bernet, and O. Bernard, “Anaerobic Digestion of Microalgae as A Necessary Step to Make Microalgal Biodiesel Sustainable,” *Biotechnology Advances*, Vol. 27, No. 4, pp. 409–416, 2009.

[66] M. M. Mendes-Pinto, M. F. J. Raposo, J. Bowen, A. J. Young, and R. Morais, “Evaluation of Different Cell Disruption Processes on Encysted Cells of *Haematococcus Pluvialis*: Effects on Astaxanthin Recovery and Implications for Bio-availability,” *Journal of Applied Phycology*, Vol. 13, No. 1, pp. 19-24, 2001.

[67] M. D. A. Zbinden, B. S. M. Sturm, R. D. Nord, W. J. Carey, D. Moore, H. Shinogle, and S. M. Stagg-Williams, “Pulsed Electric Field (PEF) as an Intensification Pretreatment for Greener Solvent Lipid Extraction from Microalgae,” *Biotechnol. Bioeng.*, Vol. 110, No. 6, pp. 1605–1615, 2013.

[68] C. Eing, M. Goettel, R. Straessner, C. Gusbeth, and W. Frey, “Pulsed Electric Field Treatment of Microalgae—Benefits for Microalgae Biomass Processing,” *IEEE Trans. Plasma Sci.*, Vol. 41, No. 10, pp. 2901–2907, 2013.

[69] S. Gnapowski, R. H. Akiyama, T. Sakugawa, and M. Akiyama, "Algae Treatment Effects by Pulse Power Discharge in the Water," *in Proc. IEEE ICOPS*, pp. 1P–111, 2012.

[70] N. Grimi, A. Dubois, L. Marchal, S. Jubeau, N. I. Lebovka, and E. Vorobiev, "Selective Extraction from Microalgae *Nannochloropsis sp.* Using Different Methods of Cell Disruption," *Bioresource Technology*, Vol. 153, pp. 254-259, 2014.

[71] M. Goettel, C. Eing, C. Gusbeth, R. Straessner, and W. Frey, "Pulsed Electric Field Assisted Extraction of Intracellular Valuables from Microalgae," *Algal Research*, Vol. 2, No. 4, pp. 401-408, 2013.

[72] T. J. Montville, and K. R. Matthews, *Food Microbiology: An Introduction, 2nd ed.,* Washington: ASM Press, 2008.

[73] J. I. Pitt, and A. D. Hocking, *Fungi and Food Spoilage, 3rd ed.,* New York: Springer-Verlag, 2009.

[74] L. Gram, L. Ravn, M. Rasch, J. B. Bruhn, A. B. Christensen, and M. Givskov, "Food Spoilage—Interactions between Food Spoilage Bacteria," *International Journal of Food Microbiology*, Vol. 78, No. 1–2, pp. 79–97, 2002.

[75] C. W. Blackburn, *Food Spoilage Microorganism*, Cambridge: Woodhead Publishing Limited, 2006.

[76] A. Rahman, and S. C. Kang, "*In Vitro* Control of Food-Borne and Food Spoilage Bacteria by Essential Oil and Ethanol Extracts of *Lonicera japonica* Thunb," *Food Chemistry*, Vol. 116, No. 3, pp. 670–675, 2009.

[77] S. S. Block, *Disinfection, Sterilization, and Preservation, 5th ed.* Philadelphia: Lippincott Williams & Wilkins, 2001.

[78] J. P. P. M. Smelt, and S. Brul, "Thermal Inactivation of Microorganisms," *Critical Reviews in Food Science and Nutrition*, Vol. 54, No. 10, pp. 1371-1385, 2014.

[79] S. S. Block, 2001. Historical Review. In: S. S. Block ed. *Disinfection, Sterilization, and Preservation. 5th ed.* Philadelphia: Lippincott Williams & Wilkins, pp: 3-17.

[80] W. D. Bigelow, "The Logarithmic Nature of Thermal Death Time Curves," *The Journal of Infectious Diseases*, Vol. 29, No. 5, pp. 528-536, 1921.

[81] M. Pelega, and M. B. Coleb, "Reinterpretation of Microbial Survival Curves," *Critical Reviews in Food Science and Nutrition*, Vol. 38, No. 5, pp. 353-380, 1998.

[82] O. Cerf, "A Review: Tailing of Survival Curves of Bacterial Spores," Journal of Applied Bacteriology, Vol. 42, No. 1, pp. 1-19, 1977.

[83] P. Mafart, O. Couvert, S. Gaillard, and I. Leguerinel, "On Calculating Sterility in Thermal Preservation Methods: Application of the Weibull Frequency Distribution Model," *International Journal of Food Microbiology*, Vol. 72, No. 1–2, pp. 107–113, 2002.

[84] G. R. Dychdala, 2001. Chlorine and Chlorine Compounds. In: S. S. Block ed. *Disinfection, Sterilization, and Preservation. 5th ed.* Philadelphia: Lippincott Williams & Wilkins, pp: 135-158.

[85] W. Gottardi, 2001. Iodine and Iodine Compounds. In: S. S. Block ed. *Disinfection, Sterilization, and Preservation. 5th ed.* Philadelphia: Lippincott Williams & Wilkins, pp: 159-184.

[86] L. K. Weavers, and G. B. Wickramanayake, 2001. Disinfection and Sterilization Using Ozone. In: S. S. Block ed. *Disinfection, Sterilization, and Preservation. 5th ed.* Philadelphia: Lippincott Williams & Wilkins, pp: 205-214.

[87] Y. Ali, M. J. Dolan, E. J. Fendler, and E. L. Larson, 2001. Alcohols. In: S. S. Block ed. *Disinfection, Sterilization, and Preservation. 5th ed.* Philadelphia: Lippincott Williams & Wilkins, pp: 229-254.

[88] G. McDonnell, and D. Pretzer, 2001. New and Developing Chemical Antimicrobials. In: S. S. Block ed. *Disinfection, Sterilization, and*

*Preservation. 5th ed.* Philadelphia: Lippincott Williams & Wilkins, pp: 431-443.

[89] G. A. Boorman, "Drinking Water Disinfection Byproducts: Review and Approach to Toxicity Evaluation," *Environmental Health Perspectives*, Vol. 107, No. 1, pp. 207-217, 1999.

[90] S. D. Richardson, and C. Postigo, 2012. Drinking Water Disinfection By-products. In D. Barceló ed. *Emerging Organic Contaminants and Human Health.* New York: Springer, pp. 93-137.

[91] A. Downes, and T. P. Blunt, "Researches on the Effect of Light upon Bacteria and other Organisms," *Proc. R. Soc. Lond.*, Vol. 26, pp. 488-500, 1877.

[92] E. R. Blatchley III, and M. M. Peel, 2001. Disinfection by Ultraviolet Irradiation. In: S. S. Block ed. *Disinfection, Sterilization, and Preservation. 5th ed.* Philadelphia: Lippincott Williams & Wilkins, pp: 823-851.

[93] J. A. Lippke, L. K. Gordon, D. E. Brash, and W. A. Haseltine, "Distribution of UV Light-Induced Damage in A Defined Sequence of Human DNA: Detection of Alkaline-Sensitive Lesions at Pyrimidine Nucleoside-Cytidine Sequences," *Proceedings of the National Academy of Sciences of the USA*, Vol. 78, No. 6, pp. 3388-3392, 1981.

[94] D. E. Brash, J. A. Rudolph, J. A. Simon, A. Lin, G. J. McKenna, H. P. Baden, A. J. Halperin, and J. Pontén, "A Role for Sunlight in Skin Cancer: UV-Induced p53 Mutations in Squamous Cell Carcinoma," *Proceedings of the National Academy of Sciences of the USA*, Vol. 88, No. 22, pp. 10124–10128, 1991.

[95] R. B. Setlow, "The Wavelengths in Sunlight Effective in Producing Skin Cancer: A Theoretical Analysis," *Proceedings of the National Academy of Sciences of the USA*, Vol. 71, No. 9, pp. 3363–3366, 1974.

[96] B. K. Armstrong, and A. Krickerb, "The Epidemiology of UV Induced Skin Cancer," *Journal of Photochemistry and Photobiology B: Biology*, Vol. 63, No. 1-3, pp. 8–18, 2001.

[97] M. A. Roberts, J. S. Rossier, P. Bercier, and H. Giraul, "UV Laser Machined Polymer Substrates for the Development of Microdiagnostic Systems," *Analytical chemistry*, Vol. 69, No11, pp. 2035-2042, 1997.

[98] J. C. Cheftel, "Review: High-Pressure, Microbial Inactivation and Food Preservation," *Food Science and Technology International*, Vol. 1, No. 2-3, pp. 75-90, 1995.

[99] D. G. Hoover, C. Metrick, A. M. Papineau, D. F. Farkas, and D. Knorr, "Biological Effects of High Hydrostatic Pressure on Food Microorganisms," *Food Technology*, Vol. 43, No. 3, pp. 99-107, 1989.

[100] D. Knorr, "Effects of High-Hydrostatic-Pressure Processes on Food Safety and Quality," *Food Technology*, Vol. 47, No. 6, pp. 156-161, 1993.

[101] D. Knorr, 1995. Hydrostatic Pressure Treatment of Food: Microbiology. In: G. W. Gould ed. *New Methods of Food Preservation. 1st ed*. New York: Blackie Academic & Professional, pp. 159-175.

[102] H. Lin, Z. Yang, and L. Chen, "An Improved Method for Disruption of Microbial Cells with Pressurized Carbon Dioxide," *Biotechnol. Prog*. Vol. 8, No. 2, pp. 165-166, 1992.

[103] B. Mertens, 1995. Hydrostatic Pressure Treatment of Food: Equipment and Processing. In: G. W. Gould ed. *New Methods of Food Preservation. 1st ed*. New York: Blackie Academic & Professional, pp. 135-158.

[104] M. Maclean, S. J. MacGregor, J. G. Anderson, G. A. Woolsey, J. E. Coia, K. Hamilton, I. Taggart, S. B. Watson, B. Thakker, and G. Gettinby, "Environmental Decontamination of A Hospital Isolation Room Using High-Intensity Narrow-Spectrum Light," *Journal of Hospital Infection*, Vol. 76, No. 3, pp. 247-251, 2010.

[105] M. Maclean, S. J. MacGregor, J. G. Anderson, and G. Woolsey, "The Role of Oxygen in the Visible-Light Inactivation of *Staphylococcus aureus*," *Journal of Photochemistry and Photobiology B: Biology*, Vol. 92, No. 3, pp. 180–184, 2008.

[106] M. Maclean, S. J. MacGregor, J. G. Anderson, and G. Woolsey, “Inactivation of Bacterial Pathogens Following Exposure to Light from A 405-Nanometer Light-Emitting Diode Array,” *Applied and Environmental Microbiology*, Vol. 75, No. 7, pp. 1932–1937, 2009.

[107] H. Ashkenazi, Z. Malik, Y. Harth, and Y. Nitzan, “Eradication of *Propionibacterium acnes* by its Endogenic Porphyrins after Illumination with High Intensity Blue Light,” *FEMS Immunology & Medical Microbiology,* Vol. 35, No. 1, pp. 17-24, 2003.

[108] R. A. Ganz, J. Viveiros, A. Ahmad, A. Ahmadi, A. Khalil, M. J. Tolkoff, N. S. Nishioka, and M. R. Hamblin, “*Helicobacter pylori* in Patients Can Be Killed by Visible Light,” *Lasers in Surgery and Medicine,* Vol. 36, No. 4, pp. 260–265, 2005.

[109] M. Maclean, S. J. MacGregor, J. G. Anderson, and G. Woolsey, “High-Intensity Narrow-Spectrum Light Inactivation and Wavelength Sensitivity of *Staphylococcus aureus*,” *FEMS Microbiology Letters,* Vol. 285, No. 2, pp. 227–232, 2008.

[110] O. Feuerstein, I. Ginsburg, E. Dayan, D. Veler, and E. I. Weiss, “Mechanism of Visible Light Phototoxicity on *Porphyromonas gingivalis* and *Fusobacterium nucleatum,*” *Photochemistry and Photobiology,* Vol. 81, No. 5, pp. 1186-1189, 2005.

[111] P. C. Wouters, and J. P. P. M. Smelt, “Inactivation of Microorganisms with Pulsed Electric Fields: Potential for Food Preservation,” Food Biotechnology, Vol. 11, No. 3, pp. 193-229, 1997.

[112] H. V. Mercado, O. M. Belloso, B. L. Qin, F. J. Chang, M. M. Góngora-Nieto, G. V. Barbosa-Cánovas, and B. G. Swanson, “Non-Thermal Food Preservation: Pulsed Electric Fields,” *Trends in Food Science & Technology,* Vol. 8, No. 5, pp. 151–157, 1997.

[113] S. Toepfl, V. Heinz, and D. Knorr, “High Intensity Pulsed Electric Fields Applied for Food Preservation,” *Chemical Engineering and Processing: Process Intensification,* Vol. 46, No. 6, pp. 537–546, 2007.

[114] A. J. Castro, G. V. Barbosa-Cánovas, and B. G. Swanson, "Microbial Inactivation of Foods by Pulsed Electric Fields," *Journal of Food Processing and Preservation*, Vol. 17, No. 1, pp. 47–73, 1993.

[115] V. Heinz, I. Alvarez, A. Angersbach, and D. Knorr, "Preservation of Liquid Foods by High Intensity Pulsed Electric Fields—Basic Concepts for Process Design," *Trends in Food Science & Technology*, Vol. 12, No. 3-4, pp. 103–111, 2002.

[116] G. V. Barbosa-Cánovas, M. M. Góngora-Nieto, U. R. Pothakamury, and B. G. Swanson, *Preservation of Foods with Pulsed Electric Fields*. London: Academic Press, 1999.

[117] H. Hashimoto, H. Morikawa, Y. Yamada, and A. Kimura, "A Novel Method for Transformation of Intact Yeast Cells by Electroinjection of Plasmid DNA," *Applied Microbiology and Biotechnology*, Vol. 21, No. 5, pp. 336-339, 1985.

[118] R. Heller, M. Jaroszeski, A. Atkin, D. Moradpour, R. Gilbert, J. Wands, and C. Nicolau, "*In Vivo* Gene Electroinjection and Expression in Rat Liver," *FEBS Letters*, Vol. 389, No. 3, pp. 225-228, 1996.

[119] L. M. Mir, M. F. Bureau, J. Gehl, R. Rangara, D. Rouyi, J. M. Caillaud, P. Delaere, D. Branelleci, B. Schwartz, snd D. Scherman, "High-Efficiency Gene Transfer into Skeletal Muscle Mediated by Electric Pulses," *Proceedings of the National Academy of Sciences of the USA*, Vol. 96, No. 8, pp. 4262-4267, 1998.

[120] U. Zimmermann, and W. M. Arnold, "Biophysics of Electroinjection and Electrofusion," *Journal of Electrostatics*, Vol. 21, No. 2-3, pp. 309-345, 1988.

[121] U. Zimmermann, and J. Vienken, "Electric Field-Induced Cell-to-Cell Fusion," *The Journal of Membrane Biology*, Vol. 67, No. 1, pp. 165-182, 1982.

[122] J. Z. Kubiak, and A. K. Tarkowski, "Electrofusion of Mouse Blastomeres," Experimental Cell Research, Vol. 157, No. 2, pp. 561-566, 1982.

[123] M. D. Guiry, and G. M. Guiry. (2016) *Arthrospira platensis* var. *tenuis* (C.B.Rao) Desikachary. [Online] Avaliable at: http://www.algaebase.Org/

search/species/detail/?species_id=u1f5b4b8e1f96f06b [Assessed 14 May 2016].

[124] J. Mader, A. Gallo, T. Schommartz, W. Handke, C. H. Nagel, P. Gunther, W. Brune, and K. Reich, "Calcium Spirulan Derived from *Spirulina platensis* Inhibits Herpes Simplex Virus1Attachment to Human Keratinocytes and Protects against Herpes Labialis," *J. Allergy Clin. Immunol*, Vol. 137, No. 1, pp. 197-203, 2016.

[125] T. Hayashi, K. Hayashi, M. Maeda, and I. Kojima, "Calcium Spirulan, an Inhibitor of Enveloped Virus Replication, from a Blue-Green Alga *Spirulina platensis*," *J. Nat. Prod.*, Vol. 59, No. 1, pp. 83-87, 1996.

[126] J. E. P. Estrada, P. B. Bescos, and A. M. V. del Fresno, "Antioxidant Activity of Different Fractions of *Spirulina platensis* Protean Extract" *Il Farmaco*, Vol. 56, No. 5-7, pp. 497-500, 2001.

[127] A. S. Babadzhanov, N. Abdusamatova, F. M. Yusupova, N. Faizullaeva, L. G. Mezhlumyan, and M. Kh. Malikova, "Chemical Composition of *Spirulina platensis* Cultivated in Uzbekistan," *Chemistry of Natural Compounds*, Vol. 40, No. 3, pp. 276-279, 2004.

[128] Z. Khan, P. Bhadouria, and P. S. Bisen, "Nutritional and Therapeutic Potential of *Spirulina*," *Current Pharmaceutical Biotechnology*, Vol. 6, No. 5, pp. 373-379, 2005.

[129] L. M. Colla, T. E. Bertolin, and J. A. V. Costa, "Fatty Acids Profile of *Spirulina platensis* Grown Under Different Temperatures and Nitrogen Concentrations," *Zeitschrift für Naturforschung C*, Vol. 59, No. 1-2, pp. 55-59, 2004.

[130] Ö. T. Oglu, and M. K. Ünal, "Biomass Nutrient Profiles of Three Microalgae: *Spirulina platensis*, *Chlorella vulgaris*, and *Isochrisis galbana*," *Journal of Food Science*, Vol. 68, No. 4, pp. 1144-1148, 2003.

[131] J. A. Barnett, 1997. Introduction: A Historical Survey of the Study of Yeast. In F. K. Zimmermann, and K. D. Entian ed. *Yeast Sugar Metabolism.* Lancaster: Technomic Pub., pp. 1-33.

[132] R. G. Garrison, and W. N. Arnold, 1981. Atlas of Cell Morphology. In W. N. Arnold ed. *Yeast Cell Envelopes: Biochemistry, Biophysics, and Ultrastructure*. Boca Raton: CRC Press, pp. 5-24.

[133] W. N. Arnold, 1981. Lipids. In W. N. Arnold ed. *Yeast Cell Envelopes: Biochemistry, Biophysics, and Ultrastructure*. Boca Raton: CRC Press, pp. 97-114.

[134] J. M. Galazka, C. Tian, W. T. Beeson, B. Martinez, N. L. Glass, and J. H. D. Cate, "Cellodextrin Transport in Yeast for Improved Biofuel Production," Science, Vol. 330, No. 6000, pp. 84-86, 2010.

[135] N. A. Buijs, V. Siewers, and J.Nielsen, "Advanced Biofuel Production by the Yeast *Saccharomyces cerevisiae*," *Current Opinion in Chemical Biology*, Vol. 17, No. 3, pp. 480-488, 2013.

[136] G. A. Mesyats, *Pulsed Power*. New York: Springer, 2005.

[137] W. J. Carey, and J. R. Mayes, "Marx Generator Design and Performance," *in Proc. Power Modulator Symp.*, pp. 625-628, 2002.

[138] A. A. Neuber, Y. J. Chen, J. C. Dickens, and M. Kristiansen, "A Compact, Repetitive, 500 kv, 500 J, Marx Generator," *in Proc. IEEE Pulsed Power Conf.*, 2005.

[139] E. Marx, Deutsches Reichpatent 455.933, 1923.

[140] J. Mankowski, and M. Kristiansen, "A Review of Short Pulse Generator Technology," *IEEE Trans. Plasma Sci.,* Vol. 8, No. 1, pp. 102-108, 2000.

[141] Y. A. Rotov, G. A. Mesyats, S. N. Rukin, A. L. Filatov, and S. K. Lyubutin, "A Novel Nanosecond Semiconductor Opening Switch for Megavolt Repetitive Pulsed Power Technology: Experiment and Applications," *in Proc. 9th Int. IEEE Pulsed Power Conf.*, pp. 134-139, 1993.

[142] A. D. Blumlien, UK Patent 589127, 1941.

[143] I. C. Somerville, S. J. MacGregor, and O. Farish, "An Efficient Stacked-Blumlein HV Pulse Generator," *Meas. Sci. Technol.,* Vol. 1, No. 9, pp. 865-868, 1990.

[144] F. Davanloo, C. B. Collins, and F. J. Agee, “High-Power, Repetitive-Stacked Blumlein Pulsers Commutated by A Single Switching Element,” *IEEE Trans. Plasma Sci.,* Vol. 26, No. 5, pp. 1463-1475, 1998.

[145] M. Rebersek, M. Kranjc, D. Pavliha, T. Batista-Napotnik, D. Vrtacnik, S. Amon, and D. Miklavcic, “Blumlein Configuration for High-Repetition-Rate Pulse Generation of Variable Duration and Polarity Using Synchronized Switch Control,” *IEEE Transactions on Biomedical Engineering*, Vol. 56, No. 11, pp. 2642-2648, 2009.

[146] N. J. Rowan, S. J. Macgregor, J. G. Anderson, R. A. Fouracre, L. Mcilvaney, and O. Farish, “Pulsed-Light Inactivation of Food-Related Microorganisms,” *Applied and Environmental Microbiology*, Vol. 65, No. 3, pp. 1312-1315, 1999.

[147] H. Li, H. Ryoo, J. Kim, G. Rim, Y. Kim, and J. Deng, “Development of Rectangle-Pulse Marx Generator Based on PFN,” *IEEE Trans. Plasma Sci.,* Vol. 37, No. 1, pp. 190-194, 2009.

[148] S. M. Turnbull, S. J. MacGregor, and J. A. Harrower, “A PFN Marx Generator Based on High-Voltage Transmission Lines,” *Meas. Sci. Technol.,* Vol. 11, No. 4, pp. N51-N55, 2000.

[149] D. D. P. Kumar, S. Mitra, K. Senthil, A. Sharma, K. V. Nagesh, S. K. Singh, J. Mondal, A. Roy, and D. P. Chakravarthy, “Characterization and Analysis of A Pulse Power System Based on Marx Generator and Blumlein,” *Rev. Sci. Instrum.*, Vol. 78, No. 11, pp. 1-4, 2007.

[150] J. Mankowski, J. Dickens, and M. Kristiansen, “High Voltage Subnanosecond Breakdown,” *IEEE Trans. Plasma Sci.,* Vol. 26, No. 3, pp. 874-881, 1998.

[151] M. Ishii, and H. Yamada, “Self-Matched High-Voltage Rectangular Wave Pulse Generator,” *Rev. Sci. Instrum.,* Vol. 56, No. 11, pp. 2116-2118, 1985.

[152] F. A. Tuema, S. J. MacGregor, and R. A. Fouracre, “The Design and Performance of A Low-Impedance, Self-Matched Transmission Line Pulse Generator,” *Meas. Sci. Technol.,* Vol. 9, No. 12, pp. 1989-1993, 1998.

[153] J. R. Beveridge, 2005. *Inactivation of Liquid-Borne Microorganisms Using Pulsed Electric Fields*. Unpublished PhD Thesis. University of Strathclyde.

[154] M. G. Hogg, 2015. *High-Performance Compact Gas Filled Spark Switches*. Unpublished PhD Thesis. University of Strathclyde.

[155] X. Zou, H. Shi, H. Xie, X. Wang, and G. Zhang, "Using Fast Moving Electrode to Achieve Overvoltage Breakdown of Gas Switch Stressed with High Direct Voltages," *Rev. Sci. Instrum.*, Vol. 86, No. 3, pp. 1-5, 2015.

[156] F. A. Tuema, 2001. *Methods of Improving the Pulse Repetition Frequency of High Pressure Gas Switches*. Unpublished PhD Thesis. University of Strathclyde.

[157] J. A. Harrower, 2001. *The Development and Characterisation of Corona-Stabilised Repetitive Closing Switches*. Unpublished PhD Thesis. University of Strathclyde.

[158] S. J. MacGregor, S. M. Turnbull, F. A. Tuema, and O. Farish, "Factors Affecting and Methods of Improving the Pulse Repetition Frequency of Pulse-Charged and DC-Charged High-Pressure Gas Switches," *IEEE Trans. Plasma Sci.*, Vol. 25, No. 2, pp. 110-117, 1997.

[159] J. A. Harrower, S. J. MacGregor, and F. A. Tuema, "Design Considerations for Corona-Stabilized Repetitive Switches," J. *Phys. D: Appl. Phys.*, Vol. 32, No. 7, pp. 790-797, 1998.

[160] J. R. Beveridge, S. J. Macgregor, M. J. Given, I. V. Timoshkin, and J. M. Lehr, "A Corona-Stabilised Plasma Closing Switch," *IEEE Trans. Dielectr. Electr. Insul.*, Vol. 16, No. 4, pp. 948-955, 2009.

[161] H. Akiyama, T. Sakugawa, T. Namihira, K. Takaki, Y. Minamitani, and N. Shimomura, "Industrial Applications of Pulsed Power Technology," *IEEE Trans. Dielectr. Electr. Insul.*, Vol. 14, No. 5, pp. 1051–1064, 2007.

[162] E. Y. Shcolnikov, S. P. Maslennikov, N. N. Netchaev, and D. V. Petrov, "Atmospheric Pulsed Diffuse Discharge in Highly Non-Uniform Field to be Used for Sterilization and Decontamination," *15$^{th}$ IEEE Pulsed Power Conf.*, pp. 1421-1424, 2005.

[163] Z. Machala, L. Chladekova, and M. Pelach, “Plasma Agents in Bio-Decontamination by DC Discharges in Atmospheric Air,” *J. Phys. D: Appl. Phys.*, Vol. 43, No. 22, pp. 1-7, 2010.

[164] S. A. Hoenig, G. T. SilL, L. M. Kelley, and K. J. Garvey, “Destruction of Bacteria and Toxic Organic Chemicals by a Corona Discharge,” *Journal of the Air Pollution Control Association*, Vol. 30, No. 3, pp. 277-278, 1980.

[165] S. E. Gilliland, and M. L. Speck, “Inactivation of Microorganisms by Electrohydraulic Shock,” *Applied Microbiology*, Vol. 15, No. 5, pp. 1031-1037, 1967.

[166] N. J. Rowan, S. Espie, J. Harrower, J. G. Anderson, L. Marsili, and S. J. MacGregor, “Pulsed-Plasma Gas-Discharge Inactivation of Microbial Pathogens in Chilled Poultry Wash Water,” *J. Food Proc.*, Vol. 12, pp. 2708-2934, 2007.

[167] K. F. McDonald, R. D. Curry, T. E. Clevenger, B. J. Brazos, K. Unklesbay, A. Eisenstark, S. Baker, J. Golden, and R. Morgan, “The Development of Photosensitized Pulsed and Continuous Ultraviolet Decontamination Techniques for Surfaces and Solutions,” *IEEE Trans. Plasma Sci.*, Vol. 28, No. 1, pp. 89-96, 2000.

[168] J. G. Anderson, N. J. Rowan, S. J. Macgregor, R. A. Fouracre, and O. Farish, “Inactivation of Food-Borne Enteropathogenic Bacteria and Spoilage Fungi Using Pulsed-Light,” *IEEE Trans. Plasma Sci.*, Vol. 28, No. 1, pp. 83-88, 2000.

[169] K. S. Cole, *Membranes, Ions and Impulses*. Berkeley: University of California Press, 1972.

[170] K. Kinosita, and T. Y. Tsong, “Hemolysis of Human Erythrocytes by Transient Electric Field,” *Proc. Natl. Acad. Sci. USA*, Vol. 74, No. 5, pp. 1923-1927, 1977.

[171] D. C. Chang, 1992. Structure and Dynamics of Electric Field-Induced Membrane Pores as Revealed by Rapid-Freezing Electron Microscopy. In: D.

C. Chang, B. M. Chassy, J. A. Saunders, and A. E. Sowers ed. *Guide to Electroporation and Electrofusion*. San Diego: Academic Press, pp. 9-27.

[172] U. Zimmermann, J. Vienken, and G. Pilwat, "Development of Drug Carrier Systems: Electrical Field Induced Effects in Cell Membranes," *J. Electroanal. Chem.*, Vol. 116, pp. 553-574, 1980.

[173] T. Kotnik, and D. Miklavcic, "Analytical Description of Transmembrane Voltage Induced by Electric Fields on Spheroidal Cells," *Biophys. J.*, Vol. 79, PP. 670-679, 2000.

[174] R. P. Joshi, and K. H. Schoenbach, "Electroporation Dynamics in Biological Cells Subjected to Ultrafast Electrical Pulses: A Numerical Simulation Study," *Phys. Rev. E*, Vol. 62, No. 1, pp. 1025-1033, 2000.

[175] J. Bernhardt, and H. Pauly, "On the Generation of Potential Differences across the Membranes of Ellipsoidal Cells in an Alternating Electrical Field," *Biophysik*, Vol. 10, No. 1, pp. 89-98, 1973.

[176] K. Kinosita, and T. Y. Tsong, "Voltage-Induced Pore Formation and Hemolysis of Human Erythrocytes," *Biochim. Biophys. Acta*, Vol. 471, No. 2, pp. 227-242, 1977.

[177] R. Narsetti, R. D. Curry, K. F. McDonald, T. E. Clevenger, and L. M. Nichols, "Microbial Inactivation in Water Using Pulsed Electric Fields and Magnetic Pulse Compressor Technology," *IEEE Trans. Plasma Sci.*, Vol. 34, No. 4, pp. 1386-1393, 2006.

[178] K. Huang, and J. Wang, "Designs of Pulsed Electric Fields Treatment Chambers for Liquid Foods Pasteurization Process: A Review," *Journal of Food Engineering*, Vol. 95, No. 2, pp. 227-239, 2009.

[179] T. Grahl, and H. Markl, "Killing of Microorganisms by Pulsed Electric Fields," *Applied Microbiology and Biotechnology*, Vol. 45, No. 1, pp. 148-157, 1996.

[180] J. E. Dunn, and J. S. Pearlman, Methods and Apparatus for Extending the Shelf Life of Fluid Food Products. US Patent 4,695,472, 1987.

[181] Y. Matsumoto, T. Satake, N. Shioji, and A. Sakuma, “Inactivation of Microorganisms by Pulsed High Voltage Application,” *Industry Applications Society Annual Meeting*, pp. 652–659, 1991.

[182] Q. Zhang, G. V. Barbosa-Cánovas, and B. G. Swanson, “Engineering Aspects of Pulsed Electric Field Pasteurization,” *J. Food Eng.*, Vol. 25, No. 2, pp. 261-281, 1995.

[183] B. L. Qin, U. R. Pothakamury, G. V. Barbosa-Cánovas, B. G. Swanson, and M. Peleg, “Nonthermal Pasteurization of Liquid Foods Using High-Intensity Pulsed Electric Fields,” *Crit. Rev. Food Sci. Nutr.*, Vol. 36, No. 6, pp. 603-627, 1996.

[184] I. Sensoy, Q. H. Zhang, and A. K. Sastry, “Inactivation Kinetics of *Salmonella dublin* by Pulsed Electric Field,” *Journal of Food Process Engineering*, Vol. 20, No. 5, pp. 367-381, 1997.

[185] B. L. Qin, G. V. Barbosa-Canovas, B. G. Swanson, P. D. Pedrow, and R. G. Olsen, “Inactivating Microorganisms using A Pulsed Electric Field Continuous Treatment System,” *IEEE Trans. Ind. Appl.*, Vol. 34, No. 1, pp. 43-50, 1998.

[186] B. Qin, Q. Zhang, G. V. Barbosa-Canovas, B. G. Swanson, and P. D. Pedrow, “Pulsed Electric Field Treatment Chamber Design for Liquid Food Pasteurization Using A Finite Element Method,” *Transactions of the ASAE.*, Vol. 38, No. 2, pp. 557-565, 1995.

[187] M. Pizzichemi, and P. D. G. Occhialini, “Application of Pulsed Electric Fields to Food Treatment,” *Nuclear Physics B: Proceeding Supplements*, Vol. 172, pp. 314-316, 2007.

[188] P. Lubicki, and S. Jayaram, “High Voltage Pulse Application for the Destruction of the Gram-negative Bacterium *Yersinia enterocolitica*,” *Bioelectrochem. Bioenergetics*, Vol. 43, No. 1, pp. 135-141, 1997.

[189] B. M. Novac, F. Babakhr, I. R. Smith, L. Pecastaing, R. Ruscassic, A. D. Ferron, and P. Pignolet, “Demonstration of a Novel Pulsed Electric Field

Technique Generating Neither Conduction Currents Nor Joule Effects", *IEEE Trans. Plasma Sci.*, Vol. 42, No. 1, pp. 216-228, 2014.

[190] D. Gášková, K. Sigler, B. Janderová, and J. Plášek, "Effect of High-Voltage Electric Pulses on Yeast Cells: Factors Influencing the Killing Efficiency," *Bioelectrochem. Bioenergetics*, Vol. 39, No. 2, pp. 195-202, 1996.

[191] K. Aronsson, and U. Ronner, "Influence of pH, Water Activity and Temperature on the Inactivation of *Escherichia coli* and *Saccharomyces cerevisiae* by Pulsed Electric Fields", *Innovative Food Sci. Emerging Technologies*, Vol. 2, No. 2, pp. 105-112, 2001.

[192] H. E. Jacob, W. Forster, H. Berg, "Microbiological Implications of Electric Field Effects II. Inactivation of Yeast Cells and Repair of their Cell Envelope," *Journal of Basic Microbiology*, Vol. 21, No. 3, pp. 225-233, 1981.

[193] S. L. Harrison, G. V. Barbosa-Canovas, and B. G. Swanson, "*Saccharomyces cerevisiae* Structural Changes Induced by Pulsed Electric Field Treatment," *LWT - Food Science and Technology*, Vol. 30, No. 3, pp. 236-240, 1997.

[194] A. Mizuno, and Y. Hori, "Destruction of Living Cells by Pulsed High-Voltage Application," *IEEE Transactions on Industry Applications*, Vol. 24, No. 3, pp. 387-394, 1988.

[195] Q. Zhang, F. Chang, G. V. Barbosa-Canovas, and B. G. Swanson, "Inactivation of Microorganisms in a Semisolid Model Food Using High Voltage Pulsed Electric Fields," *LWT - Food Science and Technology*, Vol. 27, No. 6, pp. 538-543, 1994.

[196] T. Ohshima, K. Sato, H. Terauchi, and M. Sato, "Physical and Chemical Modifications of High-Voltage Pulse Sterilization," *Journal of Electrostatics*, Vol. 42, No. 1-2, pp. 159-166, 1997.

[197] G. A. Evrendilek, Q. H. Zhang, and E. R. Richter, "Inactivation of *Escherichia coli* O157:H7 and *Escherichia coli* 8739 in Apple Juice by Pulsed Electric Fields," *Journal of Food Protection*, Vol. 62, No. 7, pp. 793-796, 1999.

[198] H. Hulsheger, and E. G. Niemann, “Lethal Effect of High Voltage Pulses on *E. coli* K12,” *Radiat. Eniron. Biophys.*, Vol. 18, No. 4, pp. 281-288, 1980.

[199] U. R. Pothakamury, H. V. Mercado, Q. Zhang, G. V. Barbosa-Cánovas, and B. G. Swanson, “Effect of Growth Stage and Processing Temperature on the Inactivation of *E. coli* by Pulsed Electric Fields,” *J. Food Protect.*, Vol. 59, No. 11, pp. 1167-1171, 1996.

[200] H. V. Mercado, O. M. Belloso, F. J. Chang, G. V. Barbosa-Cánovas, and B. G. Swanson, “Inactivation of *Escherichia coli* and *Bacillus subtilis* Suspended in Pea Soup Using Pulsed Electric Fields,” *J. Food Proc. Pres.*, Vol. 20, No. 6, pp. 501–510, 1996.

[201] H. V. Mercado, U. R. Pothakamury, F. J. Chang, Q. Zhang, G. V. Barbosa-Cánovas, and B. G. Swanson, “High Voltage Pulsed Electric Fields, pH, Ionic Strength and the Inactivation of *E. coli*,” *Food Research International*, Vol. 29, No. 2, pp. 117-121, 1996.

[202] H. Hulsheger, J. Potel, and E. G. Niemann, “Electric Field Effects on Bacteria and Yeast Cells,” *Radiat. Eniron. Biophys.*, Vol. 22, No.2, pp. 149-162, 1983.

[203] K. H. Schoenbach, F. E. Peterkin, R. W. Alden, III, and S. J. Beebe, “The Effect of Pulsed Electric Fields on Biological Cells: Experiments and Applications,” *IEEE Trans. Plasma Sci*., Vol. 25, No. 2, pp. 284-292, 1997.

[204] C. J. McDonald, S. W. Lloyd, M. A. Vitale, K. Petersson, and F. Innings, “Effects of Pulsed Electric Fields on Microorganisms in Orange Juice Using Electric Field Strengths of 30 and 50 kV/cm,” Journal of Food Science, Vol. 65, No. 6, pp. 984-989, 2000.

[205] P. Love, “Correlation of Fourier Transforms of Pulsed Electric Field Waveform and Microorganism Inactivation,” *IEEE Trans. Dielectr. Electr. Insul.*, Vol. 5, No. 1, pp. 142-147, 1998.

[206] R. M. Campbell, 2006. *On the Response of Biological Cells to Pulsed Electric Fields*. Unpublished PhD Thesis. University of Strathclyde.

[207] R. E. Bruhn, P. D. Pedrow, R. G. Olsen, G. V. Barbosa-Canovas, and B. G. Swanson, "Electrical Environment Surrounding Microbes Exposed to Pulsed Electric Fields," *IEEE Trans. Plasma Sci.*, Vol. 4, No. 6, pp. 806-812, 1997.

[208] S. Y. Ho, G. S. Mittal, J. D. Cross, and M. W. Griffiths, "Inactivation of *Pseudomonas fluorescens* by High Voltage Electric Pulses," *J. Food Sci.*, Vol. 60, No. 6, pp. 1337-1343, 1995.

[209] T. Kotnik, D. Miklavcic, and L. M. Mir, "Cell Membrane Electropermeabilization by Symmetrical Bipolar Rectangular Pulses: Part II. Reduced Electrolytic Contamination," *Bioelectrochemistry*, Vol. 54, No. 1, pp. 91-95, 2001.

[210] J. W. Loomis-Husselbee, P. J. Cullen, R. F. Irvine, and A. P. Dawson, "Electroporation can Cause Artefacts Due to Solubilization of Cations from the Electrode Plates," *Biochem. J.*, Vol. 277, No. 3, pp. 883-885, 1991.

[211] A. Sedriks, *Corrosion of Stainless Steels, 2nd ed*. New York: Wiley, 1996.

[212] S. H. Jayaram, "Sterilization of Liquid Foods by Pulsed Electric Fields," *IEEE Electrical Insulation Magazine*, Vol. 6, No. 6, pp. 17-25, 2000.

[213] A. H. El-Hag, S. H. Jayaram, O. R. Gonzalez, and M. W. Griffiths, "The Influence of Size and Shape of Microorganism on Pulsed Electric Field Inactivation," *IEEE Trans. Nanobiosci.*, Vol. 10, No. 3, pp. 133-138, 2011.

[214] N. J. Rowan, "Evidence that Inimical Food-Preservation Barriers Alter Microbial Resistance, Cell Morphology and Virulence," *Trends in Food Science and Technology*, Vol. 10, No. 8, pp. 261-270, 1999.

[215] P. C. Wouters, I. Alvarez, and J. Raso, "Critical Factors Determining Inactivation Kinetics by Pulsed Electric Field Food Processing," *Trends in Food Science and Technology*, Vol. 12, No. 3-4, pp. 112-121, 2001.

[216] R. Jeantet, F. Baron, F. Nau, M. Roignant, and G. Brulé, "High Intensity Pulsed Electric Fields Applied to Egg White: Effect on *Salmonella enteritidis* Inactivation and Protein Denaturation," *J. Food Proc.*, Vol. 62, No. 12, pp. 1381–1386, 1999.

[217] H. Hulsheger, J. Potel, and E. G. Niemann, “Killing of Bacteria with Electric Pulses of High Field Strength,” *Radiat. Eniron. Biophys.*, Vol. 20, No. 1, pp. 53-65, 1981.

[218] X. Liu, A. E. Yousef, and G. W. Chism, “Inactivation of *Escherichia coli* 0157:H7 by the Combination of Organic Acids and Pulsed Electric Field,” *J. Food Safety*, Vol. 16, No. 4, pp. 287-299, 1997.

[219] D. Garcia, N. Gomez, P. Manas, S. Condon, J. Raso, and R. Pagan, “Occurrence of Sublethal Injury after Pulsed Electric Fields Depending on the Micro-organism, the Treatment Medium pH and the Intensity of the Treatment Investigated,” *Journal of Applied Microbiology*, Vol. 99, No. 1, pp. 94-104, 2005.

[220] J. C. Weaver, and Y. A. Chizmadzhev, “Theory of Electroporation: A Review,” *Bioelectrochemistry and Bioenergetics*, Vol. 41, No. 2, pp. 135-160, 1996.

[221] T. E. Vaughan, and J. C. Weaver, 2012. A Theoretical Model for Cell Electroporation: Quantitative Description of Electrical Behavior. In F. Bersani ed. *Electricity and Magnetism in Biology and Medicine*. Springer Science & Business Media, pp. 433-435.

[222] C. L. Davey, and D. B. Kell, 1995. The Low-Frequency Dielectric Properties of Biological Cells. In D. Waltz, H. Berg, and G. Milazzo ed. *Bioelectrochemistry of Cells and Tissues.* Berlin: Birkauser, pp. 159-207.

[223] J. Gimsa, T. Müller, T. Schnelle, and G. Fuhr, “Dielectric Spectroscopy of Single Human Erythrocytes at Physiological Ionic Strength: Dispersion of the Cytoplasm,” *Biophys J.*, Vol. 71, No. 1, pp. 495-506, 1996.

[224] G. H. Markx, and C. L. Davey, “The Dielectric Properties of Biological Cells at Radiofrequencies: Applications in Biotechnology,” *Enzyme and Microbial Technology*, Vol. 25, No. 3-5, pp. 161-171, 1999.

[225] H. P. Schwan, “Electrical Properties of Tissues and Cell Suspensions: Mechanisms and Models,” *in Proc. 16$^{th}$ Annual Int. Conf. of IEEE*, Vol. 1, pp. 70-71, 1994.

[226] G. Cevc, “Membrane Electrostatics,” *Biochim. Biophys. Acta*, Vol. 1031, No. 3, pp. 311-382, 1990.

[227] Y. Huang, R. Holzel, R. Pethig, and X. Wang, “Differences in the AC Electrodynamics of Viable and Non-Viable Yeast Cells Determined through Combined Dielectrophoresis and Electrorotation Studies,” *Phys. Med. Bid.*, Vol. 37, No. 7, pp. 1499-1517, 1992.

[228] A. M. James, “The Electrical Properties and Topochemistry of Bacterial Cells,” *Adv. Coll. Interf. Sci.*, Vol. 15, No. 3-4, pp. 171-221, 1982.

[229] E. L. Carstensen, and R. E. Marquis, “Passive Electrical Properties of Microorganisms. III. Conductivity of Isolated Bacterial Cell Walls,” *Biophys. J.*, Vol. 8, No. 5, pp. 536-548, 1968.

[230] A. V. Loey, B. Verachtert, and M. Hendrickx, “Effects of High Electric Field Pulses on Enzymes,” *Trends in Food Science & Technology*, Vol. 12, No. 3-4, pp. 94-102, 2001.

[231] S. Y. Ho, G. S. Mittal, and J. D. Cross, “Effects of High Field Electric Pulses on the Activity of Selected Enzymes,” *J. Food Eng.*, Vol. 31, No. 1, pp. 69-84, 1997.

[232] O. Martín, B. L. Qin, F. J. Chang, G. V. Barbosa-Cánovas, and B. G. Swanson, “Inactivation of *Escherichia Coli* in Skim Milk by High Intensity Pulsed Electric Fields,” *Journal of Food Process Engineering*, Vol. 20, No. 4, pp. 317-336, 1997.

[233] N. J. Rowan, S. J. MacGregor, J. G. Anderson, D. Cameron, and O. Farish, “Inactivation of *Mycobacterium paratuberculosis* by Pulsed Electric Fields,” *Applied and Environmental Microbiology*, Vol. 67, No. 6, pp. 2833-2836, 2001.

[234] W. M. Haynes ed., *CRC Handbook of Chemistry and Physics, 95$^{th}$ ed.*, Boca Raton: CRC Press, 2014.

[235] Manual of the Square Impulse Generator. *SAMTECH Ltd. (UK).*

[236] F. F. Madkour, A. E. Kamil, and H. S. Nasr, “Production and Nutritive Value of *Spirulina platensis* in Reduced Cost Media,” *Egyptian Journal of Aquatic Research*, Vol. 38, No. 1, pp. 51-57, 2012.

[237] M. Coustets and J. Teissie, “The Use of Pulsed Electric Fields for Protein Extraction from *Nanochloropsis* and *Chlorella*,” *Proc. IFMBE*, Vol. 53, pp. 405-408, 2015.

[238] M. W. Washburne, L. E. Braun, G. C. Johnston, and R. A. Singer, “Stationary Phase in the Yeast *Saccharomyces cerevisiae*,” *Microbiological Reviews*, Vol. 57, No. 2, pp. 383-401, 1993.

[239] I. Stefanini, L. Dapporto, J. Legras, A. Calabretta, M. Di Paola, C. De Filippo, R. Viola, P. Capretti, M. Polsinelli, S. Turillazzi, and D. Cavalieri, “Role of Social Wasps in *Saccharomyces cerevisiae* Ecology and Evolution,” *Proceedings of the National Academy of Sciences of the USA*, Vol. 109, No. 33, pp. 13398-13403, 2012.

[240] J. R. McMillan, I. A. Watson, M. Ali, and W. Jaafar, “Evaluation and Comparison of Algal Cell Disruption Methods: Microwave, Waterbath, Blender, Ultrasonic and Laser Treatment,” *Applied Energy*, Vol. 103, pp. 128-134, 2013.

[241] K. Aronsson, M. Lindgren, B. R. Johansson, and U. Ronner, “Inactivation of Microorganisms Using Pulsed Electric Fields: The Influence of Process Parameters on *Escherichia coli, Listeria innocua, Leuconostoc mesenteroides* and *Saccharomyces cereisiae*”, *Innovative Food Sci. Emerging Technologies*, Vol. 2, No. 1, pp. 41-54, 2001.

[242] T. Meissner and F. J. Wentz, “The Complex Dielectric Constant of Pure and Sea Water from Microwave Satellite Observations,” *IEEE Trans. Geosci. Remote Sens.*, Vol. 42, No. 9, pp. 1836-1849, 2004.

[243] M. S. P. Sarah, M. Z. Musa, M. N. Asiah, and M. Rusop, “Electrical Conductivity Characteristics of $TiO_2$ Thin Film,” *in Proc. Int. Conf. on Electronic Devices, Systems and Applications (ICEDSA),* pp. 361-364, 2010.

[244] A. V. Hippel, R. G. Breckenridge, F. G. Chesley, and L. Tisza, "High Dielectric Constant Ceramics," *Industrial and Engineering Chemistry*, Vol. 38, No. 11, pp. 1097-1109, 1946.

[245] A. Wypych, I. Bobowska, M. Tracz, A. Opasinska, S. Kadlubowski, A. Krzywania-Kaliszewska, J. Grobelny, and P. Wojciechowski, "Dielectric Properties and Characterisation of Titanium Dioxide Obtained by Different Chemistry Methods," *Journal of Nanomaterials*, Vol. 2014, 2014.

[246] M. D. Earle, "The Electrical Conductivity of Titanium Dioxide," *Phys. Rev.* Vol. 61, pp. 56-62, 1942.

[247] Paschen Curve: Voltage Breakdown vs Pressure. [Online] Available at: http://www.highvoltageconnection.com/articles/paschen-curve.html. [Assessed 23 April 2016].

[248] P. C. Maness, S. Smolinski, D. M. Blake, Z. Huang, E. J. Wolfrum, and W. A. Jacoby, "Bactericidal Activity of Photocatalytic $TiO_2$ Reaction: toward an Understanding of Its Killing Mechanism," *Applied and Environmental Microbiology*, Vol. 65, No. 9, pp. 4094–4098, 1999.

[249] K. Sunada, Y. Kikuchi, K. Hashimoto, and A. Fujishima, "Bactericidal and Detoxification Effects of $TiO_2$ Thin Film Photocatalysts," *Environ. Sci. Technol.*, Vol. 32, No. 5, pp. 726–728, 1998.

[250] C. Hu, Y. Lan, J. Qu, X. Hu, and A. Wang, "Ag/AgBr/$TiO_2$ Visible Light Photocatalyst for Destruction of Azodyes and Bacteria," *J. Phys. Chem. B.*, Vol. 110, No. 9, pp. 4066-4072, 2006.

[251] O. Akhavan, and E. Ghaderi, "Photocatalytic Reduction of Graphene Oxide Nanosheets on $TiO_2$ Thin Film for Photoinactivation of Bacteria in Solar Light Irradiation," *J. Phys. Chem. C.*, Vol. 113, No. 47, pp. 20214-20220, 2009.

[252] T. Matsunaga, R. Tomoda, T. Nakajima, and H. Wake, "Photoelectrochemical Sterilization of Microbial Cells by Semiconductor Powders," *FEMS Microbiology Letters*, Vol.29, No. 1-2, pp. 211 – 214, 1985.

[253] J. Hayes, D. Kirf, M. Garvey, and N. Rowan, "Disinfection and Toxicological Assessments of Pulsed UV and Pulsed-Plasma Gas-Discharge Treated-Water Containing the Waterborne Protozoan Enteroparasite *Cryptosporidium parvum*," *Journal of Microbiological Methods*, Vol. 94, pp 325-337, 2013.

[254] D. Kirf, C. L. Higginbotham, N. J. Rowan, and S. M. Devery, "Cyto- and Genotoxicological Assessment and Functional Characterization of *N*-vinyl-2-pyrrolidone–acrylic Acid-Based Copolymeric Hydrogels with Potential for Future Use in Wound Healing Applications," *Biomed. Mater.*, Vol. 5, No. 3, pp. 1-11, 2010.

[255] H. Farrell, J. Hayes, J. Laffey, and N. Rowan, "Studies on the Relationship between Pulsed UV Light Irradiation and the Simultaneous Occurrence of Molecular and Cellular Damage in Clinically-Relevant *Candida albicans*," *Journal of Microbiological Methods*, Vol. 84, pp. 317-326, 2011.

[256] S. Griffiths, M. Maclean, J. G. Anderson, S. J. MacGregor, and M. H. Grant, "Inactivation of Microorganisms within Collagen Gel Biomatrices Using Pulsed Electric Field Treatment," *J. Mater. Sci.: Mater. Med.*, Vol. 23, pp. 507-515, 2012.

[257] J. Wall. (2009) Transient Heat Conduction: Analytical Methods. [Online] Available at: http://www.ewp.rpi.edu/hartford/~wallj2/CHT/Notes/ch05.pdf [Assessed 21 May 2016].

[258] S. Griffiths, S. Smith, S. J. MacGregor, J. G. Anderson, C. Van der Walle, J. R. Beveridge, and M. H. Grant, "Pulsed Electric Field Treatment as A Potential Method for Microbial Inactivation in Scaffold Materials for Tissue Engineering: The Inactivation of Bacteria in Collagen Gel," *Journal of Applied Microbiology*, Vol. 105, No. 4, pp. 963-969, 2008.

[259] J. R. Beveridge, K. Wall, S. J. MacGregor, J. G. Anderson, and N. J. Rowan, "Pulsed Electric Field Inactivation of Spoilage Microorganisms in Alcoholic Beverages," *Proc. IEEE*, Vol. 92, No. 7, pp. 1138-1147, 2004.

# LIST OF PUBLICATIONS

## Peer Reviewed Journal Papers

- S. Qin, I. Timoshkin, M. Wilson, M. Maclean, S. MacGregor, M. Given, J. Anderson, and T. Wang, "Pulsed Electric Field Treatment of Microalgae: Inactivation Tendencies and Energy Consumption", *IEEE Trans. Plasma Sci.*, Vol. 42, No. 10, pp. 3191-3196, Oct. 2014.

- S. Qin, I. Timoshkin, M. Maclean, M. Wilson, M. Given, T. Wang, J. Anderson, and S. MacGregor, "Pulsed Electric Field Treatment of *Saccharomyces cerevisiae* Using Different Waveforms," *IEEE Trans. Dielectrics and Electrical Insulation.*, Vol. 22, No. 4, pp. 1841-1848, Aug. 2015.

- S. Qin, I. Timoshkin, M. Maclean, S. MacGregor, M. Wilson, M. Given, T. Wang, and J. Anderson, "$TiO_2$-Coated Electrodes for Pulsed Electric Field Treatment of Microorganisms," Accepted by *IEEE Trans. Plasma Sci.*, to be published in Oct. 2016.

## Conference Proceedings and Presentations

- S. Qin, I. Timoshkin, M. Wilson, M. Maclean, S. MacGregor, M. Given, J. Anderson, and T. Wang, "Pulsed Electric Field Assisted Treatment of Microorganisms for Lysis," *in Proc. 19$^{th}$ IEEE. Pulsed Power Conf., (PPC)*, pp. 1-5, San Francisco, California, USA, 16$^{th}$-21$^{st}$ Jun. 2013.

- S. Qin, and I. V. Timoshkin, "Pulsed Electric Field Assisted Treatment of Algae for Bio-Fuel Production: Modelling and Analytical Evaluation of PEF Treatment," 6$^{th}$ *UHVnet colloquium*, Glasgow, UK, 16$^{th}$-17$^{th}$ Jan. 2013.

- S. Qin, I. Timoshkin, M. Maclean, M. Wilson, S. MacGregor, M. Given, J. Anderson, and T. Wang, "Pulsed Electric Field Treatment on Microorganisms," *12$^{th}$ Technological Plasma Workshop (TPW)*, Coventry, UK, 15$^{th}$-16$^{th}$ Oct. 2014.

# APPENDIX A:

# DERIVATION OF ANALYTICAL EXPRESSION FOR TRANSIENT FIELD IN THE MEMBRANE IN DIELECTRIC PEF CELL

## A.1 The Effective Field in the PEF Cell

Analysis in Appendix A.1 and A.2 follows the analytical work in [6] and presents the derivation of Equation III.3-III.6 used in Chapter III. A dielectric PEF test cell which consists of two identical parallel slabs of high permittivity ceramic was introduced in [6], as shown in Figure A.1. The space between the dielectric slabs is the treatment region of the PEF test cell which contains microorganism suspension. The other surface of the dielectric slabs is connected to a metal layer, forming the HV and ground electrodes.

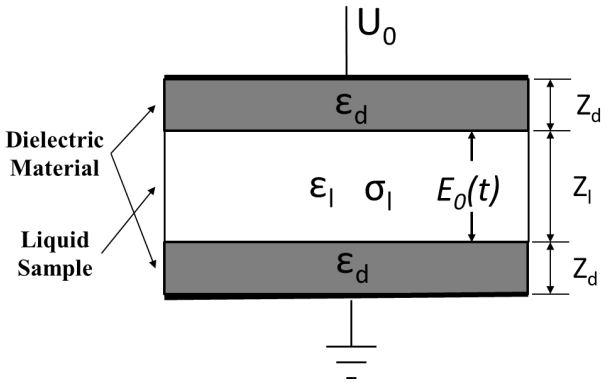


**Figure A.1** Schematic diagram of the PEF test cell with dielectric slabs proposed in [6].

To analysis the dynamic of the electric field inside the treatment region, the Ohmic conduction approach, described in [194], was applied in [6]. In this approach, the electrical potentials of different regions in the dielectric PEF test cell was written as:

$$\varphi_1(z,t) = -A_1(t) \cdot z + B_1(t)\ ;$$

$$\varphi_2(z,t) = -A_2(t) \cdot z + B_2(t)\,; \tag{A.1}$$

$$\varphi_3(z,t) = -A_3(t) \cdot z + B_3(t)\,.$$

where $\varphi_1$ and $\varphi_3$ are the potentials in the two ceramic slabs and the potential in the treatment region, is $\varphi_3$. The time-dependent coefficients, $A_x(t)$ and $B_x(t)$, were determined from the boundary conditions at the liquid-dielectric and the electrode-dielectric interfaces, where electrical potentials across these interfaces are equal:

$$\varphi_1(0,t) = U_0 \cdot f(t)\,;$$

$$\varphi_1(z_d,t) = \varphi_2(z_d,t)\,; \tag{A.2}$$

$$\varphi_2(z_d + z_l,t) = \varphi_3(z_d + z_l,t)\,;$$

$$\varphi_3(L,t) = 0\,.$$

where $U_0 \cdot f(t)$ describes the external voltage applied to the chamber. In [6], this external voltage source was a unit step function with potential $U_0$ at a time $t = 0^+$. $L = 2 \cdot z_d + z_l$ is the distance between the two electrodes. These boundary conditions assume that there is no distributed space charge in the dielectrics.

A second boundary condition was obtained as accumulation of free electrical surface charges takes place along the dielectric-liquid interface due to the conduction in the liquid. This charge continuity condition determines that the rate of change of the surface charge density equals the difference between the conduction current densities on either side of the boundary. Assuming the dielectric barriers are non-conductive ($\sigma_d$=0), this charge continuity boundary conditions at the liquid-dielectric interfaces were written as:

$$J_l - J_d = \sigma_l E_0(t) - \sigma_d E_d(t) = -\frac{\partial \gamma_s(t)}{\partial t} \tag{A.3}$$

$$\gamma_s(t) = \varepsilon_0 \varepsilon_l E_0(t) - \varepsilon_0 \varepsilon_d E_d(t) \quad \text{(A.4)}$$

$$\vec{E} = -\vec{\nabla}\varphi \quad \text{(A.5)}$$

where $J_l$ and $J_d$ are the conduction current densities on either side of the boundary; $\gamma_s(t)$ is the free surface charge at the boundaries; $E_0(t)$ and $E_d(t)$ are the electric fields in the treatment region and the dielectric barriers, respectively; and $\varepsilon_0$ is the permittivity of free space.

Therefore, the time dependent effective field in the treatment region, $E_0(t)$, was obtained by substituting the potential (Equation A.1) into boundary conditions (Equation A.2-A.5). The solution of the resulting equations provides an expression for $E_0(t)$:

$$E_0(t) = E_L e^{-t/\tau_f} \quad \text{(A.6)}$$

$$E_L = U_0 \left( z_l + 2 \frac{\varepsilon_l}{\varepsilon_d} z_d \right)^{-1} \quad \text{(A.7)}$$

$$\tau_f = \left( \frac{\varepsilon_l}{\varepsilon_d} + 2 \frac{Z_l}{Z_d} \right) \frac{\varepsilon_0 \varepsilon_d}{\sigma_l} \quad \text{(A.8)}$$

where $E_L$ is the Laplacian electric field in the treatment region and $\tau_f$ is the characteristic field relaxation time, also calls Maxwell-Wagner relaxation time. This time determines the time of existence of the field in the liquid due to the Maxwell-Wagner surface polarization mechanism.

## A.2 Transient Membrane Potential

To investigate the transient potential across the membrane when microbial cell is subjected to the external electric field in the dielectric PEF test cell, a spherical model of a microorganism cell was employed in [6]. As demonstrated in Figure A.2,

the membrane of the microbial cell was modelled as a non-conducting spherical shell, which enclosed the cytoplasm and suspended in the surrounding liquid.

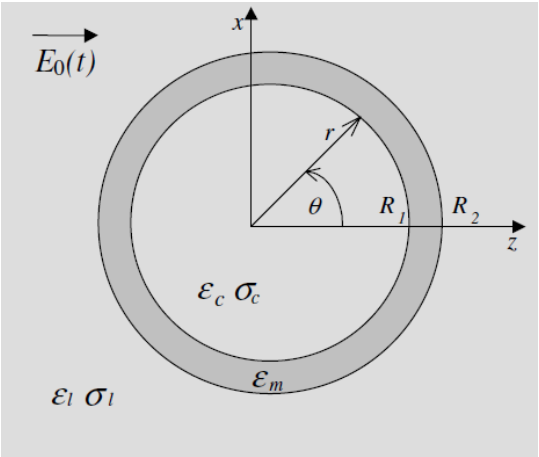


**Figure A.2** Spherical shell model of a microbial cell. Figure taken from [6].

To obtain the transient response of the membrane to a time-varying electric field $E_0(t)$, a spherical coordinate system was used in [6] and the same Ohmic conduction approach was applied in [6]. The potentials in the cytoplasm, membrane and the surrounding liquid were written as:

$$\varphi_c(r,t) = A_c(t) \cdot r\cos\theta \ ;$$

$$\varphi_m(r,t) = A_m(t) \cdot r\cos\theta + B_m(t) \cdot r^{-2}\cos\theta \ ; \qquad \text{(A.9)}$$

$$\varphi_l(r,t) = -E_0(t) \cdot r\cos\theta + B_l(t) \cdot r^{-2}\cos\theta .$$

where $\varphi_c$, $\varphi_m$ and $\varphi_l$ are the potentials in the cytoplasm, membrane and the surrounding liquid respectively. To obtain the time dependent membrane potential, the coefficients $A_m(t)$ and $B_m(t)$ need to be solved, which can be done by analysing the boundary conditions. The boundary conditions at $R_1$ and $R_2$ can be defined as the potentials and the electric flux density on either side of the membrane-cytoplasm and liquid-membrane boundaries are equal:

$$\varphi_c(R_1,t) = \varphi_m(R_1,t)\,;$$

$$\varphi_m(R_2,t) = \varphi_l(R_2,t)\,; \tag{A.10}$$

$$\sigma_c E_{rc}(t) = -\varepsilon_0\varepsilon_l \frac{\partial E_{rc}(t)}{\partial t} + \varepsilon_0\varepsilon_m \frac{\partial E_{rm}(t)}{\partial t}\,;$$

$$\sigma_l E_{rl}(t) = \varepsilon_0\varepsilon_m \frac{\partial E_{rm}(t)}{\partial t} - \varepsilon_0\varepsilon_l \frac{\partial E_{rl}(t)}{\partial t}\,.$$

where $E_{rc}(t)$, $E_{rm}(t)$ and $E_{rl}(t)$ are the normal components of the electric field in the cytoplasm, membrane and the surrounding liquid respectively. By solving the boundary equations, the coefficients $A_m(t)$ and $B_m(t)$ were obtained in [6] and expressed as:

$$A_m(t) = \frac{-3E_L}{\tau_1\tau_2 - 2(R_1/R_2)^3\tau_3\tau_4}$$

$$\times\left[\frac{e^{-t/\tau_f}}{k}\left(1 - \frac{\tau_l+\tau_1}{\tau_f} + \frac{\tau_l\tau_1}{\tau_f^2}\right)\right. \tag{A.11}$$

$$-\frac{e^{-t/\tau_5}}{\lambda}\left(1 - \frac{\tau_l+\tau_1}{\tau_5} + \frac{\tau_l\tau_1}{\tau_5^2}\right)$$

$$\left.-\frac{e^{-t/\tau_6}}{\mu}\left(1 - \frac{\tau_l+\tau_1}{\tau_6} + \frac{\tau_l\tau_1}{\tau_6^2}\right)\right]$$

$$B_m(t) = \frac{3E_L R_1^3}{\tau_1\tau_2 - 2(R_1/R_2)^3\tau_3\tau_4}$$

$$\times\left[\frac{e^{-t/\tau_f}}{k}\left(1-\frac{\tau_l+\tau_3}{\tau_f}+\frac{\tau_l\tau_3}{\tau_f^2}\right)\right. \tag{A.12}$$

$$-\frac{e^{-t/\tau_5}}{\lambda}\left(1-\frac{\tau_l+\tau_3}{\tau_5}+\frac{\tau_l\tau_3}{\tau_5^2}\right)$$

$$\left.-\frac{e^{-t/\tau_6}}{\mu}\left(1-\frac{\tau_l+\tau_3}{\tau_6}+\frac{\tau_l\tau_3}{\tau_6^2}\right)\right]$$

where $\tau_l = \varepsilon_0\varepsilon_l/\sigma_l$ is the liquid characteristic time, which determines the duration of accumulation of free charges on the external membrane surface. Coefficients $\tau_1$-$\tau_6$ are expressed as:

$$\tau_1 = \frac{2\varepsilon_m+\varepsilon_l}{\sigma_c}\varepsilon_0\,; \qquad \tau_2 = \frac{2\varepsilon_l+\varepsilon_m}{\sigma_l}\varepsilon_0\,;$$

$$\tau_3 = \frac{\varepsilon_l-\varepsilon_m}{\sigma_c}\varepsilon_0\,; \qquad \tau_4 = \frac{\varepsilon_l-\varepsilon_m}{\sigma_l}\varepsilon_0\,; \tag{A.13}$$

$$\tau_{5,6} = \frac{2}{p \mp (p^2-4q)^{1/2}}\,.$$

where coefficients $p$ and $q$ are:

$$p = \frac{(\tau_1+(\tau_2/2)-(R_1/R_2)^3(\tau_3+\tau_4))}{((\tau_1\tau_2/2)-(R_1/R_2)^3\tau_3\tau_4)} \tag{A.14}$$

$$q = \frac{(1-(R_1/R_2)^3)}{((\tau_1\tau_2/2)-(R_1/R_2)^3\tau_3\tau_4)} \tag{A.15}$$

and coefficients $k$, $\lambda$ and $\mu$ are expressed as:

$$k = \frac{1}{\tau_5\tau_6}-\frac{1}{\tau_f}\left(\frac{1}{\tau_5}+\frac{1}{\tau_6}\right)+\frac{1}{\tau_f^2}\,;$$

$$\lambda = \frac{1}{\tau_5\tau_6} - \frac{1}{\tau_f}\left(\frac{1}{\tau_6} - \frac{1}{\tau_5}\right) + \frac{1}{\tau_5^2}; \tag{A.16}$$

$$\mu = \frac{1}{\tau_5\tau_6} - \frac{1}{\tau_f}\left(\frac{1}{\tau_5} - \frac{1}{\tau_6}\right) + \frac{1}{\tau_6^2}.$$

Now with the coefficients $A_m(t)$ and $B_m(t)$ solved, the electric field at the membrane can now be expressed as:

$$E_m(r,t) = -\frac{\partial\varphi_m(r,t)}{\partial r} = -A_m(t) + 2B_m(t)\cdot r^3 \tag{A.17}$$

The field at the membrane's poles ($r=R_1$), where $\cos\theta = 1$, has no tangential components and therefore can reach its maximal value. Therefore, the time dependent maximum electric field on the membrane can now be written as:

$$E_{max}(t) = -A_m(t) + 2B_m(t)\cdot R_1^3 \tag{A.18}$$

# APPENDIX B:

# PUBLISHED WORK

## Pulsed Electric Field Treatment of Microalgae: Inactivation Tendencies and Energy Consumption

Si Qin, Igor V. Timoshkin, *Member, IEEE*, Michelle Maclean, Mark P. Wilson, *Member, IEEE*, Scott J. MacGregor, *Member, IEEE*, Martin J. Given, *Senior Member, IEEE*, John G. Anderson, and Tao Wang

***Abstract*— Pulsed electric field (PEF) treatment can be used to facilitate microbial cell lysis. The aim of this paper is to investigate this effect of PEF treatment on microalgae. The PEF system used in this paper consists of a pulse generator and treatment cell with parallel-plane metallic electrodes. The PEF treatment of microalgae, *Spirulina*, was conducted using 33.3- and 66.7-kV/cm electric field impulses. The efficiency of the PEF treatment for inactivation of microalgae was assessed by comparison of the growth curves of PEF-treated and untreated samples. Results showed that growth of microalgae can be stopped by the application between 100 and 500 high-field impulses with field magnitude 33.3 kV/cm. When the field is increased to a magnitude of 66.7 kV/cm, the growth of microalgae can be stopped by application of 50 impulses. Overall, this paper confirms that PEF treatments can be used for the inactivation of algae and the energy consumption of the PEF process can be reduced using suspensions with lower electrical conductivity.**

***Index Terms*— Inactivation, microalgae, pulsed electric field (PEF).**

### I. INTRODUCTION

HIGH-VOLTAGE impulses, with durations in the range of $10^{-8}$–$10^{-4}$ s, can be used to generate electromechanical stresses in biological membranes, which can, in turn, cause disruption of these membranes [1]. If the applied electric field is higher than a specific critical value, the electroporation process becomes irreversible [2], which inactivates the cell being treated. Pulsed electric field (PEF) treatment has been largely investigated for microbial inactivation and applications in the food industry [3]–[7].

Recently, this treatment has attracted attention as a potential process for facilitation of extraction of oil from green microalgae [8]–[13]. In [8], exponentially decaying HV pulses with a characteristic decay time of 360 ns, which developed a uniform electric field with a peak magnitude of 45 kV/cm, were used for treatment of green microalgae, *Ankistrodesmus falcatus*. The PEF treatment cell had a parallel-plane topology and consisted of two stainless steel electrodes. The efficiency of the PEF treatment was assessed by comparison of lipid extraction and by microscopic inspection of an algae cell stained with propidium iodide. The PEF treatment with a specific energy of 26 MJ/kg (dry weight) resulted in ∼90% of the algae lysed and in a 130% increase in lipid yield as compared with untreated algae. Eing *et al*. [9] used 1-$\mu$s square impulses for PEF treatment of another type of microalgae, *Auxenochlorella protothecoides*. The magnitude of electric field, which was generated between two parallel-plane stainless steel electrodes was 35 kV/cm and the maximum specific energy of 2 MJ/kg was used in this paper. The efficiency of the PEF treatment was assessed by comparison of lipid extraction from the treated and untreated algae. It was shown that PEF treatment with 2 MJ/kg specific energy resulted in a 500% increase in lipid yield as compared with untreated samples.

The aim of this paper is to investigate the PEF treatment of another type of green algae, *Spirulina*, with a higher field magnitude in low-conductivity media to examine PEF inactivation efficacy and potential structural damage to microalgae. Square HV impulses of duration 1 $\mu$s and with a rate of voltage rise of ∼500 kV/$\mu$s were used in this paper. The uniformly distributed electric fields with magnitude of 33.3 kV/cm (similar to [9]) and with a higher magnitude of 66.7 kV/cm were used. Growth curves obtained from the optical density of algae solutions was used to assess the efficiency of PEF treatment. The energy consumption of PEF treatment was obtained and compared with the literature data.

Manuscript received December 7, 2013; revised March 19, 2014; accepted April 10, 2014.

The authors are with the Department of Electronic and Electrical Engineering, University of Strathclyde, Glasgow G1 1XW, U.K. (e-mail: s.qin@strath.ac.uk; igor.timoshkin@eee.strath.ac.uk; michelle.maclean@strath.ac.uk; m.wilson@eee.strath.ac.uk; s.macgregor@eee.strath.ac.uk; m.given@eee.strath.ac.uk; j.g.anderson@strath.ac.uk; tao.wang@eee.strath.ac.uk).

Digital Object Identifier 10.1109/TPS.2014.2317522

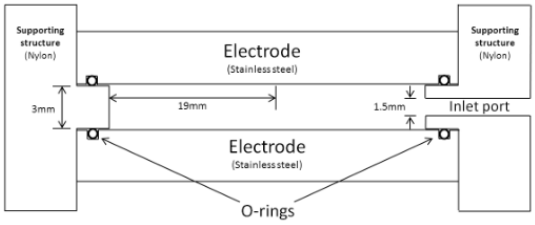


Fig. 1. Cross-sectional view of the PEF treatment cell.

### II. DEVELOPMENT OF THE PEF TREATMENT CELL AND PEF SYSTEM

A PEF treatment cell was designed and developed for this paper, a schematic diagram being shown in Fig. 1. The circular parallel-plane electrodes were made of stainless steel. The supporting structure of the treatment cell was made of nylon. The interelectrode gap is 3 mm, with two rubber O-rings used to seal the treatment cell. The liquid suspension of the algae is introduced into the cell through a 1.5-mm diameter inlet port on the side wall.

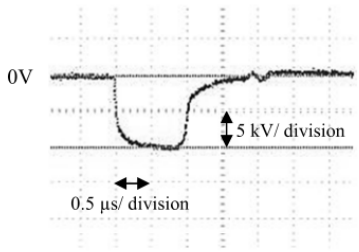


Fig. 2. Voltage waveforms across the PEF treatment cell during the PEF treatment.

The equivalent capacitance, $C$, and resistance, $R$, of the treatment sample were calculated according to

$$R = d/\sigma A \quad (1)$$

$$C = \varepsilon_0 \varepsilon_r A/d \quad (2)$$

where $d$ is the separation between the two electrodes, $A$ is the cross-sectional area of the exposed electrode surface, $\sigma$ is the conductivity of the liquid suspension, $\varepsilon_r$ is the relative permittivity of the liquid suspension, and $\varepsilon_0$ is the permittivity of free space. For a liquid with conductivity of 20 $\mu$S/cm and relative permittivity of 80, the resistance and capacitance of the treated sample were 1.3 k$\Omega$ and 268 pF, assuming that the gap length is 3 mm and an exposed surface area of 11.34 cm$^2$. The stray capacitance of the treatment cell was 21 pF, as measured by a Video Bridge 2160 (Electro Scientific Industries, Inc.). Therefore, the total capacitance of the treatment cell is 289 pF. The values of these parameters were used in calculations of the energy consumption of the PEF process.

The pulse generator used in this paper was manufactured by SAMTECH Ltd. (UK). This transmission-line-based system incorporates a voltage gain network, which allowed a voltage equal in magnitude to the charging voltage to be developed across a matched load. The pulse generator produces negative impulses of magnitude 30 kV and duration 1 $\mu$s, and can operate with pulse repetition rate from 0.1 to 10 pps (pulses per second).

The pulse generator has an output impedance of 50 $\Omega$ when incorporating the voltage gain network. For liquid with conductivity of a few tens of $\mu$S/cm, the equivalent resistance was $\sim$1 k$\Omega$. Therefore, a 50-$\Omega$ matching resistor was connected in parallel with the PEF treatment cell to match the 50-$\Omega$ output impedance of the PEF generator (including voltage gain network). A 1000:1 Tektronix P6015A high-voltage probe and a Tektronix TDS 2024 oscilloscope were used to monitor the voltage wave forms. An example of voltage waveform, developed across the PEF cell connected in parallel with the 50-$\Omega$ matching resistor is shown in Fig. 2.

## III. Experiment Procedure

The microalgae used in this paper were *Spirulina* green algae, grown for 35–40 days in a light incubator at 25 °C, under static conditions. The growth media was Zarrouk medium, [14], which is made up using sterile distilled water supplemented with $NaHCO_3$, $NaNO_3$, NaCl, $K_2SO_4$, and $K_2HPO_4$ (Sigma–Aldrich, UK). This growth media is highly conductive, with an electrical conductivity of 15–30 mS/cm. To prevent unnecessary dissipation of energy in the solution and reduction of voltage drop across the treatment cell, the *Spirulina* suspension was centrifuged at 4300 r/min for 10 min and resuspended in distilled water. Washing and resuspension of the microalgae in distilled water was carried out three times, resulting in significant reduction of the conductivity of the solution: the conductivity of all tested samples was in the range of 22.6 $\pm$ 4.5 $\mu$S/cm. The concentration of the microalgae in the solution was 13 g/l.

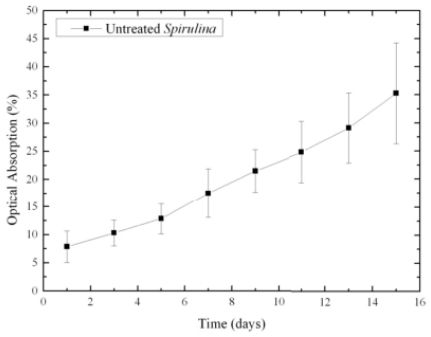


Fig. 3. Growth curve for untreated *Spirulina*. The *Spirulina* grew in a light incubator at 25 °C.

The PEF cell containing a suspension of microalgae was connected to the output of the pulse power supply. Two levels of voltage output were used 10 and 20 kV, with a pulse repetition rate of 1 pps. The resulting electric field strength in the treatment cell was 33.3 and 66.7 kV/cm, respectively. All PEF tests were repeated in triplicate.

Algae samples were subjected to different numbers of HV pulses: 50, 100, 500, and 1000. In the case of 500 and 1000 pulses, algae samples were mixed within the treatment cell after every 250 pulses to compensate for any sedimentation effects. After PEF treatment, the treated sample was removed from the treatment cell and 0.1 ml of the treated sample was transferred into 20 ml of fresh growth media and placed in a light incubator at 25 °C. A spectrophotometer (Thermo Spectronic Biomate 5) was used to measure the optical density (absorption) of the sample at 545 nm every 2 days for 15 days.

As the *Spirulina* culture grew, the sample became denser, leading to an increase in the optical absorption. Optical absorption was plotted as a function of time (the growth curve). By comparing the growth curves for treated and untreated (control) samples, the damage caused by the PEF treatment can be estimated. A typical growth curve for untreated algae is shown in Fig. 3.

## IV. Results and Discussion

### A. PEF Inactivation of Algae

The results shown in Figs. 4 and 5 show that the effect of PEF treatment on microalgae is significant. In the 10-kV (33 kV/cm) treated group, with 500 or more pulses,

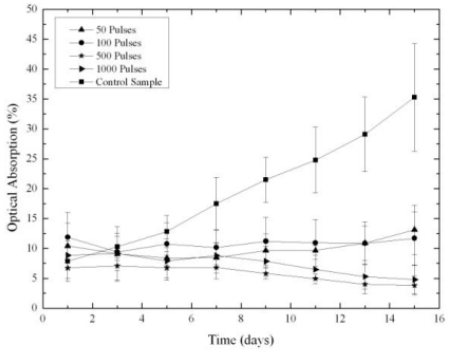


Fig. 4. Growth curves for PEF-treated (10 kV) and a nontreated (control) algae. Data points are the average value of triplicate tests (with the exception ofthe 50- and 100-pulses groups, in which one outlying group is excluded).

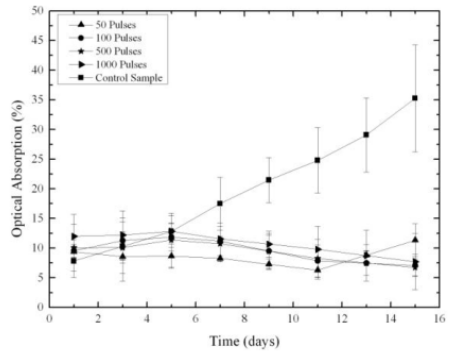


Fig. 5. Growth curves for PEF-treated (20 kV) and a nontreated (control) algae. Data points are the average value of triplicate tests.

no growth was observed by 15 days (optical absorption at day 15 even slightly decreased as compared with day 1, Fig. 4), which suggests that the vast majority of the algae had been inactivated by the applied impulses. With 50 and 100 pulses, optical density at day 15 was in general almost the same as at day 1 and the difference between the optical absorption for growth curves of these two groups of samples treated with 50 and 100 pulses is ∼7%. It must be noted that the inactivation efficacy with 50 and 100 pulses at 33 kV/cm was not consistent: two of the three replicate treatments demonstrated inactivation shown in Fig. 4 and a third run for both 50 and 100 pulses showed algae growth similar to that of the untreated control curve. These results highlight that although 50 and 100 pulses can inactivate the algae, the effect is not consistent with these electrical parameters (50 and 100 pulses at 33 kV/cm), and a larger number of impulses (500 and 1000) is required to achieve stable inactivation performance.

In the 20-kV (66.7 kV/cm) treatment (Fig. 5), the effect of the high-voltage impulses was more pronounced. Fig. 5 shows the growth curves for algae treated with 50, 100, 500, and 1000 impulses and the control (untreated) growth curve. This result indicates that virtually all microalgae have been inactivated after treatment with 50 impulses. Under these field conditions no treated sample showed an increasing optical density, indicating that a reliable inactivation of the algae had been achieved. The results of this paper show that inactivation of the microalgae can be achieved using ∼500 and more pulses at the field level of 33.3 kV/cm. When the field strength is doubled (66.7 kV/cm), the number of pulses required for inactivation is reduced to ∼50.

### *B. Temperature Measurement*

To check if the PEF treatment caused significant increases in the sample temperature, which could potentially contribute to microbial inactivation, the temperature of the treated samples was monitored using a thermocouple (Kane-May KM340, K-type) before and immediately after each test. These measurements showed that the PEF treatment regimes used in this paper did not cause significant temperature increase: the maximum registered increase in sample temperature did not exceed 2 °C. This is different from the PEF treatment reported in [8], which resulted in a 50 °C increase in the temperature of the sample when precooling of the algae suspension and ice-jacket cooling during treatment were employed. In this paper, the absence of temperature increase was a result of the use of the 50-Ω matching resistor in parallel with the treatment cell. The matching resistance is significantly smaller that the resistance of the liquid filled PEF treatment cell (∼1 kΩ). Therefore, most of the pulse energy was dissipated in the matching resistor rather than in the treated sample.

### *C. Energy Considerations*

The energy consumption during the PEF treatment was estimated using the equivalent circuit model. The PEF treatment cell was considered to form a parallel *RC* circuit. The resistance represents the conduction through the solution in the test cell. The capacitance represents the polarization of the solution within the test cell and can be modeled as an ideal capacitance in series with a resistance, $R_{\mathrm{ESR}}$ associated with the losses in these polarization processes. The energy consumption can therefore be divided into Joule energy dissipation and capacitive energy dissipation. The Joule energy dissipated in the PEF treatment cell, $E_{\mathrm{J}}$ is

$$E_{\mathrm{J}} = NV\,(t)^2\,t/R \tag{3}$$

where $N$ is the number of applied pulses, $V(t)$ is the voltage across the treatment cell, $t$ is the pulse duration, and $R$ is the equivalent resistance of the treatment cell calculated using (1). The conductivity of the liquid suspension depends on temperature which should be considered to ascertain potential changes in the equivalent resistance during the PEF treatment. It has been shown that, in this paper, the maximum increase in the conductivity due to the PEF treatment does not exceed ∼3.6%. Therefore, the constant value of the equivalent resistance obtained by (1) was used in the energy consumption calculations. It was found that the Joule energy, $E_{\mathrm{J}}$ was 0.077 and 0.308 J per pulse in the case of 10 kV (33.3 kV/cm) and 20-kV (66.7 kV/cm) treatment, respectively. The energy

dissipated in the treatment cell due to displacement current, $E_C$ is

$$E_C = N \cdot R_{\mathrm{ESR}} \cdot \int \left( C \frac{dV(t)}{dt} \right)^2 \cdot dt \quad (4)$$

$$R_{\mathrm{ESR}} = \tan\delta / (2\pi f C) \quad (5)$$

where $N$ is the number of applied pulses, $R_{\mathrm{ESR}}$ is the equivalent series resistance of the capacitor in the lumped circuit model, $f$ is the frequency that corresponds to the rise and fall times of the impulse, and $C$ is obtained by (2). The displacement current, $C \cdot dV(t)/dt$, was calculated using the actual voltage waveforms obtained in the tests. The ratio of the imaginary and real parts of permittivity of the suspension, $\tan\delta$, was modeled with the dissipation factor of tap water, which is $1.94 \cdot 10^{-4}$, at 25 °C for $f = 4$ MHz, according to [15]. This frequency corresponds to the rise and fall times of the impulse shown in Fig. 3. The values calculated using (4) and (5) for energy, $E_C$ are 0.036 mJ per pulse at 10 kV (33.3 kV/cm) and 0.150 mJ per pulse for 20 kV (66.7 kV/cm). These are significantly lower that the corresponding Joule energies of 0.077 J per pulse for 10 kV (33.3 kV/cm) and 0.308 J per pulse for 20-kV (66.7 kV/cm) impulses, respectively. Therefore, the total energy consumption of the PEF treatment can be approximated by the Joule energy losses only. The results of the tests showed that stable inactivation of the microalgae can be achieved by 500 pulses with magnitude of 10 kV (33.3 kV/cm). The volume of the treatment cell is 3.4 ml and the concentration of microalgae was ∼13 g/l, therefore the specific energy required to achieve inactivation of the microalgae is ∼0.87 MJ/kg. In the case of 20-kV (66.7 kV/cm) tests, the number of pulses is reduced to ∼50. The specific energy required to achieve inactivation of the microalgae in this case is ∼0.35 MJ/kg.

The specific energy consumption reported in [8] and [9] were 26 and 2 MJ/kg, respectively. Therefore, the specific energy consumption of the PEF treatment achieved in this paper is significantly lower than the energy values reported in [8] and [9]. There are several potential reasons which could be responsible for such significant difference in the energy consumption values. First, the conductivity of the algae suspension used in this paper was significantly lower than that in the previous work as a result of the centrifugation and resuspension processes that were used resulting in a conductivity of ∼20 $\mu$S/cm. For comparison, the microalgae suspension used in [9] had a conductivity of 0.15 S/cm. The low conductivity of the suspension used in this paper resulted in a lower conduction current in the treatment cell and therefore lower energy dissipation. Also, it was reported in [16] that square high-voltage impulses result in more efficient inactivation (∼60% increase) as compared with double-exponential waveforms. In this paper, as in [9], square impulses were used, while Zbinden *et al*. [8] used double-exponential waveforms. The energy consumption reported in [9] for 1-$\mu$s square pulses is more than 10-fold lower than the specific inactivation energy reported in [8] for exponentially decaying impulses with a characteristic decay time of 360 ns. Therefore, further decrease in the PEF specific energy achieved in this paper (for 1 $\mu$s-square impulses, as in [9]) can be attributed to other factors, including differences in cellular structure and dimensions of microorganisms. According to the Schwan equation, the field strength induced in the biomembrane increases with an increase in the external electric field [17]. It has been shown experimentally in [4], that the yeast *Saccharomyces cerevisiae* (with linear dimensions of ∼6 $\mu$m) is more susceptible to the PEF treatment than the bacterium *Staphylococcus aureus*, with linear dimensions of ∼1 $\mu$m. El-Hag *et al*. [17] also attributed an increased susceptibility of the bacterium *Bacillus subtilis* to the PEF treatment as compared with *S. aureus* to larger size of *B. subtilis*. Although the species of multicellular microalgae used in this paper and in [8] and [9] are different, linear dimensions of the individual algae cells have the same order of magnitude (tens of micrometer [18]). Therefore, it may be concluded that the size factor does not play a dominant role in the observed reduction in the energy consumption. However, further investigation into the exact mechanisms and factors, which may result in lower specific inactivation energy is required.

## V. Conclusion

The results of this paper show that PEFs can be used to inactivate the microalgae, *Spirulina*. After appropriate PEF treatment, no growth of the microalgae growth was observed over a 15 days period, which indicates that PEF treatment is able to inactivate virtually all microalgae in the sample. When exposed to ∼33.3-kV/cm electric field, stable inactivation can be achieved using at least ∼500 pulses. When exposed to ∼66.7-kV/cm field, significantly smaller number of impulses, ∼50 was required to achieve stable inactivation. This paper also demonstrated that the inactivation of microalgae could be achieved with specific energy of a few hundreds of kJ/kg rather than a few or few tens of MJ/kg as reported in the literature. This reduction has been achieved using low-conductivity algae suspensions. Reducing the conductivity of the suspensions also eliminates the heating effect of the PEF treatment. Visual inspection of microalgae did not reveal obvious damage to its structure, however, their inactivation suggested that some form of changes have been produced by electric field and further study is required to clarify potential structural damage.

## References

[1] S. Toepfl, V. Heinz, and D. Knorr, *Pulsed Electric Fields Technology for the Food Industry: Fundamentals and Applications*. New York, NY, USA: Springer-Verlag, 2006.

[2] U. Zimmermann, "Electrical breakdown, electropermeabilization and electrofusion," *Rev. Physiol. Biochem. Pharmacol.*, vol. 105, no. 6, pp. 175–256, 1986.

[3] K. H. Schoenbach, R. P. Joshi, R. H. Stark, F. C. Dobbs, and S. J. Beebe, "Bacterial decontamination of liquids with pulsed electric fields," *IEEE Trans. Dielectr. Electr. Insul.*, vol. 7, no. 5, pp. 637–645, Oct. 2000.

[4] B. L. Qin, G. V. Barbosa-Canovas, B. G. Swanson, P. D. Pedrow, and R. G. Olsen, "Inactivating microorganisms using a pulsed electric field continuous treatment system," *IEEE Trans. Ind. Appl.*, vol. 34, no. 1, pp. 43–50, Jan./Feb. 1998.

[5] J. R. Beveridge, S. J. MacGregor, L. Marsili, J. G. Anderson, N. J. Rowan, and O. Farish, "Comparison of the effectiveness of biphase and monophase rectangular pulses for the inactivation of microorganisms using pulsed electric fields," *IEEE Trans. Plasma Sci.*, vol. 30, no. 4, pp. 1525–1531, Aug. 2002.

[6] J. R. Beveridge, S. J. MacGregor, J. G. Anderson, and R. A. Fouracre, "The influence of pulse duration on the inactivation of bacteria using monopolar and bipolar profile pulsed electric fields," *IEEE Trans. Plasma Sci.*, vol. 33, no. 4, pp. 1287–1293, Aug. 2005.

[7] P. S. Brito, H. Canacsinh, J. P. Mendes, L. M. Redondo, and M. T. Pereira, "Comparison between monopolar and bipolar microsecond range pulsed electric fields in enhancement of apple juice extraction," *IEEE Trans. Plasma Sci.*, vol. 40, no. 10, pp. 2348–2354, Oct. 2012.

[8] M. D. A. Zbinden *et al.*, "Pulsed electric field (PEF) as an intensification pretreatment for greener solvent lipid extraction from microalgae," *Biotechnol. Bioeng.*, vol. 110, no. 6, pp. 1605–1615, 2013.

[9] C. Eing, M. Goettel, R. Straessner, C. Gusbeth, and W. Frey, "Pulsed electric field treatment of microalgae—Benefits for microalgae biomass processing," *IEEE Trans. Plasma Sci.*, vol. 41, no. 10, pp. 2901–2907, Oct. 2013.

[10] R. Straessner, C. Eing, M. Goettel, C. Gusbeth, and W. Frey, "Monitoring of pulsed electric field-induced abiotic stress on microalgae by chlorophyll fluorescence diagnostic," *IEEE Trans. Plasma Sci.*, vol. 41, no. 10, pp. 2951–2958, Oct. 2013.

[11] K. de Boer, N. R. Moheimani, M. A. Borowitzka, and P. A. Bahri, "Extraction and conversion pathways for microalgae to biodiesel: A review focused on energy consumption," *J. Appl. Phycol.*, vol. 24, no. 6, pp. 1681–1698, 2012.

[12] M. Vanthoor-Koopmans, R. H. Wijffels, M. J. Barbosa, and M. H. M. Eppink, "Biorefinery of microalgae for food and fuel," *Bioresour. Technol.*, vol. 135, pp. 142–149, May 2013.

[13] S. Gnapowski, R. H. Akiyama, T. Sakugawa, and M. Akiyama, "Algae treatment effects by pulse power discharge in the water," in *Proc. IEEE ICOPS*, Jul. 2012, pp. 1P–111.

[14] J. P. Pandey, A. Tiwari, and R. M. Mishra, "Evaluation of biomass production of spirulina maxima on different reported media," *J. Algal Biomass Utilization*, vol. 1, no. 3, pp. 70–81, 2010.

[15] T. Meissner and F. J. Wentz, "The complex dielectric constant of pure and sea water from microwave satellite observations," *IEEE Trans. Geosci. Remote Sens.*, vol. 42, no. 9, pp. 1836–1849, Sep. 2004.

[16] B. L. Qin, Q. Zhang, G. V. Barbosa-Canovas, B. G. Swanson, and P. D. Pedrow, "Inactivation of microorganisms by pulsed electric fields of different voltage waveforms," *IEEE Trans. Dielectr. Electr. Insul.*, vol. 1, no. 6, pp. 1047–1057, Dec. 1994.

[17] A. H. El-Hag, S. H. Jayaram, O. R. Gonzalez, and M. W. Griffiths, "The influence of size and shape of microorganism on pulsed electric field inactivation," *IEEE Trans. Nanobiosci.*, vol. 10, no. 3, pp. 133–138, Sep. 2011.

[18] M. D. Guiry. (2014, Mar. 17). *Algaebase* [Online]. Avaliable: http://www.algaebase.org

**Si Qin** was born in Guangxi, China, in 1988. He received the B.Eng. (Hons.) degree in electronic and electrical engineering and the M.Sc. degree in electrical power engineering with business from the University of Strathclyde, Glasgow, U.K., in 2011 and 2012, respectively, where he is currently pursuing the Ph.D. degree in electronic and electrical engineering.

**Igor V. Timoshkin** (M'07) received the degree in physics from Moscow State University, Moscow, Russia, and the Diploma and Ph.D. degrees from the Imperial College of Science, Technology and Medicine (ICSTM), London, U.K., in 1992 and 2001, respectively.

He was a Researcher with Moscow State Agro-Engineering University, Moscow, and with the Institute for High Temperatures, Russian Academy of Sciences, before moving to ICSTM in 1997. He joined the Department of Electronic and Electrical Engineering, University of Strathclyde, Glasgow, U.K., in 2001, where he became a Senior Lecturer in 2011. His current research interests include properties of solid and liquid dielectric materials, electronics of plasma discharges in condensed media, practical applications of electro-hydraulic and high-power ultrasound pulses, biodielectrics, and effects of electromagnetic fields on biological objects.

**Michelle Maclean** was born in the Isle of Lewis, Scotland, in 1980. She received the B.Sc. (Hons.) degree in microbiology and immunology, and the Ph.D. degree in electronic and electrical engineering from the University of Strathclyde, Glasgow, U.K., in 2002 and 2006, respectively.

She is currently a Research Fellow with the Robertson Trust Laboratory for Electronic Sterilization Technologies, University of Strathclyde. Her current research interests include the development and application of novel electrotechnologies for biological decontamination and sterilization applications in clinical and public health environments.

Dr. Maclean is a member of the Society for General Microbiology and the American Society of Microbiology.

**Mark P. Wilson** (M'10) was born in Stranraer, Scotland, in 1982. He received the B.Eng. (Hons.), M.Phil., and Ph.D. degrees in electronic and electrical engineering from the University of Strathclyde, Glasgow, U.K., in 2004, 2007, and 2011, respectively.

He is currently a Teaching Associate with the University of Strathclyde, where he is involved in investigating surface flashover of solids immersed in insulating oil.

Dr. Mark is a member of the IEEE Nuclear and Plasma Sciences Society. He was a recipient of the Graduate Scholarship Award in 2011, the IEEE Dielectrics and Electrical Insulation Society, and the Institution of Engineering and Technology.

**Scott J. MacGregor** (M'95) received the B.Sc. and Ph.D. degrees from the University of Strathclyde, Glasgow, U.K., in 1982 and 1986, respectively.

He was a Pulsed Power Research Fellow in 1986 and a Lecturer in pulsed-power technology in 1989. In 1994, he became a Senior Lecturer, with a promotion to Reader and Professor of High Voltage Engineering in 1999 and 2001, respectively. He became the Dean of Engineering Faculty with the University of Strathclyde in 2010. His current research interests include high-voltage pulse generation, high-frequency diagnostics, high-power repetitive switching, high-speed switching, electronic methods for food pasteurization and sterilization, generation of high-power ultrasound (HPU), plasma channel drilling, pulsed-plasma cleaning of pipes, and stimulation of oil wells at HPU.

**Martin J. Given** (M'99–SM'11) received the B.Sc. degree in physics from the University of Sussex, Brighton, U.K., and the Ph.D. degree in electronic and electrical engineering from the University of Strathclyde, Glasgow, U.K., in 1981 and 1996, respectively.

He is currently a Senior Lecturer with the Department of Electronic and Electrical Engineering, University of Strathclyde. His current research interests include, ageing processes and condition monitoring in solid and liquid insulation systems, high-speed switching, and pulse power applications.

**John G. Anderson** was born in Glasgow, U.K., in 1942. He received the B.Sc. degree in applied microbiology, and the Ph.D. degree in fungal physiology from the University of Strathclyde, Glasgow, U.K., in 1968 and 1971, respectively.

He has been with the Department of Bioscience and Biotechnology, University of Strathclyde, since 1971, where he became a Professor of Microbiology and the Head of Department. He is currently an Emeritus Professor with the University of Strathclyde. His current research interests include various aspects of food, biomedical, and environmental microbiology with interdisciplinary collaboration on the application of electrotechnologies for electronic pasteurization and sterilization.

**Tao Wang** received the B.Eng. and M.Sc. degrees from Northeast China Dianli University, Jilin City, China, and the Ph.D. degree from the University of Strathclyde, Glasgow, U.K., in 1993, 1996, and 2005, respectively.

He was with Newland Entech, Fuzhou, China, as a Research Fellow, developing high-efficiency industrial ozone generator, and the Department of Electronic and Electrical Engineering, University of Strathclyde, as a Lecturer, in 2010. His current research interests include nonthermal gas discharges and their applications in gas synthesis, water disinfection, and advanced oxidation process in water.

# Pulsed Electric Field Treatment of *Saccharomyces cerevisiae* Using Different Waveforms

**S. Qin, I. V. Timoshkin, M. Maclean, M. P. Wilson, M. J. Given, T. Wang, J. G. Anderson** and **S. J. MacGregor**
Department of Electronic and Electrical Engineering,
University of Strathclyde, 204 George Street,
Glasgow, G1 1XW, United Kingdom

## ABSTRACT

**Pulsed electric field (PEF) treatment can be used for non-thermal inactivation of microorganisms. The aim of this paper is to investigate PEF treatment of yeast, *Saccharomyces cerevisiae*, using three different field waveforms: square; non-oscillating exponential and oscillating exponential. The PEF system used in this paper consists of a pulsed power supply and a parallel-plane metallic electrodes treatment cell located in an air-pressurised chamber. PEF treatment of the yeast was conducted using electric field impulses with magnitudes of 67 kV/cm and 80 kV/cm. The efficacy of the PEF treatment for inactivation of the yeast cells was assessed by comparison of the PEF-treated and untreated yeast populations. Results showed that ~3-$\log_{10}$ reduction in the yeast population can be achieved with 100 impulses using all tested waveforms. Amongst all three tested waveforms non-oscillating exponential impulses demonstrated improved PEF performance. The effect of duration of treatment and peak magnitude of the field on the PEF process is discussed.**

Index Terms - **Pulsed electric field, inactivation, yeast, *Saccharomyces cerevisiae*, field waveforms.**

## 1 INTRODUCTION

**HIGH** voltage impulses can be used to generate electro-mechanical stresses in biological membranes allowing pores to be formed in the membrane [1]. The pores become irreversible if the transmembrane potential exceeds a critical value, and this irreversible electroporation results in the dysfunction of the biological membrane and the death of biological cell [2]. Therefore, pulsed electric field (PEF) treatment which results in irreversible electroporation can be used for inactivation of microorganisms. PEF induced microbiological effects have been intensively investigated in recent decades, and pulsed electric fields have been used for inactivation of yeast and bacteria [3-5], processing of liquid foodstuffs such as juice and milk [6, 7] and extraction of lipids from microalgae [8-10].

A key parameter of the PEF treatment is the critical field strength which triggers irreversible electroporation. It was found that irreversible processes of pore formation occur when the electrical potential across a membrane exceeds 0.9-1 V [2]. In several papers a relationship between the transmembrane potential and the external electric field strength has been investigated [11-13]. It was found that for a microbiological cell of 1μm in size, an external field of 10 kV/cm is required to trigger the electroporation effect [11]. However, experimental results presented in [12] showed that inactivation of yeast can be observed at a lower critical field value of 4.7 kV/cm. In [3] a similar magnitude of the critical inactivation field was obtained: 4 kV/cm for *Escherichia coli* (bacteria), 6 kV/cm for *Klebsiella pneumonia* (bacteria) and 8 kV/cm for *Candida albicans* (yeast) and *Pseudomonas aeruginosa* (bacteria). However, in both [3] and [12], only 0.2-$\log_{10}$ reduction of the microbial population was observed using the minimum (critical) field strength. When the field was increased to 7 kV/cm, the population reduction of *Saccharomyces cerevisiae* increased to 5-$\log_{10}$ [12]. It is also shown in [3], when the field was increased to 10 kV/cm, the population reduction of *E. coli* increased to 3-$\log_{10}$ and the population reduction of *C. albicans* increased to 2-$\log_{10}$ when the field was increased to 12 kV/cm. These results indicate that the field strength should exceed 10 kV/cm in order to achieve useful levels of inactivation. It has been shown that further increase in the field strength could result in a more prominent inactivation effect. For example, PEF impulses with magnitudes up to 110 kV/cm [14], and 200 kV/cm [15], were used to inactivate *E. coli* and *Bacillus subtilis* (bacteria). Such high field magnitudes require reasonably short (typically sub-μs) duration of PEF impulses in order avoid formation of spark breakdown in the treatment cell. The results obtained in [14] demonstrate that for fields which exceed a value of ~60 kV/cm, the viability of *E. coli* decreases significantly as compared with lower field magnitudes.

*Manuscript received on 22 December 2014, in final form 28 February 2015, accepted 9 April 2015.*

The effect of pulse duration on the PEF process has also been investigated [5, 16]. It was shown that PEF impulses with a longer duration produce more efficient inactivation as compared with the same number of shorter impulses. Very few studies focused on the effect of pulse wave-shapes on the PEF process had been conducted [17, 18]. In [17] a comparison between square waveforms, exponential decaying waveforms and oscillatory decaying waveforms found the square waveforms resulted in the highest energy efficacy. The PEF impulses used in [17] had a peak field strength of 12 kV/cm and their duration was a few tens of μs, depending on the wave-shape. In [18] mathematical analysis was conducted to find a correlation between the frequency components of the pulse waveform and the survival fraction of the microorganisms. These results are in good agreement with the experimental results reported in [17], which indicated that square waveforms with longest duration produce the strongest inactivation.

In the present study, PEF treatment of the yeast *S. cerevisiae* has been conducted using PEF impulses with magnitudes of 67 kV/cm and 80 kV/cm (which are above the threshold value of 60 kV/cm identified in [14]) and with three different wave-shapes: square, non-oscillating exponential and oscillating exponential wave-forms. The aim of this work is to provide a better understanding of the processes involved in the PEF inactivation of yeast at higher levels of electric field using mono-polar impulses with different wave-shapes, and with no reverse-polarity oscillations. This information can help in further optimisation of PEF wave-forms for practical applications. The yeast *S. cerevisiae* was selected for the present study as this type of yeast is commonly used in the food industry and in bio-medical applications. Also, the spherical shape of the *S. cerevisiae* cell is desirable for analytical modelling of the interaction of pulsed electric field with this microorganism which is planned in the future.

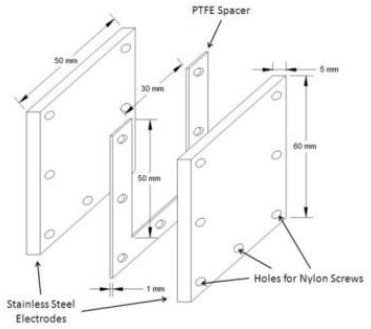


**Figure 1.** Schematic diagram of the PEF treatment cell.

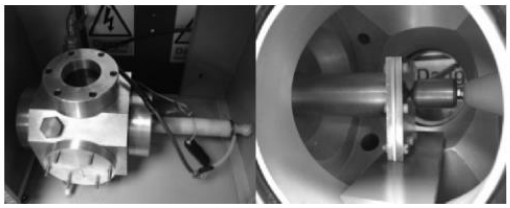

**Figure 2.** Pressurised chamber, (left), and the PEF treatment cell inside the chamber, (right).

## 2 EXPERIMENTAL PROCEDURES

### 2.1 PEF SYSTEM AND WAVEFORM

A schematic diagram of the PEF treatment cell is shown in Figure 1. The 50 mm × 60 mm rectangular parallel-plane electrodes were made of stainless steel. The 1 mm inter-electrode gap is maintained by a 1mm PTFE spacer. The electrodes and the spacer are clamped tight by 7 sets of nylon screws. The yeast suspension is transferred into the cell through the open top of the treatment cell. Due to the small gap between the electrodes, an electric breakdown is likely to occur across the liquid-air interface under atmospheric pressure. In order to avoid this undesirable breakdown, the PEF treatment cell was placed inside a sealed metallic chamber as shown in Figure 2, which is pressurised to 7.5 bars using an air compressor. Thus, the PEF treatment takes place at elevated air pressure which suppresses development of interfacial spark breakdowns.

Three different voltage waveforms (square waveform, exponential waveform and oscillating exponential waveform), were used in this PEF study. Figure 3 shows the actual wave shapes across the PEF test cell. The square high voltage impulses were generated using a transmission line pulse generator (SAMTECH Ltd., UK) described elsewhere, [8]. This transmission line based system produces negative impulses of a magnitude up to 30 kV with duration of 1 μs, and can operate with a pulse repetition rate from 0.1 to 10 pulses per second (pps). The exponential waveforms were generated by a *RC* pulse discharge circuit which consists of a HVDC charging unit (Glassman, EH50P2), a HV capacitor with capacitance of 40 nF, a self-breakdown spark gap, and a high voltage cable which connects the output terminal of the capacitor with the PEF test cell. The magnitude of the voltage across the load is regulated by the inter-electrodes gap distance of the plasma closing switch and the pulse repetition rate is controlled by the current regulator of the HV DC source. A 50 Ω resistor was connected in parallel with the PEF treatment cell in order to achieve the non-oscillating exponential waveform. The oscillating exponential waveform was formed when the 50 Ω resistor was removed. The voltage across the test cell was measured using a Tektronix HV probe with a bandwidth of 75 MHz, and the waveforms were recorded using a Tektronix TDS2024 oscilloscope with a bandwidth of 200 MHz and a sampling rate of 2 GS/s.

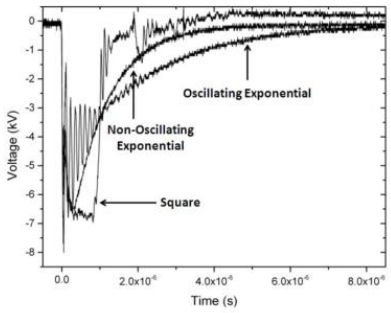


**Figure 3.** Actual waveforms obtained during the PEF treatment experiments.

### 2.2 PREPARATION OF THE YEAST SAMPLES

The yeast used in this study was *Saccharomyces cerevisiae* MUCL 28749, obtained from The Belgian Co-ordinated Collections of Microorganisms. The yeast sample was cultured in 100 ml Malt Extract Broth (Oxoid Ltd, UK) for 20 hours in a shaking incubator (120 rpm) at 30°C. Post-incubation, the yeast suspension was centrifuged at 4300 rpm for 10 minutes and re-suspended in 100 ml 0.05% Mycological Peptone (Oxoid Ltd, UK) solution. The resulting yeast suspension had a population density of ~$10^7$ colony-forming units per millilitre (CFU/ml). To investigate the PEF inactivation of different concentrations of yeast, the yeast suspension was serially diluted to prepare populations from $10^4$ to $10^7$ CFU/ml. 1.5 ml yeast suspensions were then transferred into the test cell by sterile syringe. The conductivities of yeast suspensions measured at room temperature by a portable conductivity meter, Jenway 4150, are given in Table 1. The resistance of the load (PEF test cell), $R$, and the peak conduction current through the cell during the PEF treatment, $I_{peak}$, were calculated using following equations:

$$R = d / \sigma A \quad (1)$$

$$I_{peak} = U_{peak} / R \quad (2)$$

where $d$ is the distance between the electrodes, $\sigma$ is the conductivity of the yeast suspension, $A$ is the surface area of the electrode and $U_{peak}$ is the peak voltage during the PEF treatment. The results of this analysis for the peak field of 80 kV/cm (which corresponds to the highest values of the conduction current during PEF tests) are shown in Table 1.

**Table. 1** Conductivity of yeast suspension, resistance the PEF test cell and the peak conduction current.

| Population (CFU/ml) | ~ $10^7$ | ~ $10^6$ | ~ $10^5$ | ~ $10^4$ |
|---|---|---|---|---|
| Conductivity (µS/cm) | 182 | 156 | 137 | 124 |
| Test cell resistance (Ω) | 36.6 | 42.7 | 48.7 | 53.8 |
| Peak current (A) | 218 | 187 | 164 | 149 |

### 2.3 ASSESSMENT OF PEF PERFORMANCE

Yeast samples with different initial populations were stressed with 25, 50 and 100 HV impulses of different waveforms. Two voltage levels were used in the study, 6.7 kV and 8 kV, with a pulse repetition rate of 1 pps. In the cases of the smooth and oscillating exponential waveforms, the peak voltages were set to the above values. The resulting peak electric field strength across the 1 mm inter-electrodes gap inside the PEF treatment cell was 67 kV/cm and 80 kV/cm respectively. In the case of the oscillating exponential waveform average peak fields were also calculated using an adjacent-averaging function in the Origin Pro 8 software package. These average field values for the two tested charging voltage peak levels are 47 kV/cm and 59 kV/cm. PEF treated and untreated (control) yeast samples were plated onto Malt Extract Ager (Oxoid Ltd, UK) using spiral and spread plating methods. The populations of PEF treated and untreated yeast samples were enumerated and compared in order to assess the performance of the PEF impulses. The results are presented as the mean of surviving populations ($\log_{10}$ CFU/ml) and its standard deviation obtained from 3 independent PEF tests, in which fresh yeast samples were treated with pulsed electric field. Temperature of the yeast samples was measured before and after the treatment to identify any noticeable thermal effects.

## 3 RESULTS AND DISCUSSIONS

### 3.1 TEMPERATURE EFFECTS

Measurements of the temperature of yeast samples before and after the PEF treatment indicated that there was no significant temperature change during the PEF treatment. It was reported in [8] that low conductivity of liquid samples can reduce the heating effect. In the present study, in order to reduce thermal effects 0.05% Mycological Peptone was used as the suspending media, which provided a maximum conductivity of 182 µS/cm (in the case of $10^7$ CFU/ml yeast sample). This resulted in a minimal change in temperature of the treated sample of 1.5 °C. In contrast, the sample solutions with significantly higher conductivities in the range of a few tens of mS/cm were used in [5] and [17] in PEF tests (0.9% NaCl solution and apple juice, respectively). As a result, a significant heating effect of the PEF treatment was reported: temperature of the PEF treated samples increased by a few tens of ºC. Therefore, the insignificant temperature rise observed in the present paper is likely explained by the low conductivity of liquid solutions used in the tests.

### 3.2 PEF INACTIVATION OF YEAST

Figures 4-6 show the results of the PEF treatment using different field strengths and different waveforms: square, non-oscillating exponential and oscillating exponential wave shapes. Only two initial populations, the highest, ~ $10^7$CFU/ml, and the lowest, ~ $10^4$ CFU/ml, are shown in these figures in order to provide clear viewing of the results. There were no significant differences in the behavior of the reaction kinetics for populations of $10^6$ and $10^5$ CFU/ml which are not shown in these Figures. In all cases, the PEF treatment with a higher field strength provided superior inactivation performance. As shown in Figures 4-6, the PEF treatment with 80 kV/cm provided ~1-$\log_{10}$ more efficient inactivation as compared with 67 kV/cm treatment by the same number of pulses.

The results of the PEF treatment shown in Figures 4-6 demonstrate that impulses with a higher field strength (80 kV/cm) provide on average 1-$\log_{10}$ more efficient inactivation as compared with 67 kV/cm impulses for all initial populations. However, as the conductivity of the yeast solution depends on its initial yeast concentration, it is also interesting to evaluate the energy efficacy of the PEF process (population reduction as a function of specific energy, J/l) which is done in Section 3.4 of this paper.

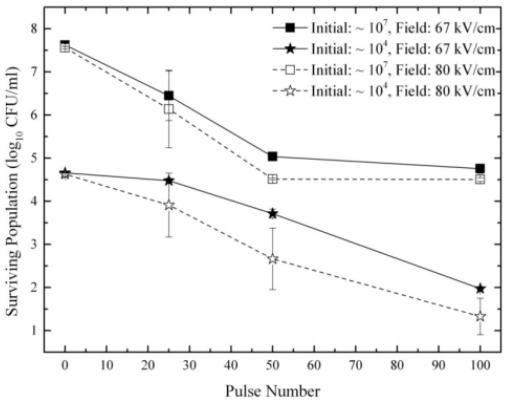


**Figure 4.** Surviving population of yeast ($\log_{10}$ CFU/ml) as a function of number of impulses. PEF treatment with square waveform of different initial populations. Solid line, 67 kV/cm; Dash line, 80 kV/cm. Error bars show standard deviation.

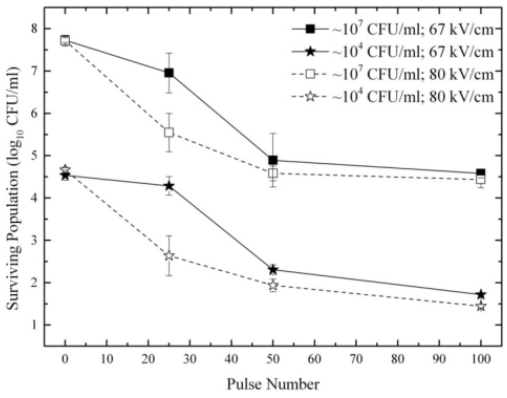


**Figure 5.** Surviving population of yeast ($\log_{10}$ CFU/ml) as a function of number of impulses. PEF treatment with non-oscillating exponential waveform of different initial populations. Solid line, 67 kV/cm; Dash line, 80 kV/cm. Error bars show standard deviation.

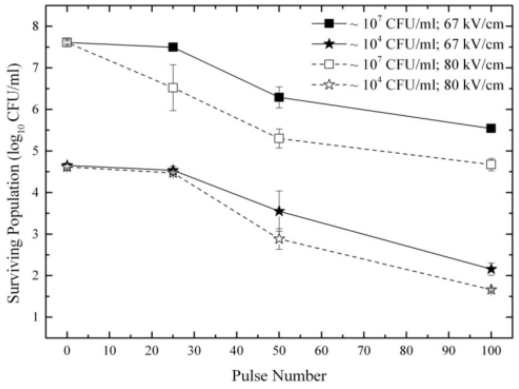


**Figure 6.** Surviving population of yeast ($\log_{10}$ CFU/ml) as a function of number of impulses. PEF treatment with oscillating exponential waveform of different initial populations. Solid line, 67 kV/cm; dashed line, 80 kV/cm. Error bars show standard deviation.

### 3.3 COMPARISON BETWEEN DIFFERENT WAVEFORMS

This section of the paper is focused on the analysis of the PEF process depending on the pulse waveform. The results of PEF inactivation using different field waveforms with the peak field of 67 kV/cm and 80 kV/cm are presented in Figure 7 and Figure 8 respectively. Again, only two initial populations, ~ $10^7$ CFU/ml and ~ $10^4$ CFU/ml, are presented in these figures. As shown in Figures 7 and 8, the PEF treatment using the simple exponential waveform provided the best inactivation performance, while the PEF treatment using the oscillating exponential waveform had the lowest inactivation performance.

### 3.4 TAILING EFFECT

During the PEF trials, it was noticed that 3-$\log_{10}$ reductions were achieved after 50 or 100 impulses regardless of the initial yeast population and the PEF waveform, resulting in a 'tailing' effect in the inactivation curves, as can be seen in Figures 7 and 8. To investigate this effect, PEF treatment with an increased number of impulses (up to 250) was conducted and the results of these tests, shown in Figure 9, confirm the 'tailing' effect. This undesirable phenomenon was also observed in [17] and [19] but no explanation of the causes of this tailing effect has been reported in these papers.

In the present work, the tailing effect was examined using all waveforms and initial populations in order to identify the causes and to find possible solutions which would eliminate or reduce this undesirable effect. Figure 9 shows that an initial population of ~ $10^4$CFU/ml can be reduced to ~ $10^1$ CFU/ml by 100 PEF impulses. However the inactivation curves for the samples with an initial population of $10^7$ CFU/ml saturated at $10^4$ CFU/ml after 50 impulses. In this work it was observed that there was significant sedimentation of the yeast during the twenty minute period associated with pressurising the test chamber, applying the PEF treatment and depressurising the test chamber.

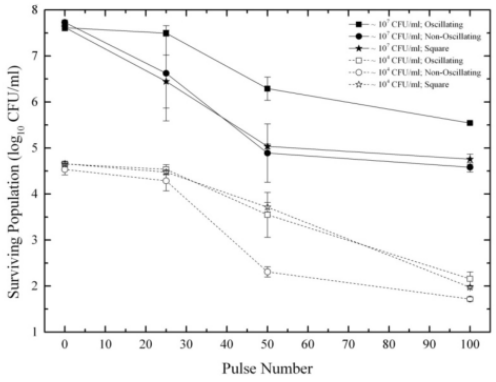


**Figure 7.** Surviving population of yeast ($\log_{10}$ CFU/ml) as a function of pulse number for 67 kV/cm waveforms: square waveform (star), non-oscillating exponential waveform (circle) and oscillating exponential waveform (square). Solid lines, $10^7$CFU/ml initial population; dashed line, $10^4$ CFU/ml initial population. Error bars show standard deviation.

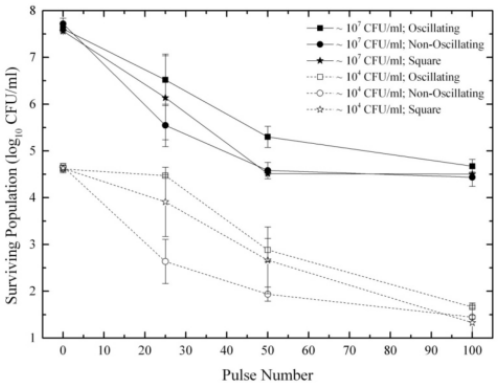


**Figure 8.** Surviving population of yeast ($\log_{10}$ CFU/ml) as a function of pulse number for 80 kV/cm waveforms: square waveform (star), non-oscillating exponential waveform (circle) and oscillating exponential waveform (square). Solid lines, $10^7$CFU/ml initial population; dashed line, $10^4$ CFU/ml initial population. Error bars show standard deviation.

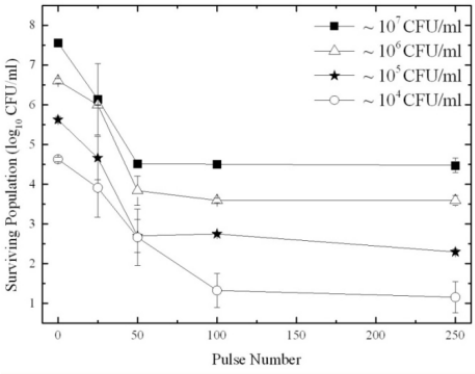


**Figure 9.** Surviving population of yeast ($\log_{10}$ CFU/ml) as a function of pulse number for larger numbers of impulses. 80 kV/cm square impulses. Error bars show standard deviation.

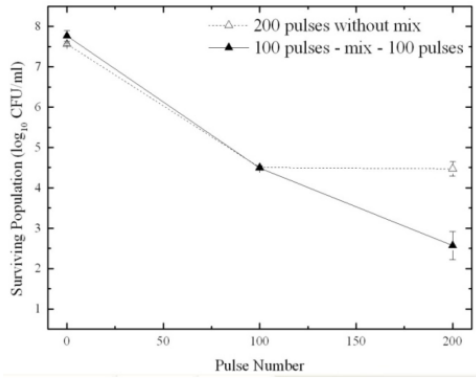


**Figure 10.** Comparison of the PEF performance between treatments with and without sample mixing after 100 pulses. Solid line and closed symbols represent the PEF treatment with mix process; Dash line and hollow spot represents PEF treatment without mix process. Error bars show standard deviation.

In [17] and [19], the batch PEF treatment process was used, which potentially may result in the tailing observed. In study [20] the tailing effect was reduced by using continuous PEF treatment (liquid flow through the PEF test cell), however no direct comparison between efficiencies of the batch and flow PEF processes of the same microorganisms was provided. Other factors, such as potential penetration of liquid with microorganisms in gaps between the electrodes and dielectric spacer (areas with reduced electric field) and clumping of microorganisms, might also contribute to the "tailing" effect in the inactivation process. More detailed analysis of actual causes of this "tailing" is required in future.

### 3.5 SPECIFIC ENERGY CONSUMPTION

Each impulse waveform delivers a different amount of energy to the liquid sample, and in order to determine the energy efficacy of the PEF process, specific energy has calculated using the following equation:

$$E = V_{vol} \cdot \sigma \cdot \int E^2(t) \cdot dt \qquad (1)$$

where $V_{vol}$ is the volume of the PEF treatment cell, $\sigma$ is electrical conductivity of the yeast sample, and $E(t)$ is the time varying electric field strength across the PEF treatment cell.

Using equation (1), experimental impulsive waveforms obtained during the PEF treatment and conductivities of the yeast samples, the specific energies delivered by each impulse have been calculated. These energies are listed in Table 2.

**Table 2.** Specific energy delivered by the different PEF waveforms.

| Waveform | Field Strength | Initial Population (CFU/ml) | | | |
|---|---|---|---|---|---|
| | | ~$10^7$ | ~$10^6$ | ~$10^5$ | ~$10^4$ |
| Square | 67 kV/cm | 1.13 J | 0.97 J | 0.85 J | 0.77 J |
| | 80 kV/cm | 1.66 J | 1.41 J | 1.24 J | 1.12 J |
| Non-Oscillating exponential | 67 kV/cm | 0.90 J | 0.77 J | 0.64 J | 0.60 J |
| | 80 kV/cm | 1.13 J | 1.04 J | 0.96 J | 0.83 J |
| Oscillating exponential | 67 kV/cm | 0.61 J | 0.69 J | 0.58 J | 0.55 J |
| | 80 kV/cm | 0.96 J | 0.96 J | 0.83 J | 0.80 J |

From here it can be seen that the largest amount of specific energy was delivered by a single square impulse, while the minimum amount of specific energy was delivered by a single oscillating exponential impulse. Figure 11 shows surviving population of yeast as a function of specific energy delivered to the test cell during the PEF treatment for three tested waveforms: non-oscillating exponential, oscillating exponential and square with peak field of 67 kV/cm and 80 kV/cm. All three waveforms provided similar PEF inactivation tendencies: the surviving population of yeast reduces gradually as the specific energy increases. Non-oscillatory wave form shows larger reduction in surviving population for the same specific energy as compared with two other wave-forms. However, it was reported in [17] and [18] that the square voltage waveform was more energy efficient than exponentially decaying waveforms in the PEF process. In [17], both waveforms produced the same peak field strength and delivered the same amount of energy per impulse. It was found that the PEF treatment using a square-wave required a lower number of impulses to achieve the same inactivation result. However, the peak field used in [17]

was 12 kV/cm, which only slightly exceeded the critical value assumed to be 10 kV/cm. For the waveforms reported, the field strength was above 10 kV/cm for only ~20 μs in the case of a single exponential impulse, while in the case of a single square impulse the field strength was above 10 kV/cm for ~50 μs.

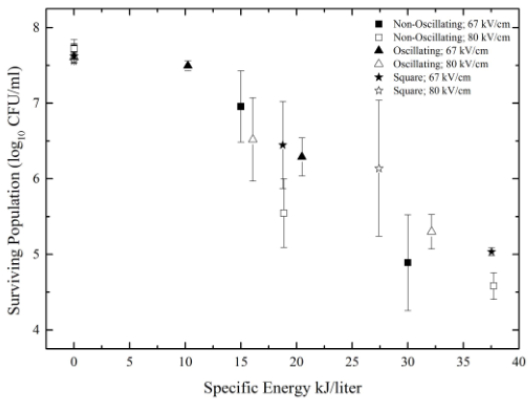


**Figure 11.** Energy efficacy of PEF treatment using non-oscillating exponential (square), Square (triangle) and Oscillating (star) waveforms with 67 kV/cm (solid) and 80 kV/cm (empty). Initial population of yeast was $10^7$ CFU/ml. Error bars show standard deviation.

In the present study, the duration of the non-oscillating exponential and square parts of impulses which exceeded 10 kV/cm were 2.5 μs and 1 μs respectively. Therefore, a correlation between the effective impulse duration (period where the field strength is above 10 kV/cm) and the PEF performance exists in the results reported in [17] and the present study. Thus, the difference in time during which the field exceeded the critical value may explain the advantage of the square impulses over the exponential waveform used in [17]. The waveform with the longer effective duration results in a better PEF performance.

In the present study, in spite of a longer effective duration, the oscillating exponential impulses demonstrated lower PEF performances compared with the non-oscillating exponential impulses. This can be explained by lower average peak fields and deep field oscillations at the peak of the former waveform.

As is indicated in Section 2.3 the average peak fields in the case of the oscillating exponential wave form are 47 kV/cm and 59 kV/cm for the two levels of charging voltage. These values are lower than the peak field magnitudes of the exponential and square waveforms, 67 kV/cm and 80 kV/cm correspondingly. This may help to explain inferior PEF inactivation results achieved with the oscillating exponential impulses as the average peak fields of 47 kV/cm and 59 kV/cm are close or below the 60 kV/cm threshold which was identified in [14] as being the magnitude below which electric fields demonstrate noticeably lower PEF performance.

Also, the oscillating exponential wave-forms have deep field oscillations at their peaks, duration of the ¼ period of these oscillations is ~ 30 ns. However, according to the model of transient membrane charging developed in [13], time required to achieve the maximum field across yeast membrane is ~ 1 μs and during ~ 30 ns the field across the membrane can reach only ~ 10% of its potential maximum value.

Therefore, in order to achieve high efficacy in the PEF inactivation process it is desirable to increase duration of exposure to the maximum field and to the critical field. However, it is not clear which of these two factors play a dominant role and further investigation is required to clarify their contribution to pulsed electric field inactivation.

## 4 CONCLUSION

The present study is focused on investigation of the PEF inactivation process of the yeast *Saccharomyces cerevisiae* using three types of field impulses (square, non-oscillating exponential and oscillating exponential impulses) with pulse duration of a few μs and two levels of field strength of 67 kV/cm and 80 kV/cm. The results of this study show that PEF performance depends on multiple factors.

It was established that measures which minimise the sedimentation of the yeast during the batch PEF treatment, (either by using continuous flow PEF system, [20], or by applying a mixing procedure), improves PEF performance.

It was shown that surviving population of yeast depends on the magnitude of the PEF pulses: pulses with a higher peak field magnitude produce a greater inactivation effect as compared with the same number of pulses with a lower field peak magnitude. However, the specific energy delivered by the same number of pulses with different field magnitudes is different. Therefore, further analysis of the obtained PEF inactivation curves has been conducted in order to establish the dependency of PEF performance on the specific energy delivered to the test cell. It was demonstrated that surviving population of yeast reduces with an increase in the specific energy delivered to the cell and the rate of this decrease does not depend on the peak field magnitude (for pulses with magnitudes of 67 kV/cm or 80 kV/cm).

Three types of waveforms were used in the PEF tests and it was shown that non-oscillating exponential impulses provided better PEF performance: higher decrease in surviving yeast population for the same number of impulses and the same specific energy as compared with two other waveforms. It was also shown that lower effective duration of the waveform may result in lower PEF performance. Therefore, in order to optimise PEF inactivation of yeast all these factors (the maximum field strength, the critical pulse duration and the specific energy) should be taken into account. However, further investigations are required in order to establish individual role of each of these factors in the PEF treatment.

## REFERENCES

[1] S. Toepfl, V. Heinz, and D. Knorr, *Pulsed Electric Fields Technology for the Food Industry: Fundamentals and Applications*, *Springer-Verlag*, 2006.

[2] U. Zimmermann, "Electrical Breakdown, Electropermeabilization and Electrofusion", Rev. Physiol. Biochem. Pharmacol., Vol. 105, No. 6, pp. 175-256, 1986.

[3] H. Hulsheger, J. Potel, and E.G. Niemann, “Electric Field Effects on Bacteria and Yeast Cells”, Radiation and Enironmental Biophysics, Vol. 22, pp. 149-162, 1983.

[4] B. L. Qin, G. V. Barbosa-Canovas, B. G. Swanson, P. D. Pedrow, and R.G. Olsen, "Inactivating Microorganisms Using a Pulsed Electric FieldContinuous Treatment System," IEEE Trans. Industry Applications, Vol. 34, No. 1, pp. 43-50, 1998.

[5] K. Aronssona, M. Lindgrena, B. R. Johanssonb, and U. Ronner, “Inactivation of Microorganisms Using Pulsed Electric Fields:the Influence of Process Parameters on Escherichia Coli, Listeria Innocua, Leuconostoc Mesenteroides andSaccharomyces Cereisiae”, Innovative Food Sci. Emerging Technologies, Vol. 2, No. 1, pp. 41-54, 2001.

[6] P. S. Brito, H. Canacsinh, J. P. Mendes, L. M. Redondo, and M. T. Pereira, “Comparison between Monopolar and Bipolar Microsecond Range Pulsed Electric Fields in Enhancement of Apple Juice Extraction,” IEEE Trans. Plasma Sci., Vol. 40, No. 10, pp. 2348-2354, 2012.

[7] H. Jaeger, N. Meneses, and D. Knorr, “Impact of PEF Treatment Inhomogeneity such as Electric Field Distribution, Flow Characteristics and Temperature Effects on the Inactivation of E. Coli and Milk Alkaline Phosphatase”, Innovative Food Sci. Emerging Technologies, Vol. 10, No. 4, pp. 470-480, 2009.

[8] S. Qin, I. Timoshkin, M. Wilson, M. Maclean, S. MacGregor, M. Given, J. Anderson, and T. Wang, “Pulsed Electric Field Treatment of Microalgae: Inactivation Tendencies and Energy Consumption”, IEEE Trans. Plasma Sci., Vol. 42, No. 10, pp. 3191–3196, 2014.

[9] M. D. A. Zbinden, B. S. M. Sturm, R. D. Nord, W. J. Carey, D. Moore, H. Shinogle, and S. M. Stagg-Williams, “Pulsed Electric Field (PEF) as an Intensification Pretreatment for Greener Solvent Lipid Extraction from Microalgae," Biotechnol. Bioeng., Vol. 110, No. 6, pp. 1605-1615, 2013.

[10] C. Eing, M. Goettel, R. Straessner, C. Gusbeth, and W. Frey, “Pulsed Electric Field Treatment of Microalgae—Benefits for Microalgae Biomass Processing,” IEEE Trans. Plasma Sci., Vol. 41, No. 10, pp. 2901–2907, 2013.

[11] K. H. Schoenbach, F. E. Peterkin, R. W. Alden, III, and S. J. Beebe, “The Effect of Pulsed Electric Fields on Biological Cells: Experiments and Applications”, IEEE Trans. Plasma Sci., Vol. 25, No. 2, pp. 284–292, 1997.

[12] T. Grahl, and H. Markl, “Killing of Microorganisms by Pulsed Electric Fields”, Appl. Microbiology Biotechnology, Vol. 45, No. 1-2, pp. 148-157, 1996.

[13] I. Timoshkin, S. MacGregor, R. Fouracre, B. Crichton, and J. Anderson, "Transient Electrical Field across Cellular Membranes: Pulsed Electric Field Treatment of Microbial Cells", J. Phys. D: Appl. Phys., Vol. 39, pp. 569-603, 2006.

[14] R. Narsetti, R. D. Curry, K. F. McDonald, T. E. Clevenger, and L. M. Nichols, “Microbial Inactivation in Water Using Pulsed Electric Fields and Magnetic Pulse Compressor Technology”, IEEE Trans. Plasma Sci., Vol. 34, No.4, pp. 1386-1393, 2006.

[15] B. M. Novac, F. Babakhr, I. R. Smith, L. Pecastaing, R. Ruscassic, A. D. Ferron, and P. Pignolet, “Demonstration of a Novel Pulsed Electric Field Technique Generating Neither Conduction Currents Nor Joule Effects”, IEEE Trans. Plasma Sci., Vol. 42, No. 1, pp. 216-228, 2014.

[16] J. Beveridge, S. MacGregor, J. Anderson, and R. Fouracre, “The Influence of Pulse Duration on the Inactivation of Bacteria using Monopolar and Bipolar Profile Pulsed Electric Fields,” IEEE Trans. Plasma Sci., Vol. 33, No. 4, pp. 1287–1293, 2005.

[17] B. L. Qin, Q. Zhang, G. V. Barbosa-Canovas, B. G. Swanson, and P. D. Pedrow, “Inactivation of Microorganisms by Pulsed Electric Fields of Different Voltage Waveforms,” IEEE Trans. Dielectr. Electr. Insul., Vol. 1, No. 6, pp. 1047–1057, 1994.

[18] P. Love, “Correlation of Fourier Transforms of Pulsed Electric Field Waveform and Microorganism Inactivation”, IEEE Trans. Dielectr. Electr. Insul., Vol. 5, No. 1, pp. 142–147, 1998.

[19] J. R. Beveridge, S. J. MacGregor, L. Marsili, J. G. Anderson, N. J. Rowan, and O. Farish, “Comparison of the Effectiveness of Biphase and Monophase Rectangular Pulses for the Inactivation of Microorganisms using Pulsed Electric Fields,” IEEE Trans. Plasma Sci., Vol. 30, No. 4, pp. 1525–1531, 2002.

[20] J. R. Beveridge, K. Wall, S. J. MacGregor, J. G. Anderson, and N. J. Rowan, “Pulsed Electric Field Inactivation of Spoilage Microorganisms in Alcoholic Beverages”, Proc. IEEE, Vol. 92, No. 7, pp. 1138-1147, 2004.

**Si Qin** was born in Guangxi, China, in 1988. He received the B.Eng. (with honours) degree in electronic and electrical engineering in 2011, and the M.Sc. degree in electrical power engineering with business in 2012, both from the University of Strathclyde, Glasgow, U.K. He is currently pursuing the Ph.D. degree in electronic and electrical engineering at the University of Strathclyde.

**Igor V. Timoshkin** (M’07-SM’14) received a degree in physics from the Moscow State University (Russia) in 1992, and the Diploma and the Ph.D. degree from the Imperial College of Science, Technology and Medicine, (London, UK) in 2001. After graduation from MSU he worked as a Researcher at Moscow State Agro-Engineering University, and then at the Institute for High Temperatures of Russian Academy of Sciences before moving to ICSTM in 1997. He joined the Department of Electronic and Electrical Engineering of the University of Strathclyde (Glasgow, UK) in 2001 where he became a Senior Lecturer in 2011. His research interests include properties of solid and liquid dielectric materials, electronics of plasma discharges in condensed media, practical applications of electro-hydraulic and high-power ultrasound pulses, bio-dielectrics and effects of electromagnetic fields on biological objects.

**Michelle Maclean** was born on the Isle of Lewis, Scotland, in 1980. She received the B.Sc. (1st class honors) degree in Microbiology and Immunology in 2002, and the Ph.D. degree in electronic and electrical engineering in 2006, both from the University of Strathclyde, Glasgow, U.K. She is presently working as a Lecturer at the University of Strathclyde, and her interdisciplinary research work involves the development and application of novel electro-technologies for biological decontamination and sterilization applications in clinical and public health environments. She is a member of The Society for General Microbiology and The American Society of Microbiology**.**

**Mark P. Wilson** (M’10) was born in Stranraer, Scotland, in 1982. He received the B.Eng. (with honours), M.Phil., and Ph.D. degrees in electronic and electrical engineering from the University of Strathclyde, Glasgow, U.K., in 2004, 2007, and 2011, respectively. He is presently working as a Teaching Associate at the University of Strathclyde, where he continues to investigate surface flashover of solids immersed in insulating oil. Mark is a member of the IEEE Nuclear and Plasma Sciences Society, from whom he received a Graduate Scholarship Award in 2011, the IEEE Dielectrics and Electrical Insulation Society, and the IET.

**Martin J. Given** (M’99-SM’11) is currently a Senior Lecturer in the Department of Electronic and Electrical Engineering at the University of Strathclyde. He received a degree in physics from the University of Sussex in 1981 and a PhD in electronic and electrical engineering from the University of Strathclyde in 1996. His research interests include, ageing processes and condition monitoring in solid and liquid insulation systems, high speed switching and pulse power applications.

**Tao Wang** received the B.Eng and M.Sc degrees from Northeast China Dianli University (China) in 1993 and 1996 respectively, and the Ph.D. degree from the University of Strathclyde (Glasgow, UK) in 2005. He then joined the Newland Entech as a research fellow developing high efficiency industrial ozone generator. He joined the department of Electronic and Electrical Engineering of University of Strathclyde as a lecturer in 2010. His research interests include non-thermal gas discharges and their applications in gas synthesis, water disinfection and advanced oxidation process in water.

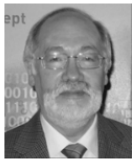

**John Anderson** was born in Glasgow, U.K., on September 2, 1942. He received the B.Sc. degree in applied microbiology in 1968, and the Ph.D. degree in fungal physiology in 1971, both from the University of Strathclyde, Glasgow. Since 1971, he has been with the Department of Bioscience and Biotechnology, University of Strathclyde, where he became a Professor of Microbiology and Head of Department. He is currently an Emeritus Professor at the University of Strathclyde. His research interests include various aspects of food, biomedical and environmental microbiology with interdisciplinary collaboration on the application of electro-technologies for electronic pasteurization and sterilization.

**Scott J. MacGregor** (M'95-SM'14) received the B.Sc. and Ph.D. degrees from the University of Strathclyde, Glasgow, U.K., in 1982 and 1986, respectively. He became a Pulsed Power Research Fellow in 1986 and a Lecturer in pulsed-power technology in 1989. In 1994, he became a Senior Lecturer, with a promotion to Reader and Professor of High Voltage Engineering, in 1999 and 2001, respectively. From 2010 he became a Dean of the Engineering Faculty of the University of Strathclyde. His research interests include high-voltage pulse generation, high-frequency diagnostics, high-power repetitive switching, high-speed switching, electronic methods for food pasteurization and sterilization, generation of high-power ultrasound (HPU), plasma channel drilling, pulsed-plasma cleaning of pipes, and stimulation of oil wells with HPU.

# $TiO_2$-Coated Electrodes for Pulsed Electric Field Treatment of Microorganisms

Si Qin, Igor V. Timoshkin, *Senior Member, IEEE*, Michelle Maclean, Scott J. MacGregor, *Senior Member, IEEE*, Mark P. Wilson, *Member, IEEE*, Martin J. Given, *Senior Member, IEEE*, Tao Wang, and John G. Anderson

***Abstract*— Pulsed electric fields (PEFs) can cause irreversible damage to bio-membranes and may result in inactivation of microorganisms. The aim of this paper is to investigate the PEF treatment of the yeast Saccharomyces cerevisiae, using a novel treatment cell with parallel-plane electrodes coated with a 2-$\mu$m thin $TiO_2$ film. Two different PEF waveforms, square and exponential, with magnitudes of 67 and 80 kV/cm were used in this study. The efficacy of the PEF treatment was assessed by a comparison of the surviving treated and untreated yeast populations, and it was shown that a treatment cell with $TiO_2$-coated electrodes can be successfully used for the PEF treatment of microorganisms: 3-$\log_{10}$ reduction in the yeast population was achieved with 100 impulses. The energy efficacy of the PEF process in the proposed treatment cell has been compared with the energy losses in the PEF treatment cell with uncoated, conductive electrodes. It is shown that the electrodes coated with $TiO_2$ provide better performance compared with the traditional uncoated electrodes.**

***Index Terms*— Inactivation of microorganisms, pulsed electric field (PEF), $TiO_2$-coated electrodes, yeast.**

## I. Introduction

INTENSIVE electric field impulses with durations from a few nanoseconds to a few tens of microseconds can generate electromechanical stresses in biological membranes, which allow pores to be formed in the membrane [1]. Such field-induced pores become irreversible if the transmembrane potential exceeds a critical value, ∼1 V [2]. Irreversible electroporation results in the dysfunction of the biological membrane and the death of the cell. Therefore, pulsed electric field (PEF) treatment can be used for nonthermal inactivation of microorganisms. In recent decades, the PEF inactivation process has been intensively investigated and this technology is used for treatment of yeast and bacteria [3]–[5], for processing of liquid foodstuffs such as juice and milk [6], [7], and for extraction of lipids from microalgae [8]–[10].

Typically, the electrodes in traditional PEF systems, including commercially available apparatuses, are made of stainless steel. The liquid being treated in such PEF systems is in direct contact with the metallic electrodes, which creates some significant drawbacks. First, significant conduction current, as high as a few hundreds of amperes, can flow through the liquid during PEF treatment [11], [13]. As a result of Joule heating [5], [13], the treated liquid should be cooled to maintain a desirable temperature during the PEF treatment. Energy losses due to Joule heating and cooling imply a significant energy consumption of the PEF process. Second, the direct contact between the liquid and the electrodes can cause undesirable electrochemical reactions during the treatment. Metallic particles can be introduced into the liquid and other toxic reactive chemical species such as hydrogen peroxide can also be produced [14]. Moreover, air bubbles can be generated at the interface between the liquid and the metallic electrodes [15], which increases the probability of undesired dielectric breakdown in the PEF treatment cell.

A conceptually new treatment cell with dielectric electrodes is discussed in [16] and [17]: it is proposed to cover the electrodes of the cell with a layer of dielectric material with a high permittivity. Thus, direct contact between the metal surface and the liquid is prevented, and conduction current through the liquid is eliminated. This concept was proved theoretically in [16] and tested experimentally in [17]. The results presented in [17] showed that a treatment cell with dielectric electrodes could be successfully used for inactivation of the bacterium *Escherichia coli*, while maintaining a relatively low sample temperature and low energy consumption. However, the maximum field magnitude that was tested in [17], 200 kV/cm, is significantly higher than a typical field used in the PEF treatment, ∼30 kV/cm. In addition, no comparison between the PEF performance achieved in the novel and traditional PEF treatment cells was made.

In this paper, a treatment cell with metallic electrodes coated with a 2-$\mu$m thick $TiO_2$ film has been developed. Titanium dioxide can form a stable dielectric ceramic in a low-temperature condition [18], [19]. It was reported in [18] that the dielectric constant of $TiO_2$ is ∼95 at room temperature. It was also shown in [20] that the conductivity of a dry, thin $TiO_2$ film is $\sim 5 \times 10^{-7}$ $\mu$S/cm. However, as found in this work, when $TiO_2$ film is in contact with water, its conductivity increases significantly and an ionic current can also flow through the liquid when treated with PEF impulses. Nevertheless, the magnitude of this conduction current is lower than the magnitude of the current in the case of metallic electrodes. Therefore, the $TiO_2$-coated electrodes can be potentially considered for the design and development of a low-conductivity PEF treatment cell.

PEF treatment of the yeast *Saccharomyces cerevisiae* has been conducted using this $TiO_2$-coated treatment cell. In order

Manuscript received December 23, 2015; revised April 12, 2016; accepted May 15, 2016.

The authors are with the Department of Electronic and Electrical Engineering, University of Strathclyde, Glasgow G1 1XW, U.K. (e-mail: s.qin@strath.ac.uk; igor.timoshkin@strath.ac.uk; michelle.maclean@strath.ac.uk; scott.macgregor@strath.ac.uk; mark.p.wilson@strath.ac.uk; m.given@strath.ac.uk; t.wang@strath.ac.uk; j.anderson@strath.ac.uk).

Digital Object Identifier 10.1109/TPS.2016.2571628

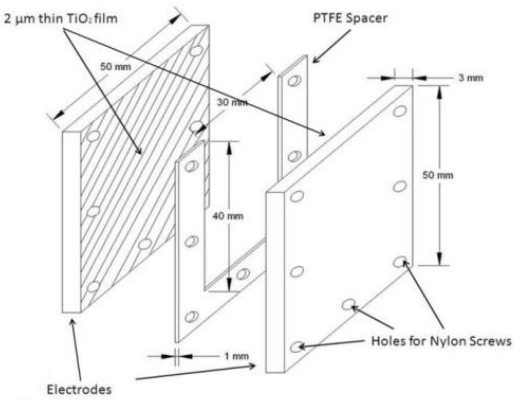


Fig. 1. Schematic of the PEF treatment cell with $TiO_2$-coated electrodes.

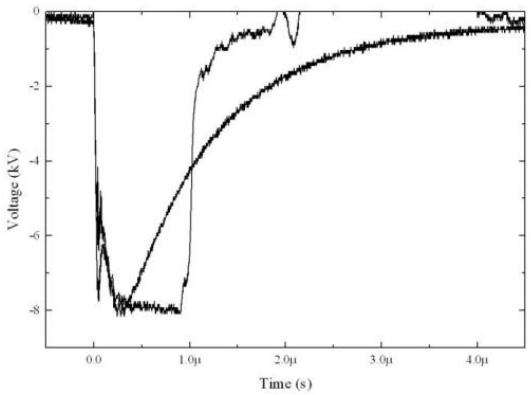


Fig. 2. Exponential and square voltage waveforms used to stress the PEF cell.

to provide a direct comparison between this $TiO_2$-coated and traditional metallic PEF treatment cells, the PEF treatment procedure was identical to the procedure used in [12], where the same microorganisms were subjected to PEFs in a treatment cell with uncoated conductive electrodes. In [12], voltage impulses with two different waveshapes, square and exponential, and two peak electrical-field magnitudes, 67 and 80 kV/cm, were used. In order to make comparison with this test cell, identical field strengths and waveshapes were used in this work. The inactivation kinetics and energy consumption for the PEF process performed in the treatment cell with $TiO_2$-coated electrodes have been obtained. The results of PEF inactivation obtained using the treatment cell with $TiO_2$-coated electrodes are compared with the recently published results [12]: the results of the PEF treatment obtained using the treatment cell with uncoated conductive electrodes and the same high-voltage (HV) waveforms.

## II. Experimental Procedures

### A. PEF Treatment Cell With Coated Electrodes

The topology of the PEF treatment cell used in this work is shown in Fig. 1. In this treatment cell, 50 mm × 50 mm square metallic plates, coated with a 2-$\mu$m $TiO_2$ thin-film, were used as parallel-plane electrodes. The interelectrode gap was maintained by a 1-mm-thick Polytetrafluoroethylene (PTFE) spacer. The electrodes and the spacer were clamped tightly together by nylon screws in order to seal the treatment cell. The treatment cell was filled with the yeast suspensions through its open top.

### B. PEF System and Voltage Waveforms

Under atmospheric pressure, an electrical breakdown event is likely to occur across the top liquid–air interface, due to the short (1 mm) gap between the electrodes. To avoid this undesirable breakdown, the PEF treatment cell was placed inside a sealed metallic chamber, described in [12], which was pressurized up to 7.5 bar (absolute pressure) with compressed air. The elevated air pressure suppresses the development of interfacial spark breakdowns.

Two different voltage waveforms, square and exponential, were used in this PEF study. An impulse generator based on a transmission-line topology (SAMTECH Ltd., UK [8]), was used to generate square HV impulses. This impulse generator was used to produce negative impulses with a magnitude of 30 kV and a duration of 1 $\mu$s.

A capacitive pulsed-power system was built to generate exponential HV impulses. This system consisted of an HVdc charging unit (Glassman, EH50P2), a protective resistor of 28 MΩ, a 40-nF HV capacitor (nominal capacitance), a self-breaking plasma closing switch, and a 2-m length of URM67 coaxial cable, which connects the output terminal of the capacitor with the PEF treatment cell. The magnitude of the voltage across the PEF treatment cell was regulated by the interelectrode gap distance of the switch, and the pulse repetition rate was controlled by the current regulator of the HVdc source. A 50-Ω resistor was connected in parallel with the PEF treatment cell to match the impedance of the pulse generator. A Tektronix P6015 A HV probe with a bandwidth of 75 MHz was used to measure the voltage across the PEF treatment cell, and a Pearson 6585 current monitor was used to measure the current through the PEF treatment cell. Both voltage and current waveforms were recorded using a Tektronix TDS2024 digital storage oscilloscope with a bandwidth of 200 MHz and a sampling rate of 2 GS/s. Fig. 2 shows the typical voltage waveshapes across the treatment cell during PEF treatment. The current waveforms for both types of applied HV impulses will be discussed in Section III-A.

### C. Preparation of the Yeast Sample

The yeast used in this work was *S. cerevisiae* (MUCL 28749), obtained from the Belgian Coordinated Collections of Microorganisms. The yeast was cultured in 100 ml 2% (w/v) malt extract broth (Oxoid Ltd, UK) at 30 °C in a shaking incubator (120 rpm). After 20 h incubation, the *S. cerevisiae* culture was centrifuged at 4300 rpm for 10 min and resuspended in 100 ml 0.05% (w/v) mycological peptone (Oxoid Ltd, UK). The population density of the

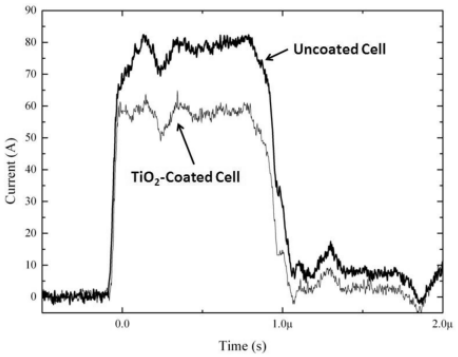


Fig. 3. Current waveform obtained during PEF treatment using exponential impulse. Dark line: current waveform in the treatment cell with stainless steel electrodes. Gray line: current waveform in the treatment cell with $TiO_2$-coated electrodes.

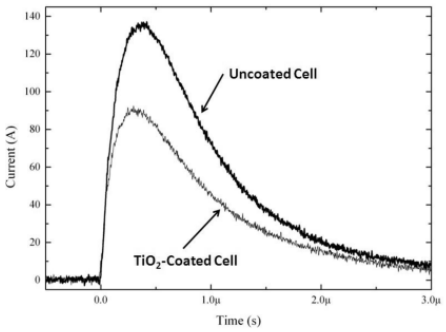


Fig. 4. Current waveform obtained during PEF treatment using exponential impulse. Dark line: current waveform in the treatment cell with stainless steel electrodes. Gray line: current waveform in the treatment cell with $TiO_2$-coated electrodes.

resulting yeast suspension was $\sim 10^7$ CFU/ml. The yeast suspension was then serially diluted 0.05% (w/v) with mycological peptone to prepare samples with population densities of $10^4$–$10^7$ CFU/ml.

### *D. Assessment of PEF Performance*

Yeast suspensions were treated in the PEF treatment cell with $TiO_2$-coated electrodes. *S. cerevisiae* samples were subjected to 25-, 50-, and 100-HV impulses, which had square and exponential waveforms, with peak magnitudes of 67 and 80 kV/cm. The pulse repetition rate was 1 pps for all tests. In order to exclude any potential antimicrobial effect from the electrode itself, a control group of samples was also used. In this group, the samples were placed inside the treatment cell for the same period of time without PEF treatment, to detect any antimicrobial effect. The treated and untreated (control) yeast samples were plated onto malt extract agar (Oxoid Ltd, UK) using spiral- and spread-plating methods, as detailed in [12]. Agar plates were then incubated at 30 °C for 20 h. Post incubation, the surviving populations of the treated and untreated (control) *S. cerevisiae* samples were enumerated and compared to assess the effect of the PEF treatment. The mean of the yeast populations ($\log_{10}$ CFU/ml) and its standard deviation have been obtained from triplicate independent PEF tests ($n = 3$), with each test using a fresh yeast culture.

## III. Results and Discussion

### *A. Current Waveform*

Figs. 3 and 4 show the current waveforms obtained during PEF treatments using the square impulse and exponential impulse, respectively. As can be seen from both Figs. 3 and 4, there is a noticeable ionic conduction current in the case of both PEF treatment cells, conductive (uncoated) and $TiO_2$-coated cells. It was found that the conduction current through the treated liquid was reduced by ~23% with $TiO_2$-coated electrodes compared with the conduction current with the stainless steel treatment cell.

### *B. Temperature Effects*

The temperature of the yeast suspension was measured using a K-type thermocouple before and after PEF treatment, in order to identify any notable thermal effects. The maximum registered change (increase) in the temperature of the yeast samples treated in the test cell with $TiO_2$-coated electrodes was only ~0.5 °C. As a comparison, an increase of ~1.5 °C in the sample temperature was observed after PEF treatment of a yeast suspension in a test cell with uncoated stainless steel electrodes using the same treatment parameters, i.e., the same field magnitude, pulse waveshape, and pulse repetition rate [12]. As the Joule heating of the liquid sample is directly related to the conduction current, the lower temperature increase of the sample treated in the $TiO_2$-coated treatment cell can be explained by the lower conduction current through the sample. Low electrical conductivity of the yeast solutions used in this work is also an important factor which helps to minimise the thermal effect of PEF treatment [8], [12]. In contrast, in the case of a highly conductive solution, an increase of a few tens of degree Celsius in temperature was reported [5], [13]. Therefore, the lower temperature change observed in this work (~0.5 °C) is likely to be explained by the use of less conductive $TiO_2$-coated electrodes and the low conductivity sample solution.

### *C. PEF Inactivation of Yeast in the Treatment Cell With $TiO_2$-Coated Electrodes*

The results of the PEF treatment of yeast suspensions ($\sim 10^7$ CFU/ml and $\sim 10^4$ CFU/ml) with $TiO_2$-coated electrodes are shown in Figs. 5 and 6. Figs. 5 and 6 show that both types of impulses (square and exponential) lead to a notable reduction in the yeast population. The control populations, which were held in the $TiO_2$-coated test cell but not subjected to electrical fields, were unchanged compared with the untreated starting populations, thus confirming that direct contact with the $TiO_2$ coating alone had no antimicrobial effect.

It was found that the PEF treatment with the higher field strength, 80 kV/cm, provides ~1-$\log_{10}$ greater reduction of

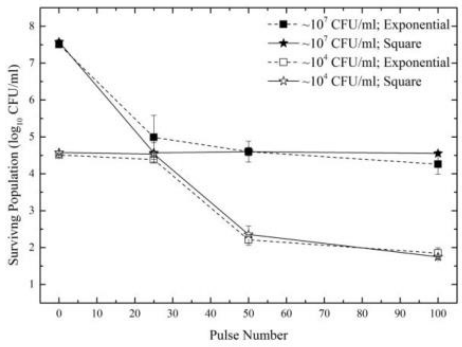


Fig. 5. Surviving populations of yeast ($\log_{10}$ CFU/ml) as a function of pulse number for 67 kV/cm waveforms: square waveform (stars and solid line) and exponential waveform (squares and dashed line). Error bars show standard deviation ($n = 3$).

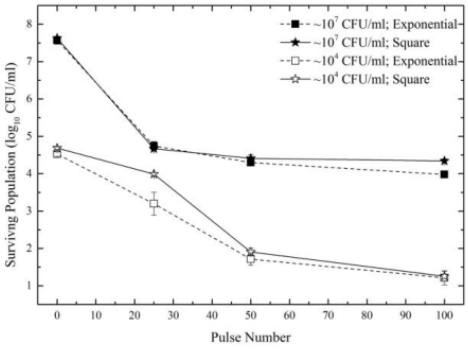


Fig. 6. Surviving populations of yeast ($\log_{10}$ CFU/ml) as a function of pulse number for 80 kV/cm waveforms: square waveform (stars and solid line) and exponential waveform (squares and dashed line). Error bars show standard deviation ($n = 3$).

the yeast population compared with the 67 kV/cm treatment, for all initial populations. The energy efficacy of the PEF treatment in the treatment cell equipped with $TiO_2$-coated electrodes is discussed in Section III-F.

The results shown in Figs. 5 and 6 demonstrate that the PEF treatment using the exponential waveform provides a greater inactivation effect compared with the PEF treatment using the square waveform. A similar tendency was reported in [12], where it was shown that exponential HV impulses resulted in a higher PEF efficacy compared with square impulses. It was suggested that the superior performance of the exponential waveform could be a result of its longer effective duration, during which the field in the treatment cell exceeds the critical inactivation field value, ∼10 kV/cm, [12].

### *D. Tailing Effect*

The PEF inactivation results presented in Figs. 5 and 6 demonstrate that after a 3-$\log_{10}$ population reduction

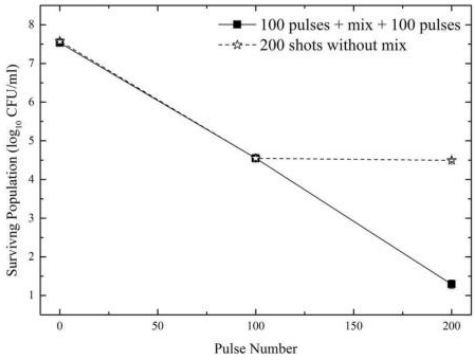


Fig. 7. Surviving populations of yeast in the case of the batch PEF treatment (dashed line, star symbols) and PEF treatment with remixing procedure (solid line, square symbols). Field strength: 67 kV/cm; square waveform. Error bars show standard deviation ($n = 3$).

(for all initial yeast populations and for all applied HV waveforms), further increase in the number of applied impulses leads to a tailing effect in the inactivation curves. This undesirable phenomenon was also reported in [12], [13], and [21]. In [12], the tailing effect was examined using different impulse waveforms and different initial populations of the yeast, in order to identify the potential causes of this effect. It was found that there was a sedimentation of the yeast cells during a ∼20-min period associated with pressurizing/depressurizing the test chamber. Conducting PEF treatment and remixing of the samples after every 100 impulses allowed a further reduction in the yeast population to be achieved. The same approach was used in this work, and it was shown that a further 3-$\log_{10}$ reduction in the *S. cerevisiae* population was achieved using this remixing process (Fig. 7). Therefore, a continuous flow of the liquid through the PEF treatment cell may help to eliminate the tailing effect, as was shown in [22]. However, no direct comparison between batch and continuous PEF processes has been made. As suggested in [12], other factors such as the potential penetration of liquid in the gaps between the electrodes and the dielectric spacer (areas with a reduced electric field), and clumping of microorganisms might also contribute to the tailing effect in the inactivation process.

### *E. Comparison of PEF Inactivation of Yeast in the Treatment Cell With $TiO_2$-Coated Electrodes and Uncoated Electrodes*

As discussed in Section III-B, the electrodes coated with $TiO_2$ film resulted in a lower Joule heating of the liquid compared with a treatment cell with uncoated conductive electrodes [12]. In this section, the results of the PEF treatment of yeast in the treatment cell with $TiO_2$-coated electrodes (Fig. 1) are compared with those following PEF treatment of the same strain of yeast in a treatment cell with uncoated conductive electrodes, published in [12]. The same initial populations of yeast were used in both this work and in [12]. The PEF inactivation curves for two initial populations,

TABLE I
ENERGY LOSSES ASSOCIATED WITH POLARIZATION PROCESS

| Waveform | Field Strength | Initial Population (CFU/ml) | |
|---|---|---|---|
| | | $10^7$ | $10^4$ |
| Square | 67 kV/cm | 0.058mJ | 0.055mJ |
| | 80 kV/cm | 0.072mJ | 0.069mJ |
| Exponential | 67 kV/cm | 0.094mJ | 0.096mJ |
| | 80 kV/cm | 0.152mJ | 0.152mJ |

TABLE II
TOTAL ENERGY LOSSES PER PULSE

| Waveform | Field Strength | Initial Population (CFU/ml) | |
|---|---|---|---|
| | | $10^7$ | $10^4$ |
| Square | 67 kV/cm | 394 mJ | 327 mJ |
| | 80 kV/cm | 641 mJ | 459 mJ |
| Exponential | 67 kV/cm | 401 mJ | 299 mJ |
| | 80 kV/cm | 544 mJ | 409 mJ |

losses have been calculated using the experimental voltage and current waveforms for both impulses and these losses are given in Table II.

Analysis of Tables I and II shows that the energy losses due to the polarization process (55–152 $\mu$J) only accounted for a very small portion of the total energy loss (which are in the range of 299–641 mJ). Therefore, the energy dissipation during PEF treatment in the test cell with $TiO_2$-coated electrodes is mainly due to the ionic conduction through the liquid sample. However, these conduction losses are lower than the conduction energy losses reported in [12] for the treatment cell with uncoated electrodes, which were in the range of 0.6–1.7 J.

Table II also shows that the energy delivered by a single impulse increased with the increase in the initial population of the yeast due to an increase in the conductivity of the yeast solution: the conductivity of the $10^7$ CFU/ml samples is $\sim$182 $\mu$S/cm, while the conductivity of the $10^4$ CFU/ml samples is $\sim$124 $\mu$S/cm. As a result, the ionic conduction current is higher in the case of $10^7$ CFU/ml samples than that of the samples with $10^4$ CFU/ml. Therefore, the energy losses due to the conduction current are higher in the case of a higher concentration of the yeast samples. Table II shows that the energy losses are higher for a higher electric field; also, there is a tendency toward a decrease in the energy losses for exponential impulses compared with the square impulses.

Comparison of the energy losses in the treatment cell with $TiO_2$-coated electrodes obtained in this work and in the treatment cell with uncoated electrodes has been made. The data for the treatment cell with uncoated electrodes are taken from [12], where the same HV impulses and the same strain of yeast were used. The results of this analysis are

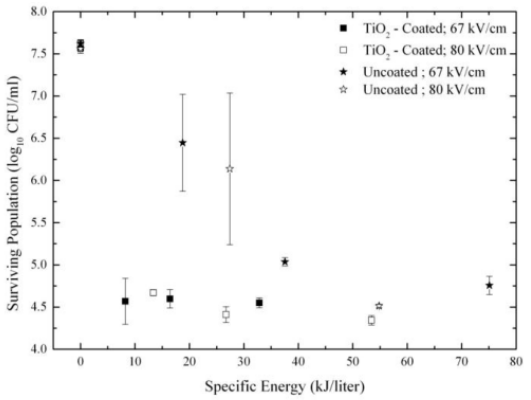


Fig. 10. Energy efficacy of the PEF treatment using the square waveform. Squares, $TiO_2$-coated electrodes; stars uncoated electrodes (data from [12]). Solid points, 67 kV/cm impulses; open points, 80 kV/cm impulses. Initial population of yeast was $10^7$ CFU/ml. Error bars show standard deviation ($n = 3$).

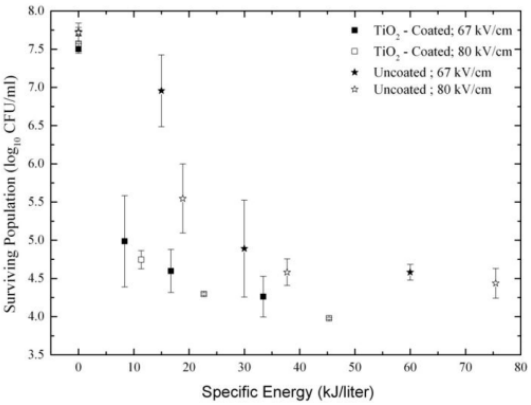


Fig. 11. Energy efficacy of the PEF treatment using the exponential waveform. Squares, $TiO_2$-coated electrodes; stars uncoated electrodes (data from [12]). Solid points, 67 kV/cm impulses; open points, 80 kV/cm impulses. Initial population of yeast was $10^7$ CFU/ml. Error bars show standard deviation ($n = 3$).

shown in Figs. 10 and 11, which demonstrate a reduction in the surviving population of the yeast for both treatment cells as a function of the specific energy. Figs. 10 and 11 show similar PEF inactivation tendencies for both types of electrodes: the surviving population of the yeast reduces as the specific energy increases. However, in the case of $TiO_2$-coated electrodes, the energy losses that are associated with the same $\log_{10}$ reduction in the yeast population are significantly lower compared with the uncoated electrodes. The main reason for this reduction in the energy losses is a lower conduction current through the yeast suspension in the test cell with $TiO_2$-coated electrodes. Therefore, this result suggests that the main mechanism of PEF inactivation is a

nonthermal process, which potentially involves electromechanical disruption of the yeast membrane. Potentially, further reduction in the specific energy consumption could be achieved if completely nonconductive electrodes are used. Such a design of the PEF treatment cell was implemented in [17], where only displacement current during the PEF process was observed.

## IV. Conclusion

This paper investigated the PEF inactivation of the yeast *S. cerevisiae*, using a treatment cell with $TiO_2$-coated electrodes. The $TiO_2$ coating acts as a barrier, reducing the ionic conduction current in the system. Two types of impulsive waveforms, square and exponential, with peak electrical-field magnitudes of 67 kV/cm and 80 kV/cm were used. The results obtained in this work show that a treatment cell with $TiO_2$-coated electrodes provides similar or better PEF inactivation performance compared with uncoated conductive electrodes. Moreover, it was demonstrated that $TiO_2$-coated electrodes result in a significant reduction in the energy losses during the treatment. Thus, this paper demonstrates that there are clear advantages in the use of electrodes coated with a thin less-conductive film in the PEF process.

It was also found that the tailing effect (reduction in the efficacy of the PEF treatment with an increase in the number of the applied impulses), which was evident in the initial inactivation kinetics, can be minimized by mixing the yeast suspension after every 100-HV impulses. A flowing system could be employed to eliminate this tailing effect in the future system design. These results are similar to the results obtained in [12] for the PEF process in a treatment cell with uncoated conductive electrodes. The PEF performances of square and exponential waveforms were investigated for comparison, and it was shown that the exponential waveform, which has a longer effective duration, provides a better PEF performance compared with the square waveform. This result confirms a similar finding reported in [12], for PEF treatment with uncoated electrodes.

The results of the PEF treatment of yeast in a treatment cell with $TiO_2$-coated electrodes demonstrate that such electrodes can be successfully used in the design of PEF reactors for practical applications. Electrodes coated with a thin less-conductive film lead to a substantial reduction in the energy losses due to Joule heating, and provide similar PEF inactivation performance compared with uncoated conductive electrodes. Therefore, a further reduction in the energy consumption could potentially be achieved if completely nonconductive electrodes are used. Further investigation of the PEF process using this novel approach is required in order to establish the PEF efficacy for other types of microorganism and energization regimes.

## References

[1] S. Toepfl, V. Heinz, and D. Knorr, "High intensity pulsed electric fields applied for food preservation," *Chem. Eng. Process.*, vol. 46, no. 6, pp. 537–546, 2007.

[2] U. Zimmermann, "Electrical breakdown, electropermeabilization and electrofusion," *Rev. Physiol. Biochem. Pharmacol.*, vol. 105, no. 6, pp. 175–256, 1986.

[3] H. Hülsheger, J. Potel, and E.-G. Niemann, "Electric field effects on bacteria and yeast cells," *Radiat. Environ. Biophys.*, vol. 22, no. 2, pp. 149–162, 1983.

[4] B.-L. Qin, G. V. Barbosa-Cánovas, B. G. Swanson, P. D. Pedrow, and R. G. Olsen, "Inactivating microorganisms using a pulsed electric field continuous treatment system," *IEEE Trans. Ind. Appl.*, vol. 34, no. 1, pp. 43–50, Jan. 1998.

[5] K. Aronssona, M. Lindgrena, B. R. Johanssonb, and U. Rönner, "Inactivation of microorganisms using pulsed electric fields: The influence of process parameters on *Escherichia coli*, Listeria innocua, Leuconostoc mesenteroides and Saccharomyces cerevisiae," *Innov. Food Sci. Emerg. Technol.*, vol. 2, no. 1, pp. 41–54, 2001.

[6] P. S. Brito, H. Canacsinh, J. P. Mendes, L. M. Redondo, and M. T. Pereira, "Comparison between monopolar and bipolar microsecond range pulsed electric fields in enhancement of apple juice extraction," *IEEE Trans. Plasma Sci.*, vol. 40, no. 10, pp. 2348–2354, Oct. 2012.

[7] H. Jaeger, N. Meneses, and D. Knorr, "Impact of PEF treatment inhomogeneity such as electric field distribution, flow characteristics and temperature effects on the inactivation of E. coli and milk alkaline phosphatase," *Innov. Food Sci. Emerg. Technol.*, vol. 10, no. 4, pp. 470–480, 2009.

[8] S. Qin *et al.*, "Pulsed electric field treatment of microalgae: Inactivation tendencies and energy consumption," *IEEE Trans. Plasma Sci.*, vol. 42, no. 10, pp. 3191–3196, Oct. 2014.

[9] M. D. A. Zbinden *et al.*, "Pulsed electric field (PEF) as an intensification pretreatment for greener solvent lipid extraction from microalgae," *Biotechnol. Bioeng.*, vol. 110, no. 6, pp. 1605–1615, 2013.

[10] C. Eing, M. Goettel, R. Straessner, C. Gusbeth, and W. Frey, "Pulsed electric field treatment of microalgae—Benefits for microalgae biomass processing," *IEEE Trans. Plasma Sci.*, vol. 41, no. 10, pp. 2901–2907, Oct. 2013.

[11] R. Narsetti, R. D. Curry, K. F. McDonald, T. E. Clevenger, and L. M. Nichols, "Microbial inactivation in water using pulsed electric fields and magnetic pulse compressor technology," *IEEE Trans. Plasma Sci.*, vol. 34, no. 4, pp. 1386–1393, Aug. 2006.

[12] S. Qin *et al.*, "Pulsed electric field treatment of Saccharomyces cerevisiae using different waveforms," *IEEE Trans. Dielectr. Electr. Insul.*, vol. 22, no. 4, pp. 1841–1848, Aug. 2015.

[13] B.-L. Qin, Q. Zhang, G. V. Barbosa-Cánovas, B. G. Swanson, and P. D. Pedrow, "Inactivation of microorganisms by pulsed electric fields of different voltage waveforms," *IEEE Trans. Dielectr. Electr. Insul.*, vol. 1, no. 6, pp. 1047–1057, Dec. 1994.

[14] S. H. Jayaram, "Sterilization of liquid foods by pulsed electric fields," *IEEE Elect. Insul. Mag.*, vol. 16, no. 6, pp. 17–25, Nov./Dec. 2000.

[15] Q. Zhang, G. V. Barbosa-Cánovas, and B. G. Swanson, "Engineering aspects of pulsed electric field pasteurization," *J. Food Eng.*, vol. 25, no. 2, pp. 261–281, 1995.

[16] I. V. Timoshkin, S. J. MacGregor, R. A. Fouracre, B. H. Crichton, and J. G. Anderson, "Transient electrical field across cellular membranes: Pulsed electric field treatment of microbial cells," *J. Phys. D, Appl. Phys.*, vol. 39, no. 3, pp. 569–603, 2006.

[17] B. M. Novac *et al.*, "Demonstration of a novel pulsed electric field technique generating neither conduction currents nor Joule effects," *IEEE Trans. Plasma Sci.*, vol. 42, no. 1, pp. 216–228, Jan. 2014.

[18] A. von Hippel, R. G. Breckenridge, F. G. Chesley, and L. Tisza, "High dielectric constant ceramics," *Ind. Eng. Chem.*, vol. 38, no. 11, pp. 1097–1109, Nov. 1946.

[19] A. Wypych, I. Bobowska, M. Tracz, A. Opasinska, S. Kadlubowski, A. Krzywania-Kaliszewska, J. Grobelny, and P. Wojciechowski, "Dielectric properties and characterisation of titanium dioxide obtained by different chemistry methods," *J. Nanomater.*, vol. 2014, pp. 1–9, Mar. 2014, Art. no. 124814.

[20] M. S. P. Sarah, M. Z. Musa, M. N. Asiah, and M. Rusop, "Electrical conductivity characteristics of $TiO_2$ thin film," in *Proc. Int. Conf. Electron. Devices, Syst. Appl. (ICEDSA)*, Apr. 2010, pp. 361–364.

[21] J. R. Beveridge, S. J. MacGregor, L. Marsili, J. G. Anderson, N. J. Rowan, and O. Farish, "Comparison of the effectiveness of biphase and monophase rectangular pulses for the inactivation of microorganisms using pulsed electric fields," *IEEE Trans. Plasma Sci.*, vol. 30, no. 4, pp. 1525–1531, Aug. 2002.

[22] J. R. Beveridge, K. Wall, S. J. MacGregor, J. G. Anderson, and N. J. Rowan, "Pulsed electric field inactivation of spoilage microorganisms in alcoholic beverages," *Proc. IEEE*, vol. 92, no. 7, pp. 1138–1143, Jul. 2004.

[23] T. Meissner and F. J. Wentz, "The complex dielectric constant of pure and sea water from microwave satellite observations," *IEEE Trans. Geosci. Remote Sens.*, vol. 42, no. 9, pp. 1836–1849, Sep. 2004.

**Si Qin** received the B.Eng. (Hons.) degree in electronic and electrical engineering and the M.Sc. degree in electrical power engineering from the University of Strathclyde, Glasgow, U.K., in 2011 and 2012, respectively, where he is currently pursuing the Ph.D. degree in electronic and electrical engineering.

**Igor V. Timoshkin** (M'07–SM'14) received the Degree in physics from the Moscow State University, Moscow, Russia, in 1992, and the Diploma and Ph.D. degrees from Imperial College of Science, Technology and Medicine (ICSTM), London, U.K., in 2001.

He was a Researcher with Moscow State Agro-Engineering University, Moscow, and with the Institute for High Temperatures of Russian Academy of Sciences. He moved to ICSTM in 1997. He joined the Department of Electronic and Electrical Engineering, University of Strathclyde, Glasgow, U.K., in 2001, where he became a Reader in 2016. His current research interests include properties of solid and liquid dielectric materials, bio-dielectrics and effects of electromagnetic fields on biological objects, gas discharges, non-thermal plasma for environmental, and bio-medical applications plasma in liquids.

**Michelle Maclean** was born in Isle of Lewis, U.K., in 1980. She received the B.Sc. (Hons.) degree in microbiology and immunology and the Ph.D. degree in electronic and electrical engineering from the University of Strathclyde, Glasgow, U.K., in 2002 and 2006, respectively.

She is currently a Lecturer with the University of Strathclyde, where she is involved in the development and application of novel electro-technologies for biological decontamination and sterilization applications in clinical and public health environments.

Dr. Maclean is a member of The Society for General Microbiology and The American Society of Microbiology.

**Scott J. MacGregor** (M'95–SM'14) received the B.Sc. and Ph.D. degrees from the University of Strathclyde, Glasgow, U.K., in 1982 and 1986, respectively.

He became a Pulsed Power Research Fellow in 1986, and a Lecturer in pulsed-power technology in 1989. In 1994, he became a Senior Lecturer, with a promotion to Reader and a Professor of High Voltage Engineering, in 1999 and 2001, respectively. In 2006 and 2010, he became the Head of the Department of Electronic and Electrical Engineering and the Executive Dean of the Faculty of Engineering, and has been the Vice Principal of the University of Strathclyde since 2014.

Dr. MacGregor was a recipient of the 2013 IEEE Peter Haas Award, and he was appointed as an Associate Editor of the IEEE TRANSACTIONS ON DIELECTRICS AND ELECTRICAL INSULATION in 2015. His current research interests include high-voltage pulse generation, high-frequency diagnostics, high-power repetitive switching, high-speed switching, electronic methods for food pasteurization and sterilization, generation of high-power ultrasound (HPU), plasma channel drilling, pulsed-plasma cleaning of pipes, and stimulation of oil wells with HPU.

**Mark P. Wilson** (M'10) was born in Stranraer, U.K., in 1982. He received the B.Eng. (Hons.), M.Phil., and Ph.D. degrees from the University of Strathclyde, Glasgow, U.K., in 2004, 2007, and 2011, respectively, all in electronic and electrical engineering.

He is currently a Teaching Associate with the University of Strathclyde, where he continues to investigate surface flashover of solids immersed in insulating oil.

Dr. Wilson is a member of the IEEE Nuclear and Plasma Sciences Society, the IEEE Dielectrics and Electrical Insulation Society, and the Institution of Engineering and Technology. He received a Graduate Scholarship Award in 2011.

**Martin J. Given** (M'99–SM'11) received a B.Sc. xegree in physics from the University of Sussex, Brighton, U.K., in 1981, and the Ph.D. degree in electronic and electrical engineering from the University of Strathclyde, Glasgow, U.K., in 1996.

He is currently a Senior Lecturer with the Department of Electronic and Electrical Engineering, University of Strathclyde. His current research interests include ageing processes and condition monitoring in solid and liquid insulation systems, and high speed switching and pulse power.

**Tao Wang** received the B.Eng. and M.Sc. degrees from Northeast China Dianli University, Jilin City, China, in 1993 and 1996 respectively, and the Ph.D. degree from the University of Strathclyde, Glasgow, U.K., in 2005.

He joined the Newland Entech, Fuzhou, China, as a Research Fellow, where he is involved in developing high efficiency industrial ozone generator. He joined the Department of Electronic and Electrical Engineering, University of Strathclyde, as a Lecturer, in 2010. His current research interests include non-thermal gas discharges and their applications in gas synthesis, water disinfection, and advanced oxidation process in water.

**John G. Anderson** was born in Glasgow, U.K., in 1942. He received the B.Sc. degree in applied microbiology and the Ph.D. degree in fungal physiology from the University of Strathclyde, Glasgow, in 1968 and 1971, respectively.

He has been with the Department of Bioscience and Biotechnology, University of Strathclyde, since 1971, where he became a Professor of Microbiology and the Head of Department. He is currently an Emeritus Professor with the University of Strathclyde. His current research interests include various aspects of food, biomedical and environmental microbiology with interdisciplinary collaboration on the application of electro-technologies for electronic pasteurization and sterilization.